Am J Clin Exp Urol 2020;8(Supplementary Issue 1):1-181
www.ajceu.us /ISSN:2330-1910/2020 SBUR Annual Meeting

Cellular Interactions and Identities in Urologic Biology: Meeting Report of the 2020 Society for Basic Urologic Research Annual Meeting

Rosalyn M Adam[1,2], Daniel E Frigo[3,4,5], Allen C Gao[6,7], Thomas S Griffith[8,9], Beatrice S Knudsen[10], Shawn E Lupold[11], Larisa Nonn[12], Arun Sreekumar[13], LaMonica V Stewart[14], Chad M Vezina[15], Zongbing You[16,17], Jindan Yu[18], Scott M Dehm[19]

[1]Department of Urology, Boston Children's Hospital, Boston, MA, USA; [2]Department of Surgery, Harvard Medical School, Boston, MA, USA; [3]Department of Cancer Systems Imaging and Department of Genitourinary Medical Oncology, The University of Texas MD Anderson Cancer Center, Houston, TX, USA; [4]Center for Nuclear Receptors and Cell Signaling, Department of Biology and Biochemistry, University of Houston, Houston, TX, USA; [5]The Houston Methodist Research Institute, Houston, TX, USA; [6]Department of Urologic Surgery and UC Davis Comprehensive Cancer Center, University of California, Davis, Sacramento, CA, USA; [7]VA Northern California Health Care System, Sacramento, CA, USA; [8]Department of Urology, Center for Immunology, and Masonic Cancer Center, University of Minnesota, Minneapolis, MN, USA; [9]Minneapolis VA Health Care System, Minneapolis, Minnesota, USA; [10]Department of Pathology, University of Utah, Salt Lake City, UT, USA; [11]The James Buchanan Brady Urologic Institute and Department of Urology, Johns Hopkins School of Medicine, Baltimore, MD, USA; [12]Department of Pathology and University of Illinois Cancer Center, University of Illinois at Chicago, Chicago, IL, USA; [13]Verna and Marrs McLean Department of Biochemistry and Molecular Biology, Department of Molecular and Cellular Biology, Center for Metabolism and Experimental Therapeutics and Dan L Duncan Comprehensive Cancer Center, Baylor College of Medicine, Houston, TX, USA; [14]Department of Biochemistry, Cancer Biology, Neuroscience, and Pharmacology, Meharry Medical College, Nashville, TN, USA; [15]Department of Comparative Biomedical Sciences, School of Veterinary Medicine and Molecular and Environmental Toxicology Center, School of Medicine, and Public Health and George M O'Brien Benign Urology Center, University of Wisconsin- Madison, Madison, WI, USA; [16]Department of Structural & Cellular Biology, Tulane Cancer Center and Louisiana Cancer Research Consortium, Tulane University, New Orleans, LA, USA; [17]Southeast Louisiana Veterans Health Care System, New Orleans, LA, USA; [18]Department of Medicine, Division of Hematology/Oncology, Department of Biochemistry and Molecular Genetics, and Robert H Lurie Comprehensive Cancer Center, Northwestern University Feinberg School of Medicine, Chicago, IL, USA; [19]Department of Laboratory Medicine and Pathology, Department of Urology, and Masonic Cancer Center, University of Minnesota, Minneapolis, MN, USA

In his Leland W.K. Chung Lecture, Dr. Hans Clevers from the Utrecht Institute shared his laboratory's discoveries of Wnt-driven stem cells in crypts of mouse colonic epithelium, and the identification of Lgr5 as a key stem cell effector that marks colonic stem cells in the crypts [1, 2]. Lineage tracing of Lgr5-positive cells led to label incorporation in mature differentiated epithelial cells lining the villi as well as the lumen, confirming that they originated from the Lgr5-positive stem cells. Characterization of Lgr5-positive colonic stem cells determined that they are relatively abundant and bind R-spondin to enable sustained signaling from Wnt receptors in colonic stem cells. These discoveries enabled Dr. Clevers and his team to identify a set of defined growth factors and conditions, consisting of R-spondin, Noggin, EGF, and matrigel, that supported the formation of "mini-gut" organoid structures *in vitro* from individual Lgr5-positive stem cells [3]. Dr. Clevers presented his group's characterization of these colonic organoids, including their ability to expand organoids *in vitro* from a single Lgr5-positive stem cell, and then use these organoids to regenerate injured colons by transplanting them via the anus in an experimental mouse model of inflammatory bowel disease, thus acting as a "living bandage" [4]. Dr. Clevers then presented several application of organoid technology to address problems in human disease. One application was generating colonic organoids from children with cystic fibrosis, and applying these organoids for *in vitro* drug test-

ing to predict patient drug responses [5]. Another application was to generate organoids from several human tissues, and use these organoids to test infectivity of these tissues by the SARS-CoV2 virus responsible for the current COVID-19 pandemic [6]. Dr. Clevers knocked out the ACE2 receptor and TMPRSS2 protease in these organoids to confirm the requirement for these proteins for SARS-CoV2 virus priming and cellular entry. Approaches for generating organoids from cancer cells were presented, with applications including drug screening to identify effective therapeutics as well as elucidating genetic dependencies of specific cancer types. Transitioning to research in urologic biology, Dr. Clevers discussed the development of kidney "tubuloids" for studying kidney viral infections by BK virus [7], the generation of pediatric kidney cancer organoid biobanks from Wilms' tumor and malignant rhabdoid tumors of the kidney [8], the generation of mouse and human bladder organoids from cells captured in urine, and the development of a biobank of bladder cancer organoids derived from surgical procedures [9].

The first plenary session discussed New Models and Technologies for Studying Urologic Biology. Drs. X. Sean Li (Cedars-Sinai Medical Center) and Paula Hurley (Vanderbilt University) were discussion leaders for this plenary session. Dr. Woonyoung Choi from Johns Hopkins University presented a consensus classification system of muscle invasive bladder cancer based on the use of network analysis to consolidate published RNA-seq and DNA-seq studies of muscle invasive bladder cancer into 6 distinct molecular subtypes. Dr. Choi presented the clinical correlates and treatment outcomes for these 6 subtypes, as well as research designed to understand mechanisms of therapy response and resistance within subtypes [10]. Dr. Justin Drake from University of Minnesota presented the use of mass spectrometry-based proteomics profiling to understand kinase signaling networks that are de-regulated in prostate cancer, leading to the identification of RET kinase as a molecular driver of the lethal neuroendocrine manifestation of advanced castration-resistant prostate cancer [11]. Dr. Drake also presented on the use of targeted proteomics to characterize protein expression of androgen receptor variants in prostate cancer cell lines and patient-derived xenograft tissues. Dr. Margot Damaser presented her work on development of animal models to study stress urinary incontinence. Dr. Damaser presented regenerative medicine approaches using mesenchymal stem cells and electrical stimulation to promote innervation of the neuromuscular junction as a treatment for stress urinary incontinence [12, 13]. Dr. John Lee from Fred Hutchinson Cancer Research Center presented his strategy for identifying genetic combinations of cDNAs and short hairpin RNAs (shRNAs) that can initiate bladder cancer in basal bladder urothelial cells. Dr. Lee demonstrated that specific combinations of cDNAs and shRNAs could promote distinct bladder cancer histologies. Dr. Scott Hultgren from Washington University discussed mouse models for studying recurrent urinary tract infections by uropathogenic *Escherichia coli* (UPEC) [14]. He demonstrated that bladders of mice infected with UPEC are remodeled and display defects in terminal differentiation due to neutrophil damage, which sensitizes the urinary tract to subsequent infections. Dr. Hultgren further discussed the development of vaccines against UPEC virulence factors as a strategy to prevent recurrent urinary tract infection [15]. Dr. Ashleigh Theberge at University of Washington presented her group's advances in bioengineering for developing microfluidic platforms for studying cellular interactions *in vitro* using cell co-culture [16]. Dr. Theberge also presented devices developed in her lab to enable at-home blood capture and RNA stabilization.

The second plenary session focused on Advances in Urologic Pathologies by National Institutes of Diabetes and Digestive and Kidney Disease (NIDDK) Urology Centers and Training Programs. NIDDK O'Brien Center Directors Drs. William Ricke (University of Wisconsin), Zhou Wang (University of Pittsburgh) and Cathy Mendelsohn (Columbia University) were discussion leaders for this plenary session. To emphasize NIDDK Training Programs and their importance for developing the next generation of investigators in the field, the design of this session was for senior investigators at NIDDK-funded O'Brien Centers to give short talks, and NIDDK-funded trainees to give longer talks. Dr. Chad Vezina from the University of Wisconsin O'Brien Center discussed the role of prostatic collagen accumulation in benign prostatic hyperplasia (BPH) and urinary voiding function in aging males [17, 18]. Dr. Donald DeFranco from the University of Pittsburgh presented

research on the role of progressive, age-related mitochondrial dysfunction in prostatic cells in the development and progression of BPH. Dr. DeFranco provided evidence that electron transport chain complex I dysfunction contributes to BPH pathogenesis. Dr. Jonathan Barasch from Columbia University discussed the role of iron in urinary tract infection and the complex interactions between siderophore iron chelators produced by UPEC and heme in host red blood cells that comprise the "heme machine" required for urinary tract infection. Dr. Teresa Liu, a trainee at the University of Wisconsin expanded on the role of mitrochondrial dysfunction in BPH pathology, and discussed the hypothesis that defective mitochondria accumulate in prostatic cells due to insufficient mitophagy as males age. She also presented data showing that mitrochondrial dysfunction leads to cellular senescence, collagen accumulation, and prostatic fibrosis, which may be reversed with anti-fibrotic drugs [19]. Dr. Laura Pascal, a trainee at University of Pittsburgh, discussed a mouse model of prostatic CHD1 knock-out (encodes E-cadherin), which displayed features of altered prostate epithelial barrier function, inflammation, BPH, and lower urinary tract dysfunction [20]. Dr. Pascal used this model to test non-steroidal anti-inflammatory drugs for treating these pathogenic symptoms. Dr. Eric Gonzalez, a trainee at Duke University, presented his detailed characterization of bladder voiding and muscle contractility dysfunction that he identified in a mouse model of detrusor underactivity caused by diet-induced obesity [21]. Following this session, Dr. Carolyn Best, Director of Research at the AUA presented an update on AUA activities in education, research, and advocacy.

The third plenary session focused on Genes and Development in Urologic Health and Disease. SBUR president Dr. Rosalyn Adam (Boston Children's Hospital) and Dr. Jason Van Batavia (University of Pennsylvania) served as discussion leaders for this plenary session. The first lecture of this session was the AUA lecture delivered by Dr. Linda Baker from University of Texas Southwestern Medical Center at Dallas. Dr. Baker presented her research on genetics and treatment of congenital birth defects affecting the genitourinary tract. The genitourinary tract is the second most common organ system affected by birth defects. These birth defects can manifest externally or internally, and have profound effects on the function of genitourinary organs including kidney, bladder, and the reproductive tract. Dr. Baker presented her work using forward genetics and reverse genetics approaches to understand the genetic basis for various congenital birth defects affecting the genitourinary tract, with focus on cryptorchidism, testicular torsion, hypospadias, vaginal anomalies, and prune belly syndrome. Dr. Baker presented her group's identification of insulin-3 signaling and INSL3 gene alterations in cryptorchidism [22, 23] and her use of near-infrared imaging to identify testicular torsion rapidly and prioritize patients for surgery [24]. She discussed hypospadias, which is the most common genitourinary birth defect, and her studies with an ephrin B2 knock-out mouse model that develops hypospadias [25]. She presented an autologous buccal vaginoplasty strategy that she developed for surgical reconstruction of vaginal birth anomalies [26]. Finally, Dr. Baker presented her research on prune belly syndrome. Dr. Baker developed an organ system-based phenotyping scoring system for grouping patients based on disease severity [27]. Using this scoring system, she was able to study discrete cohorts of patients and their families using forward genetics. This approach led to Dr. Baker and her group identifying mutations in the MYOCD and FLNA genes as underlying causes of prune belly syndrome [28]. Following the AUA lecture, Dr. Michelle Southard-Smith from Vanderbilt University discussed development and innervation of the lower urogenital tract, and presented her group's characterization of the timing and mechanisms of neural crest cell migration and population of the urogenital sinus during mouse embryonic development [29]. Dr. Margaret Vizzard from University of Vermont presented her research on mechanosensation in the urinary bladder. Dr. Vizzard presented the basis for micturition reflex in the urinary bladder, and discussed the role of TRPV4 mechanoreceptor expression and function in bladder function, with potential for targeting TRPV4 to improve bladder dysfunction and pain [30].

The fourth plenary session presented recent advances in Cancer Cell Biology and Communication. Drs. Gail Prins (University of Illinois at Chicago) and Li Xin (University of

Washington) were discussion leaders for this session. Dr. A. Ari Hakimi from Memorial Sloan Kettering Cancer Center presented his research on RNA-seq and single-cell RNA-seq profiling of the tumor microenvironment in clear cell kidney cancer to characterize immune cell infiltrates [31]. Dr. Hakimi discussed how immune cell phenotyping in kidney cancer could be used to predict and improve clinical responses to immune checkpoint blockade therapy. Dr. Bethany Kerr from Wake Forest University presented her work on developing microfluidic platforms for prostate cancer cell chemotaxis assays, with the goal of modeling bone tropism of metastatic prostate cancer and identifying therapeutic targets for preventing bone metastasis [32]. Dr. Kerr also discussed the use of mouse models to understand how co-morbidities such as osteoarthritis impacts prostate cancer bone metastasis. Dr. Jennifer Wu from Northwestern University addressed the role of MHC Class I Chain Related Molecule (MIC) as an immune-suppressor when cleaved and shed by prostate cancer cells. Dr. Wu developed a therapeutic antibody targeted to soluble MIC that may overcome the general resistance of prostate cancer to T-cell and natural killer cell-mediated killing [33, 34]. Dr. Jelani Zarif from Johns Hopkins University presented the role of macrophages in prostate cancer. Dr. Zarif discussed the role and biomarker potential of CD206 enrichment on the surface of M2-polarized tumor-associated macrophages, as well as therapeutic targeting of glutamine dependence of M2 macrophages, in advanced, castration-resistant prostate cancer [35]. Dr. Daniel Frigo from University of Texas MD Anderson Cancer Center presented his group's research on CAMKK2 as a biomarker and therapeutic target in castration-resistant prostate cancer [36]. Dr. Frigo demonstrated that CAMKK2 phosphorylates the CREB transcription factor to regulate oxidative phosphorylation in prostate cancer cells, which may present a therapeutic vulnerability.

The fifth plenary session discussed Cellular Identity and Lineage Plasticity. Drs. Yuanyuan Zhang (Wake Forest University) and Wendy Huss (Roswell Park Comprehensive Cancer Center) were discussion leaders for this session. Dr. David Rickman from Weill Cornell Medical College presented his laboratory's development of a mouse model of neuroendocrine prostate cancer achieved by transgenic overexpression of N-Myc and knock-out of Rb1. Dr. Rickman discussed his group's characterization of the neuroendocrine prostate cancer molecular program in this mouse model using RNA-seq and chromatin immunoprecipitation (ChIP)-seq approaches. Dr. Donald Vander Griend from University of Illinois at Chicago presented studies on lineage tracing of the SOX2 transcription factor in prostatic regeneration, and the role of SOX2 in the development and progression of prostate cancer to an advanced, castration-resistant phenotype [37]. Dr. Tanya Stoyanova from Stanford University presented her group's identification of Trop2 overexpression in advanced prostate cancers. Characterization of Trop2 demonstrated that this protein can promote aggressive disease phenotypes, including the neuroendocrine manifestation of castration-resistant prostate cancer [38].

The sixth plenary session highlighted Emerging Cellular Targets and Therapies for Urologic Pathologies. Discussion leaders for this session were Drs. Amina Zoubeidi (Vancouver Prostate Centre) and Ganesh Raj (University of Texas Southwestern Medical Center at Dallas). Dr. Leah Cook from University of Nebraska Medical Center initiated this session by discussing the role of neutrophils in restraining growth of bone metastatic prostate cancer. Dr. Cook presented evidence that prostate cancer cells can reprogram tumor-associated neutrophils to lose this tumor suppressor activity [39]. Dr. John David Spencer from Nationwide Children's Hospital presented his group's research on the antimicrobial properties of ribonuclease A superfamily proteins, emphasizing the mechanisms by which RNase 7 protects the urothelial tract from UPEC infection [40]. Dr. Leigh Ellis from Cedars-Sinai Medical Center discussed his group's development of a mouse model of advanced prostate cancer driven by transgenic overexpression of Ezh2 and c-Myc, which revealed a major role of Ezh2 in regulating the interferon gamma pathway thorough an epigenetic mechanisms involving histone H3 lysine 27 acetylation. He demonstrated that treating these mice with Ezh2 inhibitors increased efficacy of immune checkpoint blockade therapy. Dr. Kerry Burnstein from University of Miami demonstrated that the arginine vasopressin receptor 1A (AVPR1A) is overexpressed

in castration-resistant prostate cancer. Targeting AVPR1A with the antagonist relcovaptin inhibited the growth of castration-resistant prostate cancer *in vivo* [41]. Dr. Daniel Gioeli from University of Virginia presented his group's identification of a long-noncoding RNA residing in the *LCK* gene locus as a driver of prostate cancer growth. Dr. Gioeli named this lncRNA HULLK (hormone-upregulated lncRNA within *LCK*) and demonstrated the potential for HULLK detection in urine as a prostate cancer biomarker [42]. Dr. Veronica Rodriguez-Bravo from Sidney Kimmel Cancer Center at Thomas Jefferson University highlighted the role of nucleoporins in promoting prostate cancer progression [43]. Dr. Rodriguez-Bravo discussed the therapeutic potential for targeting nucleoporins with nuclear import inhibitors. Finally, Dr. Trinity Bivalacqua from Johns Hopkins University discussed his group's research to engineer Bacillus Calmette-Guerin (BCG) to improve intravesical immunotherapy for treating bladder cancer [44].

There were 20 trainees selected to receive Virtual Travel Awards from over 100 submitted abstracts and 7 of these trainees were selected to give oral presentations within these plenary sessions. The remaining 13 Virtual Travel Awardees gave oral presentations during a special online session moderated by Drs. Nonn and Lupold. Drs. Sreekumar and Frigo organized a trainee affairs symposium for all trainee attendees, held on the first day of the meeting. The trainee affairs symposium discussed strategies for pursuing and advancing careers in academia and industry. SBUR promotes the training of next generation of urologic researchers.

Acknowledgements

The authors comprise the SBUR 2020 Annual Meeting Program Committee, chaired by S.M.D., the SBUR Trainee Affairs Symposium Committee, chaired by A.S., and advisors to these committees. The authors thank the meeting registrants for attending the annual meeting virtually amid the COVID-19 global pandemic. The authors are grateful to all attendees for the wonderful presentations and robust discussions throughout the meeting. A.S. and D.E.F. thank panelists that participated in the trainee affairs symposium and provided valuable career advice: Drs. Gopi Shanker (Novartis Institutes for Biomedical Research), Steven Kregel (University of Michigan), Ciara Metcalfe (Genentech), Leigh Ellis (Cedars-Sinai Medical Center), Vinata Lokeshwar (Augusta University), Andrea Sherk (Womble Bond Dickinson, LLP) and Nikki Delk (University of Texas at Dallas). The authors are grateful to Shelley Warnock, Regina Legoo, and the rest of the Affinity Strategies team for providing efficient administration, management, and digital meeting support. The SBUR 2020 Annual Meeting and activities reported in this publication were supported by the National Institute of Diabetes and Digestive and Kidney Diseases of the National Institutes of Health under Award Number R13DK127671 (to S.M.D.). The content is solely the responsibility of the authors and does not necessarily represent the official views of the National Institutes of Health. The SBUR 2020 Annual Meeting also received generous financial support from Astellas Pharma, Inc., and Bristol Myers Squibb.

Disclosure of conflict of interest

None.

Address correspondence to: Scott M Dehm, Masonic Cancer Center, University of Minnesota, MCRB 560D, Mayo Mail Code 806, 420 Delaware Street SE, Minneapolis, MN 55455, USA. Tel: 612-625-1504; Fax: 612-625-4915; E-mail: dehm@umn.edu

References

[1] Barker N, Tan S and Clevers H. Lgr proteins in epithelial stem cell biology. Development 2013; 140: 2484-2494.

[2] Clevers H. Stem cells: a unifying theory for the crypt. Nature 2013; 495: 53-54.

[3] Sato T, Vries RG, Snippert HJ, van de Wetering M, Barker N, Stange DE, van Es JH, Abo A, Kujala P, Peters PJ and Clevers H. Single Lgr5 stem cells build crypt-villus structures in vitro without a mesenchymal niche. Nature 2009; 459: 262-265.

[4] Andersson-Rolf A, Zilbauer M, Koo BK and Clevers H. Stem cells in repair of gastrointestinal epithelia. Physiology (Bethesda) 2017; 32: 278-289.

[5] Berkers G, van Mourik P, Vonk AM, Kruisselbrink E, Dekkers JF, de Winter-de Groot KM, Arets HGM, Marck-van der Wilt REP, Dijkema JS, Vanderschuren MM, Houwen RHJ, Heijerman HGM, van de Graaf EA, Elias SG, Majoor CJ, Koppelman GH, Roukema J, Bakker M, Janssens HM, van der Meer R, Vries RGJ, Clevers HC, de Jonge HR, Beekman JM and

van der Ent CK. Rectal organoids enable personalized treatment of cystic fibrosis. Cell Rep 2019; 26: 1701-1708, e1703.

[6] Lamers MM, Beumer J, van der Vaart J, Knoops K, Puschhof J, Breugem TI, Ravelli RBG, Paul van Schayck J, Mykytyn AZ, Duimel HQ, van Donselaar E, Riesebosch S, Kuijpers HJH, Schipper D, van de Wetering WJ, de Graaf M, Koopmans M, Cuppen E, Peters PJ, Haagmans BL and Clevers H. SARS-CoV-2 productively infects human gut enterocytes. Science 2020; 369: 50-54.

[7] Schutgens F, Rookmaaker MB, Margaritis T, Rios A, Ammerlaan C, Jansen J, Gijzen L, Vormann M, Vonk A, Viveen M, Yengej FY, Derakhshan S, de Winter-de Groot KM, Artegiani B, van Boxtel R, Cuppen E, Hendrickx APA, van den Heuvel-Eibrink MM, Heitzer E, Lanz H, Beekman J, Murk JL, Masereeuw R, Holstege F, Drost J, Verhaar MC and Clevers H. Tubuloids derived from human adult kidney and urine for personalized disease modeling. Nat Biotechnol 2019; 37: 303-313.

[8] Custers L, Khabirova E, Coorens THH, Oliver TRW, Calandrini C, Young MD, Vieira Braga FA, Ellis P, Mamanova L, Segers H, Maat A, Kool M, Hoving EW, van den Heuvel-Eibrink MM, Nicholson J, Straathof K, Hook L, de Krijger RR, Trayers C, Allinson K, Behjati S and Drost J. An organoid biobank for childhood kidney cancers that captures disease and tissue heterogeneity. Nat Commun 2020; 11: 1310.

[9] Mullenders J, de Jongh E, Brousali A, Roosen M, Blom JPA, Begthel H, Korving J, Jonges T, Kranenburg O, Meijer R and Clevers HC. Mouse and human urothelial cancer organoids: a tool for bladder cancer research. Proc Natl Acad Sci U S A 2019; 116: 4567-4574.

[10] Kamoun A, de Reyniès A, Allory Y, Sjödahl G, Robertson AG, Seiler R, Hoadley KA, Groeneveld CS, Al-Ahmadie H, Choi W, Castro MAA, Fontugne J, Eriksson P, Mo Q, Kardos J, Zlotta A, Hartmann A, Dinney CP, Bellmunt J, Powles T, Malats N, Chan KS, Kim WY, McConkey DJ, Black PC, Dyrskjøt L, Höglund M, Lerner SP, Real FX and Radvanyi F; Bladder Cancer Molecular Taxonomy Group. A consensus molecular classification of muscle-invasive bladder cancer. Eur Urol 2020; 77: 420-433.

[11] VanDeusen HR, Ramroop JR, Morel KL, Bae SY, Sheahan AV, Sychev Z, Lau NA, Cheng LC, Tan VM, Li Z, Petersen A, Lee JK, Park JW, Yang R, Hwang JH, Coleman I, Witte ON, Morrissey C, Corey E, Nelson PS, Ellis L and Drake JM. Targeting RET kinase in neuroendocrine prostate cancer. Mol Cancer Res 2020; 18: 1176-1188.

[12] Balog BM, Deng K, Labhasetwar V, Jones KJ and Damaser MS. Electrical stimulation for neuroregeneration in urology: a new therapeutic paradigm. Curr Opin Urol 2019; 29: 458-465.

[13] Janssen K, Lin DL, Hanzlicek B, Deng K, Balog BM, van der Vaart CH and Damaser MS. Multiple doses of stem cells maintain urethral function in a model of neuromuscular injury resulting in stress urinary incontinence. Am J Physiol Renal Physiol 2019; 317: F1047-F1057.

[14] Tamadonfar KO, Omattage NS, Spaulding CN and Hultgren SJ. Reaching the end of the line: urinary tract infections. Microbiol Spectr 2019; 7.

[15] O'Brien VP, Hannan TJ, Nielsen HV and Hultgren SJ. Drug and vaccine development for the treatment and prevention of urinary tract infections. Microbiol Spectr 2016; 4: 10.1128/microbiolspec.UTI-0013-2012.

[16] Day JH, Nicholson TM, Su X, van Neel TL, Clinton I, Kothandapani A, Lee J, Greenberg MH, Amory JK, Walsh TJ, Muller CH, Franco OE, Jefcoate CR, Crawford SE, Jorgensen JS and Theberge AB. Injection molded open microfluidic well plate inserts for user-friendly coculture and microscopy. Lab Chip 2020; 20: 107-119.

[17] Ruetten H, Wegner KA, Romero MF, Wood MW, Marker PC, Strand D, Colopy SA and Vezina CM. Prostatic collagen architecture in neutered and intact canines. Prostate 2018; 78: 839-848.

[18] Wegner KA, Mueller BR, Unterberger CJ, Avila EJ, Ruetten H, Turco AE, Oakes SR, Girardi NM, Halberg RB, Swanson SM, Marker PC and Vezina CM. Prostate epithelial-specific expression of activated PI3K drives stromal collagen production and accumulation. J Pathol 2020; 250: 231-242.

[19] Liu TT, Thomas S, McLean DT, Roldan-Alzate A, Hernando D, Ricke EA and Ricke WA. Prostate enlargement and altered urinary function are part of the aging process. Aging (Albany NY) 2019; 11: 2653-2669.

[20] Pascal LE, Mizoguchi S, Chen W, Rigatti LH, Igarashi T, Dhir R, Tyagi P, Wu Z, Yang Z, de Groat WC, DeFranco DB, Yoshimura N and Wang Z. Prostate-specific deletion of Cdh1 induces murine prostatic inflammation and bladder overactivity. Endocrinology 2020; 162: bqaa212.

[21] Gonzalez EJ and Grill WM. The effects of neuromodulation in a novel obese-prone rat model of detrusor underactivity. Am J Physiol Renal Physiol 2017; 313: F815-F825.

[22] Harrison SM, Bush NC, Wang Y, Mucher ZR, Lorenzo AJ, Grimsby GM, Schlomer BJ, Bullesbach EE and Baker LA. Insulin-like peptide 3 (INSL3) serum concentration during human male fetal life. Front Endocrinol (Lausanne) 2019; 10: 596.

[23] Sozubir S, Barber T, Wang Y, Ahn C, Zhang S, Verma S, Lonergan D, Lorenzo AJ, Nef S and Baker LA. Loss of Insl3: a potential predisposing factor for testicular torsion. J Urol 2010; 183: 2373-2379.
[24] Schlomer BJ, Keays MA, Grimsby GM, Granberg CF, DaJusta DG, Menon VS, Ostrov L, Sheth KR, Hill M, Sanchez EJ, Harrison CB, Jacobs MA, Huang R, Burgu B, Hennes H and Baker LA. Transscrotal near infrared spectroscopy as a diagnostic test for testis torsion in pediatric acute scrotum: a prospective comparison to gold standard diagnostic test study. J Urol 2017; 198: 694-701.
[25] Yucel S, Dravis C, Garcia N, Henkemeyer M and Baker LA. Hypospadias and anorectal malformations mediated by Eph/ephrin signaling. J Pediatr Urol 2007; 3: 354-363.
[26] van Leeuwen K, Baker L and Grimsby G. Autologous buccal mucosa graft for primary and secondary reconstruction of vaginal anomalies. Semin Pediatr Surg 2019; 28: 150843.
[27] Wong DG, Arevalo MK, Passoni NM, Iqbal NS, Jascur T, Kern AJ, Sanchez EJ, Satyanarayan A, Gattineni J and Baker LA. Phenotypic severity scoring system and categorisation for prune belly syndrome: application to a pilot cohort of 50 living patients. BJU Int 2019; 123: 130-139.
[28] Iqbal NS, Jascur TA, Harrison SM, Edwards AB, Smith LT, Choi ES, Arevalo MK, Chen C, Zhang S, Kern AJ, Scheuerle AE, Sanchez EJ, Xing C and Baker LA. Prune belly syndrome in surviving males can be caused by Hemizygous missense mutations in the X-linked Filamin A gene. BMC Med Genet 2020; 21: 38.
[29] Wiese CB, Deal KK, Ireland SJ, Cantrell VA and Southard-Smith EM. Migration pathways of sacral neural crest during development of lower urogenital tract innervation. Dev Biol 2017; 429: 356-369.
[30] Girard BM, Campbell SE, Perkins M, Hsiang H, Tooke K, Drescher C, Hennig GW, Heppner TJ, Nelson MT and Vizzard MA. TRPV4 blockade reduces voiding frequency, ATP release, and pelvic sensitivity in mice with chronic urothelial overexpression of NGF. Am J Physiol Renal Physiol 2019; 317: F1695-F1706.
[31] Vuong L, Kotecha RR, Voss MH and Hakimi AA. Tumor microenvironment dynamics in clear-cell renal cell carcinoma. Cancer Discov 2019; 9: 1349-1357.
[32] Jinnah AH, Zacks BC, Gwam CU and Kerr BA. Emerging and established models of bone metastasis. Cancers (Basel) 2018; 10: 176.
[33] Basher F, Dhar P, Wang X, Wainwright DA, Zhang B, Sosman J, Ji Z and Wu JD. Antibody targeting tumor-derived soluble NKG2D ligand sMIC reprograms NK cell homeostatic survival and function and enhances melanoma response to PDL1 blockade therapy. J Hematol Oncol 2020; 13: 74.
[34] Zhang J, Liu D, Li G, Staveley-O'Carroll KF, Graff JN, Li Z and Wu JD. Antibody-mediated neutralization of soluble MIC significantly enhances CTLA4 blockade therapy. Sci Adv 2017; 3: e1602133.
[35] Zarif JC, Baena-Del Valle JA, Hicks JL, Heaphy CM, Vidal I, Luo J, Lotan TL, Hooper JE, Isaacs WB, Pienta KJ and De Marzo AM. Mannose receptor-positive macrophage infiltration correlates with prostate cancer onset and metastatic castration-resistant disease. Eur Urol Oncol 2019; 2: 429-436.
[36] White MA, Tsouko E, Lin C, Rajapakshe K, Spencer JM, Wilkenfeld SR, Vakili SS, Pulliam TL, Awad D, Nikolos F, Katreddy RR, Kaipparettu BA, Sreekumar A, Zhang X, Cheung E, Coarfa C and Frigo DE. GLUT12 promotes prostate cancer cell growth and is regulated by androgens and CaMKK2 signaling. Endocr Relat Cancer 2018; 25: 453-469.
[37] McAuley E, Moline D, VanOpstall C, Lamperis S, Brown R and Vander Griend DJ. Sox2 expression marks castration-resistant progenitor cells in the adult murine prostate. Stem Cells 2019; 37: 690-700.
[38] Hsu EC, Rice MA, Bermudez A, Marques FJG, Aslan M, Liu S, Ghoochani A, Zhang CA, Chen YS, Zlitni A, Kumar S, Nolley R, Habte F, Shen M, Koul K, Peehl DM, Zoubeidi A, Gambhir SS, Kunder CA, Pitteri SJ, Brooks JD and Stoyanova T. Trop2 is a driver of metastatic prostate cancer with neuroendocrine phenotype via PARP1. Proc Natl Acad Sci U S A 2020; 117: 2032-2042.
[39] Costanzo-Garvey DL, Keeley T, Case AJ, Watson GF, Alsamraae M, Yu Y, Su K, Heim CE, Kielian T, Morrissey C, Frieling JS and Cook LM. Neutrophils are mediators of metastatic prostate cancer progression in bone. Cancer Immunol Immunother 2020; 69: 1113-1130.
[40] Eichler T, Bender K, Murtha MJ, Schwartz L, Metheny J, Solden L, Jaggers RM, Bailey MT, Gupta S, Mosquera C, Ching C, La Perle K, Li B, Becknell B and Spencer JD. Ribonuclease 7 shields the kidney and bladder from invasive uropathogenic escherichia coli infection. J Am Soc Nephrol 2019; 30: 1385-1397.
[41] Zhao N, Peacock SO, Lo CH, Heidman LM, Rice MA, Fahrenholtz CD, Greene AM, Magani F, Copello VA, Martinez MJ, Zhang Y, Daaka Y, Lynch CC and Burnstein KL. Arginine vasopressin receptor 1a is a therapeutic target for castration-resistant prostate cancer. Sci Transl Med 2019; 11: eaaw4636.

[42] Ta HQ, Whitworth H, Yin Y, Conaway M, Frierson HF Jr, Campbell MJ, Raj GV and Gioeli D. Discovery of a novel long noncoding RNA overlapping the LCK gene that regulates prostate cancer cell growth. Mol Cancer 2019; 18: 113.

[43] Rodriguez-Bravo V, Pippa R, Song WM, Carceles-Cordon M, Dominguez-Andres A, Fujiwara N, Woo J, Koh AP, Ertel A, Lokareddy RK, Cuesta-Dominguez A, Kim RS, Rodriguez-Fernandez I, Li P, Gordon R, Hirschfield H, Prats JM, Reddy EP, Fatatis A, Petrylak DP, Gomella L, Kelly WK, Lowe SW, Knudsen KE, Galsky MD, Cingolani G, Lujambio A, Hoshida Y and Domingo-Domenech J. Nuclear pores promote lethal prostate cancer by increasing POM121-driven E2F1, MYC, and AR nuclear import. Cell 2018; 174: 1200-1215, e1220.

[44] Becker REN, Kates MR and Bivalacqua TJ. Identification of candidates for salvage therapy: the past, present, and future of defining bacillus calmette-guerin failure. Urol Clin North Am 2020; 47: 15-21.

Deciphering the role of *PRAC1* in castration resistant prostate cancer

Jin-Yih Low[1], David M. Esopi[2], Yiting Lim[1], Ajay M. Vaghasia[1], Harrison Tsai[2], Qizhi Zheng[2], Jessica Hicks[2], Nicolas Wyhs[2], Nicole Castagna[2], Tamara L. Lotan[2,3], William B. Isaacs[2,4], Angelo M. De Marzo[2,3,4], William G. Nelson[2,3,4], Andrew C. Hsieh[1], Srinivasan Yegnasubramanian[2] and Michael C. Haffner[1,3]

Affiliations: [1]Division of Human Biology, Fred Hutchinson Cancer Research Center, Seattle, Washington, [2]Sidney Kimmel Comprehensive Cancer Center, Johns Hopkins School of Medicine, Baltimore, Maryland, [3]Department of Pathology, Johns Hopkins School of Medicine, Baltimore, Maryland, [4]Brady Urological Institute, Johns Hopkins School of Medicine, Baltimore, Maryland.

Introduction and objective
Resistance to androgen receptor (AR) targeting therapies is one of the key drivers of prostate cancer mortality. Although several molecular alterations involved in castration resistant prostate cancer (CRPC) have been catalogued, a deep mechanistic understanding of the diverse resistance pathways operative in CRPC is still lacking. Here, we investigate DNA methylation changes as potential drivers of castration resistance.

Methods
We aimed to specifically investigate CpG methylation changes that are associated with the acquisition of castration resistance. To this end, we applied a reductionist approach by performing whole genome methylation analyses using MBD-seq on paired androgen dependent and castration resistant cell lines to identify candidate gene loci with differential methylation in CRPC. Results from this screen were validated in metastatic CRPC (mCRPC) samples from rapid autopsy cohorts. *In vitro* and *in vivo* loss and gain of function experiments were used to delineate phenotypic and transcriptomic alterations.

Results
We identified *PRAC1* as a differentially expressed and hypermethylated gene locus in castration resistant models. In clinical mCRPC samples, *PRAC1* hypermethylation was found in 42% of cases, but not in primary hormone naïve tumors, suggesting that epigenetic silencing of *PRAC1* is induced by and/or selected for by AR targeted therapies. *PRAC1* knock down or knock out resulted in a conversion to castration resistance of multiple cell lines *in vitro* and *in vivo*. Conversely, overexpression of the protein coding open reading frame of *PRAC1* inhibited growth of CRPC models in the absence of androgens. Mechanistically, depletion of *PRAC1* resulted in widespread transcriptional changes affecting in particular androgen regulated genes and genes involved in cell cycle progression.

Conclusion
Our data suggests that *PRAC1* is epigenetically silenced and may regulate AR signaling in CRPC. We are committed to further investigate the impact of *PRAC1* alterations in mCRPC and delineate the role of *PRAC1* in physiological androgen receptor signaling and resistance to AR directed therapies.

Funding: DoD, Safeway foundation.
Keywords: PRAC1, castration resistant prostate cancer, epigenetics, methylation

Background: Neuroendocrine prostate cancer (NEPC) is an aggressive variant of prostate cancer that either develops de novo or arises from prostate adenocarcinoma as a result of treatment resistance. Although the prostate basal cells have been shown to directly generate tumor cells with neuroendocrine features when transduced with oncogenic signaling, the identity of the cell-of-origin for de novo NEPC remains unclear.

Methods: The sorted TACSTD2high and TACSTD2low luminal cells from human benign prostate tissues are infected with caAKT and c-Myc-expressing lentiviruses and cultured under organoid assay. Established tumor organoids are analyzed by qRT-PCR and immunostaining of lineage markers.

Results: We show that the TACSTD2high human prostate luminal epithelia cells highly express SOX2 and are relatively enriched in the transition zone prostate. Both TACSTD2high and TACSTD2low luminal cells transduced by activated AKT and c-Myc can form organoids containing versatile clinically relevant tumor cell lineages with regard to the expression of androgen receptor and the neuroendocrine cell markers Synaptophysin and Chromogranin A. Tumor organoid cells derived from the TACSTD2high luminal cells are more predisposed to neuroendocrine differentiation along passaging and are relatively more castration resistant. Knocking down TACSTD2 and SOX2 both attenuate neuroendocrine differentiation of tumor organoid cells.

Conclusions: This study demonstrates de novo neuroendocrine differentiation of the human prostate luminal epithelial cells induced by caAKT and c-Myc and reveals an impact of cellular status on initiation of lineage plasticity.

Smartphone Thermal Imaging in the Detection of Testicular Ischemia

Background: In the setting of testicular torsion, the duration of symptoms prior to operative detorsion is the most important variable which determines risk of necrosis and testicular loss. A quick point-of-care test for testicular ischemia would be useful to confirm the diagnosis and proceed more quickly with operative treatment. Thermal Imaging detects the infrared (heat) pattern of an object and the technology is now available as an inexpensive ($400) attachment to smartphones.

Methods: Smartphone Thermal Imaging was studied as a point-of-care diagnostic test for testicular ischemia in an IACUC approved study that prioritized survival of all animal subjects. Thirty canines weighing over 12 kg (range 13.6 – 37.2 kg, avg 23.9 kg) were observed during elective neuter procedures with consent from owners. Randomization determined ligation of the right vs left spermatic cord. With both testicles remaining in the scrotum, blinded inspection was performed with a FLIR ONE Pro Thermal Imaging camera for smartphone use. Inspection halted when ischemia was diagnosed by comparison of the two testicular thermal images. Temperature measurements of the testicles were taken with the same device. The bilateral orchiectomy procedures were then completed as planned and subjects were discharged home after postoperative recovery.

Results: Within 11 minutes of ligation of the randomized spermatic cord, an obvious change in the thermal imaging pattern allowed for the correct diagnosis of the ischemic testicle in 30 of the 30 subjects in a blinded fashion. The average observation time was 7.3 minutes. The ischemic testicle always had the lower measured temperature. Temperature differences between testicles at the time of ischemia diagnosis ranged from 0.7° to 3.7° C with an average difference of 1.79° C [95% CI: (1.50, 2.08)]. A Thermal Imaging evaluation of the testicles takes 30 seconds to perform.

Conclusion: Within 11 minutes after ligation of the blood supply, blinded inspection of Smartphone Thermal Images allowed the correct diagnosis of testicular ischemia in 100% of subjects. Prospective evaluation of this emerging point-of-care technology in the clinical diagnosis of testicular ischemia is suggested.

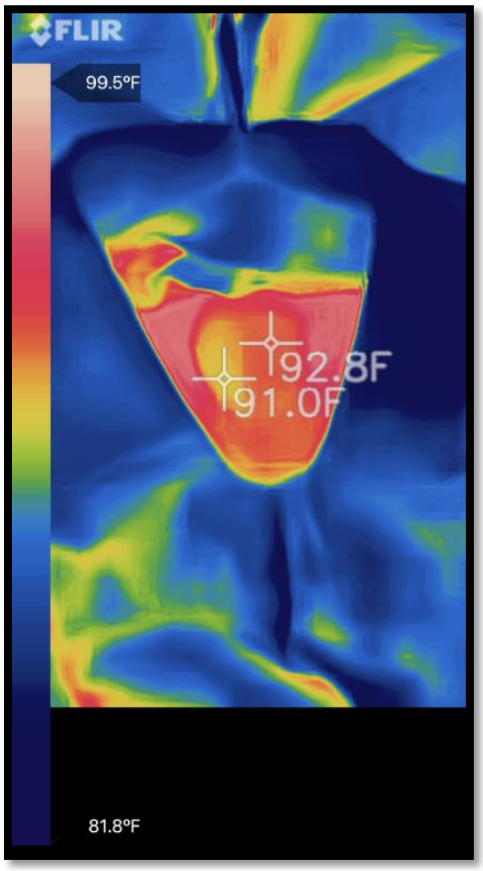

Smartphone thermal image obtained by FLIR ONE Pro Thermal Camera.
Right testicular ischemia is confirmed (in yellow).

Hormonal control and therapeutic targeting of TMPRSS2 and ACE2 as a potential strategy to combat COVID-19

Background: The novel SARS-CoV-2 infection responsible for the COVID-19 pandemic is expected to have an adverse effect on the progression of multiple cancers, including prostate cancer, due to the ensuing cytokine storm associated oncogenic signaling. A better understanding of the host cell factors and their regulators will help identify potential therapies to block SARS-CoV-2 infection at an early stage and thereby prevent cancer progression. Host cell infection by SARS-CoV-2 requires the binding of the viral Spike S protein to ACE2 receptor and priming by the serine protease TMPRSS2 – encoded by a well-known androgen response gene and highly expressed in hormone-sensitive and castration-resistant prostate cancer. Epidemiological data showing increased severity and mortality of SARS-CoV-2 disease in men suggest a possible role for androgen in the transcriptional activation of ACE2 and TMPRSS2 in the lungs and other primary infection sites.

Methods: Experimental methods used are physical castration of mice, immunohistochemistry for AR, TMPRSS2 and ACE2 in multiple organs, qRT-PCR, ChIP-seq, immunoblotting, Co-IP, SARS-CoV-2 pseudovirus spinoculation, and viral entry reporter assays in prostate and lung cells.

Results: We present evidence for the transcriptional regulation of SARS-CoV-2 host cell receptor ACE2 and co-receptor TMPRSS2 by androgen in mouse organs (lungs and small intestine), and human prostate and lung cells. Additionally, we provide the first evidence for the endogenous interaction between TMPRSS2 and ACE2 in human cells. In an overexpression system as well as endogenous TMPRSS2 expression cells, camostat – a serine-protease inhibitor specific to TMPRSS2 - inhibited the cleavage of pseudotype SARS-CoV-2 surface Spike S protein without disrupting TMPRSS2-ACE2 interaction. Thus demonstrating a direct role of TMPRSS2 in priming the viral Spike S protein, a prerequisite for an active infection. Importantly, androgen deprivation, anti-androgens (enzalutamide/AR-PROTAC), or camostat attenuated the SARS-CoV-2 pseudovirus infection in lung and prostate cells.

Conclusions: Our preclinical data provide a strong rationale for clinical evaluation of TMRPSS2 inhibitors, androgen-deprivation therapy such as GnRH antagonist, and AR-signaling blockers alone or in combination with antiviral drugs as early as clinically possible. This will likely prevent progression to pneumonia, and multi-organ failure because of hyper-inflammatory responses in COVID-19 patients with or without cancer.

Reduced HOXB13 expression in neuroendocrine prostate cancer represents a loss of prostate identity

Siyuan Cheng1, Shu Yang[1], Yingli Shi[1], Runhua Shi[2], Yunshin Yeh[3,4], Xiuping Yu[1,4]

1. Department of Biochemistry & Molecular Biology, LSU Health-Shreveport, Shreveport, LA, USA
2. Department of Medicine, LSU Health-Shreveport, Shreveport, LA, USA
3. Pathology & Laboratory Medicine Service, Overton Brooks VA Medical Center, Shreveport, LA, USA
4. Department of Urology, LSU Health-Shreveport, Shreveport, LA, USA

Background: About 30% patients acquire the neuroendocrine (NE) phenotype after androgen deprivation therapy fails. Evidences support that neuroendocrine prostate cancer (NEPCa) arise from prostate adenocarcinoma (AdPCa) through trans-differentiation. HOXB13, a homeobox gene, is primarily expressed in prostate. Previous research suggests that the different HOX genes expression pattern represents the anatomic origins of cells.

Methods: Using publicly available RNASeq data, we analyzed the expression of HOX genes in 1019 human cancer cell lines that reflect 24 anatomic origins. Additionally, immunohistochemistry (IHC), Western blot and RT-qPCR were used to assess the expression of HOXB13. Dual immunofluorescence staining was used to visualize the expression of HOXB13 in prostate glands. In silico analysis based on R was used to perform data mining.

Results: We established HOX codes for 24 anatomic origins using the transcriptomic data of 1019 human cancer cell lines. We found that NEPCa cell line H660 has a distinct expression pattern of HOX genes, different from prostatic HOX code. Additionally, analysis of RNASeq data of human NEPCa samples indicated that AdPCa tumors maintained prostatic HOX code but majority NEPCa tumors lost prostate HOX code. However, the NEPCa samples did not show consistent correlation with the HOX codes of any tissues. This suggests that NEPCa tumors have lost prostate identity but have yet gained a clear-cut new tissue identity. Further, we found that HOXB13 was expressed in prostatic luminal epithelial cells. The expression of HOXB13 was elevated along with AdPCa progression but was decreased in NEPCa. Furthermore, we found the all-trans retinoic acid induced the expression of HOXB13, AR and AR targeting genes in NEPCa cells.

Conclusion: 1) HOXB13 expression is reduced or lost in NEPCa. 2) A loss of prostate-specific HOX code in NEPCa represents a loss of prostatic identity. 3) the lost expression of HOXB13 in NEPCa is reversible. **Significance:** 1) The HOX codes we established can be used in pan cancer research to identify the tissue of origin and to study the trans-differentiation of cancer cells. 2) We propose all-trans retinoic acid can be used to revert NE differentiation in human patients.

This research was supported by NIH R01 CA226285

Title: *SRD5A2* Promoter Methylation is associated with Estrogen Receptor β in BPH

Background: Steroid 5α-reductase type II (SRD5A2) is the predominant enzyme responsible for prostatic development and growth. We found that expression of SRD5A2 in the prostate is variable, and that one-third of prostate tissue samples from BPH patients do not express SRD5A2. We demonstrated that the absence of SRD5A2 expression is associated with *SRD5A2* methylation in the promoter region. We also demonstrated that there is an "androgenic to estrogenic switch" when SRD5A2 is absent in the prostate gland. Here we wished to identify if *SRD5A2* methylation in the promoter region effects on the expression of estrogen receptors (ERs). **Methods:** We used human prostatic stromal and epithelium cells, and prostate specimens collected from patients who underwent transurethral resection of the prostate (TURP). The expression of ERα and ERβ was determined by immunohistochemistry and semi-quantified with immunoreactive scores. Genome DNA was extracted and *SRD5A2* promoter methylation was determined with DNA methylation-specific PCR. The level of *SRD5A2* promoter methylation was correlated to ER expression. **Results:** Both of ERα and ERβ were expressed in prostatic stroma and epithelia compartments. In cultured prostatic stromal and epithelium cells, ERα was expressed in both cytoplasm and nuclei, and ERβ was only expressed in the nuclei. Six out of twenty patients had *SRD5A2* hypermethylation at the promoter region, which was associated with the expression of ERβ in the epithelia compartment ($p=0.023$). **Conclusions:** ERα and ERβ co-localize in human benign prostatic tissue. Specifically, ERβ is expressed in the nuclei of both the prostatic stromal and epithelium cells. *SRD5A2* promoter methylation is associated with the expression of ERβ. Targeting the estrogenic signaling may serve as an effective treatment strategy in subset of *SRD5A2* hypermethylation and ER-sensitive BPH patients.

The microphthalmia transcription factor (MITF) contributes to castration resistance via an actionable translation mechanism in lethal prostate cancer

Santasusagna S 1, Pippa R 1, Zhu S 2, Ertel A 1, Kelly WK 1, Knudsen KE 1, Hoshida Y 2, Rodriguez-Bravo V 1, Domingo-Domenech J 1

1 Sidney Kimmel Cancer Center, Thomas Jefferson University, Philadelphia, PA 19107, USA

2 Simmons Comprehensive Cancer Center, University of Texas Southwestern Medical Center, Dallas, TX 75390, USA

Deciphering transcription factor-dependent signaling networks and molecular mechanisms that rewire the cancer cell may provide actionable therapeutic targets to improve patient survival. Here, we show that the master regulator microphthalmia transcription factor (MITF) is downregulated in advanced lethal prostate cancer (PC) patient samples and has a major role in regulating a subset of biologically relevant signaling pathways that control PC growth and confer resistance to androgen deprivation therapy (ADT).

Mechanistically, MITF directly represses protein synthesis by regulating the assembly of the translation initiation complex, which impacts on the protein levels and activity of key PC drivers, such as MYC and AR. Since AR overexpression is a frequent adaptive trait that confers resistance to ADT, we investigated if low MITF levels contribute to castration resistance. Indeed, knockdown of MITF in the hormone therapy sensitive cell lines, LNCaP and VCaP, allowed PC cells to proliferate when cultured in charcoal-stripped serum medium. Likewise, the proliferation of MITF knockdown cells was higher than control cells in presence of 1nmol/L dihydrotestosterone (DHT) than when cultured with 10nmol/L DHT. Most notably, in vivo, subcutaneous tumors generated from shMITF LNCaP and VCaP luciferase tagged cells continued to grow in castrate mice as measured by photon flux and tumor volume. Altogether, these results indicate that low MITF cells continue to proliferate under ADT, suggesting that the MITF signaling axis contributes to the acquisition of castration resistance. Finally, based on the regulatory function of MITF on translation initiation, we unveil that the pharmacologic inhibition of protein synthesis decreases tumor growth, sensitizes PC tumors to ADT and improves survival most robustly in low MITF expressing patient-derived preclinical models.

Overall, this study sheds insight into the role MITF has in the pathogenesis of lethal PC and identifies an actionable mechanism that may transcend into effective combined therapeutic strategies.

Effective combinatorial immunotherapy for penile cancer demonstrated in the first GEM model of penile squamous cell carcinoma

Background: Penile cancer is a rare but highly morbid disease, with penile squamous cell carcinoma (PSCC) accounting for over 95% of all cases. Compared with other urological malignancies, PSCC is among the least understood with very limited treatment options.

Methods: We developed of the first genetically engineered mouse model (GEM) of PSCC by co-deletion of *Smad4* and *Apc* in penile epithelia. Transcriptomics of the penile tumor and normal penile epithelium was profiled by RNA-seq for mechanistic investigation and comparison to human penile cancer transcriptomics. Immunophenotyping of the model was performed by CyTOF. Targeted proteomics by RPPA on the model informed inhibitor screening for finding novel drugs against PSCC. Targeted therapeutics and immune checkpoint blockade antibodies (PD1, CTLA4) were combined as key preclinical evidence of new treatment strategy.

Results: The GEM model is highly relevant to the human disease by virtue of sharing up- and down-regulated genes and pathways. Both cancer cell-intrinsic (β-catenin and SOX2 transcription activation) and extrinsic (COX2-dependent inflammatory microenvironment) mechanisms drive the progression of PSCC. Mouse PSCC fosters an immunosuppressive microenvironment with myeloid-derived suppressor cells (MDSCs) as the dominant population. Preclinical trials in the model demonstrate synergistic efficacy of immune checkpoint blockade with the MDSC-debilitating drugs cabozantinib or celecoxib. Drug screen studies informed by targeted proteomics identified potential drugs (e.g. mubritinib).

Conclusion: Our studies have established the essential resources for studying PSCC biology and therapy (Figure 1). The combinatorial immunotherapy approach illuminates a promising clinical path for treating aggressive PSCC.

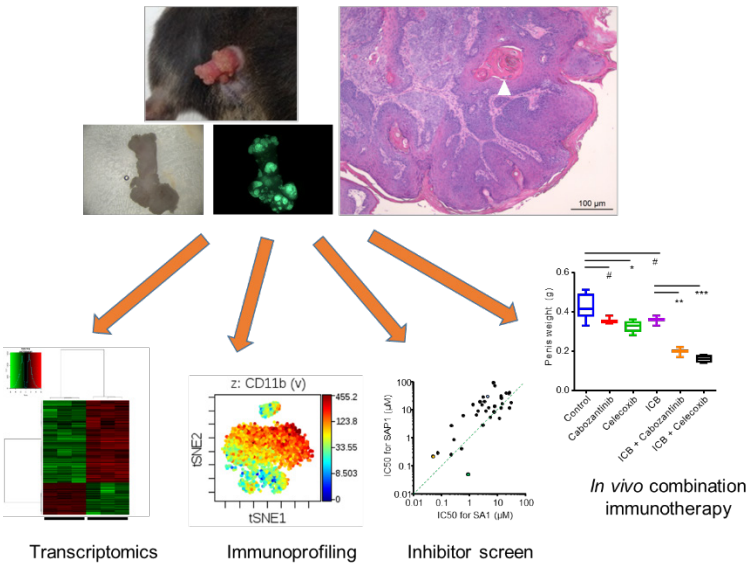

Figure 1. First genetically engineered mouse model of penile cancer and its application in preclinical studies

ADT/ANTI-AR THERAPY RESULTS IN GAPDH UPREGULATION IN PROSTATE CANCER

Wang Liu, **Ting Li**, Haixia Xu, Changlin Li, Jeffrey Holzbeierlein and Benyi Li

Departments of Urology, The University of Kansas Medical Center, Kansas City, KS 66160

Introduction

As the widespread use of potent anti-AR drugs in castration-resistant prostate cancer patients, neuroendocrine progression (t-NEPC or CRPC-NE) has emerged as a major clinical obstacle, accounting for more than 25-30% mortality of prostate cancers. Recent studies with patient-derived xenografts (PDX) revealed that t-NEPC model LTL-331R exerted a highly upregulated glycolytic activity, indicating a metabolic reprogramming in t-NEPC progression. Currently, targeting the altered glycolysis pathway in cancer cells has emerged as a potent cancer therapy. Especially, inhibition of glyceraldehyde-3-phosphate dehydrogenase (GAPDH), a critical glycolytic enzyme, achieved a profound anti-cancer outcome specifically in highly glycolytic cancers. Therefore, we investigated the role of GAPDH alteration in t-NEPC/CRPC-NE models and identified a novel GAPDH inhibitor Alternol as a potential therapy for NEPC patients.

Methods

GAPDH gene expression profiles in prostate cancers were analyzed using the published NCBI GDS datasets. GAPDH promoter-driven luciferase reporter assay and glucose consumption assay was conducted in LNCaP cells after Enzalutamide treatment. GAPDH protein expression was evaluated in tissue microarray sections, NEPC PDX tissue and xenograft tissues by immunohistochemistry. The novel small compound Alternol isolated from fungi fermentation was used in multiple prostate cancer cell lines for GAPDH activity assay. Cellular thermal shift assay (CETSA) was used to verify the interaction of Alternol with GAPDH protein in cells.

Results

Data mining for GAPDH expression showed that it is slightly higher in primary (1.7-2.18 folds) and significantly higher in metastatic prostate cancers (>5-folds) compared to normal or benign adjacent tissues (Fig 1). In addition, castration in mice caused a significant increase of GAPDH expression in prostate gland or subcutaneous xenograft tissues of prostate cancer (Fig 2). Consistently, GAPDH-LUC reporter activity was increased about 2-fold after androgen depravation, which was further enhanced (> 9-fold) by Enzalutamide in LNCaP cells. Interestingly, Enzalutamide also enhanced glucose consumption rate under androgen depravation condition (Fig 3). Molecular docking study confirmed our previous report that Alternol interacts with GAPDH at the catalytic active/NAD+ binding sites with a binding affinity at -10.1 kcal/mol (Fig 4A). This interaction was validated in CETSA assay in C4-2 and 22RV1 cells (Fig 4B & 4C). The functional consequence of Alternol-GAPDH interaction was evaluated using in vitro and in vivo GAPDH assays (Fig 5).

Conclusion

Androgen depravation plus anti-AR therapy resulted in GAPDH up-regulation in prostate cancer cells and tissues, suggesting a strong clinical relevance of GAPDH up-regulation in anti-AR treatment-induced NE progression of CRPC patients. Alternol interacts with GAPDH and potently suppressed GAPDH glycolytic activity *in vitro* (IC_{50} = 5.794 nM), which is 37.5-fold more potent than an existing GAPDH inhibitor Korningic Acid (IC_{50} = 217.6 nM). Alternol also lowered down the excessive GAPDH glycolytic activity in prostate cancer cells to the level close to benign cells without a total blockage, indicating a safe therapeutic feature.

Funding

DoD PCRP190026

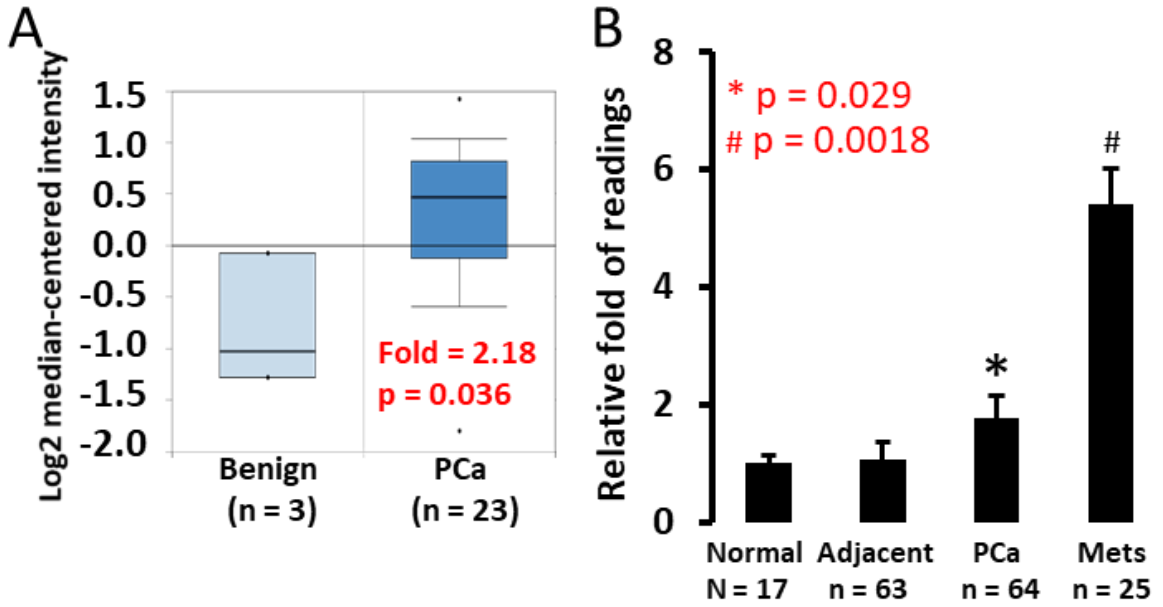

Fig 1. GAPDH expression in prostate cancers. Data mining for GAPDH expression was conducted using datasets from human prostate specimens (A, GSE6888236 and (B, GDS254537).

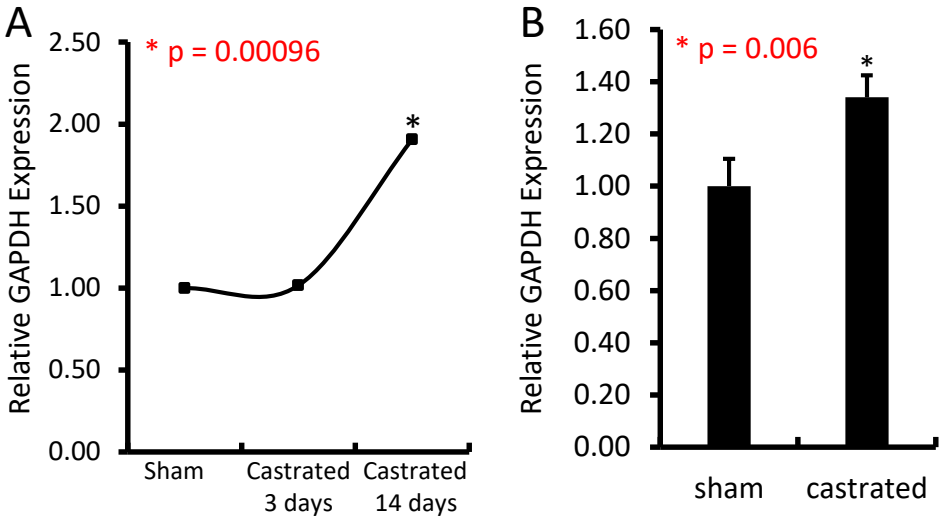

Fig 2. GAPDH expression after castration. Data mining for GAPDH expression was conducted using datasets from (A) mouse prostate tissue after 3-14 days of castration (GDS2562) and (B) LuCaP35 s.c. xenografts in SCID mice after 4-weeks castration (GDS4120). Epithelium-specific gene KRT18 was used for data normalization.

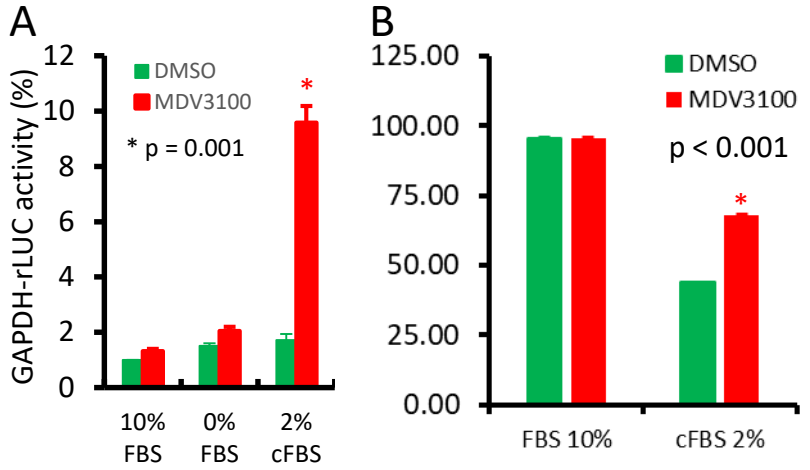

Fig 3. Enzalutamide enhances GAPDH expression and activity. **A** LNCaP cells transfected with GAPDH-rLUC constructs (Addgene#82479) were treated with DMSO or MDV3100 (Enzalutamide, 10 μM) for 24 h. Reporter activities were normalized with protein concentrations in corresponding samples. **B** Glucose levels in cell culture media were measured with a pre-assembled kit from Signa (catalog #GAGO20) in LNCaP cells after 24-h treatment as indicated.

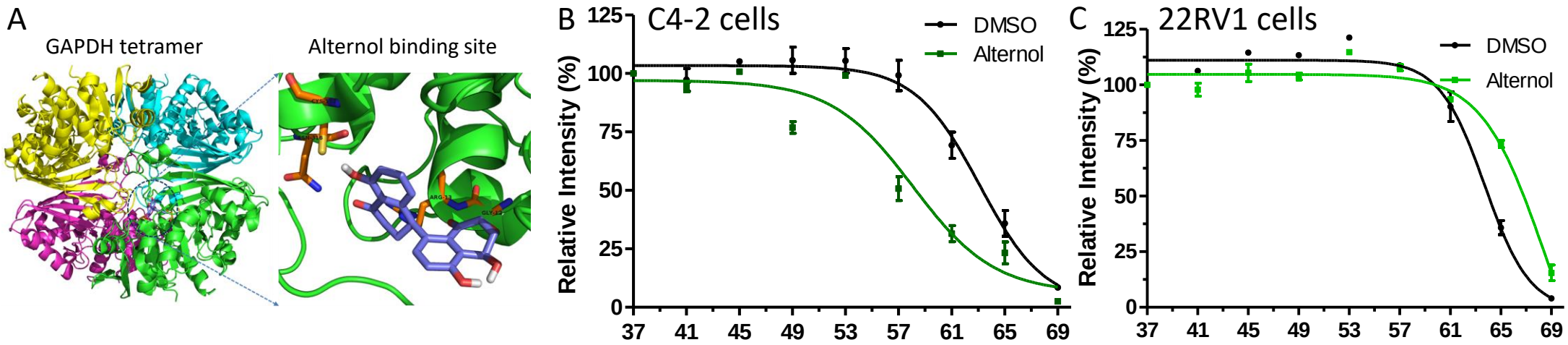

Fig 4. Alternol interacts with GAPDH. **A** in silicon docking analysis was conducted using crystal structure for human liver GAPDH protein derived from Research Collaboratory for Structural Bioinformatics Protein Data Bank (1ZNQ). **B&C** C4-2 and 22RV1 cells were treated with Alternol (10 μM) for 4 h, followed by CETSA assays.

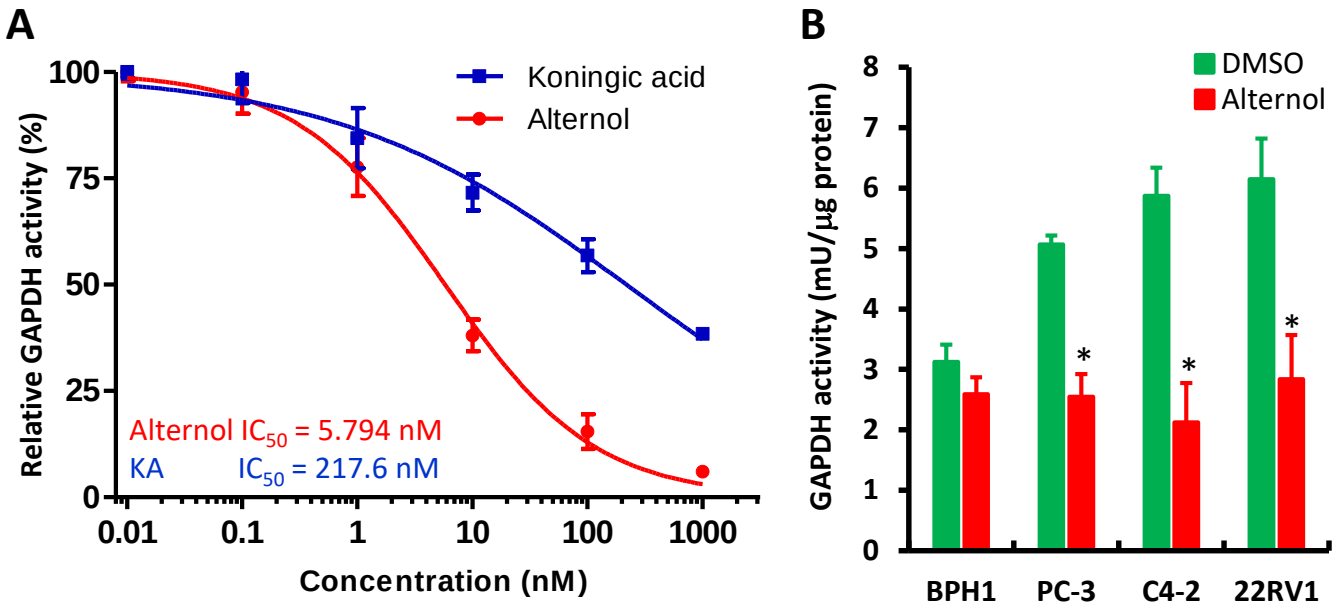

Fig 5. Alternol suppresses GAPDH activity. **A** GAPDH in vitro activity assay. **B** Cells were treated with DMSO or Alternol (10 μM) for 4 h and cellular proteins were extracted for GAPDH activity assay using the BioVision kit. The asterisk indicates a significant difference compared to DMSO ($p < 0.05$, Student t-test).

Spatial Heterogeneity of Tumor Associated Macrophages in the Tumor Immune Microenvironment in ccRCC

Background

Tumor associated macrophages (TAM) stimulate tumor proliferation and facilitate immune escape via production of immunosuppressive cytokines. We hypothesize that non-random spatial clustering of TAMs within the tumor are associated with poor survival in ccRCC patients.

Methods

Tumor specimens were obtained from 41 patients with metastatic ccRCC who received immunotherapy (IT). Sections from the tumor core underwent multiplex immunofluorescence staining for CD68, CD163, and CD206. Digital pathologic analysis was used to convert the digital images to spatial point pattern plots (PPP). Ripley's K function, the current standard metric for spatial heterogeneity, was utilized. Novel metrics were developed using a probability density function (PDF) for distances between cells, assuming that cells can be located anywhere with equal probability. Empirical histograms were generated from the PPPs. Deviation from the PDF demonstrates a non-random distribution. Deviations were quantified with the Kolmogorov-Smirnov (KS) test and Cramér-von Mises (CVM) criterion. Overall survival (OS) was assessed between groups stratified by the median value for each metric using Kaplan-Meier and log-rank analysis. Figure 1A.

Results

75 slides were analyzed from the 41 patients. The three metrics for measuring spatial heterogeneity had moderate and statistically significant correlation with each other (Spearman's R: Ripley/KS=0.68, $p<0.01$; Ripley/CVM=0.54, $p<0.01$; KS/CVM=0.47, $p<0.01$; Figure 1B). Using CVM, increasingly non-random distribution of the Tumor-CD68+ cell relationship was associated with worse OS ($p<0.01$, Figure 1C), and increasingly non-random distribution of CD163+ cells suggested an association with worse OS without reaching statistical significance ($p=0.06$, Figure 1C). No statistically significant associations were identified using the KS or Ripley's K metrics.

Conclusion

We describe CVM and KS as novel metrics for measuring spatial heterogeneity of immune cells. Increased spatial heterogeneity of CD68+ TAMs and tumor cells was associated with worse OS in patients with metastatic ccRCC who received IT. These findings corroborate prior reports of TAMs eliciting an immunosuppressive effect on the tumor-immune microenvironment, and demonstrate the novel finding of a clinically significant effect of TAM spatial clustering on OS.

Figure 1. A: Diagram illustrating the workflow for the described methodology. B: Spearman's correlation for the three metrics for spatial heterogeneity utilized in the analysis (1: Ripley's K and KS; 2: Ripley's K and CVM; 3: KS and CVM). C: Kaplan-Meier analysis for OS, log-rank p values reported (1: Tumor/CD68+ CVM; 2: CD163+ CVM).

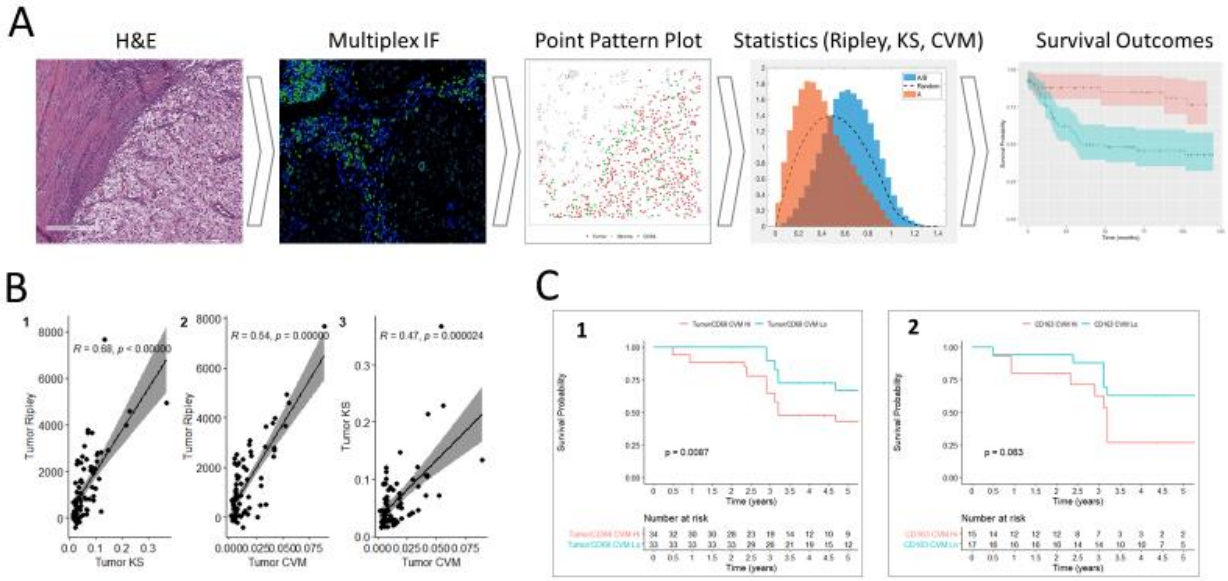

Splice-site Variants as Promising Novel Biomarkers in Clear Cell Renal Cell Carcinoma

Background
Splice-site variants (SV) are DNA mutations that ultimately result in abnormal mRNA splicing and a dramatically altered protein-coding sequence. SVs in clear cell renal cell carcinoma (ccRCC) have been largely unexplored. Our primary objective was to identify the most prevalent SVs in ccRCC, determine their prevalence in other malignancies, and analyze associations with clinical outcomes.

Methods
Specific SVs were identified in RCC cell lines from the Broad Institute Cancer Cell Line Encyclopedia (CCLE). Patients with a diagnosis of ccRCC were then identified in the Moffitt Cancer Center Total Cancer Care (TCC) cohort and RNA-seq data was utilized in a bioinformatics pipeline to identify the SVs among the TCC cohort. SVs identified in the TCC ccRCC cohort were then identified in TCC patients with non-ccRCC malignancies. The 10 most prevalent SVs in ccRCC were selected for analysis, using a minimum SV read count threshold of 10. SV read count and SV dominance (specific SV read count / total SV read count) were assessed as metrics. Kaplan-Meier analysis and log-rank testing were utilized to assess differences in overall survival (OS) and recurrence free survival (RFS) between groups, stratified by the top quartile.

Results
We identified 4,278 tumor samples in TCC with available RNA-seq. 104 were ccRCC. Ten distinct SVs were found to have high ccRCC prevalence and low prevalence in non-ccRCC malignancies. Figure 1A. The OXR1, GAL3ST1-alpha, and GAL3ST1-beta SVs had the highest prevalence in ccRCC, as well as the highest read count per patient. Figure 1B. Low read counts of GAL3ST1-alpha, GAL3ST1-beta, and ASTN2, and high read counts of TMEM44 were associated with stage cM1. Figure 1C. None of the survival analyses demonstrated a statistically significant difference in OS. 81 patients had non-metastatic disease at diagnosis and were therefore eligible for RFS analysis. Patients with high OXR1-SV dominance had improved RFS ($p=0.05$). Figure 1D.

Conclusions
We identified SVs that are highly prevalent in ccRCC tumors and minimally prevalent in other malignancies. Particularly striking were the OXR1, GAL3ST1-alpha, and GAL3ST1-beta SVs. The total read count of several SVs was associated with clinical M stage. Increasing dominance of the OXR1 SV was associated with improved RFS. These SVs warrant further investigation as potential biomarkers in ccRCC.

Figure 1. A: The 10 most frequently identified SVs in ccRCC, ordered by prevalence in ccRCC. B: Heatmap plot for SV read count in ccRCC for the included SVs. C: Box-plot diagrams for M stage by SV read count for each included SV, asterix in the plot title denotes Wilcoxon rank-sum $p < 0.05$. D: Kaplan-Meier analysis for RFS, groups stratified by top quartile for OXR1 dominance and quartiles 1-3, log-rank p reported.

A

Gene	SV Location	ccRCC (n=104)	Non-ccRCC (n=4,174)
OXR1	8:107593479-107691437	104 (100%)	289 (6.9%)
GAL3ST1	22:30953388-30956727	101 (97.1%)	67 (1.6%)
GAL3ST1	22:30953388-30960811	96 (92.3%)	59 (1.4%)
PDZD2	5:31995744-32000244	77 (74.0%)	321 (7.7%)
TMEM44	3:194309368-194313769	75 (72.1%)	1106 (26.5%)
MVK	12:110032708-110032832	73 (70.2%)	39 (0.9%)
RNASET2	6:167369679-167370715	67 (64.4%)	911 (21.8%)
ASTN2	9:119739064-119741597	61 (58.7%)	42 (1.0%)
MVK	12:110032624-110032832	53 (50.1%)	25 (0.6%)
EGFR	7:55259222-55259411	51 (49.0%)	107 (2.6%)

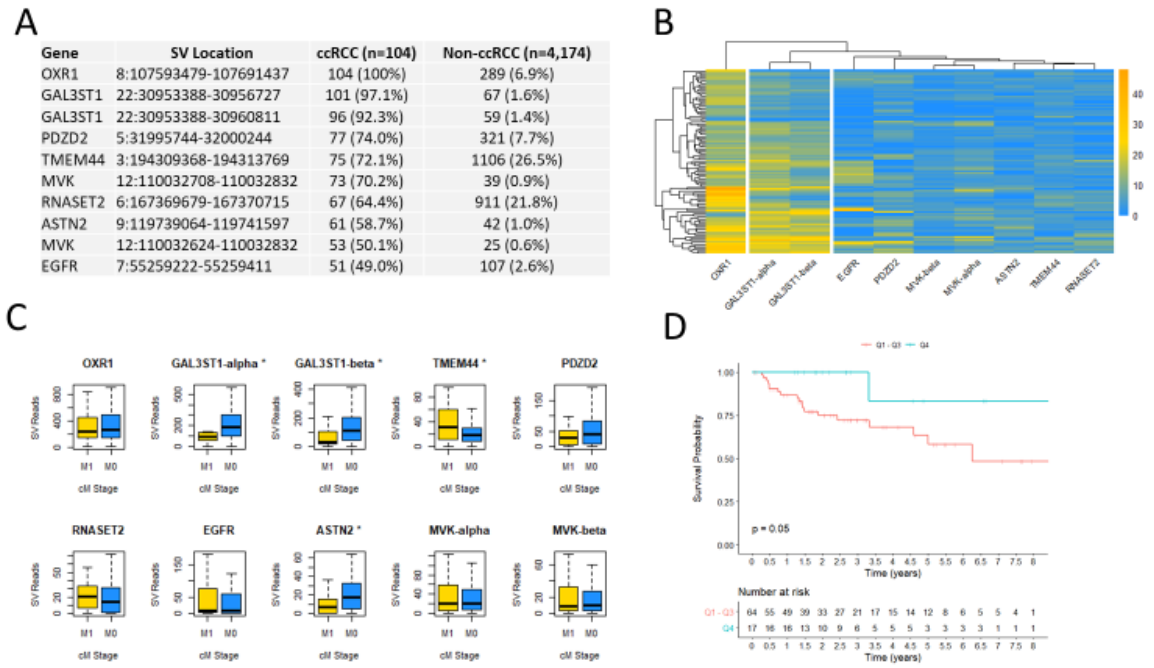

Interferon-STAT1 signaling induces lineage plasticity of castration-resistant prostate cancer

Background: Research has revealed the association of prostate cancer stem cells (PCSCs) with initiation and progression of metastatic castration-resistant prostate cancer (mCRPC). CSCs are reservoir cancer cells possessing self-renewal capacities and abilities to differentiate into heterogeneous lineages. Tumor heterogeneity is the major cause of treatment failure in PCa. In particular, genetic alterations during the development of drug resistance in PCa empower the lineage plasticity to PCSCs. Despite accumulating studies have shown the involvement of PCSCs with cancer relapse, metastasis and drug resistance, mechanisms underlying the acquisition of lineage plasticity in PCSCs remained to be elucidated. The signal transducer and activator of transcription 1 and 2 (STAT1/2) are essential components in interferon (IFN)-induced signaling pathway. Studies have demonstrated that STAT1 is highly overexpressed in tumors with acquired radio-resistance *in vivo*, and facilitates tumor cell survival after irradiation *in vitro*. Meanwhile, the IFN-related DNA damage resistance signature (IRDS) encompassed a subset of STAT1-driven genes with pro-survival functions are associated with intrinsic resistance to chemotherapy and radiotherapy in many malignancies. However, the involvement of STAT1 signaling in driving lineage plasticity of mCRPC remain unclear.

Methods: Tumor sphere assay, cell viability MTT assay, and subcutaneous transplant model of PCa lines were applied to examine tumorigenesis *in vitro* and anti-tumor activity of STAT1 inhibitors *in vivo*, along with bioinformatics approaches such as RNA sequencing followed by Ingenuity pathway analysis and Gene Set Enrichment Analysis (GSEA) to study the clinical correlation of STAT1 in PCa progression.

Results: We observed several IFN-inducible STAT1-driven genes are significantly upregulated in metastatic PCa and CRPC lines with acquired lineage plasticity. Inhibition of JAK-STAT1 signaling by Fludarabine or Ruxolitinib suppresses self-renewal capacity of tumor spheres *in vitro*, and attenuates tumor growth *in vivo*. In particular, STAT1-mediated induction of IFIT5 appears to facilitate the acquisition of stemness properties in PCSCs via regulating Bmi1 and Sox2 through targeting miR-128 and miR-101. Loss of IFIT5 leads to attenuated sphere forming ability *in vitro*, and decreased tumor incidence *in vivo*.

Conclusion: This study delineates the mechanistic impact of STAT1-IFIT5-mediated microRNA turnover on the acquisition of lineage plasticity in advanced PCa.

Background: Benign prostatic hyperplasia (BPH) is highly prevalent in men between the ages of 60-80. Due to the enlargement of the prostate, men develop lower urinary tract symptoms (LUTS). Prostate is the only solid organ that grows during adulthood, and its growth rate is quite variable amongst men. Currently, one of the main medical therapies for BPH is 5-alpha reductase (SRD5A) inhibitor (5ARI). While the variable growth rate of the total prostate gland is recognized, the variable growth rate of different prostate zones and their response to 5ARI treatment among adult male remains largely unclear. **Methods:** Prostate MRI data and clinical information of 160 patients who had at least three prostate MRI's from 2003 – 2020 with BPH and low grade prostate cancer were collected retrospectively. Prostate volume was measured for the central zone, peripheral zone and total prostate. **Results:** We demonstrated that prostate growth rate vary depending on age, the prostate zone and 5ARI use. Specifically, between ages 60-70, peripheral zone had the highest growth rate ($p=0.026$), whereas the central zone did not. Furthermore, multivariate analysis showed that age and comorbidities are independently associated with the peripheral zone ($p=0.026$ and $p=0.048$, respectively), but not the central zone. Lastly, 5ARI use is significantly associated with the reduction in growth rate in the central zone ($p=0.025$), not the peripheral zone. **Conclusion:** The growth pattern of the prostate vary between the central and peripheral zones, and is dependent on age and comorbidities. In addition, reduction of the prostate size as a result of the 5ARI treatment occur mainly at the central zone. Therefore, assessing the growth pattern of different prostate zones will better inform us about the underlying biology and responsiveness to therapy.

Adeno-associated viral vector (AAV)-mediated pharmacogenetic inhibition of lumbosacral sensory neurons alleviates visceral hypersensitivity in a mouse model of urological chronic pelvic pain syndrome (UCPPS)

Alison X. Xie*, Randall B. Meacham, Anna P. Malykhina

Division of Urology, Department of Surgery, School of Medicine, University of Colorado, Denver, Anschutz Medical Campus

New Models and Technologies for Studying Urologic Biology

Background: Patients with UCPPS experience chronic pelvic pain (CPP) and overactive lower urinary tract symptoms (LUTS). The UCPPS symptoms are closely associated with nociceptive sensitization in the nervous system, which contributes to visceral hypersensitivity. Previous studies suggested that increased excitability of lumbosacral sensory neurons innervating pelvic organs plays an important role in the generation and maintenance of UCPPS symptoms, especially of bladder pain and urinary urgency. In this study, we tested the hypothesis whether inhibition of lumbosacral sensory neurons alleviate pelvic hypersensitivity and overactive LUTS in a mouse model of UCPPS.

Methods: To silence neuronal activity *in vivo*, Gi-coupled DREADDs (designer receptor exclusively activated by a designer drug, hM4Di) were expressed in lumbosacral sensory neurons via targeted AAV intrathecal injections. Transgenic mice expressing *Cre*-recombinase and fluorescent reporters in sensory neurons and afferent nerves were used to guide cellular expression of DREADDs, as well as to track potential nerve remodeling *via* neuroimaging. Intravesical instillation of $VEGF_A$ was used to induce bladder hypersensitivity and LUTS. Detrusor contractility recordings using isolated bladder strips were used to evaluate neuronal control of bladder functions. Spontaneous voiding spot assay, awake cystometry, and Von Frey filament testing were used to assess pelvic sensitivity and voiding function *in vivo*.

Results: Intravesical instillation of $VEGF_A$ induced sensory nerve remodeling in the bladder, visceral hypersensitivity, and increased responses to sensory nerve-mediated contractility of the detrusor in mice. The $VEGF_A$-induced symptoms were likely due to increased VEGF receptor 1 signaling in peripheral nerve terminals in the bladder wall, and subsequent up-regulation of bladder nociceptors. Pharmacogenetic inhibition of lumbosacral sensory pathways with Gi-DREADDs effectively reversed $VEGF_A$-induced pelvic hypersensitivity in mice. Awake cystometry revealed decreased number of non-voiding contractions in mice when their lumbosacral sensory afferent activity was inhibited.

Conclusions: Our data suggests that decreasing afferent neuronal excitability *in vivo* can serve as a potential therapeutic strategy for treating the symptoms of UCPPS in an animal model of upregulated VEGF signaling in the urinary bladder.

Funding Source: The study was funded by the NIH/NIDDK grant DK121506 (APM)

Identifying and treating *ROBO1*$^{-ve}$/*DOCK1*$^{+ve}$ prostate cancer: An aggressive cancer type highly prevalent in African-American patients

Marina G Ferrari, Arsheed Ganaie, Adrian P Mansini, Badrinath R Konety, Paari Murugan, Luke Heppner, Christopher Warlick, Mohammad Saleem

Grant Funding: R01CA193739

Metastasis is the principal cause of death in prostate cancer (CaP) patients. The prognosis is very poor for metastatic CaP. On comparison, African-American patients exhibit high mortality rates than Caucasian counterparts. The failure of therapies for metastatic CaP is observed very high in patients belonging to African-American race. There is a need to identify new target-based therapies which could be either (i) beneficial to patients regardless of race or (ii) treat high-risk patients such as African-Americans who fail standard therapies compared to Caucasians. This requires identification of molecular pathways which are either (i) preferentially active in African-Americans or (ii) highly active in both races. We posit that the loss of *ROBO1* in advanced stage CaP contributes to the disparity observed between African-Americans and Caucasian. We conducted a comprehensive analysis of race-based primary and metastatic tumors for ROBO1 and its downstream targets (RAC1, DOCK1, E-Cadherin, and β-catenin). We show that ROBO1 expression is progressively lost with the increasing stage of CaP in African-American patients. Next, in order to explore the underlying mechanism that leads to *ROBO1* loss, we analyzed matching tumor DNA from patients and found that the *ROBO1* promoter is methylated in the majority of African-American cases in agreement with the CaP stage. In addition, we found that ROBO1 loss is associated to increasing RAC1 activation in tumors and representative cell models. We show that loss of ROBO1

results in increased DOCK1 activity that in turn induces Rac1 signaling in CaP cells. We hypothesized that targeting DOCK1/Rac1 network could be an ideal strategy to treat metastatic CaP, particularly in *ROBO1*$^{-/-}$ cases. To test the hypothesis, we tested the therapeutic efficacy of a selective inhibitor of DOCK1/Rac1 interaction in ROBO1^{+ve} and ROBO1^{-ve} CaP cells. We observed that DOCK1-inhibitor treatment significantly decreased the RAC1 activation and β-catenin activity in metastatic CaP cells. Notably, inhibition of DOCK1/Rac1 was observed to significantly decrease the motility and invasiveness of aggressive metastatic CaP cells. Furthermore, DOCK1-inhibitor significantly blocked the potential of metastatic CaP cells to extravasate (cross-over) through the endothelial lining (constituted of HUVEC cells).

These data suggested the significance of DOCK1/Rac1 pathway in a metastasis of CaP particularly in African-Americans. We conclude that the ROBO1/RAC1 ratio in tumor biopsies could be developed as an early biomarker of metastasis in African-American patients. We suggest that DOCK1-inhibitor therapy would be more beneficial to patients who exhibit *ROBO1*$^{-}$ tumor, and African-American patients are such as group who likely to benefit this therapy.

Metastatic prostate cancer (PCa) and is the major cause of mortality in PCa patients. The poor prognosis and failure of therapies in metastatic PCa could be associated with the heterogeneous nature of tumor cells. We previously showed that S100A4 protein drives the metastasis of PCa in preclinical models. Based on recent genomic data of >1000 patients, we now provide evidence that S100A4 in association with CD52 forms a unique and aggressive class of PCa in patients. The tumor genome data of patients show a direct correlation between S100A4 and CD52, a small glycoprotein expressed on T, B, NK, dendritic cells and monocytes. We posit that aggressive type of PCa cells during progression acquire immunosuppressive properties. Here, by employing a progressive panel of human PCa cell lines and primary prostate tumors and metastatic tumors, we show the presence of a subpopulation of PCa cells that express high levels of CD52 and S100A4. We were successful in isolating $CD52^{+}/S100A4^{+}$ subpopulation of aggressive PCa cells from DU145 (brain metastasis model) and PC3 (bone metastasis model). On analysis, the $CD52^{+}/S100A4^{+}$ metastatic cells exhibited high degree of invasiveness and the cells are characterized by the high expression of S100A4, VEGF and MMP9, phosphorylated-NFκB-p65 and phosphorylated-ERK. By using IHC, we observed that metastatic tumors exhibiting high S100A4 levels also exhibited a high expression of CD52. A marked increase in the number of $CD52^{+}/S100A4^{+}$ metastatic PCa cells was found in brain in patient metastatic specimens (Mets), which well explains the increased number of such tumor cell types found in the DU145 model. Furthermore, by employing the DECIPHER test we identified *CD52* as a biomarker of seminal vesicle metastasis, which is associated with an increased risk of lymph node metastasis and tumor recurrence. We provide data showing that genetic suppression CD52 significantly reduces the growth, migration and invasive potential of metastatic cells, and modulation of S100A4 expression could bring changes in the expression of CD52 in PCa cells. In addition, we found that $CD52^{+}/S100A4^{+}$ cells exhibit a strong immune- and radio- resistant behavior and treatment of the immune NK-92 cell line with recombinant CD52 induced down-regulation of activating receptors and cytolytic molecules, which are involved in immune surveillance, tumor recognizing and anti-

tumor activity. These data suggest a potential link between the S100A4, CD52 and immunosuppressive type PCa cells human disease. In conclusion, the novelty of this study is that we for the first time identified a new PCa subtype that is aggressive and resistant to radiation therapy. Another novel finding is that we identified CD52 as a novel target for treating metastatic PCa. These findings warrant future clinical studies in investigating *CD52*$^{+}$*/S100A4*$^{+}$ signature as a biopsy biomarker to identify patients who are prone to develop metastasis. In addition, our data open the opportunity to develop new therapies targeting CD52/S100A4 for treating aggressive metastatic PCa which otherwise remains a non-treatable disease.

Molecular Dissection of Renal Cell Carcinoma with Inferior Vena Cava Thrombus Highlights Prognostic Significance of Epithelial—Mesenchymal Transition and Cellular Proliferation Signatures

Randy Vince[1,2], Srinivas Nallandhighal[1,2], Razeen Karim[2], Skylar Groves[2], Judith Stangl-Kremser[1,7], Christopher Russell[1], Kevin Hu[3,5], Trinh Pham[1,2], Andi K. Cani[2,3,4,6], Chia-Jen Liu[2,3,6], Todd M. Morgan[1,2,3], Ganesh S. Palapattu[1,2,3,7], Aaron M. Udager[2,3,6], Simpa S. Salami[1,2,3]

[1]Department of Urology, Michigan Medicine, Ann Arbor, Michigan, USA.
[2]University of Michigan Rogel Cancer Center, Ann Arbor, Michigan, USA.
[3]Michigan Center for Translational Pathology, Michigan Medicine, Ann Arbor, Michigan, USA.
[4]Molecular and Cellular Pathology Graduate Program, University of Michigan, Ann Arbor, Michigan, USA.
[5]Department of Computational Medicine and Bioinformatics, University of Michigan Medical School, Ann Arbor, Michigan, USA
[6]Department of Pathology, Michigan Medicine, Ann Arbor, Michigan, USA.
[7]Department of Urology, Medical University of Vienna, Vienna, Austria

Intro:

5-year survival in clear cell renal cell carcinoma (ccRCC) varies based on stage and grade at diagnosis. However, some patients with similar disease stages have different survival outcomes, highlighting the importance of identifying molecular aberrations that lead to progression or recurrence. Our study aims to identify gene expression pathways enriched in patients with advanced disease and evaluate their prognostic significance.

Methods:

After IRB approval, we retrospectively identified 5 patients with ccRCC and IVC thrombus who underwent surgery(discovery cohort). Pathologists identified 3 areas of FFPE specimen from the primary and tumor thrombus for targeted RNA next-generation sequencing. Differential expression analysis was performed to identify gene expression. Using The Cancer Genome Atlas (TCGA) ccRCC gene expression data (n=466), we evaluated the potential prognostic significance of differentially expressed genes in the discovery cohort. We stratified patients on the enrichment of epithelial-mesenchymal transition (EMT) and cell cycle proliferation (CCP) pathways. Kaplan-Meier (KM) survival analysis and multivariable cox-proportional hazard testing to investigate the independent prognostic impact of the interaction between EMT and CCP on disease-free survival (DFS) and overall survival (OS).

Results:

In our discovery cohort, *WT1* and CCP genes were overexpressed in tumor thrombi. In the TCGA cohort, tumors with *WT1* overexpression also overexpressed EMT and CCP genes. Using expression data of 200 EMT genes, we calculated EMT scores and derived CCP scores for all TCGA tumors. KM analysis demonstrates patients with CCP^{low} and EMT^{low} tumors have the lowest risk of recurrence and death. Interestingly, EMT enrichment allows stratification of patients with CCP^{low} tumors, showing patients CCP^{low} and EMT^{high} have shorter DFS and worse OS (Fig. 2A-B). Multivariable analysis confirms patients with CCP^{low} tumors and EMT enrichment have a shorter DFS (Fig. 2C-D).

Conclusion:

Our study reveals the independent prognostic significance of the interaction between EMT and CCP genes on disease-free and overall survival. While further validation in prospective clinical cohorts is warranted, these findings could potentially impact treatment recommendations in patients undergoing biopsy for small renal masses.

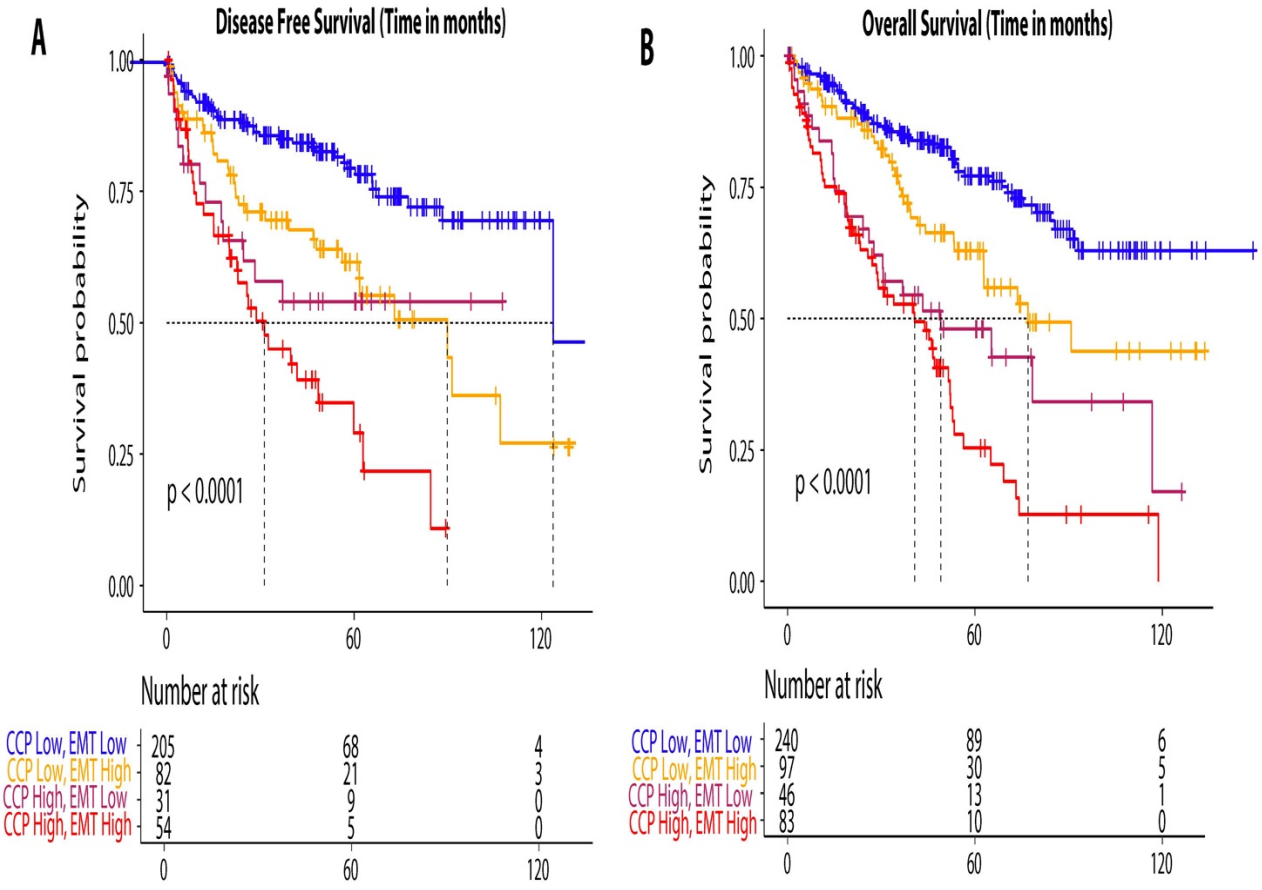
A
Disease Free Survival (Time in months)
Survival probability
1.00
0.75
0.50
0.25
0.00
p < 0.0001
0
60
120
Number at risk
CCP Low, EMT Low 205 68 4
CCP Low, EMT High 82 21 3
CCP High, EMT Low 31 9 0
CCP High, EMT High 54 5 0
0
60
120
B
Overall Survival (Time in months)
Survival probability
1.00
0.75
0.50
0.25
0.00
p < 0.0001
0
60
120
Number at risk
CCP Low, EMT Low 240 89 6
CCP Low, EMT High 97 30 5
CCP High, EMT Low 46 13 1
CCP High, EMT High 83 10 0
0
60
120

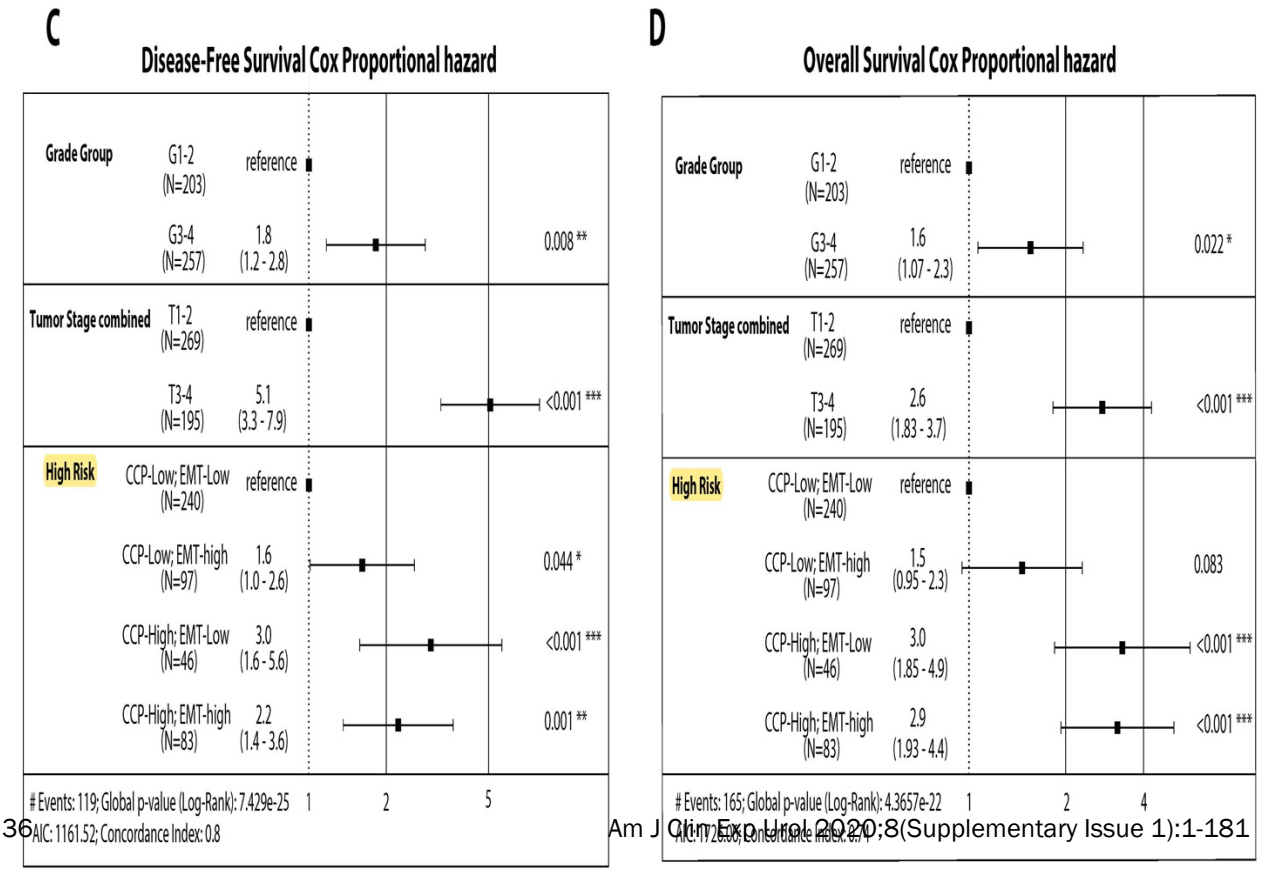
C
Disease-Free Survival Cox Proportional hazard
Grade Group
G1-2 (N=203) reference
G3-4 (N=257) 1.8 (1.2 - 2.8) 0.008 **
Tumor Stage combined
T1-2 (N=269) reference
T3-4 (N=195) 5.1 (3.3 - 7.9) <0.001 ***
High Risk
CCP-Low; EMT-Low (N=240) reference
CCP-Low; EMT-high (N=97) 1.6 (1.0 - 2.6) 0.044 *
CCP-High; EMT-Low (N=46) 3.0 (1.6 - 5.6) <0.001 ***
CCP-High; EMT-high (N=83) 2.2 (1.4 - 3.6) 0.001 **
Events: 119; Global p-value (Log-Rank): 7.429e-25
AIC: 1161.52; Concordance Index: 0.8
1
2
5
D
Overall Survival Cox Proportional hazard
Grade Group
G1-2 (N=203) reference
G3-4 (N=257) 1.6 (1.07 - 2.3) 0.022 *
Tumor Stage combined
T1-2 (N=269) reference
T3-4 (N=195) 2.6 (1.83 - 3.7) <0.001 ***
High Risk
CCP-Low; EMT-Low (N=240) reference
CCP-Low; EMT-high (N=97) 1.5 (0.95 - 2.3) 0.083
CCP-High; EMT-Low (N=46) 3.0 (1.85 - 4.9) <0.001 ***
CCP-High; EMT-high (N=83) 2.9 (1.93 - 4.4) <0.001 ***
Events: 165; Global p-value (Log-Rank): 4.3657e-22
1
2
4

Decoding Stromal Heterogeneity across BPH Phenotypes

Background: Benign Prostatic Hyperplasia (BPH) is a non-malignant enlargement of the prostate that occurs with aging and is associated with Lower Urinary Tract Symptoms (LUTS). Therapeutic options often fail, necessitating surgical resection of the prostate. The phenotypic and cellular heterogeneity of BPH is thought to contribute to treatment resistance. BPH patients present with multiple nodules grouped around the prostatic urethra in the transition zone. The composition of these nodules vary with some being solely comprised of stromal cells and others containing a mixture of stromal and epithelial cells. In addition, some patients present with a band of fibrotic tissue around the prostatic urethra that we term as peri-urethral fibrosis. Here, we describe stromal cell heterogeneity in the normal human prostate and across the different BPH phenotypes.

Methods: We used unbiased single cell RNA-sequencing (scRNA-seq) to obtain transcriptomic identities of stromal cells from normal human prostates and prostates from BPH patients who underwent simple prostatectomy. Cell clusters identified from scRNA-seq were validated *in situ* using immunohistochemistry and RNA *in situ* hybridization.

Results: We found that the stromal composition of the normal prostate consists of two major fibroblast populations, a prostate smooth muscle cell type, a vascular smooth muscle cell type and pericytes. One fibroblast sub-type, marked by expression of MFAP4, is abundant around the prostatic urethra and in the interstitial space between prostate glands. The second fibroblast population, marked by expression of APOD, is found closely associated with the secretory epithelium of the prostate and is absent from the spaces between prostate glands. The MFAP4+ fibroblast subtype extends into the bladder and represents a lower urinary tract fibroblast whereas APOD+ fibroblasts are restricted to the prostate. MFAP4+ fibroblasts are present within stromal and glandular nodules from BPH patients and are increased in peri-urethral fibrosis. APOD+ fibroblasts are absent from stromal nodules and regions of peri-urethral fibrosis. Desmin expressing smooth muscle cells are largely absent from regions of peri-urethral fibrosis. Wisps of smooth muscle are present in stromal nodules while glandular nodules are packed with Desmin expressing cells.

Conclusions: Our results highlight the identity and anatomical location of stromal cell types in the normal and BPH prostate. We expect that a molecular understanding of stromal cell types in the prostate will aid in a better understanding of the etiology of BPH.

Nucleolar Protein BOP1 Expression, Localization, and Function in Prostate Cancer Progression

Background

Differentiating between indolent and aggressive prostate cancers (CaP) is important to decrease over-treatment and increase survival for men with aggressive disease. Nucleolar prominence is a histologic hallmark of CaP; however, the expression, localization, and functional significance of specific nucleolar proteins has not been thoroughly investigated. Nucleolar protein BOP1 has been associated with multiple cancers, but it has not been previously implicated in CaP.

Methods

Meta-analysis of publicly available data was used to determine BOP1 expression changes in CaP progression, recurrence, and survival. Multiplexed immunohistochemistry was used to analyze the expression and localization of BOP1 and nucleolar marker NOP56 in human tissue samples. BOP1 functional significance was assessed in cell line models using siRNA knockdown followed by cell viability and motility assays.

Results

Meta-analysis of publicly available data showed increased BOP1 expression in metastatic CaP, recurrent CaP, and was inversely associated with overall survival. In human tissue samples, increased BOP1 expression was observed at later stages of CaP progression coinciding with a localization change from nuclear to cytoplasmic. Importantly, BOP1 expression was inversely associated with overall survival in meta-analysis and patient samples. In models of prostate cancer progression, BOP1 expression showed similar expression and localization to the human patient samples. Functional significance of BOP1 in metastatic CaP was assessed by genetic knockdown, where knockdown of BOP1 resulted in decreased proliferation and motility compared to control.

Conclusions

These data suggest a prognostic significance of BOP1 in CaP, where increased overall BOP1 expression concurrent with localization to the cytoplasm was associated with advanced disease and decreased survival. Functionally, BOP1 may be involved in CaP proliferation and motility, suggesting a functional role for nucleolar proteins in CaP progression.

LINC00992 contributes to the oncogenic phenotypes in prostate cancer via targeting miR-3935 and augmenting GOLM1 expression

Xuezhen Yang[1], Xu Jiang[1], Xueping Ma[1], Tomonori Habuchi[2], Yinglu Guo[3]

[1]Department of Urology, the Second Affiliated Hospital of Bengbu Medical College, Bengbu, 233000, Anhui, China

[2]Department of Urology, Akita University School of Medicine, Akita, 010-8543, Japan

[3]Department of Urology, Peking University First Hospital, Beijing 100034, China

[*]**Correspondence to:** Xuezhen Yang, Department of Urology, the Second Affiliated Hospital of Bengbu Medical College, 220 Hongye Road，Bengbu, 233000, Anhui, China. Email: engineyang@sina.com

Abstract

Background: Accumulating evidence has revealed the critical role of long non-coding RNAs (lncRNAs) in cellular processes during tumor progression. As documented in cancer-related literatures, LINC00992 expression is associated with cancer progression, whereas its function in tumors including prostate cancer has not been characterized yet.

Methods: Data from GEPIA database suggested LINC00992 expression in prostate cancer tissues. The expression levels of RNAs were monitored via qRT-PCR. Western blot evaluated the levels of proteins. The proliferation, apoptosis and migration of prostate cancer cells were assessed by CCK-8, EdU, TUNEL, Transwell and wound healing assays. Luciferase reporter, RNA pull down and RIP assays were applied to detect the interplays among LINC00992, miR-3935 and GOLM1.

Results: Elevated levels of LINC00992 and GOLM1 were detected in prostate cancer tissues and cells. LINC00992 exerted facilitating functions in prostate cancer cell proliferation and migration. Mechanically, LINC00992 interacted with and negatively regulated miR-3935 to elevate GOLM1 expression in prostate cancer cells. In addition, the in vitro suppressive effect of silenced LINC00992 on prostate cancer cell proliferation and migration was reversed by GOLM1 upregulation. Likewise, LINC00992 depletion restrained tumor growth in vivo was offset by enhanced GOLM1 expression.

Conclusions: LINC00992 competitively bound with miR-3935 to elevate GOLM1 expression and therefore facilitate the oncogenic phenotypes of prostate cancer cells, implying a potential LINC00992-targeted therapy for prostate cancer.

Keywords: LINC00992; miR-3935; GOLM1; prostate cancer

A role of increased transcription and high translation efficiency in upregulated androgen receptor splice variant expression in castration-resistant prostate cancer

Background

Upregulated expression of androgen receptor splice variants (AR-Vs), especially the most frequently expressed variant, AR-V7, is associated with resistance of prostate cancer to androgen deprivation therapy (ADT). At the RNA level, AR-V7 upregulation is generally coupled with increased expression of the full-length AR (AR-FL); consequently, AR-V7 mRNA and also the collective abundance of AR-V mRNAs constitute a minority of the AR population. However, Western blot analyses have shown that the relative abundance of the AR-V proteins is much higher in a sizable proportion of castration-resistant prostate cancers (CRPCs).

Methods

To address the mechanism underlying this discrepancy, we first analyzed RNA-seq data from ~350 CRPC samples for correlation between canonical and alternative AR splicing. We then knocked down AR-FL expression via shRNA or a PROTAC degrader and CRISPR-deleted the AR-binding site in the AR gene in preclinical models to determine the involvement of a negative autoregulatory circuit, in which androgen-bound AR-FL represses the transcription of the AR gene, in AR-V induction by ADT. We also measured the mRNA and protein stabilities of AR-FL and AR-Vs in response to ADT by mRNA and protein stability assays and pulse-chase analysis. Lastly, we examined the translation efficiency of AR-FL and AR-V mRNAs by nascent protein synthesis assays and polysome profiling analysis.

Results

Our analysis of clinical samples revealed a strong positive correlation between all canonical and alternative AR splicing, indicating that increased alternative splicing is not at the expense of canonical splicing. Instead, ADT disrupts the AR negative autoregulatory circuit to induce coordinated increase of AR-FL and AR-V mRNAs. At the protein level, however, ADT induces AR-FL degradation without affecting AR-V stability, and AR-V7 is translated at a faster rate than AR-FL irrespective of androgen levels.

Conclusions

Thus, ADT-induced AR-gene transcription and AR-FL protein decay, together with efficient AR-V7 translation, provide the first explanation for the discrepancy between the relative AR-V mRNA and protein abundances in many CRPCs. This mechanism highlights the inevitability of AR-V induction after ADT.

Targeting Wnt5a/FZD2 signaling overcomes resistance to enzalutamide in advanced CRPC

Shu Ning, Cameron M Armstrong, Chengfei Liu, Wei Lou, Alan P Lombard, Leandro S D'Abronzo, Jinge Zhao, Neelu Batra, Aiming Yu, Allen C Gao*
Department of Urology · University of California Davis

Background Androgen receptor (AR) blockade using antiandrogens is a mainstay for the treatment of castration resistant prostate cancer (CRPC). Unfortunately, drug resistance occurs frequently due to mechanisms that are not completely understood. Wnt5a, a representative ligand of non-canonical Wnt signaling, is expressed in circulating tumor cells from CRPC patients treated with enzalutamide. FZD2, the cognate frizzled receptor for Wnt5a, is the most commonly co-upregulated non-canonical Wnt signaling molecules in prostate cancer. Here we determine the contribution of non-canonical Wnt5a/FZD2 to enzalutamide treatment resistance, and explore the potential of targeting Wnt5a/FZD2 to overcome antiandrogen resistance in castration resistant prostate cancer.

Methods Wnt5a/FZD2 expression was examined in enzalutamide resistant C4-2B cells (C4-2B MDVR). Wnt5a and FZD2 expression were modulated using specific siRNAs. Cell growth, colony formation, and migration were studied *in vitro*. RNA sequencing analysis was performed on C4-2B MDVR cells with FZD2 knocked down; gene expression of non-canonical Wnt signaling, AR activity and AR-V7 related genes were analyzed. A novel RNA bioengineered Wnt5a siRNA (tRNA-siWnt5A) was developed to target Wnt5a/FZD2 signaling. The effect of tRNA-siWnt5a on tumor growth and sensitivity to enzalutamide treatment was evaluated *in vitro* and *in vivo*.

Results Wnt5a and FZD2 are highly co-upregulated in castration resistant prostate cancer patients. Wnt5a and FZD2 are overexpressed in enzalutamide resistant C4-2B MDVR cells compared to parental C4-2B cells. Knocking down FZD2 abrogates the increase of full-length AR and AR variant expression and diminishes the enrichment of genes involved in the non-canonical Wnt signaling pathway. Blocking FZD2 using specific siRNAs suppresses prostate cancer cell growth, colony formation, and migration. FZD2 knockdown with siRNA resensitized C4-2B MDVR cells to enzalutamide treatment. Down regulation of Wnt5a using the bioengineered tRNA-siWnt5A inhibited the growth of enzalutamide resistant prostate cancer cells and resensitized cells to enzalutamide treatment *in vitro*, and resistant CRPC PDX tumor growth *in vivo*.

Conclusions Our studies suggest that Wnt5a/FZD2 confers enzalutamide resistance and prostate cancer survival and proliferation. Targeting the non-canonical Wnt5a/FZD2 pathway could provide benefit for CRPC patients with tumors expressing high level of Wnt5a and FZD2, not only overcoming resistance but potentiating anti-tumor effects of enzalutamide in CRPC patients.

Steroid sulfatase stimulates intracrine androgen synthesis and is a therapeutic target for advanced prostate cancer

Background: DHEAS is the most abundant steroid in blood circulation and significant concentrations of DHEAS are present in prostate cancer patients even after ketoconazole or abiraterone therapy, suggesting that this may act as a depot for downstream androgen production. Steroid sulfatase (STS) catalyzes the hydrolysis of DHEAS to biologically active DHEA, which is further metabolized to active androgens that bind the androgen receptor (AR) leading to cell proliferation. Currently the role of STS in AR signaling and CRPC is largely unknown. This study determines the role of STS in AR signaling and explores the potential of targeting STS to overcome castration resistance in prostate cancer.

Methods: Quantitative rt-PCR and Western blots were used to detect expression of STS and AR. STS was downregulated using siRNA specific to STS. Stable cell lines overexpressing STS were generated and characterized. RNA-seq was performed on the stable clones. The steroid profiles of the cells were analyzed by LC-MS using the Thermo Scientific Vanquish UPLC/AB Sciex Qtrap system. Testosterone was assessed by ELISA in tumor extracts and cell culture media. Eleven potent STS inhibitors (SI) were synthesized and characterized. Prostate cancer cell sensitivity to SI was tested using cell growth assays and clonogenic assays. Efficacy of two SI was tested *in vivo* in castration relapsed VCaP xenograft tumor models.

Results: STS is overexpressed in CRPC patients and resistant prostate cancer cells including VCaP and C4-2B MDVR. Stable STS overexpression in C4-2B and LNCaP cells increases the levels of androgen. This resulted in increased cell growth and PSA expression *in vitro*. Inhibiting STS with siRNA or SI suppresses cell growth and AR signaling. STS overexpression in C4-2B and LNCaP cells promoted resistance to enzalutamide and this could be reversed by STS siRNA and SI. SI significantly suppressed AR transcriptional activity, suggesting that inhibition of STS activity by SI downregulates AR signaling. RNAseq analysis determined that enrichment of AR and AR variant signaling gene sets was reduced by SI-1 and SI-2. SI-1 and SI-2 significantly suppressed the growth of relapsed VCaP tumors, reduced intratumoral testosterone, and improved enzalutamide treatment *in vitro* and *in vivo*.

Conclusions: These studies suggest that STS drives intracrine androgen synthesis and prostate cancer proliferation. Targeting STS represents a therapeutic strategy to treat CRPC and improve second generation anti-androgen therapy.

Novel dual targeting of AKR1C3 and AR/AR variants inhibits androgen signaling and overcomes resistance to antiandrogen treatment

Background: AR/AR-V7 and AKR1C3 play key roles in prostate cancer progression and drive resistance to current therapies. Thus far, there are no clinically available therapies to specifically target either AR-V7 or AKR1C3, nor are there dual inhibitors for AR/AR-V7 and AKR1C3. We have developed a number of novel small molecules (LX) that are dual inhibitors of AR/AR-V7 and AKR1C3.

Methods: We designed and synthesized a library of novel compounds according to structure based computer modeling. Fourteen were selected for initial study. Cell growth assays were used to assess their efficacy at inhibiting CRPC growth. The effects of the LXs on AR/AR variants and AKR1C3 expression were determined by Western blot. PSA-luciferase assays were used to determine effects on AR signaling activity. RNA-seq was performed on selected LXs (LX-1 and LX-5) based on their improved efficacy over the other LX compounds. Resistant cell sublines generated from C4-2B cells resistant to enzalutamide (MDVR), apalutamide (ApalR), darolutamide (DaroR), or abiraterone (AbiR) were treated with LX-1 or their respective antiandrogen and cell number was determined. Mice bearing VCaP xenograft tumors and LuCaP35CR PDX tumors were treated with LX-1 and the effects on tumor growth were determined.

Results: Of the 14 LX compounds, LX-1 had the greatest effect at reducing cell number, AR/AR variant expression, and AKR1C3 activity. LX-5 was the next most effective compound. PSA-luciferase activity was greatly reduced by both LX-1 and LX-5. RNA-seq analysis demonstrated a robust reduction in AR and AR-V7 signaling gene expression by both LX-1 and LX-5. MDVR, ApalR, DaroR, and AbiR cells all showed a reduction in cell number when treated with LX-1. LX-1 inhibited conversion of the testosterone precursor androstenedione into testosterone in AKR1C3 overexpressing C4-2B and LNCaP cells. Additionally, LX-1 treatment reduced testosterone production by LUCaP35CR tumor cells which express high levels of AKR1C3 in the presence of androstenedione in a dose-dependent manner *ex vivo*. In addition, treatment with LX-1 reduced tumor growth in both VCaP and LuCaP35CR PDX models. Furthermore, LX-1 treatment reduced intratumoral testosterone.

Conclusions: We generated novel small molecule inhibitors that dual target AKR1C3 and AR/AR variants. These compounds, specifically LX-1, effectively reduce CRPC growth *in vitro* and *in vivo,* suggesting a clinical potential for treating advanced prostate cancer.

Cross-resistance among next generation anti-androgen drugs through the AKR1C3/AR-V7 axis in advanced prostate cancer

*Jinge Zhao, Shu Ning, Wei Lou, Joy C. Yang, Cameron M. Armstrong, Alan P. Lombard, Leandro S D'Abronzo, Christopher P. Evans, Allen C. Gao, Chengfei Liu**

Department of Urologic Surgery, UC Davis Comprehensive Cancer Center, University of California at Davis, Sacramento, CA, USA

INTRODUCTION AND OBJECTIVES: The next generation anti-androgen drugs, XTANDI® (Enzalutamide), ZYTIGA® (Abiraterone acetate), ERLEADA™ (Apalutamide) and NUBEQA (Darolutamide) extend survival times and improve quality of life in advanced prostate cancer patients. Despite these advances, resistance occurs frequently and there is currently no definitive cure for Castration-Resistant Prostate Cancer (CRPC). Our previous studies identified that similar mechanisms of resistance to enzalutamide or abiraterone occur following treatment and cross-resistance exists between these therapies in advanced prostate cancer. In this study, we will investigate the role of the AKR1C3/AR-V7 axis in apalutamide and darolutamide resistance.

METHODS: C4-2B cells were chronically exposed to increasing concentrations of apalutamide (5 μM ~ 40 μM) by passage in media containing apalutamide for >12 months in complete FBS and stored for further analysis. Cells resistant to apalutamide were referred to as C4-2B APALR. The effects of AKR1C3 expression and activation were examined by knock down of AKR1C3 expression using lenti-shRNA or inhibition of AKR1C3 enzymatic activity by indomethacin. AR and AR-V7 activity were determined by luciferase reporter assay. The effects of AKR1C3 activation on anti-androgen sensitivity were examined by growth assay and clonogenic assay.

RESULTS: Enzalutamide and abiraterone resistant prostate cancer cells are further cross-resistant to apalutamide and darolutamide. Mechanistically, we have determined that the AKR1C3/AR-V7 axis confers this cross-resistance. Knockdown of AR-V7 in enzalutamide resistant cells re-sensitize cells to apalutamide and darolutamide treatment. Furthermore, targeting AKR1C3 re-sensitizes resistant cells to apalutamide and darolutamide treatment through AR-V7 inhibition. Chronic apalutamide treatment in C4-2B cells activates the steroid hormone biosynthesis pathway and increases AKR1C3 expression which confers resistance to enzalutamide, abiraterone and darolutamide.

CONCLUSION: Apalutamide and darolutamide share similar resistant mechanisms with enzalutamide and abiraterone. The AKR1C3/AR-V7 complex confers cross-resistance to second generation AR-targeted therapies in advanced prostate cancer.

Expression of mutant *Pik3ca* in murine urothelial cells provides a novel model of early stage bladder cancer

Lauren Shuman MS, Hironobu Yamashita PhD, Thomas Wildermuth BS, Xue-Ru Wu MD, Joshua Warrick MD, David DeGraff PhD

Background

Despite the fact that approximately 70% of newly diagnosed bladder cancers are non-invasive tumors with high rates of recurrence, non-invasive bladder cancer is significantly understudied. In part, the general lack of appropriate models to validate the contribution of specific molecular drivers in bladder tumorigenesis is a significant issue. Activating mutations in phosphatidylinositol-4,5-bisphosphate 3-kinase catalytic subunit alpha (*PIK3CA*) are a frequent event in early stage bladder cancer, yet an *in vivo* model for understanding these mutations in bladder cancer is not available.

Methods

To address this gap, we have created a novel *Upk2-Cre/Pik3ca*^{H1047R} mouse model which expresses one or two copies of mutant *Pik3ca*^{H1047R} in a urothelial-specific manner. Experimental and genetic control mice were aged for 6 or 12 months, and bladders were collected for analysis. Western blotting and immunohistochemistry was used to confirm the functionality of mutant *Pik3ca* as well as to characterize urothelial expression differences.

Results

Mutant *Pik3ca* activity was confirmed by immunohistochemistry for phospho-Akt(Ser473). At 6 months of age, mice carrying one or two copies of mutant *Pik3ca* developed urothelial hyperplasia. While mice with one copy of *Pik3ca*^{H1047R} failed to progress to frank malignancy, activation of two copies of mutant *Pik3ca* resulted in the development of papillary bladder cancer at 12 months of age. Increased proliferation of bladder urothelium was confirmed by measuring urothelial thickness as well as immunohistochemistry for Ki67. Consistent with human papillary bladder cancer, immunohistochemistry also revealed high expression of luminal markers Foxa1, Pparγ, and Gata3, as well as low expression of basal markers Krt5/6 and Krt14.

Conclusions

These data provide evidence of the establishment and characterization of *Upk2-Cre/Pik3ca*^{H1047R} mice as a novel, clinically relevant model of non-invasive bladder cancer.

Title: *RB*-loss prostate cancer confers vulnerability to LSD1 inhibition

Authors: Mingyu Liu, Wanting Han, Muqing Li, Anna Besschetnova, Dong Han, Anthia A Toure, Shuai Gao, and Changmeng Cai

Background: Retinoblastoma protein (Rb) forms a repressor complex with E2Fs to prevent G1/S cell cycle progression. Genomic *RB*-loss is frequently occurred in castration-resistant prostate cancer (CRPC) and is significantly associated with poor clinical outcomes. However, it remains unclear how Rb/E2F repressor complex functions in modulating transcriptional networks in CRPC. In this study, we performed a comprehensive analysis to functionally characterize the activities of Rb/E2F in CRPC models and aimed to identify vulnerabilities in CRPC with *RB*-loss.

Methods: C4-2 CRPC cells stably infected with doxycycline-inducible lentiviral shRNA against *RB* were generated. The chromatin landscape of Rb/E2F complex was determined by ChIP-seq of Rb. Rb/E2F transcriptome was obtained from RNA-seq analysis in the stable line treated with/out doxycycline. An integrated analysis that combines the ChIP-seq and RNA-seq data was also performed to characterize the direct targets of Rb/E2F. We have additionally assessed the effect of *RB* silencing on AR transcriptional program using AR ChIP-seq.

Results: Using Bing and Expression Target Analysis, we have identified the direct transcriptional targets of Rb/E2F repressor complex. These genes include known E2F targets and genes mediating cell cycle and DNA damage repair pathways. The expression of these Rb/E2F directly repressed genes is increased in the clinical cohort of CRPC with *RB* deletion and neuroendocrine-like CRPC. Remarkably, we found that *RB* silencing led to a dramatic redistribution of AR chromatin binding, a potential mechanism for tumor resistance to enzalutamide. Furthermore, we found that *RB*-loss CRPC has higher gene expression of *LSD1*/*KDM1A* (a lysine-specific demethylase that demethylate histone and non-histone proteins) and that Rb/E2F targets are correlated with the activator function of LSD1. Using ChIP-qPCR, we found that E2F chromatin binding was suppressed by LSD1 inhibition, indicating E2F activity may be directly controlled by LSD1. Importantly, LSD1 inhibitor treatment was more effective in CRPC xenograft tumors with *RB* silencing.

Conclusions: This study provided novel insights into the molecular function of Rb/E2F repressor complex in CRPC progression and identified LSD1 as a regulator of E2F chromatin binding. These results also demonstrated that *RB*-loss CRPC may be vulnerable to LSD1 inhibition treatment.

Susceptibility-associated genetic variation in *NEDD9* contributes to prostate cancer progression

Background: In the US, African American (AA) patients show higher prostate cancer (PCa) incidents and worse treatment outcomes in comparison to European Americans (EA). This PCa disparity is largely contributed by socioeconomic factors, but race-associated genetic variations may also play a role. From GWAS analyses, we identified a panel of PCa risk-associated single nucleotide polymorphisms (SNPs) with significantly different allele frequencies in AA versus EA. The top-ranked SNP, rs4713266, is located at an intronic region of the *NEDD9* gene and the risk allele frequency is significantly higher in AA. *NEDD9* encodes for a focal adhesion protein that is phosphorylated by FAK and Src and acts as a signaling hub to regulate multiple downstream pathways. Clinically, *NEDD9* amplification was found in castration-resistant PCa (~3%) and neuroendocrine PCa (~15%). The chromatin region containing this SNP is highly enriched for enhancer marks, indicating it may contain a putative enhancer (we named it NEDD9-Int1Enh) to drive *NEDD9* transcription.

Methods: To determine the role of rs4713266 in regulating *NEDD9* expression, we performed: (1) CRISPRa to determine if NEDD9-Int1Enh mediates *NEDD9* transcription; (2) reporter assays to determine if the nucleotide variation of this SNP can alter binding of specific transcription factors; (3) CRISPR editing to modify the nucleotide at the SNP to determine the effects on *NEDD9* expression. To determine NEDD9 function in PCa, we silenced *NEDD9* in VCaP cells and then assessed its effects on the global gene profile using RNA-seq and on PCa tumor growth and metastasis using *in vivo* and *in vitro* models, such as zebrafish embryo injection.

Results: We found that forced activation of NEDD9-Int1Enh can increase *NEDD9* expression and modifying the nucleotide of the SNP altered *NEDD9* expression by interacting with distinct transcription factors such as ERG (non-risk) and NANOG (risk). Moreover, RNA-seq results revealed that NEDD9 may promote several oncogenic pathways, including epithelial-mesenchymal transition (EMT), JAK/STAT3, and KRAS signaling pathways. Indeed, we show that *NEDD9* silencing decreased PCa tumor growth and metastasis *in vitro* and *in vivo*.

Conclusion: Our study indicates a critical role of rs4713266 on modulating *NEDD9* expression in PCa of different racial subgroups. We also demonstrate strong oncogenic activities of NEDD9 in promoting PCa progression and metastasis. Together, our study provides novel insights into genetic mechanisms driving PCa racial disparities.

Title: SPARC: A Bladder Cancer Tumor-Suppressor via Targeting Metabolic Programming

Background:

Bladder cancer (BC) has limited treatments and low survival in advanced disease. We identified Secreted Protein Acidic and Rich in Cysteine (SPARC) as a tumor suppressor in BC whose expression decreases in advanced disease. We sought to elucidate SPARC's role in regulating metabolic programming in BC and identify pathways that may serve as biomarkers and treatment targets.

Methods:

We used human BC cell lines UMUC3, T24, T24T. We assessed SPARC's effect on bioenergetics by knocking it down and treating with exogenous SPARC. We profiled transcriptomes of T24, T24T, and T24 SPARC-knockout to identify aggressive phenotype signatures using Gene Signature Enrichment Analysis. We compared signatures with survival data from BC cohorts from the Gene Expression Omnibus and The Cancer Genome Atlas. To determine SPARC's effect on several pathways, we performed in vitro mechanistic studies.

Results:

SPARC inhibited ATP production, basal and maximal respiration, and spare respiratory capacity in BC cells. The effect was greater on T24T cells than T24 cells. Depleting SPARC in T24 cells restored an aggressive phenotype, increased ATP production and mitochondrial respiration. Integrated transcriptomic profiling indicated SPARC loss is associated with enriched mitochondrial metabolic pathways. SPARC loss is also associated with oncogenic signatures. In patient samples, SPARC expression negatively correlated with enzymes in metabolic pathways associated with lower survival.

Conclusion:

Our data reveals a novel function of SPARC: inhibiting mitochondrial bioenergetics and ATP production that fuel growth and invasion in BC cells. Loss of SPARC in BC cells is associated with enriched oncogenic signatures. SPARC loss is linked to activation of pathways for proliferation, invasiveness, and metabolic programming of BC cells. This programming supports increased energy production to fill demands for malignant tumors. The SPARC-treated metabolic profile reveals BC cell vulnerabilities suggestive of a promising therapeutic target.

Figure 1:

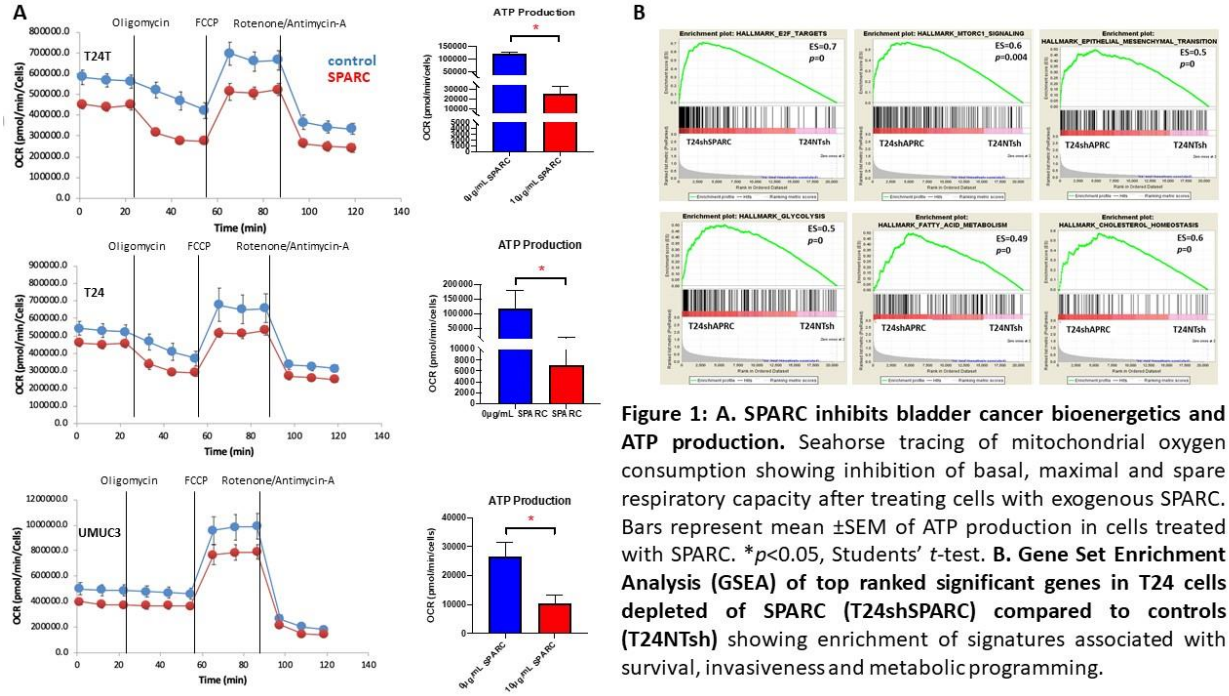

Figure 1: A. SPARC inhibits bladder cancer bioenergetics and ATP production. Seahorse tracing of mitochondrial oxygen consumption showing inhibition of basal, maximal and spare respiratory capacity after treating cells with exogenous SPARC. Bars represent mean ±SEM of ATP production in cells treated with SPARC. *p<0.05, Students' t-test. **B. Gene Set Enrichment Analysis (GSEA) of top ranked significant genes in T24 cells depleted of SPARC (T24shSPARC) compared to controls (T24NTsh)** showing enrichment of signatures associated with survival, invasiveness and metabolic programming.

Figure 2:

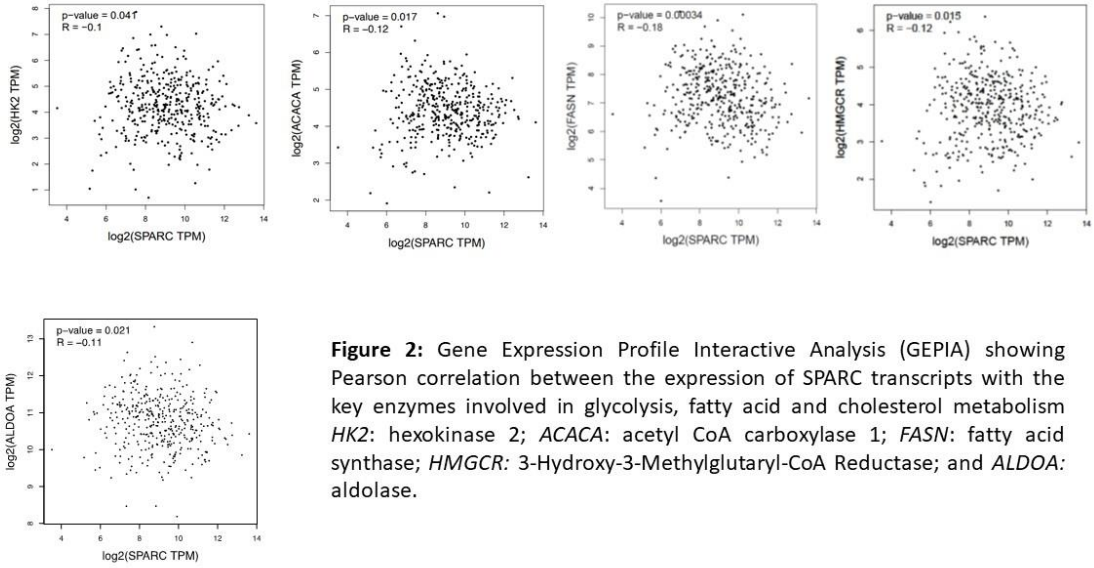

Figure 2: Gene Expression Profile Interactive Analysis (GEPIA) showing Pearson correlation between the expression of SPARC transcripts with the key enzymes involved in glycolysis, fatty acid and cholesterol metabolism *HK2*: hexokinase 2; *ACACA*: acetyl CoA carboxylase 1; *FASN*: fatty acid synthase; *HMGCR:* 3-Hydroxy-3-Methylglutaryl-CoA Reductase; and *ALDOA:* aldolase.

Connective tissue structure of women with POP and LUTS

Tryfonyuk L.[1], Baranowski W.[2], Ushenko O.[3]

1 - Rivne Regional Hospital, Rivne, Ukraine

2 – Warsaw Military Instytut, Warsaw, Poland

3 - Chernivtsi National University, Chernivtsi, Ukraine

About 40% of women with Pelvic Organ Prolapse (POP) coexist with LUTS. The study of morphological changes in the structure of connective tissue (CT) in these disorders is only descriptive. The results of polarimetric studies are fair, because they can be described using mathematical methods that in fact allow to assess the quantitative degree of changes in CT at the level of subcellular structures.

319 women aged 35-87 assessed with questionnaires before and 1 and 6 months after reconstruction, the investigated IA-B group, the II(control)- treated surgically on other gynecological diseases(without POP and LUTS, patients with similar demographic characteristics). During the operation collected sections from the anterior wall of the vagina and the uterosacral and round ligaments of the uterus; subjected to classical histpat evaluation, IHC and microscopic laser polarization investigation.

After corrective surgery, objective improvement (good anatomic effect, POPQ<=2) in 96.3% women. All tissue samples taken from patients in the study group, significant histological changes were observed in the microscopic pattern in relation to control group women. The IGC investigation revealed a significant decrease in the content of collagen type I and elastin with significant fragmentation of this protein, and change in the proportion in the content of certain types of collagen (prevalence of collagen type III). QoL after surgery has improved significantly (IA-PFDI-20 171.01/37.05,POPIQ-7 196.27/34.37,UDI-6 75.9/15.22, IB- PFDI-20 171.97/43.18, POPIQ-7 201.1/39.63,UDI-6 80.24/17.2($p<0.01$). Was discovered that the method of phase polarimetry can be used in the study of a large number of samples, a polarization-correlation method can be used as a refinement of the phasometric method, the polarization-correlation method of Stokes vector distribution. These can be used not only to detect but also to differentiate the severity of the pathology of the CT of the pelvic floor, as well as the method of laser induced AF, which can be used in screening for women with risk factors for the occurrence of POP.

The degree of degenerative changes (estimated by different methods) in the range of CT depends on the degree of progression of the POP. Optical-physical methods using methods of polarization microscopic analysis can be useful due to the possibility of accurate diagnosis of the severity of morphological changes in the CT and thus allow to make a more rational choice of surgical techniques (classical operations or operations with primary use of SM).

Developmental exposure to the environmental toxicant, polychlorinated biphenyls, leads to increases in mouse bladder volume and nerve density

Kimberly Keil Stietz, Kathy Wang, Alexandra Nunez, Conner L. Kennedy

Department of Comparative Biosciences, School of Veterinary Medicine, University of Wisconsin-Madison, Madison, WI.

Background: Environmental contaminants are risk factors for several disorders, yet their ability to contribute to lower urinary tract (LUT) function is understudied. Polychlorinated biphenyls (PCBs) are a group of chemicals for which developmental exposures have been linked to elevated autism risk. Children with autism often suffer from higher incidence of LUT symptoms, yet whether there is a connection between PCBs and bladder function in this population, or in typically developing individuals, is a current gap in fully understanding the etiology of LUT dysfunction. As a first step in addressing this gap, we test the hypothesis that developmental exposure to PCBs in mice, results in alterations to the bladder which could contribute to urinary function.

Methods: An environmentally relevant mixture of PCBs was used to mimic the top congeners and their proportions found in serum of mothers at risk of having a child with a neurodevelopmental disorder. Wild type mouse dams were dosed daily with either 0, 0.1, 1 or 6 mg/kg/d PCB, two weeks prior to mating, through gestation and lactation. Resultant offspring were weaned at 3 weeks of age, and bladders collected for morphometric and immunohistochemical analysis at 4 and 7 weeks of age.

Results: Effects of PCBs on bladder morphology were sex- and dose-dependent. Males more greatly affected than females. In developmentally exposed male mice there was a significant increase in bladder volume in the 6mg/kg PCB versus control group in 4 week old mice, which persisted to at least 7 weeks of age. In 4 week old mice there were no changes in bladder mass, muscle or epithelial thickness. However, βIII-tubulin, a marker of total nerve fiber density, was increased in bladder suburothelium of male mice of the 6mg/kg PCB versus control group. Expression of calcitonin gene related protein (CGRP), a marker of sensory nerve fibers, was also increased in the highest compared to lowest PCB dose groups. These measures are underway in 7 week old animals.

Conclusions: Developmental PCB exposure can alter bladder morphology in mice weeks after the final PCB exposure. While we did not observe evidence of obstruction, we did observe PCB-induced increases in bladder innervation, especially within the suburothelium. The functional consequences of PCB-induced increases in suburothelial nerve density on sensation, bladder contractility and ultimately voiding function are areas of future study. Supported by NIH awards R00ES029537 and T32ES007015.

Background: Bladder cancer remains a significant health problem, and a major cost to the health care system. While the majority of cases of bladder cancer are non-muscle invasive and are treated by cystoscopic resection, for those with muscle-invasive disease, therapy consists of either a radical cystectomy or radiation therapy. Even with definitive treatment, the mortality from muscle-invasive bladder cancer and metastatic disease remains high. Despite numerous clinical trials, treatment options for advanced bladder cancer have not improved, demonstrating the need for predictive models. Patient derived models (PDMs) are a powerful tool to study preclinical responses, however the benefits of each model have not been compared in head-to-head when models are derived from the same surgical specimen. Models of bladder cancer are needed to improve the preclinical testing of novel therapeutics and to predict response to therapy.

Methods: Surgical specimens (n=48) were implanted in hosts and were classified as no growth, some growth, or established lines. The PDMs representing xenografts (PDX), organoids (PDO), and spheroids (PDS) were characterized pathologically and molecularly by RNA sequencing. The universal molecular subtype and model-specific gene signatures were determined in order to compare PDMs to each other and their matching surgical specimen. Differential gene expression between the PDMs and surgical specimens were determined. PDMs and surgical specimens were clustered using the Euclidian distance analysis to test model fidelity.

Results: PDX models were established from 9/48 specimens. Overall, the molecular profiles of PDXs were the most similar to their matching patient specimen than the PDO and PDS from that patient. Likewise, each model was more similar to its matching patient sample than surgical samples and models from another patient. It is interesting to note that only Basal/Squamous (Ba/Sq) or Luminal Papillary (LumP) tumors established PDX models.

Conclusion: Surgical specimens had the most differentially expressed genes reflecting loss of immune and stromal compartments in PDMs. Moreover, PDMs upregulated a clear, patient-specific bladder cancer signal. Surgical specimens with the Ba/Sq molecular subtype are the most likely to form PDX models, alternative strategies to have models represent the other molecular subtypes are needed to provide models representing all subtypes of the disease.

A Uropathogenic *E. coli* UTI89 model of prostatic inflammation and collagen accumulation for use in studying aberrant collagen production in the prostate

Background: Bacterial infection is one known etiology of prostatic inflammation. Prostatic inflammation is associated with prostatic collagen accumulation and both are linked to progressive lower urinary tract symptoms in men. We characterized a model of prostatic inflammation utilizing transurethral instillations of uropathogenic *E. coli* UTI89 (UPEC UTI89) in C57BL/6J male mice with the goal of determining the optimal instillation conditions, understanding the impact of instillation conditions on urinary physiology, and identifying ideal prostatic lobes and collagen 1a1 (COL1A1) producing prostatic cell types for further analysis.

Methods: Transurethral instillation of 50, 100, 200, or 500μL of green tissue dye to determine fluid distribution (n=3 per volume). Transurethral instillation of sterile PBS, and UPEC UTI89 in sterile PBS with optical density (OD) of 0.2, 0.4, and 0.8 to collect prostate lobes and determine UPEC UTI89 distribution (n=2-5 per OD). Transurethral instillation of 50μL OD 0.35 UPEC UTI89 or 100μL OD 0.7 UPEC UTI89 to compare instillation conditions (n= 8-12 per condition). Sterile PBS instillation of equal volume were used as controls (n=8-12 per group). Spontaneous void spot assay and cystometry were used to assess changes in urinary function. Picrosirius red staining was used to assess collagen accumulation and ProCOL1A1 immunostaining in combination with smooth muscle actin (ACTA2) and protein tyrosine phosphatase, receptor type C (PTPRC also known as CD45) immunostaining was used to determine COL1A1 producing cell types.

Results: A 50 μL instillation volume distributes exclusively to bladder, 100 and 200 μL volumes distribute to bladder and prostate, and a 500 μL volume distributes to bladder, prostate and ureter. A threshold OD of 0.4 UPEC UTI89 in the instillation fluid is necessary for significant ($p < 0.05$) prostate colonization. UPEC UTI89 infection results in a low frequency, high volume spontaneous voiding pattern. This phenotype is due to exposure to UPEC UTI89, not catheterization alone. Prostate inflammation is isolated to the dorsal prostate and is accompanied by increased collagen density. This is partnered with increased density of PTPRC+, ProCOL1A1+ co-positive cells and decreased density of ACTA2+, ProCOL1A1+ co-positive cells.

Conclusions: Overall, we determined that this model is effective in altering urinary phenotype and producing prostatic inflammation and collagen accumulation in mice.

A Retrospective Medical Record Review of Dogs with Benign Prostatic Hyperplasia: 37 Cases (2014-2018)

Objective: Describe clinical signs of benign prostatic hyperplasia (BPH), in a well-defined clinical population of client-owned dogs.

Animals: 37 intact male dogs of any age, breed, or weight, and absent of prostatic neoplasia that were clinically diagnosed with BPH, and had a prostatic ultrasound and bacterial culture of urine, semen, or prostatic cytology performed.

Procedures: The Zambelli Symptom Index for BPH in Dogs (ZSI-BPH) was used to assess symptom severity in dogs meeting our case definition. Expected prostate size was calculated, prevalence of concurrent bacterial prostatitis and ultrasound characteristics were recorded, and response to treatment in cases with a minimum of 2 months follow-up summarized.

Results: There were no significant associations between prostate size and ZSI-BPH. True prostate size was less than expected, not greater. In patients with non-cystic BPH, there was a significant increase in ZSI-BPH in those cases with concurrent bacterial infection. After dogs with BPH were neutered prostatic size decreased, however there was no significant reduction in ZSI-BPH scores for dogs treated with castration or medical therapy.

Conclusions and Clinical Relevance: Prostate volume is a poor predictor of symptom severity, and urine culture is more informative. Measurement of prostate size and comparison to expected based on the dogs weight and age should be performed to quantitatively confirm prostatomegaly and reduce overdiagnosis. Future focus on reducing clinical signs in addition to prostate size is needed in order to improve BPH treatment practices.

DEVELOPMENTAL POLYCHLORINATED BIPHENYL (PCB) EXPOSURE CONTRIBUTES TO BLADDER DYSFUNCTION IN MICE

Conner L. Kennedy[1], Zunyi Wang[2], Kimberly Keil Stietz[1]

[1]Department of Comparative Biosciences, School of Veterinary Medicine, University of Wisconsin-Madison, Madison, WI.

[2]Department of Surgical Sciences, School of Veterinary Medicine, University of Wisconsin-Madison, Madison, WI.

Background: Lower urinary tract symptoms (LUTS) are a marked comorbidity in individuals with neurodevelopmental disorders (NDDs). Yet underlying factors contributing to LUTS risk in individuals with and without NDDs, is not completely understood. Early life environmental exposures to polychlorinated biphenyls (PCBs), have been implicated in NDD risk, however, their effects on peripheral targets like bladder are unknown. With the link of early life PCB exposure and NDD risk, it is worth considering whether LUT comorbidities are related to PCB exposure. As an initial step in addressing this question, we test the hypothesis that developmental PCB exposure contributes to bladder dysfunction in young adult wild type mice.

Methods: C57Bl/6J mouse dams were dosed with a PCB mix which mimic those found in serum of women at risk of having a child with a NDD. Dams were dosed daily via the diet at 0, 0.1, 1 or 6mg/kg PCB two weeks prior to mating, through gestation and lactation. Voiding function was assessed in offspring 6-8 weeks of age using void spot assay (VSA, n=17-24), uroflowmetry (n=14-24), and anesthetized cystometry (n=7-10) to provide assessment of voiding function in awake and anesthetized mice. Bladder bath assays (n=3-5) were used to examine bladder contractility in *ex vivo* bladder preparations.

Results: Developmental PCB exposure significantly alters urine spot size distribution during VSA testing. Compared to control, PCBs increase the number of small diameter (0-0.1cm) urine spots in the 0.1 and 6mg/kg PCB groups in males, and all dose groups in females. Uroflowmetry testing reveals that in male mice only, PCBs decrease void stream strength rating in the 0.1mg/kg PCB dose group versus control, indicative of a more drop like void pattern. In mice undergoing anesthetized cystometry, PCBs have a significant overall dose effect, decreasing intervoid interval in the 0.1 mg/kg/d and 6 mg/kg/d PCB groups compared to control. Ongoing preliminary studies from bladder bath assays suggest that PCBs may alter sensitivity to contractile stimuli.

Conclusions:These results support the hypothesis that developmental PCB exposures can contribute to voiding function in mice. Overall PCB effects on voiding function correspond to increased small diameter urine spots, drop like voids and shorter time intervals between voids. Further studies into mechanisms associated with these sex and dose-dependent effects for PCB exposure are warranted. Supported by NIH awards [R00ES029537, T32ES007015, and U54DK104310].

Resistance to Olaparib is Dependent on Re-Emergence from G2/M Arrested Senescence

Background: Inhibition of poly (ADP-ribose) polymerase (PARP) is an exciting treatment strategy recently approved for prostate cancer patients with homologous recombination repair defects. Despite this advance in the field, there are important unanswered questions regarding PARP inhibitor (PARPi) use; 1) How do PARPi sensitive cells respond to treatment? 2) What mechanisms give rise to PARPi resistance? To address these questions, we sought to characterize response to PARP inhibition using PARPi sensitive LNCaP and C4-2B cells and two PARPi resistant cell line derivatives.

Methods: LN-OlapR and 2B-OlapR olaparib resistant cell lines were generated from LNCaP and C4-2B cells through chronic exposure to increasing doses of olaparib. Western blot was used to detect PARP activity, apoptosis, and DNA damage. Flow cytometry and beta-galactosidase activity assays tested response to PARPi's. CDK1 was inhibited using RNAi and small molecule drug, BMS-265246.

Results: OlapR cells exhibit marked resistance to olaparib versus parental cells. OlapR models are also cross-resistant to other clinically relevant PARPi's including rucaparib, niraparib, and talazoparib. Mechanistically, PARPi treatment inhibits PARP catalytic activity, induces DNA double strand breaks, and activates apoptosis in LNCaP and C4-2B cells. We also observed a cytostatic response in a significant proportion of cells. Flow cytometry showed a robust G2/M arrest in response to olaparib treatment, accompanied by marked increases in p21 expression and beta-galactosidase activity, suggestive of senescence. In contrast, OlapR cells do not exhibit G2/M arrest, increased p21, or senescence in response to PARP inhibition, suggesting that resistance is dependent upon re-emergence from p21 dependent senescence. CDK1 activity governs the G2/M cell cycle phases and is a primary p21 target. Thus, we tested if CDK1 inhibition re-sensitizes OlapR cells to PARPi treatment. Indeed, we found that CDK1 inhibition by either siRNA or BMS-265246 re-sensitized OlapR cells to treatment.

Conclusions: We find that response to PARP inhibition is characterized largely by a G2/M arrested senescence, which may give rise to resistance through re-emergence from this state. PARPi induced senescence provides an escape route from PARPi cytotoxicity, creating a repository of persistent cells which can give rise to resistance. Targeting CDK1 may prove to be an efficacious strategy for the treatment of re-emerged, PARPi resistant prostate cancer.

Bmi1-driven PTEN/TP53 loss promotes prostate cancer progression and treatment resistance by leveraging metabolic dependency.

Introduction and Objective: Concurrent inactivation of PTEN and TP53 is often observed in aggressive prostate cancers (PCs) that resist androgen deprivation therapy (ADT) and show poor clinical outcomes. The identification of targetable vulnerabilities that result from loss of both PTEN and TP53 is urgently needed. Here, we used transgenic, cell line and PDX models to investigate the functional roles of Bmi1-driven PTEN/TP53 loss in PC progression and treatment resistance, and potential vulnerabilities that could be targeted therapeutically.

Methods: We have established clinically relevant animal models of prostate cancer recurrence using transgenic Bmi1-CreER; PTENf/f; TP53f/f (hereafter referred to as BC-PTEN/TP53 mice) and PDX mice. A tissue recombination strategy was used to rescue transgenic BC-PTEN/TP53 mouse prostates by regeneration as grafts in SCID mice. Tumors were characterized by histology, immunohistochemistry for relevant markers, and gene expression profiling by RNA-seq. Our findings were validated using genetic and pharmacologic approaches in relevant cell lines and mouse models.

Results: Combined PTEN and TP53 deletion in Bmi1-expressing prostate cells strongly accelerated formation of prostate cancer comprising diverse phenotypes including AR-negative PCs. Notably, following castration, BC-PTEN/TP53 mice develop castration-resistant PC (CRPC) that exhibits extensive phenotypic plasticity and cellular heterogeneity. In BC-PTEN/TP53 mice, CRPC phenotype is significantly associated with enhanced cell proliferation, the loss of AR expression, and a profound decrease in the fraction of p16-mediated senescent cells. Genomic profiling analysis revealed significant enrichment of genes involved in mitochondrial and amino acid metabolism. Genetic or pharmacological inhibition of Bmi1 significantly suppressed the survival of enzalutamide-resistant PC cells lacking PTEN/TP53 with simultaneous decrease in gene sets associated with metabolic pathways. Moreover, inhibition of mitochondrial or amino acid metabolism resulted in significant growth suppression.

Conclusions: These results highlight the cooperative roles of Bmi1 with PTEN/TP53 loss in facilitating PC progression and therapeutic resistance by regulating metabolic vulnerabilities. This may provide a rational for targeted therapy to selectively eradicate PTEN/TP53-deficient tumors.

Inhibition of Wntless expression suppresses growth of neuroendocrine tumors

Leandro S D'Abronzo, Alan Lombard, Shu Ning, Cameron M Armstrong, Chengfei Liu, Wei Lou, Jinge Zhao, Allen C Gao
Department of Urology · University of California Davis

BACKGROUND: The current mainstream treatment for advanced prostate cancer (PCa) is AR-targeted therapies such as enzalutamide and abiraterone. Unfortunately, prostate tumors may develop mechanisms by which they can circumvent therapeutics. Neuroendocrine differentiation, which can occur *de novo* or in response to AR-targeted therapy, is one such means by which tumor cells can resist treatment. Neuroendocrine prostate cancer (NEPC) cells often do not respond to AR-targeted therapy and respond only transiently to chemotherapy. Therefore, there is an urgent need to understand the mechanism of NEPC development and develop therapeutic strategies that are independent of the androgen/AR axis. In this study we investigate the role and potential targeting of Wntless (WLS) in the development and treatment of NEPC.

METHODS: To examine the expression of WLS in NEPC, we utilized western blotting and qPCR to compare protein and mRNA levels of WLS in prostate cancer cells with neuroendocrine features as well as the established neuroendocrine cell line NCI-H660. Cell proliferation was assessed by CCK8. In vivo studies were carried out by treating H660 tumor bearing mice with a novel WLS inhibitor, NicS, via gavage administration.

RESULTS: We found that WLS is overexpressed in models of NEPC including NCI-H660, PC3 and CWR22rv1 cells. Downregulation of WLS by siRNA inhibits the markers of NEPC differentiation including chromogranin A (CHGA), neuron-specific enolase (NSE) and synaptophysin (SYP). WLS inhibition also reduces cellular viability. We synthesized a library of drug derivatives from niclosamide, and found one of the derivatives, NicS, can inhibit WLS expression and cellular viability and decrease neuroendocrine markers. To examine if NicS can inhibit tumor growth in vivo, we treated H660 tumor bearing mice with NicS and found that it significantly reduced tumor growth of H660 cells.

CONCLUSIONS: Our results show that WLS is overexpressed in NEPC cells and targeting WLS by either siRNA or NicS suppresses tumor cell growth, suggesting that NicS could be potentially developed to treat NEPC.

Altering the gastrointestinal microbiome to improve treatment response in prostate cancer models

Anuradha A. Shastri[1], Tiziana DeAngelis[1], Kevin Ko[1], Leonard G. Gomella[2], Edouard Trabulsi[2], Matthew J. Schiewer[2], Karen S. Sfanos[3], Nicole L. Simone[1]

1. Department of Radiation Oncology, Sidney Kimmel Medical College at Thomas Jefferson University, Philadelphia, PA
2. Department of Urology, Sidney Kimmel Medical College at Thomas Jefferson University, Philadelphia, PA
3. Department of Pathology, Johns Hopkins University School of Medicine, Baltimore, MD

Background: The gastrointestinal microbiome (GIM) is a critical regulator of inflammation. Recent research suggests that targeting the microbiome may alter the systemic inflammation known to be associated with progression, metastasis and resistance to therapy in prostate cancer (PC). Previously, our lab has successfully used calorie restriction (CR) in conjunction with irradiation (IR) to reduce the inflammatory/miR-21 axis thereby decreasing tumor progression. Here we sought to determine if CR could alter the GIM to reduce inflammation and improve therapy outcomes.

Methods: To assess the effect of CR with IR *in vivo*, 6-week-old male nude mice were injected with $4x10^6$ LNCaP (hormone sensitive) cells. Once tumors were palpable, mice were randomized to one of 4 treatments: ad libitum (AL) diet, 6Gy IR, CR diet, or CR+IR. On day 21, stool samples were collected of all cohorts for 16S sequencing. Tumors and serum were collected when they reached $2cm^3$. In a clinical trial using 25% CR prior to prostatectomy in 16 patients (pts.) with PC, blood and rectal swab samples were collected pre and post intervention.

Results: In the mouse model, CR sensitized the tumor to IR showing a 35% growth delay compared to IR and increase in survival. Mice treated with CR+IR had increased β-diversity and anti-inflammatory species of the GIM. The less inflammatory GIM phenotype of CR treated mice, reduced the LPS that crossed the gut wall by 5 fold, which reduced inflammatory cytokines IL-1β, IL-6, pP65 and increased anti-inflammatory pIKBα. IKB is known to promote tumor progression by increasing miR-21 expression, however with CR treatment, miR-21 reduced ~2.4 fold, which increased expression of its target PDCD4 by ~18 fold leading to decreased inflammation in tumor and increased apoptosis noted by reduced levels of Bcl2 and BclxL. Pts. in the clinical trial of CR showed similar results with increased anti-inflammatory GIM including Propionobacterium, Eubacterium, Ruminococcus, Akkermansia and Lactobacillus and a simultaneous decrease in systemic inflammation noted by decrease in ESR (1.5 fold) and inflammatory cytokines linked with PC metastasis including CXCL10, CXCL12, CXCL16, and TGF-β2. miR-21 decreased in half the pts.

Conclusions: Dietary alterations are known to have positive effects on cancer growth as we and others have shown. Here, we demonstrate in *in vivo* model and in a clinical trial, that CR may decrease tumor growth in PC models by positively affecting the GIM leading to decreased systemic inflammation and decreased tumor growth. Further investigation into precision nutrition approaches to alter the GIM to decrease cancer growth should be performed.

The p75^{NTR} Antagonist Mediates Anti-Inflammatory Responses to LPS in Urothelial and Smooth Muscle Cells

Background: Current evidence links acute bacterial cystitis by E. coli to the progression of interstitial cystitis in aging women. Lipopolysaccharide found on these bacteria activates the TLR4 receptor to induce proinflammatory responses. Much as the TLR4, the p75NTR receptor also sets inflammation with proNGF to remodel bladder tissues and impair urodynamics, suggesting that it might be a key contributor of recurrences and onsets of chronic cystitis. As we showed previously that antagonism of p75^{NTR} can impede the development of diabetic voiding dysfunction, we aimed to demonstrate a molecular interplay in p75^{NTR} inflammatory signals through activation of TLR4.

Methods: We pre-treated rat primary urothelial (UTC) and detrusor smooth muscle (SM) cells with a specific p75^{NTR} antagonist (THX-B), followed by exposure to LPS. We evaluated the recruitment of the Traf6 ubiquitinase by p75^{NTR}, as well as its downstream activation of caspase-3/8, NF-κB and MAPKs pathways by immunoprecipitation, enzymatic assay and immunoblotting. Cytokinesis of TNF-α and its diffusion in cell medium with NO were examined by Western blotting and Griess' colorimetric method. Disruption of E-Cadherin, ZO-1 and Occludin on cell surface was identified using immunochemistry and immunoblotting.

Results: Both cell types showed expression of p75^{NTR} independently of TLR4 activity and absence of caspase activity under LPS or THX-B conditions. In UTC, LPS induced cytokinesis of TNF-α and NO release. Antagonizing p75^{NTR} before LPS exposure also decreased cytokinesis/release of TNF-α, without interfering with NO diffusion in these cells. While Traf6, Jnk and NF-κB were unchanged, increased levels of Erk were noted in presence of LPS, with no changes under p75^{NTR}antagonism. Expression of Occludin and ZO-1 on UTC surface greatly decreased with exposure to LPS, while this effect was prevented on occludin by THX-B. In SMC, LPS soared the recruitment of Traf6 by p75^{NTR}, which was then suppressed by pre-treatment. Similarly, pre-treating SMC with THX-B decreased Jnk and NF-κB activation by LPS. Expression of all tight junctions remained stable with LPS or p75^{NTR} antagonism.

Conclusions: Together, our results demonstrated cell-specific interplay between TLR4 and p75^{NTR} inflammatory pathways sensitizing hosts to recurrent bacterial cystitis and chronic interstitial cystitis. We emphasize the merit of characterizing the anti-inflammatory value of p75^{NTR} antagonism *in vivo*, as a potential therapeutic approach for women with cystitis.

Authors: **Anna Besschetnova**, Wanting Han, Yanfei Gao, Mingyu Liu, Dong Han, Shuai Gao, and Changmeng Cai

Title: EHMT1 activity in prostate cancer is regulated by dual lysine-methylations

Background: Lysine methylation is an important post-translational regulation on histones, but its molecular functions on non-histone proteins remain largely unknown. In a pilot study, we identified novel lysine methylations at non-histone proteins in prostate cancer (PCa) cells through an affinity pull-down assay. EHMT1/GLP, containing monomethylated K450 and K451, was one of these proteins, and it was known to repress transcription through methylating H3K9. EHMT1 and EHMT2/G9a are members of the REST repressor complex, that includes LSD1/CoREST/HDACs and represses neuronal genes in non-neuronal cells. Loss of function for this complex has been suggested as a mechanism to drive neuroendocrine (NE) transition of PCa. We hypothesize that the K450/451 methylations may inhibit the activity of EHMT1 and that LSD1 may demethylate these lysines and thus enhance EHMT1 activity.

Methods: LNCaP stable cell lines overexpressing doxycycline-regulated V5-tagged EHMT1-WT, K450R, K451R, and K450/451R were generated. We performed ChIP-seq analyses of V5 and H3K9me2, and RNA-seq analyses in all four cell lines treated with/out doxycycline. We also conducted *in vitro* demethylation assays to examine whether LSD1 directly demethylates EHMT1. Moreover, we performed co-immunoprecipitation assays to determine the effect of LSD1 inhibition on the interaction of LSD1 with EHMT1.

Results: The K450/451R mutant had a significant increase of chromatin binding in V5 and elevated levels of H3K9me2 compared to the weak chromatin binding seen in WT, K450R and K451R**.** Analyses in RNA-Seq revealed that the K450/K451R mutant repressed genes enriched for neuronal pathways, which was not seen in WT, K450R or K451R. The demethylation assays indicated that methylated K450 but not K451 is a potential substrate of LSD1. Furthermore, we confirmed the interactions of LSD1 with EHMT1 and found that LSD1 inhibition repressed the interaction of LSD1 with EHMT1.

Conclusions: Our studies suggest that K450 of EHMT1 is specifically demethylated by LSD1, but this alone is not sufficient to induce the chromatin recruitment of EHMT1. However, demethylation at both K450/K451 can dramatically increase the chromatin binding of EHMT1, which subsequently represses neuronal pathways. This mechanism may be particularly important for maintaining the prostate epithelial cell lineage and loss of this demethylation might lead to the emergence of NE-like PCa.

MAP3K11 promotes enzalutamide resistance in castration-resistant prostate cancer *in vitro*

Kohrt SE[1,2], Awadallah WN[2,3], Grabowska MM[1,2,3,4]

[1]Department of Pharmacology, Case Western Reserve University, Cleveland, OH; [2]Case Comprehensive Cancer Center, Case Western Reserve University, Cleveland, OH; [3]Department of Urology, Case Western Reserve University, Cleveland, OH; [4]Department of Biochemistry, Case Western Reserve University, Cleveland, OH

Background: Castration-resistant prostate cancer (CRPC) patient tumors can be treated with androgen receptor (AR) pathway antagonists such as enzalutamide that target AR signaling and transcriptional activity. CRPC patient tumors inevitably gain enzalutamide resistance. Our lab previously identified and validated *MAP3K11* as a putative driver of resistance in a short hairpin RNA screen. MAP3K11, also known as mixed lineage kinase 3 (MLK3), has been shown to be involved in multiple signaling pathways including the JNK, ERK, and p38 MAPK pathways. MAP3K11 has also been implicated in regulating AR activity via signaling cascades related to changes in phosphorylation of Serine 650 (AR-Ser650). The purpose of this study was to investigate the mechanism of MAP3K11 in CRPC to promote enzalutamide resistance.

Methods: To investigate the mechanism of MAP3K11 in enzalutamide resistance, we utilized enzalutamide sensitive (LNCaP, C4-2B) and enzalutamide resistant cells (22Rv1, CWR-R1-EnzR, C4-2B MDVR, PC-3, DU145). We used Western blotting to measure changes in MAP3K11, AR, and phospho-AR-Ser650. We furthermore investigated activation of JNK, p38, and ERK via Western blot. Finally, we performed cell survival assays using crystal violet to measure cell survival in response to MAP3K11 KD or inhibition with the inhibitor CEP-1347 in cells treated with DMSO or enzalutamide.

Results: Our studies show MAP3K11 KD or treatment with CEP-1347 decreased cell survival in CRPC and enzalutamide-resistant cell lines. Combination of enzalutamide with MAP3K11 inhibition further decreased cell survival. MAP3K11 KD and CEP-1347 treatment decreased phosphorylation of AR-Ser650 with no change in AR protein expression. To understand the cellular effects of phosphorylated AR-Ser650, we show phospho-AR-Ser650 localizes to the nucleus and is absent in the cytoplasm. We furthermore observed an increase in MAP3K11 expression and activation of JNK, p38, and ERK in enzalutamide-resistant compared to enzalutamide-sensitive cells.

Conclusions: This data suggests MAP3K11 plays a role in CRPC cell line survival and in enzalutamide-resistance mechanisms. We found MAP3K11 acts through the related JNK, p38, and ERK pathways in CRPC cells and effects AR localization via phosphorylation of AR-Ser650. Importantly, this data also shows MAP3K11 inhibition with CEP-1347 can sensitize cells to enzalutamide treatment. Future studies will further determine the mechanism of MAP3K11 in enzalutamide resistance, and evaluate MAP3K11 inhibition in pre-clinical models of CRPC.

Comparative analysis of *AR* gene aberrations in circulating tumor cells and plasma cell-free DNA from prostate cancer patients

Background

Reactivation of the androgen receptor (AR) transcription factor is a key step in the progression to endocrine therapy resistance in castration-resistant prostate cancer (CRPC). One mechanism supporting the reactivation of AR signaling is the generation of constitutively active AR variants through genomic rearrangements that change the architecture of the *AR* gene. The landscape of *AR* gene rearrangements has been examined in solid tumor samples and plasma cell-free DNA (cfDNA) from CRPC patients. However, the detection of *AR* gene rearrangements in patient circulating tumor cells (CTCs) represents a gap in knowledge.

Methods

We used the Versatile Exclusion-based Rare Sample Analysis (VERSA) platform to capture CTCs and isolate DNA. DNA was subjected to whole genome amplification and analyzed using a targeted DNA-sequencing (DNA-seq) approach. DNA-seq data were analyzed by four different DNA structural variant (SV) detection algorithms and two different single nucleotide variant (SNV) detection algorithms. This CTC capture and analysis pipeline was first optimized using prostate cancer cell lines with known *AR* gene aberrations. Following optimization, we analyzed CTCs from ten patients with metastatic CRPC and compared the results with a parallel analysis of matched plasma cfDNA samples.

Results

Out of ten CRPC CTC samples analyzed, there was one sample harboring a 2.6 Mb inversion with one breakpoint occurring in intron 1 of *AR*, and the other breakpoint occurring within *ZC4H2*. This *AR* gene rearrangement was not detected in matched cfDNA. Conversely, two cfDNA samples were found to harbor *AR* gene rearrangements that were not detected in matched CTC samples. These findings demonstrated an unexpected discordance of *AR* gene rearrangement detection between liquid biopsy sources. Interestingly, we also observed discordance in the detection of *AR* T878A SNVs between matched CTC/cfDNA samples.

Conclusions

We optimized a CTC capture and analysis pipeline for detection of *AR* gene rearrangements in CRPC patient liquid biopsies. Comparing this pipeline to standard cfDNA analysis revealed that *AR* gene rearrangements and SNVs found in both liquid biopsy sources provide complementary information on *AR* gene aberrations. These findings suggest that analysis of CTC DNA and cfDNA may be necessary to obtain an accurate understanding of the *AR* gene aberration landscape in CRPC.

Background: Aging is the single largest risk factor for many common diseases that burden public health. For example, as men age, the prostate undergoes a prototypical aging change, fibrosis. The aged fibrotic prostate contributes to urinary symptoms, which will afflict nearly every man if they live long enough. However, the molecular mechanisms responsible for the aging-dependent promotion of fibrosis in prostate are largely unknown and understudied. We sought to reveal the contribution of mitochondrial dysfunction to fibrosis in the aging prostate, ultimately leading to urinary symptoms, and overall poor health.

Methods: Immunohistochemistry was performed on formalin-fixed, paraffin-embedded human and rodent tissue samples using Ndufs3 and PINK1 as markers for altered mitochondrial homeostasis. Additionally, tissues were assessed for fibrosis using picrosirius red (PSR) staining. BHPrS1 cells, a human prostate stromal cell line, were treated with 25nM rotenone to inhibit mitochondrial electron transport chain complex I. qPCR was performed to assess gene expression of collagen genes.

Results: The demise of mitochondrial function is well established in other aging-associated diseases but has not been investigated in the prostate. Our analysis revealed altered mitochondrial homeostasis in benign prostatic hyperplasia (BPH) patient tissue compared to normal prostates. A selective inhibition of mitochondrial complex I by rotenone in cultured human prostate fibroblasts led to myofibroblast phenoconversion as characterized by increased expression of Col1a1, Col3a1, and ACTA2. Furthermore, rotenone treatment of Lewis rats leads to an increase in prostatic collagen as measured by PSR. To determine the contribution of mitochondrial dysfunction on lower urinary tract dysfunction (LUTD), we examined the prostate lobes in both aging and steroid-induced LUTD in mice. These models have been extensively characterized and exhibit an age-mediated increase in LUTD and fibrosis. We observed a altered mitochondrial homeostasis corresponding to an increase in fibrosis and LUTD.

Conclusions: Our data suggest that normal aging-dependent reductions in mitochondrial function may contribute to BPH and lower urinary tract symptoms. Specifically, the inhibition of mitochondrial complex I leads to an increase in collagen gene expression and increases collagen deposition in an animal model. Additionally, mouse models of LUTD show an increase in mitochondrial dysfunction. The findings in this study could lead to new avenues of treatment for BPH that target mitochondrial deficiencies to reverse fibrosis.

Spindle assembly checkpoint serine / threonine kinases BUB1 and BUB1B have distinct actions in castration-resistant and chemo-resistant prostate cancer

Background

Using a systems biology approach, we identified a clinically relevant androgen receptor (AR) variant-driven seven gene network[(1)]. This gene set includes BUB1 and BUB1B, serine threonine kinases, which are related proteins that exert different functions on the spindle assembly checkpoint (SAC). Although the expression of both BUB1 and BUB1B genes are upregulated in CRPC patient samples, little is known regarding their roles in PC progression or their link to the AR pathway.

Methods and Results

To understand BUB1 and BUB1B function within the seven gene network, we individually depleted both kinases and measured expression of the other gene set members. Depletion of BUB1B, but not BUB1, downregulated all but one member of the set, suggesting that BUB1B is of particular importance in regulating the gene network in CRPC. While all evaluated PC cell lines expressed similar amounts of BUB1 and BUB1B, individual depletion of these kinases resulted in decreased proliferation in CRPC but not androgen-dependent PC cells. The anti-proliferative effects of BUB1 and BUB1B depletion was associated with prolonged mitosis and cell cycle inhibition in CRPC cells. Depletion of BUB1 and BUB1B also decreased expression of specific AR and AR-V7 target genes in CRPC cells under androgen-depleted conditions suggesting that BUB1 and BUB1B enhance AR ligand-independent signaling. BUB1B knockdown resulted in decreased levels of AR and AR-V7 protein, but not mRNA, in CRPC cells. In contrast, neither BUB1 nor BUB1B depletion in androgen-dependent PC cells affected AR transcriptional activity or AR levels. Since SAC dysregulation is a well characterized mechanism of taxane resistance, we analyzed the expression of BUB1 and BUB1B in taxane sensitive (TxS), resistant (TxR) and cabazitaxel resistant (cabR) PC cell lines. Expression of both genes was higher in TxR and cabR compared to their chemosensitive counterparts. Furthermore, inhibition of BUB1 kinase activity (BAY1816032) sensitized TxR and cabR cells to docetaxel and cabazitaxel treatment.

Conclusion

Collectively, our data indicate that both BUB1 and BUB1B have important but distinct roles in CRPC. Our results suggest that BUB1B represents a vulnerability in CRPC since it participates in a positive feedback loop to AR signaling likely through post-translational regulation of AR and AR-V7. On the other hand, BUB1 plays a role in taxane resistance. These results support investigation of BUB1 and BUB1B as therapeutic targets in CRPC.

(1) Magani F, Bray ER, Martinez MJ, Zhao N, Copello VA, Heidman L, Peacock SO, Wiley DJ, D'Urso G, Burnstein KL. 2018. Identification of an oncogenic network with prognostic and therapeutic value in prostate cancer. Mol Syst Biol. 14(8): e8202. doi: 10.15252/msb.20188202.

Background: There is tremendous need for improved prostate cancer (PCa) models. The murine prostate is anatomically and developmentally different from the human prostate, and does not form sporadic tumors. Furthermore, engineered mouse models lack the heterogeneity of human disease, are often driven in a contrived manner, and rarely (if ever) establish metastatic growth. Human xenografts represent an alternative, but they rely on tumor growth in an immunocompromised host, preventing the study of tumor-immune interactions and immunotherapies. Accordingly, we generated PCa xenograft models in a murine system with an intact human immune system to test the hypothesis that humanizing tumor-immune interactions would improve modeling of metastatic PCa, and further-enable improved modeling of hormonal and immunotherapies.

Methods: Male huNOG mice were produced at Taconic Biosciences by engrafted juvenile NOG mice with human CD34+ hematopoietic stem cells. These mice stably maintain multiple human cell linages, including functional human T-cells. We utilized two human PCa xenograft cell line models transduced with luciferase to assay organ-specific metastatic growth. First, castrated and intact control mice were injected subcutaneously with 22Rv1 cells. When tumors reached >100mm^3, half of the castrated mice were treated with enzalutamide (enza), then tumor growth was monitored to endpoint. Additionally, VCaP tumor–bearing mice were castrated when the tumors were ~200 mm^3 in size, and once the tumor grew back, they were randomized and treated with enza and/or the anti-PD-1 antibody pembrolizumab (pembro), with vehicle controls. At sacrifice, organs were *ex-vivo* analyzed for metastatic growth, tumor infiltrating lymphocytes, and splenic immune reconstitution.

Results: With 22Rv1, subcutaneous tumor size was not significantly altered across conditions; however, the extent and growth at the secondary sites differed markedly in castrate huNOG vs conventional NOG mice treated with enza. VCaP xenograft tumors showed marked decreases in growth with enza and pembro treatments in huNOG mice, and no effect was seen for either of these treatments in NOG mice. Furthermore, enza responses in huNOG and NOG mice were distinct, and associated with increased CD3+ T-cells within tumors of enza treated huNOG mice, and increased CD3+ T-cell activation, accessed by intracellular interferon-γ.

Conclusions: These results illustrate, to the best of our knowledge, the first model of human PCa that metastasizes to clinically relevant locations, has intact human immune system, and responds appropriately to standard-of-care hormonal therapies.

Interactions between Androgen- and Hedgehog-Signaling maintain the cellular niche for pubertal prostate morphogenesis and growth

Background: The essential role of mesenchymal androgen signaling in the development of prostate epithelium has been known for over 30 years. However, the identity of the mesenchymal cells responsible for this paracrine regulation is unknown. In addition, the underlying mechanisms underlying stromal androgen action as the cell niche in facilitating prostatic stem/progenitor cells in pubertal prostatic epithelial morphogenesis and growth are largely unknown.

Methods: *ROSA26R*$^{mTmG/+}$*:Ar*$^{LoxP/Y}$*:Gli1*$^{CreERT2/+}$ mice and *ROSA26R*$^{mTmG/+}$*:Gli1*$^{CreERT2/+}$ control littermates were administered Tamoxifen (TM) at postnatal day 14 (P14), and then systematically examined at P17, P35, and P56: before, during, and after puberty, respectively. Prostate tissues were dissected from AR-deficient and control mice at P35 following TM administration at P14, and prostatic cells were isolated for single cell RNA sequencing analyses.

Results: Selective deletion of androgen receptor (AR) in stromal Shh-responsive cells significantly impedes pubertal prostatic epithelial morphogenesis and growth. AR deletion increased *Gli1* expression in prostatic stromal cells, elevated *Shh* expression in adjacent epithelial cells, and induced stark inhibition of prostate epithelial growth. Dysregulation of Shh and other developmental pathways revealed in both prostatic stromal and epithelial cells of AR-deficient mice at single-cell resolution. Trajectory analysis further revealed abnormal differentiation patters of prostatic epithelia in mutant mice. Recombination of wild-type prostatic epithelial cells with AR-deficient stromal *Gli1*-expressing cells failed to develop normal prostatic epithelia.

Conclusions: These data provide novel, high-resolution insight into the regulatory mechanisms for androgen-Shh signaling in the cellular niche to control pubertal prostate morphogenesis and growth.

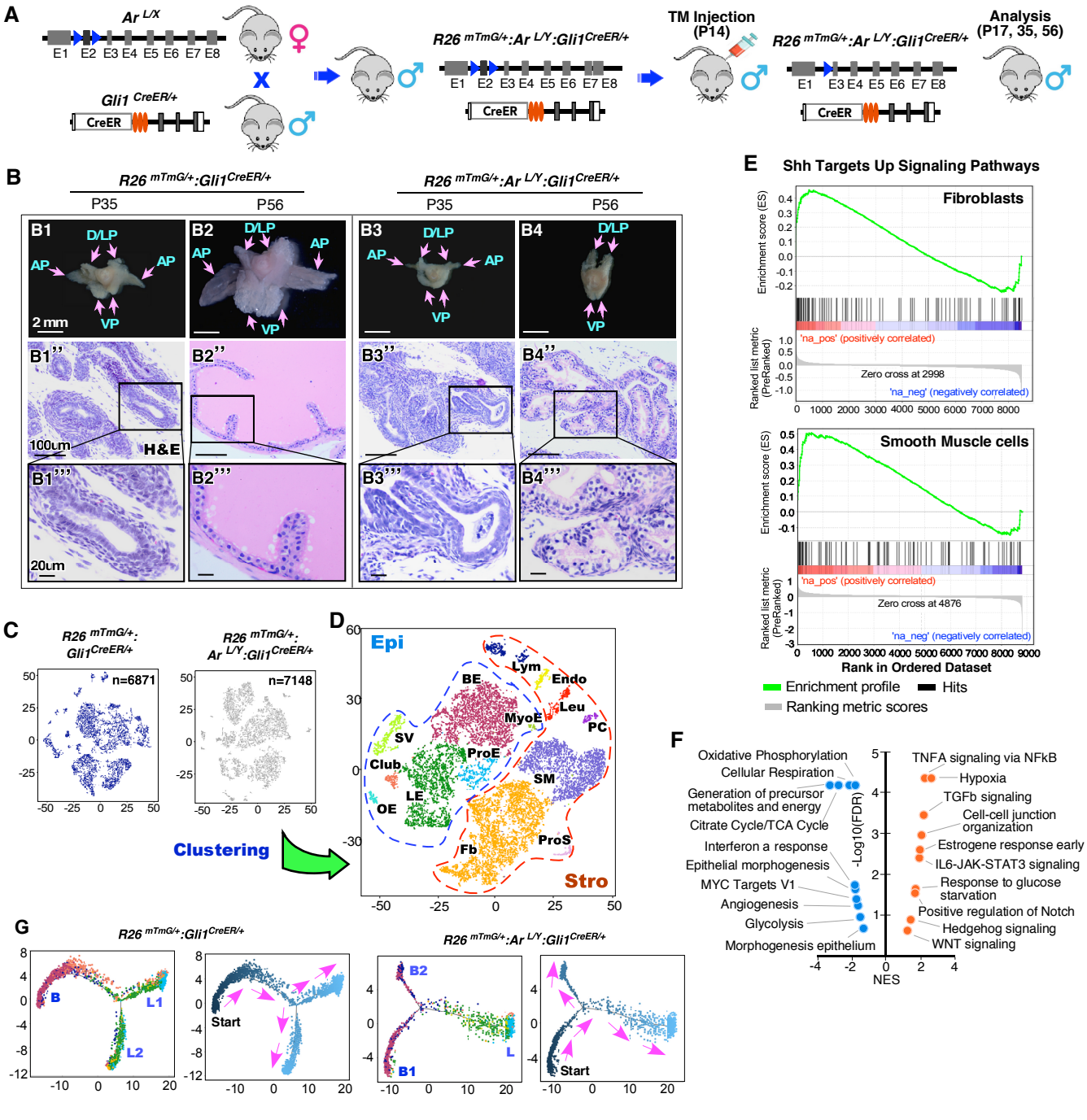

(A) Schematic for generating *R26*$^{mTmG/+}$*:Gli1*$^{CreER/+}$, and *R26*$^{mTmG/+}$*:Ar*$^{L/Y}$*:Gli1*$^{CreER/+}$ mice.
(B) Representative images of prostates isolated from the indicated genotypes at day 35 and 56 postnatal. AP: anterior prostate; DLP: dorsolateral prostate; VP: ventral prostate.
(C) tSNE plot showing dimensional reduction of the distribution of 6871 individual cell transcriptomes from *R26*$^{mTmG/+}$*:Gli1*$^{CreER/+}$ and 7148 individual cell transcriptomes from *R26*$^{mTmG/+}$*:Ar*$^{L/Y}$*:Gli1*$^{CreER/+}$.
(D) tSNE plot showing major clusters of epithelial and stromal lineages based on their transcription profiles.
(E) GSEA enrichment plots showing similar significant positive enrichment of Shh pathway in fibroblasts and smooth muscle.
(F) GSEA analysis with a p-value based, pre-ranked gene list comparing basal cells from ARKO versus control samples.
(G) Trajectory analysis of epithelial cells shows the differences in cell differentiation from *R26*$^{mTmG/+}$*:Gli1*$^{CreER/+}$ and *R26*$^{mTmG/+}$*:Ar*$^{L/Y}$*:Gli1*$^{CreER/+}$.

ANDROGEN ACTION IN CELL FATE AND COMMUNICATION DURING PROSTATE DEVELOPMENT AT SINGLE-CELL RESOLUTION

Background: Androgen signaling pathways are essential for prostate development, morphogenesis, and regeneration. Early tissue recombination studies showed that mesenchymal, rather than epithelial, AR signaling plays a decisive role in inducing development of the prostatic epithelium through paracrine regulation. However, the molecular mechanisms underlying AR-initiated mesenchymal-epithelial interactions in prostate development remain unclear.

Methods: Using gene-targeting approaches, we generated a new mouse model, $Ar^{IRES\text{-}Cre}$ mice, by inserting *Cre* recombinase into the mouse *Ar* gene locus on the X chromosome through an engineering internal ribosome entry site (IRES) within the 3' untranslated region. Utilizing single-cell mRNA sequencing (scRNAseq) and other experimental approaches, we evaluated the cellular properties of AR-expressing cells at single cell resolution in prostate early development.

Results: We profiled the transcriptomes of more than 9000 cells isolated from murine E17.5 UGS tissues and identified a variety of urogenital mesenchyme (UGM) and epithelial (UGE) cell populations. The expression of AR and other regulators were assessed in different cell types at single cell resolution to determine their roles and interactions during early prostate development. Pseudotime analyses further explored the differentiation trajectory of UGM and UGE cell populations, and identified a *Zeb1*-expressing progenitor population. Using mouse genetic tools, the decisive role of mesenchymal AR action in prostate initiation was further determined.

Conclusions: These data provide novel, high-resolution insight into AR signaling and its roles in initiating dynamic interactions with distinct signaling pathways between prostatic mesenchymal-epithelial cells.

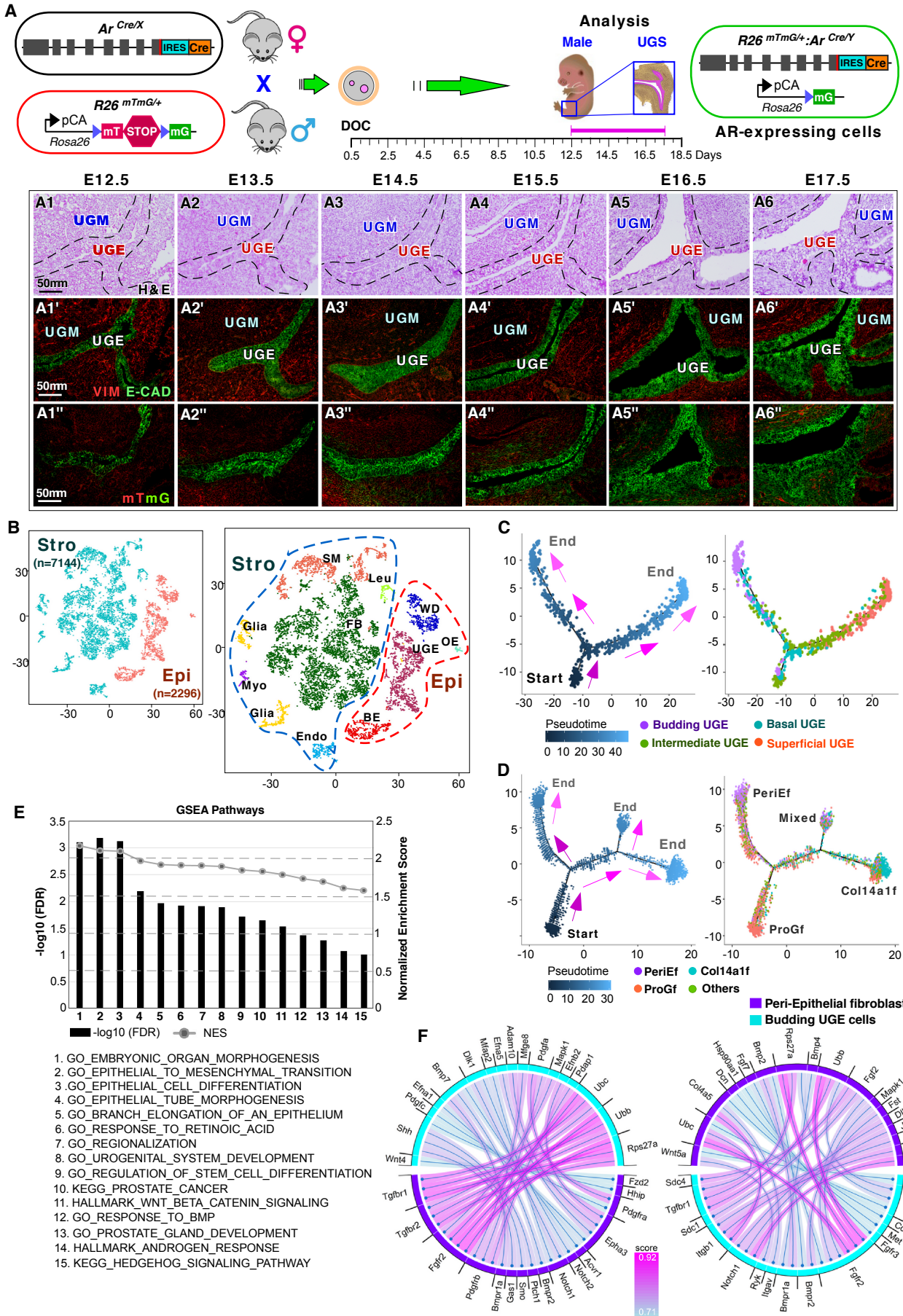

A. Generation and characterization of *Ar*$^{IRES\text{-}Cre}$ mice. Genetic construct of the targeted *Ar* allele displaying the inserted IRES and Cre sequences. Schematics of the *Ar*$^{IRES\text{-}Cre}$ and *R26*$^{mTmG/+}$ alleles are shown in relation to the mating strategy for this experiment. Following the day of conception (DOC), a timeline is provided indicating the days of analysis as shown. A construct is displayed demonstrating the recombination event that will take place in *Ar* expressing cells resulting in a change from red to green fluorescence. A1-A6 Representative H&E images with dashed lines separating urogenital sinus epithelium and mesenchyme at the indicated time points. A1'-A6" Representative fluorescence imaging for the indicated proteins/antibodies. **B. Single-cell RNA sequencing of E17.5 male mouse UGS.** Gene expression tSNE plots for the indicated epithelial and stromal cell marker genes. Identification of cell types as indicated within the original clustering results. **C. Trajectory analysis of the urogenital sinus epithelium.** Pseudotime plot displays a predicted directional path of differentiation between cell types as indicated. **D. Trajectory analysis of fibroblast cells.** Pseudotime indicates a predicted pathway of differentiation between the fibroblast subtypes as indicated. **E. GSEA pathway analysis.** GSEA pathway analysis results comparing the peri-epithelial fibroblast clusters to the remaining fibroblasts. **F. Predicted ligand-receptor interactions** between budding UGE cells and peri-epithelial fibroblasts as indicated, generated using SingleCellSignalR. Color scale corresponds to interaction scores for each interaction.

Urinary levels of miR-491-5p and miR-592 as potential clinical biomarkers in female aging patients with OAB.

Philippe Cammisotto[1], Abubakr H Mossa[1], Samer Shamout[1,2], Lysanne Campeau[1,2]

1, Lady Davis Institute, McGill University, Montreal, Quebec, Canada.

2, Urology Department, Jewish General Hospital, Montreal, Quebec, Canada

Background: Overactive bladder syndrome (OAB), a common condition associated with aging, is characterized by a decrease in the ratio NGF/proNGF in urine of patients. In order to reinforce the clinical value of this observation, we measured the relative amount of several urinary microRNAs (miRNAs) involved in the processing of these neurotrophins and their receptors.

Methods: Urine and blood samples from women with OAB ad controls between the age of 50 and 80 years old were gathered together with validated questionnaires. Results were adjusted for age, sex, medication and insulin sensitivity. MiRNAs were measured by RT-qPCR.

Results: Levels of miRNAs (miR-98-5p, let-7b-5p and let-7d-5p) implicated in the translational control of proNGF were similar between groups. On the other hand, levels of miR-491-5p was strongly decreased in OAB. The latter directly controls the translation of matrix metalloproteinase-9 (MMP-9), the main enzyme hydrolysing NGF into peptides. MiR-885-5p, associated with indirect translational control of MMP-9, was expressed at similar levels between groups. The microRNAs MiR-92a-3p and 221-5p that control expression of the survival receptor TrkA were unchanged between groups. However, lower levels of miR-592 were measured in OAB group, which suggests an increase in the pro-inflammatory receptor $p75^{NTR}$ synthesis as miR-592 normally downregulates it. Finally, no change was observed for markers of nerve integrity (miR-21-5p, miR-132 and miR-212-5p). ROC curves confirmed a high sensitivity of miR-491-5p and miR-592 for diagnosis.

Conclusions: Together, our results suggest that OAB is associated with enhanced inflammatory pathways through: 1) elevated proteolysis of NGF consecutive to high MMP-9 activity; and 2) increased expression of the proinflammatory receptor $p75^{NTR}$. These results may prove useful for diagnosis and treatment of OAB.

The LOU rat, a new model of healthy aging to study bladder diseases

Philippe Cammisotto[1], Abubakr H Mossa[1], Monica Velasquez-Flores[1], Lysanne Campeau[1,2]

1, Lady Davis Institute, McGill University, Montreal, Quebec, Canada.

2, Urology Department, Jewish General Hospital, Montreal, Quebec, Canada

Background: Aging is associated with the development of several benign urological conditions such as voiding dysfunction and benign prostatic hyperplasia. Using a rodent model of healthy aging (the LOU rats), we examined the effect of partial urethral obstruction on proteins involved in bladder contraction and protein markers of OAB (NGF and proNGF).

Methods: LOU rats aged 6 or 36 months were subjected to partial bladder urethral obstruction (PUO) for 2 weeks. Conscious cystometry was then carried out to assess voiding parameters, followed by in vitro assessment of detrusor contractile properties. Tissue proteins were examined by immunoblotting and microscopy (Masson trichrome and hematoxylin-eosin).

Results: Body weight and glycaemia were not affected by age or surgery. PUO increases significantly the ratio bladder mass/body weight with increased thickness and fibrosis of the bladder wall as revealed by histology. Cystometry parameters were unchanged by PUO in old LOU rats while the inter-micturition intervals, micturition volume and bladder capacity were increased in young LOU rats. Contraction of bladder strip in vitro was not affected by age or PUO, which could be related to an increase of smoothelin content with PUO in both age groups, a protein of the cytoskeleton essential to detrusor contraction. On the other hand, levels of smooth muscle myosin heavy chain 1 (SMMHC1), alpha- and beta- actin and connexin were not different across all groups. CK17 expression, an index of urothelial integrity, was also similar between groups. PUO in old rats only led to an increase in E-cadherin, a junction protein essential in cell

proliferation, as well in phospho-JNK, an index of detrusor contractility. Finally, the ratio NGF/proNGF, a marker of OAB was decreased with PUO in both groups of animals, with decreased expression of $p75^{NTR}$ and unchanged expression of its cofactor sortilin.

Conclusions: Young LOU rat bladders respond to PUO by increasing their bladder capacity and micturition volume, while old ones maintain the same voiding parameters. The old LOU rats, a model of healthy aging, showed several changes in protein expression in response to PUO, all the while maintaining their voiding efficiency after PUO. Together, our findings introduce a new interesting model to study the effect of age and the evolution of diseases affecting the bladder.

Regulation of megalin by vitamin D as the mechanism for differential levels of intra-prostatic androgens between African American and Caucasian men

J Garcia, Z Richards, M Zenner, Y Wang, P Gann, G Prins, L Nonn

Prostate cancer (PCa) is a hormonally driven cancer and is currently the third most common cancer in the US. African American (AA) men are disproportionately at risk for both PCa and vitamin D (vitD) deficiency compared to white men. The numerous chemopreventative properties of vitD and epidemiological relationship of vitD status with PCa aggressiveness and mortality has led to the hypothesis that vitD deficiency is a biological contributor to PCa disparity in AA men. Our lab recently reported an unexpected relationship between serum and intraprostatic vitD metabolites 25-hydroxyvitamin D (25(OH)D) and 1,25-dihydroxyvitamin D in AA men. We also observed that Megalin, a multi-liganded endocytic membrane receptor encoded by the gene *LRP2,* was expressed in the prostate epithelium and is regulated by vitD. Extra-renal activity of Megalin has not been well studied as the widely accepted Free Hormone Hypothesis assumes passive diffusion of circulating free hormones into tissues. The presence of megalin suggests that globulin bound hormones from the circulation, including 25(OH)D bound to vitamin D binding protein (DBP) and testosterone (T) bound to sex hormone binding globulin (SHBG), are imported into the prostate in a regulated manner. Here we examine megalin as a potential mechanism to regulate globulin bound hormone import into the prostate. 25(OH)D decreased expression of *LRP2* in primary prostate epithelial cells and fresh human prostate tissue slice explants. DBP-bound 25(OH)D and SHBG-bound T were imported into these prostate models and transcriptionally active. Lastly, we quantified T and its active metabolite dihydrotestosterone (DHT) in the patient cohort from our prior study. Prostatic DHT levels inversely correlated with serum 25(OH)D status. AA men had higher levels of DHT in prostate tissue compared to white men. These clinical findings support our hypothesis that vitD status regulates intraprostatic hormone levels. In summary, we report the presence of a negative feedback loop in which vitD deficiency increases hormone import into prostate epithelium via megalin. Therefore, the upregulation of megalin in the setting of vitamin D deficiency may facilitate increased import of circulating sex steroids into the prostate contributing to carcinogenesis in AA men.

Global changes in membrane lipid metabolism by inhibition of fatty acid synthase in prostate cancer

Yeung Ho, Frank Vanderhoydonc, Jonas Dehairs, Giorgia Zadra, Caroline Ribeiro, Johan Swinnen, Massimo Loda, Scott Dehm

Background: A hallmark of prostate cancer progression is dysregulation of lipid metabolism via overexpression of fatty acid synthase (FASN), a key enzyme in de novo fatty acid synthesis. Castration resistant prostate cancer (CRPC) develops resistance to inhibitors of androgen receptor (AR) signaling through a variety of mechanisms, including the emergence of constitutively active AR variants. Previously, we studied an irreversible FASN inhibitor (IPI-9119) and demonstrated that IPI-9119 promoted endoplasmic reticulum (ER) stress, which inhibited protein expression and transcriptional activity of both full-length AR and AR variants. Because ER stress is known to be influenced by membrane lipids, the goal of this study was to investigate the lipid metabolic effects of IPI-9119 in prostate cancer.

Methods: AR-positive LNCaP and AR/AR-variant positive LNCaP95 cells were treated with IPI-9119 over a 6-day time course. Cell pellets were subjected to comprehensive lipidomic profiling of over 1800 lipid species across 16 different lipid classes. We performed integrative analysis of lipidomic changes and gene expression changes observed in RNA-seq data from IPI-9119 treated cells.

Results: IPI-9119 induced a progressive decrease in the levels of abundant triacylglyceride (TAG) species in both cell lines. Interestingly, treatment with IPI-9119 promoted a progressive increase in specific membrane sphingolipid species, which matched the kinetics of reduced AR and AR variant protein expression in these cell line models. An increase in sphingolipid levels in response to IPI-9119 treatment was consistent with concomitant up-regulation in gene expression levels of *CERS2* and *CERS4*, which encode sphingolipid synthesis enzymes ceramide synthase 2 and 4. IPI-9119 treatment also increased the levels of specific glycerophospholipid (GPL) species, which was accompanied by altered expression of GPL regulators *ACSL1*, *AGPAT2*, and *AGPAT6*.

Conclusions: Inhibition of FASN with IPI-9119 promotes widespread changes in lipid metabolites and expression of genes that regulated lipid metabolism. Our work demonstrates up-regulation of sphingolipids and GPL species with kinetics that mirror the reduction in expression of AR and AR variants in IPI-9119-treated prostate cancer cell line models. We have further identified key regulators of these lipid species that display altered gene expression in response to IPI-9119.

Discovery of PTN as a serum-based early biomarker for poor prognosis prostate cancer

Shiqin Liu[1,2], Michelle Shen[1,2], En-Chi Hsu[1,2], Chiyuan Amy Zhang[3], Fernando Garcia-Marques[1,2], Rosalie Nolley[3], Kashyap Koul[1,2], Meghan A. Rice[1,2], Merve Aslan[1,2], Sharon J. Pitteri[1,2], Charlie Massie[4,5,6], Anne George[5], James D. Brooks[2,3], Vincent J Gnanapragasam[4,7*] and Tanya Stoyanova[1,2*]

1. Department of Radiology, Stanford University, Stanford, CA, USA. 2. Canary Center at Stanford for Cancer Early Detection, Stanford University, Palo Alto, CA, USA. 3. Department of Urology, Stanford University, Stanford, CA, USA. 4. Cambridge Urology Translational Research and Clinical Trials, Cambridge University Hospitals NHS Trust & University of Cambridge Cambridge, UK. 5. Urological Malignancies Programme, CRUK Cambridge Cancer Centre, Cambridge, UK. 6. Early Detection Programme, CRUK Cambridge Cancer Centre, Cambridge, UK. 7. Academic Urology Group, Department of Surgery, University of Cambridge, Cambridge, UK.

Abstract

Background: Prostate cancer is the most common non-cutaneous cancer and the second leading cause of cancer-associated deaths in men in the US and UK. One of the major clinical challenges in prostate cancer is distinguishing clinically significant from indolent disease. Here, we utilized a targeted human protein biomarker discovery approach and identified pleiotrophin (PTN) as a potential prognostic serum and tissue biomarker for clinically significant prostate cancer.

Methods: Serum samples from 4 different groups: 1) cancer-free group, 2) Cambridge Prognostic Group 1 (CPG1) disease with 97% 10 year survival, 3) Cambridge Prognostic Group 5 (CPG5) disease with 50% 10 year survival, and 4) men with metastatic disease at diagnosis were analyzed using high-multiplex immunoassays from Olink Proteomics (n=20 samples per group). PTN was selected for further validation by sandwich ELISA in the discovery cohort and immunohistochemical analysis in a validation cohort.

Results: We discovered that nine out of 174 proteins are significantly elevated in metastatic prostate cancer patients when compared to all other groups. PTN levels are significantly increased in CPG5 and metastatic prostate cancer serum samples in comparison to those from cancer-free and CPG1 groups. Moreover, high levels of PTN in localized prostate cancer tissues are predictive for biochemical recurrence ($p<0.05$) and correlate with pre-operative serum prostate specific antigen levels ($p=0.003$), pathological tumor stage ($p=0.0083$), and biopsy Gleason Score ($p=0.0012$). High tissue PTN level was an independent predictor of biochemical recurrence in patients with low pathological Gleason Grades ($p<0.05$).

Conclusions: Serum PTN expression may be specific for the presence of poor prognosis local and metastatic disease. PTN may also serve as a predictor of disease progression. Our data justifies its further evaluation as a potential early detection biomarker of lethal disease.

Background:
Prostate cancer is the second leading cause of male cancer death in the United States. While localized disease can be cured by radiation or surgery, metastatic prostate cancer presents a clinical challenge. Metastatic prostate cancer can initially be controlled by endocrine therapies that target the androgen receptor (AR), however, these tumors will inevitably develop resistance. This stage of the disease, termed castration-resistant prostate cancer (CRPC), is responsible for practically all prostate cancer-specific deaths. Truncated AR variant (AR-V) proteins are broadly enriched in CRPC cell lines and clinical samples, and can function as ligand-independent, constitutively active transcription factors. Recent studies have indicated that AR-V expression levels are regulated by mRNA polyadenylation.

Methods:
To understand the mechanism of *AR* polyadenylation in greater detail, we conducted biochemical assays examining the roles of candidate trans-acting factors and cis-regulatory elements in regulation of *AR* alternative polyadenylation and growth of CRPC cells. We used siRNA and shRNA strategies to perform knockdown of trans-acting factors and used antisense-oligomers to disrupt cis-regulatory sequences that regulate alternative polyadenylation of *AR*.

Results:
Several well-characterized AR-Vs, such as AR-variant-7 (AR-V7) and AR variant-9 (AR-V9) arise from splicing of different cryptic exons (CEs), located within intron 3 of the *AR* gene to *AR* exon 3. We found that blocking the alternative poly(A) site in *AR* exon CE3 reduced expression of AR-V mRNAs and protein and increased expression of full-length AR mRNA and protein in 22Rv1 CRPC cells, suggesting this single alternative poly(A) site in exon CE3 is utilized to generate AR-Vs, including AR-V7 and AR-V9. We also found the CPSF complex component, CPSF1, regulated selection of this alternative poly(A) site based on the finding that knockdown of CPSF1 in 22Rv1 cells reduced expression of AR-Vs and increased expression of full-length AR. Our data has also nominated a negative regulatory region ~50 bp downstream of the poly(A) site in exon CE3, which can be repressed to induce *de novo* expression of AR-V7 in AR-V negative LNCaP cells.

Conclusions:
These results have identified a single alternative poly(A) site in exon CE3 of *AR* that regulates expression of full-length AR and AR-Vs in CRPC cells and have determined CPSF1 as a trans-acting regulator of the poly(A) site, highlighting new drug targets for CRPC treatment.

DAB2IP modulates primary cilia formation associated with renal tumorigenesis

Chun-Jung Lin, Andrew Dang, Elizabeth Hernandez, Jer-Tsong Hsieh

UT Southwester Department of Urology, University of Texas Southwestern Medical Center, Dallas, TX, 75390, USA

ABSTRACT

Background:

Primary cilium is a microtubule-based organelle that projects from the surfaces in most mammalian cell types. Primary cilia protrude into the extracellular milieu (ciliogenesis) as an antenna-like sensor to senses extracellular physical and biochemical signals, then transmit signals into cell to regulate numerous physical and developmental processes. Also, loss of primary cilia is often found in many cancer types, including skin, breast, pancreas, ovarian, prostate and kidney cancers. Our previous studies demonstrate that loss of DAB2/DOC2 Interacting Protein (DAB2IP) is frequently associated with renal cell carcinoma (RCC). Recently, we observed that loss of DAB2IP in normal kidney epithelial cell significantly impairs primary cilia formation. Thus, we hypothesize that the tumor suppressor function of DAB2IP is mediated by regulating primary cilia formation.

Methods:

Serum starvation (1% FBS) was used to induce ciliogenesis throughout this study. Primary cilia were visualized by Immunofluorescence staining, and ciliated cells were calculated into percentage. The interaction of KIF3a with DAB2IP was determined by immunoprecipitation, and the interaction between KIF3a and DAB2IP domains was measured by dot blot assay. Tumorigenesis was determined by using colony formation assay, anchorage independent growth assay, and confirm the tumor take in SCID mice model.

Results:

In this present study, we observed an association of DAB2IP with primary cilia structure in normal kidney cell. Therefore, immunoprecipitation of DAB2IP complex was subjected to mass spectrum analysis and KIF3a was identified as an interactive partner. KIF3a is, the most abundant kinesin-2 family protein expressed in cells, one subunit of the heterotrimeric motor protein necessary for ciliogenesis. Data demonstrate a new mechanism of primary cilia maintenance via the physical interaction between KIF3a and the Pleckstrin homology (PH) domain of DAB2IP in which DAB2IP is able to prevent KIF3a protein turnover. Thus, DAB2IP can stabilize KIF3a proteins localized in the axoneme of primary cilia, which is

critical for the integrity of primary cilia. Furthermore, loss of KIF3a could promote renal tumorigenesis, suggesting that DAB2IP-KIF3a complex associated with primary cilia is one of critical homeostatic machinery in normal kidney epithelia.

Conclusions:

In conclusion, these data highlight a new function of DAB2IP in normal kidney cells by regulating primary cilia formation, which is independent from starvation-induced primary cilia pathway. Mechanistically, KIF3a is identified to be a key target that physically interacts with N-terminal PH domain of DAB2IP to stabilize this protein in maintaining primary cilia complex. As expected, loss of KIF3a can leads to the destruction of primary cilia underlying renal tumorigenesis.

Oncolipid Sphingosine Kinase is involved in neuroendocrine transdifferentiation of prostate cancer (NEPC)

Yu-An Chen[1, 2], Cheng-Fan Lee[1,3], Ming-Shyue Lee[3], Chih-Ho Lai[2], Ho Lin[4], Haiyen E Zhou[5], Leland WK Chung[5], Ganesh Raj[1] and Jer-Tsong Hsieh[1]

[1] Department of Urology, University of Texas Southwestern Medical Center, Dallas, TX

[2] Department of Microbiology and Immunology, Graduate Institute of Biomedical Sciences, College of Medicine, Chang Gung University, Taoyuan, Taiwan

[3] Department of Biochemistry and Molecular Biology, College of Medicine, National Taiwan University, Taipei, Taiwan

[4] Department of Life Sciences, National Chung Hsing University, Taichung, Taiwan

[5] Department of Medicine, Cedars-Sinai Medical Center, Los Angeles, CA.

Introduction

Androgen deprivation therapy (ADT) is considered the most effective regimen to treat metastatic prostate cancer (PCa). Eventually, almost all patients develop castration resistant PCa (CRPC) that is often associated with neuroendocrine phenotypes. Until now, there is very limited agents available for NEPC therapy. Obviously, identifying underlying mechanism of NEPC could provide new targeting strategies to eradicate this disease. From cBioPortal of PCa database, it appears that 22% NEPC patients exhibit sphingosine kinase-1 (SphK1) gene amplification as well as positive correlation of expression between SphK1 and NE genes; this enzyme produces sphingosine 1-phosphate (S1P) that is known for tumor cell growth, survival, and therapeutic resistance. Thus, in this study, we have dissected the underlying mechanism of Sphk1-elicited NEPC and further explored Sphk1 as a potential druggable target.

Methods

CRISPR technology was used to knockout (KO) Sphk1 gene in PC3, 22RV1, ARCaP-IIB5 and ARCaP-IIG5 cells and SphK1 cDNA vector was used for overexpression (OE) in LNCaP. The gene expression is measured via qRT-PCR and Western blot. ChIP assay is used to map the interactive site of REST. The REST–transcriptional activity is determined using the luciferase assay from BRN2 and SOX2 gene promoter. The SCID male mice carrying 22RV1 or IIG5 tumor are subjected to experimental therapy.

Results

Elevation of Sphk1 can be detected in several PCa cell lines treated with anti-androgens. Data from SphK1-KO or -OE cells demonstrated the Sphk1-S1P-S1P receptors (S1PRs) is a key pathway to up-regulate the master neural transcription factors (NETFs: BRN2, EZH2, FOXA2 and SOX2) and NE biomarkers leading to the onset of NEPC that is resistant to ADT. Mechanistically, Erk activation by S1P appears to be the key downstream effector of S1PRs, which further phosphorylates REST (a master neural transcriptional repressor) at the S861 and S864 sites resulted in protein degradation. Indeed, elevated REST expression was detected in SphK1 KO cells. ChIP and reporter gene data confirmed the activity of REST in NETF expression and REST OE in PC3, 22RV1 and IIG5 cells significantly reduced NE phenotypes. Noticeably, FTY720 or

SKI-II (Sphk1 inhibitors) exhibited high potency to suppress the growth of 22RV1 and IIG5 using xenograft mouse models.

Conclusions

SphK1-S1P-S1PRs is a critical upstream pathway involved in NEPC progression. SphK1 targeted small molecule inhibitors have potential impact on clinical application on NEPC therapy.

Background: Treatment for localized prostate cancer consists of Androgen Deprivation Therapies (ADTs), which inhibit the androgen receptor (AR). Though initially effective, a subset of patients will develop resistance to ADTs and the tumors will transition to Castration-Resistant Prostate Cancer (CRPC). Treatment of CRPC consists of newer hormonal therapies such as enzalutamide, but it is not curative. Two mechanisms contributing to enzalutamide resistance are the presence of androgen-independent truncated AR proteins called AR splice variants (ARVs) and increased tyrosine kinase pathway activity. Previous work has shown that tyrosine kinase SRC can bind to and phosphorylate critical residues on full-length AR (AR-FL), increasing AR activity in the presence of low androgens. What is unknown is how kinase signaling directly contributes to ARV function in this setting or in lieu of enzalutamide and does this mechanism aid in the observed resistance with newer hormonal therapies.

Methods: We have begun evaluating synergy between enzalutamide or chemotherapy with SRC kinase inhibitors, saracatinib and dasatinib, in prostate cancer cell line models using the Combination Equation via Chou-Talay method. We have chosen four cell lines: DU145, AD-1, R1-D567, and 22Rv1, all of which have SRC. Each cell line expresses a range of AR-FL and ARVs allowing us to elucidate the role of each AR species in synergy. We also have begun to define the mechanism of synergy using IP-western blots, antibody immunofluorescence, and phosphoproteomics to assess SRCs contribution to AR signaling.

Results: We observed synergy between enzalutamide and SRC kinase inhibitors in AR-FL+ cell lines, AD-1, which contains one copy of AR-FL, and 22Rv1, which contains AR-FL and ARVs. We have also observed less synergy between docetaxel and SRC kinase inhibitors in 22rv1 cells. In our variant ARv12 cell line, R1-D567, there is less synergy for both combinations as this cell line is missing AR-FL, allowing us to conclude AR-FL is required for significant synergy. We have also found that enzalutamide and SRC kinase inhibitors when together, can have a dose fold reduction up to five fold, which was not seen in the docetaxel and SRC kinase inhibitor combinations.

Conclusions: By elucidating this synergy, we will provide critical pre-clinical data that could influence how future clinical trials are designed via combining specific SRC kinase inhibitors with enzalutamide, ultimately leading to the goal of increasing survival for men suffering from lethal CRPC.

Background. Risk of prostate cancer (PCa) associates with reduced vitamin D receptor (VDR) signaling in African American (AA) compared to European American (EA) patients, but the mechanism remains enigmatic.

Methods. VDR-dependent ChIP-Seq and RNA-Seq was undertaken in EA (non-malignant HPr1AR and malignant LNCaP) and AA (non-malignant RC43N and malignant RC43T) cells, combined with transcriptomic studies in three PCa patient cohorts.

Results. AA cells have higher VDR protein expression, which genomically binds more frequently, and is more enriched in active and poised enhancers than EA models. SMAD4 and VDR motifs were common in all models, whereas AA peaks were enriched for a larger motif repertoire including RUNX2 and ZBTB33/KAISO, and ERG motifs were enriched in EA peaks. Overlapping with ~10,000 publicly available cistromes revealed that in AA models VDR significantly overlapped with core circadian rhythm transcription factors (e.g. NONO). Integrating VDR-dependent ChIP-Seq and RNA-Seq revealed significantly stronger VDR transcriptional responses in AA models, again enriched for circadian rhythm (NES 2.7) and inflammation.

Using clinical cohorts, we identified serum miRNA expression associated with progression from HGPIN to PCa. In AA men ~30% predicative miRNAs were VDR bound and $1\alpha,25(OH)_2D_3$ regulated in AA cell lines, whereas only ~5% of miRNAs in EA men were VDR-responsive in EA cell lines. For example, miR-199b down-regulation associates with AA progression from HGPIN to PCa, VDR binds and $1\alpha,25(OH)_2D_3$ up-regulates miR-199b in RC43N, but is repressed in RC43T. MiR-199b regulates NPAS2, a core circadian transcription factor. Similarly, we previously reported AA tumors are more $1\alpha,25(OH)_2D_3$-responsive *in vivo*, and we now revealed these genes are enriched for circadian transcriptional regulators (e.g. NOCT) and inflammatory signals. A genome-wide analyses of coregulators in TCGA identified significantly reduced BAZ1A/SMARCA5 expression in TMPRSS2:ERG fusion negative AA PCa. We are currently analyzing RNA-Seq from AA and EA cells with restored BAZ1A expression.

Together, these data suggest VDR transcriptional control in the prostate is most potent and dynamic in AA men, and is primed to govern inflammatory and circadian

pathways. This is suppressed, by altered BAZ1A/SMARCA5 expression and/or reduced environmental-regulated serum vitamin D_3 levels. Therefore, the VDR axis lies at the cross-roads of biopsychosocial processes that contributes to PCa health disparities.

Cooperative actions of a novel ERβ ligand, WTIV012, and enzalutamide in advanced prostate cancer

Jaimie S. Gray, Moray J. Campbell

Background: Early successful therapies in prostate cancer (PCa) included the use of estrogens but were discontinued due to serious side effects. Given estrogen receptor alpha (ERα) and estrogen receptor beta (ERβ) appear to have opposing actions, it is unclear how estrogen actions control PCa growth. The OSU Drug Development Institute has developed a novel compound, WTIV012, that selectively targets ERβ, allowing for the possibility to study ERβ effects in androgen deprivation therapy (ADT) resistant or sensitive PCa.

Methods: A combination high-throughput drug viability screen was undertaken in ADT-sensitive and resistant PCa models that combined multiple concentrations of WTIV012 with 30 compounds including Enzalutamide (Enza), and epigenomic regulators. Quantitative PCR (qPCR) for key genes and RNA-Seq was undertaken for selected WTIV012 combinations.

Results: The 30 different WTIV012 multi-dose combinations were tested in one ADT-sensitive and four ADT-resistant PCa cell lines in duplicate; equivalent to 23,040 dose/drug combinations. Drug interaction delta values were calculated as observed percent inhibition of drug combination minus the expected additive percent inhibition of each drug. All cell lines were sensitive to high doses of WTIV012 alone (1-10μM) whereas each cell line displayed unique responses to WTIV012 drug interactions; 22RV1 cells responded with the greatest additive effects to combinations of WTIV012 with Enza and several histone deacetylase inhibitors (Istodax). We focused on WTIV012 plus Enza for pathway analyses. In the first instance, qPCR in cells treated with WTIV012 plus Enza revealed a significant decrease in transcription of AR target genes including *TMPRSS2* and reduced transcription of AR itself. Currently, we are undertaking RNA-Seq LNCaP, 22RV1 and LNCaP C4-2B in response to estrogen plus Enza or WTIV012 plus Enza to reveal the unique pathways regulated by WTIV012 plus Enza.

Conclusion: The possibility of targeting ERβ in the context of PCa is now becoming a reality with development of the novel, highly selective ERβ agonist, WTIV012. Specifically, this ligand is a powerful tool to understand the specific role of ERβ has on transcriptomic and epigenetic regulation. Our initial data suggest that there is a promising cooperative action between WTIV012 and the ADT drug Enza. Overall, using WTIV012 may prove to be a powerful tool to study estrogen anticancer functions in PCa.

SLC-mediated metabolic reprogramming: A new paradigm for targeting enzalutamide resistance in prostate cancer

Shiv Verma [1,2], Eswar Shankar[1,2] Ricky Chen[3], Sanjay Gupta [1,2,4,5,6*]

1.Department of Urology, Case Western Reserve University, School of Medicine, Cleveland, OH 44106, USA
2.The Urology Institute, University Hospitals Cleveland Medical Center, Cleveland, OH 44106, USA
3.Institute of Computational Biology, Case Western Reserve University, School of Medicine, Cleveland, OH 44106, USA
4.Department of Urology, Louis Stokes Cleveland Veterans Affairs Medical Center, Cleveland, OH 44106, USA
5.Department of Nutrition, Case Western Reserve University, Cleveland, OH 44106, USA
6.Division of General Medical Sciences, Case Comprehensive Cancer Center, Cleveland, OH 44106, USA
*Correspondence: Sanjay Gupta, Ph.D., Department of Urology, The James and Eilleen Dicke Research Laboratory, Case Western Reserve University, 10900 Euclid Avenue, Cleveland, Ohio 44106 USA
Phone: (216) 368 6162; Fax: (216) 368 0213; E-mail: sanjay.gupta@case.edu

Background

Androgen deprivation therapy (ADT) is standard-of-care for advanced-stage prostate cancer, and enzalutamide (Xtandi®), a second generation antiandrogen, is frequently prescribed for use in clinical setting. Response to this medication is usually temporary, and prolong treatment results in the emergence of drug resistance. Therefore, an understanding of molecular mechanism and its association with enzalutamide resistance will facilitate circumventing this problem.

Methods

We employed next generation sequencing (NGS) and compared the transcriptomic profile of paired enzalutamide-sensitive and resistant in two cell lines of prostate cancer; Lymph Node Carcinoma of the prostate (LNCaP) and C4-2 bone metastatic (C4-2B) for identification of genes involved in drug resistance along with *in silico* analysis. Pathway analysis was performed by IPA/iPathway and subset of differentially expressed genes in both cell lines were validated at transcript and protein level by qRT-PCR and western blot respectively.

Results

NGS data identified 9409 and 7757 genes differentially expressed in LNCaP and C4-2B cells respectively compared to their parental counterparts. Pathway analysis revealed metabolic signaling pathway was overrepresented and membrane transporters including solute carrier proteins, ATP-binding cassette transporters and other metabolizing enzymes as the most prominent genes dysregulated during metabolic reprogramming in resistant cell lines. RNA-Seq data of resistant cells demonstrate predominance of solute carrier genes, in particular, *SLC12A5*, *SLC25A17* and *SLC27A6*, during metabolic reprogramming and in the development of drug resistance as showed in figure. Upregulation of these genes were associated with an increase in stemness; higher uptake of lactic/citric acid and lower glucose intake in resistant cells.

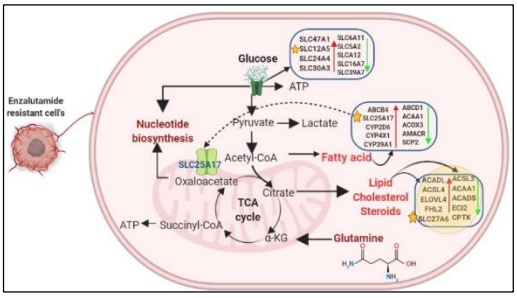

Conclusion

Our data suggest predominance of solute carrier genes (SLCs) during metabolic reprogramming of prostate cancer cells in an androgen-deprived environment. SLCs are important in cellular uptake of nutrients and drug absorption, thus could play a significant role in the emergence of drug-resistant phenotype, designating SLC genes as potentially attractive therapeutic targets.

Supported in parts by the Department of Defense Grants W81XWH-18-1-0618, W81XWH-19-1-0720 and VA Merit Review 1I01BX002494.

TROP2 regulates prostate cancer growth and metastasis through distinct molecular mechanisms

Authors: En-Chi Hsu[1], Shiqin Liu[1], Fernando Jose Garcia Marques[1], Abel Bermudez[1], Merve Aslan[1], Michelle Shen[1], Sharon Pitteri[1], James D. Brooks[2] and Tanya Stoyanova[1]

Affiliations: [1]Department of Radiology, Canary Center at Stanford for Cancer Early Detection, Stanford University, [2]Department of Urology, Stanford University

Background: Prostate cancer is the most common non-cutaneous cancer and second leading cause of cancer related deaths in men in the United States. The first line of treatment for men with advanced prostate cancer is androgen deprivation therapy. Although initial responses are observed, prostate cancer commonly relapses in its lethal metastatic form referred to as castration resistant prostate cancer (CRPC) with 1-2 years mean survival time. Neuroendocrine prostate cancer (NEPC) is highly aggressive, AR independent subtype and usually emerges post castration resistance. We recently identified that the cell surface receptor TROP2, is a new driver of NEPC. Moreover, we demonstrated that TROP2 regulates prostate cancer growth and metastasis. In this study, we set out to delineate the molecular mechanisms through which TROP2 regulates prostate cancer growth and metastasis.

Methods: Proximity-dependent Biotin Identification (BioID) was performed by expressing TROP2-Biotin ligase fusion protein in prostate cancer cell lines to identify TROP2 interactome with biotinylated labels utilizing pull-down methods following with mass spectrometry. Lentiviral infection was used to generate prostate cancer cell lines with over-expression of TROP2 and knock-down of NOTCH1, SLC4A7, PLEC, and OCLN shRNA to modulate gene expression levels. *In vitro* functional assays were performed including colony formation, and Matrigel drop 3D cell invasion assays.

Results: The TROP2 membrane interactome was identified utilizing Proximity-dependent Biotin Identification (BioID) in living cells and uncovered that TROP2-mediated prostate cancer growth and metastasis are orchestrated by distinct downstream pathways including Notch signaling (NOTCH1), control of intracellular pH (SLC4A7), exosome secretion (PLEC), and tight junctions (OCLN). Interaction of TROP2 binding partners including NOTCH1, SLC4A7, PLEC and OCLN with TROP2 were further validated by fluorescence resonance energy transfer (FRET) using confocal microscopy. Moreover, knocking down the TROP2 interacting partners in TROP2 over-expressing prostate cancer cells suppressed TROP2-driven growth and invasion ability.

Conclusions: In a previous study, we identified cell surface receptor, TROP2, as a novel driver of metastatic NEPC. Herein, our new findings reveal that TROP2 interacts with NOTCH1, SLC4A7, PLEC, and OCLN, which may highlight novel biological functions of TROP2 in prostate tumorigenesis and provide new understanding of the potential mechanism of neuroendocrine differentiation and metastasis to develop new therapeutic strategy for metastatic CRPC with neuroendocrine features.

RET Kinase in Neuroendocrine Prostate Cancer

Background: Increased treatment of metastatic castration resistant prostate cancer (mCRPC) with second-generation anti-androgen therapies (ADT) has coincided with a greater incidence of lethal, aggressive variant of prostate cancer (AVPC) tumors that have lost androgen receptor (AR) signaling. AVPC tumors may also express neuroendocrine markers, termed neuroendocrine prostate cancer (NEPC). Recent evidence suggests kinase signaling may be an important driver of NEPC. While kinases such as AURKA have been identified as important for NEPC growth, targeting these kinases for treatment has not dramatically improved patient survival and there remains a need to improve NEPC treatment options.

Methods: To identify targetable kinases in NEPC, we performed global phosphoproteomics comparing AR-negative to AR-positive prostate cancer cell lines and identified multiple altered signaling pathways, including enrichment of RET kinase activity in the AR-negative cell lines. We also analyzed multiple clinical and patient derived xenografts transcript datasets to look for RET kinase expression and enrichment in subsets of patient populations. Finally, we utilized genetic and pharmacological approaches to reduce RET kinase activity in multiple models of NEPC to determine if RET kinase is necessary for NEPC cell growth and proliferation.

Results: We found that RET kinase was highly upregulated and enriched in the NEPC patient samples relative to AdCa or double negative tumor samples. Additionally, we found that knockdown of RET kinase reduced cell proliferation by 80% in NCI-H660 cells and 50% in PC3 cells. Pharmacological inhibition of RET with multiple inhibitors, including AD80, Blu-6667, and LOXO-292, dramatically reduced downstream signaling of ERK1/2 and reduced growth and viability in multiple mouse and human NEPC models.

Conclusions: There are limited treatment options for patients with metastatic aggressive variant prostate cancer and none are curative. Identification of aberrantly expressed RET kinase as a driver of tumor growth in multiple models of NEPC provides a significant rationale for testing the clinical application of RET inhibitors in patients with AVPC.

Epigenetic control of RARγ cross-talk with AR is distorted in advanced prostate cancer

Sajad A Wani, Jaimie S Gray, Hedieh Jafari, Manjunath Siddapa, Moray J Campbell

Division of Pharmaceutics and Pharmacology, The Ohio State University

Background: Epigenetic mechanisms in prostate cancer (PCa) alter androgen receptor (AR) enhancer access resulting in re-wired AR signaling. Reduced RARγ expression is common in PCa, and we sought to understand how miR-96 targeting of RARγ impacts AR signaling, cell fates and promotes PCa progression.

Methods: In HPr1AR, LNCaP and 22RV1 cells we undertook; miR-96 mimic RNA-Seq and mass spectrometry; biotinylated miR-96 to capture binding sites (IMPACT-Seq (*i*dentification of *MiRNA* REs by *p*ull-down and *a*lignment of *c*aptive *t*ranscripts—*seq*uencing)); RIME (*R*apid *i*mmuno- precipitation *m*ass spectrom*e*try) to test RARγ interactions; RARγ Cut and Run ChIP-Seq; viability, invasion and apoptisis assays to test phenotypic consequences.

Results: MiR-96 regulated 1032 mRNA and 891 proteins in LNCaP cells with fewer in HPr1AR and 22RV1, including RARγ and coregulators such as TACC1, and were enriched for miR-96 motifs (e.g. LNCaP RNA NES 5.6, p.adj=0.0005; LNCaP protein NES 2.6, p.adj=0.005) as well as Androgen and MYC networks, and response to Tretinoin (retinoid). IMPACT-seq identified 777 significant miR-96 recognition elements (MREs) in LNCaP cells (log OddRatio > 1, p.adj > 0.1), and fewer in HPr1-AR cells ~ 50% were shared. MiR-96 bound and regulated targets were common. For example, TACC1 contains MREs, was signifantly miR-96 downregulated (-1.6 fold mRNA; p.adj=1.2e^{-8}; - 1.7 fold protein; p.adj = 0.0025), and RARγ and TACC1 physically interact. RARγ-dependent RIME revealed ~ 300 interacting proteins 61% of which contained miR-96 MREs including the AR corepressor PA2G4. Given roles for m6A to regulate MREs access, we are investigating its levels at MREs on miR-96 target genes. The most altered miR-96 bound and regulated genes, including TACC1, plus enzymes that govern m6A, cluster tumors from the SU2C cohort with worse overall survival ($p < 0.001$). 22RV1 cells with modulated RARγ expression display altered regulation of neuroendocrine markers such as CHGA further supporting a role for RARγ to control AR signaling and cell phenotypes. We are currently defining the TACC1-dependent and independent RARγ-AR cistromes and how this controls gene enhancer access for cell fate decision genes.

Conclusions: In summary, our data support the concept that miR-96, a known oncomir, evolves in its choice of binding sites in PCa progression to increasingly suppress the actions of the RARγ network, which cooperates with TACC1 to promote luminal differentiation. Distortion to this network predicts overall survival in advanced PCa.

Tristetraprolin Loss Drives the Progression of Aggressive Prostate Cancer

Katherine L. Morel[1], Anis A. Hamid[2,3], Mariana Secundes[1], Deborah L. Burkhart[1], Massimo Loda[4], Christopher J. Sweeney[2], Leigh Ellis[1,5,6]

[1]Department of Oncologic Pathology, Dana-Farber Cancer Institute, Harvard Medical School, Boston, MA, USA
[2]Lank Center for Genitourinary Oncology, Department of Medical Oncology, Dana-Farber Cancer Institute, Boston, MA, USA
[3]University of Melbourne, Melbourne, VIC, Australia
[4]Pathology and Laboratory Medicine, Weill Cornell Medical College, Cornell University, New York, NY, USA
[5]Department of Pathology, Brigham and Women's Hospital, Harvard Medical School, Boston MA, USA
[6]The Broad Institute, Cambridge, MA, USA

Background:
Lineage plasticity drives therapy resistance and progression of lethal disease, so it is critical to identify actionable targets to inhibit or reverse such cellular changes. Recently, we and others have characterized the molecular landscape of androgen indifferent castrate resistant prostate cancer (CRPC-AI) and have identified and validated genetic-epigenetic mechanisms, including concurrent loss of PTEN and RB1 and/or TP53, and induction of specific epigenetic modifiers, such as EZH2, required for driving prostate cancer (PCa) lineage plasticity. Preliminary data from mouse and human samples of CRPC-AI indicate significant reduction in mRNA destabilizing protein known as Tristetraprolin (TTP - encoded by the *ZFP36* gene) when compared to CRPC adenocarcinomas. TTP binds to AU-rich elements in the 3`-untranslated regions of target mRNAs to promote their degradation. TTP regulates NF-κB through TNF-α mRNA degradation and inhibiting p65 nuclear translocation, and is an important regulator of proper neuronal differentiation.

Methods:
RNA and protein expression in clinical and GEMM PCa data sets were analyzed. Novel genetically engineered mouse models (GEMMs) were generated to represent loss of Ttp alone or in combination with Pten. GEMM tissues were examined by IHC, IF, WB and qPCR, and human and GEMM-derived cell lines were utilized for therapy studies.

Results:
Specific deletion of Ttp in GEMM prostate tissue induces prostatic intraepithelial neoplasia. Co-deletion of Pten and Ttp shows significant acceleration of disease progression, including dissemination of tumor cells to distant tissues, compared to Pten deletion. Further, both low TTP and concurrent low PTEN/TTP expression in multiple PCa patient cohorts selects for most aggressive disease. These patients demonstrate an increased gene signature score of lineage plasticity and EZH2 gene expression. Deletion of Ttp in mouse PCa cells results in an inflammatory tumor phenotype, increased p65 (NF-κB) expression and signaling, reduced AR expression, increased expression of synaptophysin and resistance to androgen deprivation therapy (ADT) with enzalutamide. Dimethylaminoparthenolide (DMAPT), an NF-κB inhibitor, preferentially slows growth of TTP-deficient PCa cells compared to TTP-proficient cells and restores sensitivity to enzalutamide in TTP-deficient cell lines.

Conclusions:
Together, our data demonstrates that TTP is an important regulator of prostate cellular identity, and loss of TTP drives progression of an aggressive prostate cancer phenotype. Of clinical significance, TTP loss provides a novel therapeutic vulnerability to either prevent or reverse resistance to ADT due to lineage plasticity in PCa patients.

TIME- AND DOSE-DEPENDENT, RADIATION CYSTITIS-INDUCED ALTERATIONS TO BLADDER WALL MECHANICAL BEHAVIOR

Authors: Marissa Grobbel, Bernadette M.M. Zwaans, Elijah P. Ward, Laura E. Lamb, Sara Roccabianca

Background

Following radiation treatment for pelvic organ cancer, patients can develop a debilitating disease of the urinary bladder, called radiation cystitis (RC). This can cause bleeding, pain, and kidney disease, limiting a cancer patient's ability to fully recover. To create a deeper understanding of the development of this disease, we have examined the effects of RC on the mechanics of the urinary bladder following radiation.

Methods

At 8 weeks, of age, C57BL female mice were subjected to varying doses of bladder-centered radiation treatment. The doses were: 1x40Gy, 2x28Gy, or 3x22Gy (multiple doses separated by two weeks). Along with age-matched controls, the mice were euthanized at either 3 months or 6 months after treatment, and their urinary bladders isolated (sample sizes in **Figure 1**). Each bladder was decellularized, sliced into circumferential rings, and subjected to a uniaxial stress-strain test. The resulting stress-strain curve and stiffness at an estimated "micturition" point (based on bladder capacity and geometry) were calculated.

Results

From the stress-strain curves, at 3 months, the 1x40Gy dose was slightly less distensible ($P < 0.1$) than the control group, **Figure 1**. At 6 months, no irradiated bladders showed differences from the controls, though the 3x22Gy was less distensible ($P < 0.05$) at mid-level stresses than the 1x40Gy. There were no time-related differences in the stress-strain curves. The stiffness at micturition was significantly higher ($P < 0.05$) for 1x40Gy and 2x28Gy (as well as the compiled irradiated data) than the controls, at 3 months following treatment, **Figure 1**. These significantly increased stiffnesses returned to control levels at 6 months.

Conclusions

Though differences between doses, controls, and time points were limited in the stress-strain curves, there were several significant differences in the stiffness at micturition. Namely, at 3 months, two radiation doses showed a significantly higher stiffness, which decreased by the 6-month time point. Overall, this study suggests the possibility of a dose-dependent increased bladder stiffness as a response to radiation, followed by a time-dependent recovery.

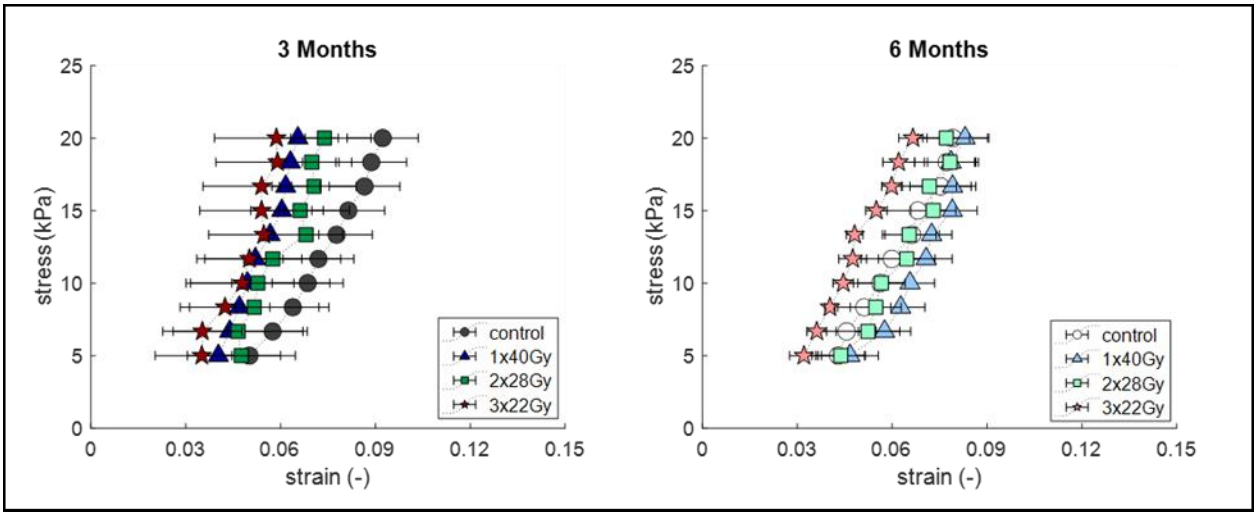

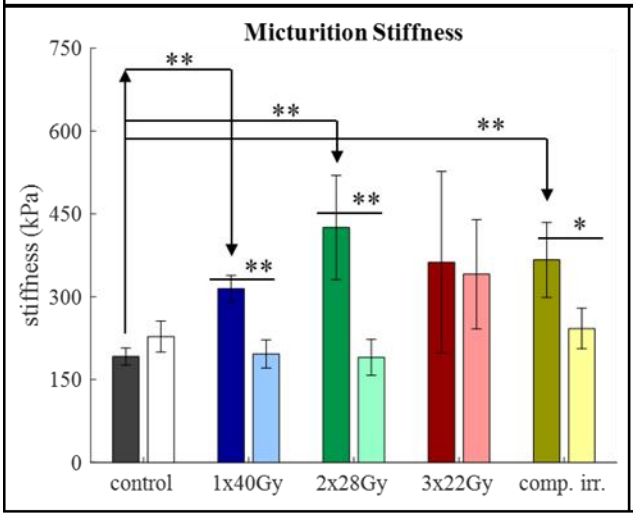

Figure 1. Top: stress-strain curves. Bottom-Left: stiffness at micturition (3 months in dark colors, 6 months in light).

3-month sample sizes: control (n = 7), 1x40Gy (n = 2), 2x28Gy (n = 2), 3x22Gy (n = 3).

6-month sample sizes: control (n = 4), 1x40Gy (n = 5), 2x28Gy (n = 5), 3x22Gy (n = 4).

Statistics: * - $P < 0.1$, ** - $P < 0.05$

Narla, Sridhar T[1]; Duara, Joanne[3], Bushnell, Daniel S[1]; Bates, Carlton M[1,2].

1: Division of Nephrology, Department of Pediatrics, University of Pittsburgh School of Medicine, Pittsburgh, Pennsylvania
2: Division of Nephrology, UPMC Children's Hospital of Pittsburgh, Pittsburgh, Pennsylvania
3: Division of Neonatology, UPMC Children's Hospital of Pittsburgh, Pittsburgh, Pennsylvania

KGF protects bladder urothelium after cyclophosphamide via AKT

Background:
Cyclophosphamide (CPP), a drug used to treat lymphoma and other diseases, can cause severe acute bladder urothelial injury and chronic problems including fibrosis and cancer. We previously showed that treatment with keratinocyte growth factor (KGF) prior to CPP blocked Basal and Intermediate cell apoptosis. Our objective is to determine the mechanism of cytoprotection and long term benefits of KGF.

Methods:
We treated female mice with 5mg/kg KGF or PBS (vehicle) 24 hours before intraperitoneal (IP) CPP (150mg/kg) or sham injection and harvested mice at various time points. To identify the role of AKT, we administered LY294002 (50mg/kg), a potent AKT inhibitor IP every 12 hours to CPP injured mice ± KGF and harvested mice 12 hours after CPP. We performed H&E staining, TUNEL assays and immunofluorescence (IF) for many proteins on collected samples.

Results:
In PBS treated injured mice, we observed robust urothelial apoptosis 12 hours after CPP in PBS-treated mice and no apoptosis in KGF-treated mice. Addition of LY294002 partially blocked induction of urothelial pAKT staining by KGF and led to breakthrough apoptosis 12 hours after CPP (the inhibitor had no effects in PBS-treated mice). We next interrogated AKT-targets known affect apoptosis such as mammalian target of rapamycin (mTORC1, anti-apoptotic), and BCL2 associated agonist of cell death (BAD, pro-apoptotic). CPP injury alone led to a loss of baseline staining of phospho-P70S6K, a readout of mTORC1 activity. KGF treatment prevented the loss of pS6K staining, consistent with preservation of anti-apoptotic mTORC1 activity. In addition, pretreatment with KGF increased expression of phospho-BAD, which inactivates BAD and thus blocks BAX-triggered apoptosis. To assess long term benefits of KGF, we examined mice 6 months after CPP + KGF/PBS. PBS treated mice had many regions of hyperplasia, ongoing proliferation of $KRT14^+$ Basal cells, and many foci of ectopic $KRT14^+$ cells in the superficial layer. In contrast, KGF treated mice showed few regions of hyperplasia, $KRT14^+$ cell proliferation and no ectopic $KRT14^+$ cells.

Conclusion:
KGF appears to block CPP-induced urothelial cell apoptosis via AKT signaling. KGF-AKT appears to drive cytoprotection by preventing CPP induced loss of mTORC1 activity and by inactivating BAD. KGF treatment appears to improve long term recovery from CPP vs. PBS-treated mice.

Background and Objective:
MIBC is genetically and immunogenically heterogenous disease. Recent molecular classification of MIBC identifies six different molecular subtypes that differ in the immune features. Bladder cancer patients show a high variability in response to treatment, which includes the recently approved checkpoint inhibitors as well as chemotherapeutic interventions. To study the different molecular subtypes and their inter-play with the immune microenvironment that enables the tumors to escape immune surveillance, we have developed immune competent syngeneic BURP (BBN induced Urothelial carcinoma Roswell Park) model of bladder cancer.

Methods: BURP tumor lines were developed by serial sub-cutaneous passaging of BBN induced primary bladder tumors into sex-matched wild-type C57BL/6 mice. The tumor models were first classified by histological features following identification of molecular subtypes by applying the consensus molecular subtype classifiers to the bulk RNA-seq data of each tumor line. Immune cell composition of the BURP lines was determined by applying CIBERSORT deconvolution algorithm using the ImmuCC immune cell signatures. We treated two BURP lines of different molecular and immune subtype with cisplatin and compared the difference in tumor growth rates between them.

Results: We have established eight BURP tumor lines, that differ in their histological, molecular and immunological characteristics. Histologically, the tumor lines show squamous and sarcomatoid differentiation. Molecularly, the tumor lines are divided into basal/ squam, stroma-rich and neuroendocrine subtypes. All the tumor lines have a low estimated CD8+ T-cell fraction, but differ in their estimated fraction of macrophages and differentiated CD4+ T-cells. The BURP tumor line classified as stroma-rich subtype (BURP16) showed a strong response to cisplatin treatment but BURP24, classified as basal/ squam subtype, was resistant to cisplatin treatment.

Conclusion: The BURP tumor lines are suitable model systems to study the dynamics between molecular sub-types and the tumor immune microenvironment. The difference in response to cisplatin treatment between the BURP tumor lines, indicates that the BURP tumor lines can provide a deeper understanding of the interplay between the molecular drivers and immune cell players in inherent treatment response and resistance.

LOSS OF PUTATIVE TUMOR SUPPRESSOR EPHB2 INDUCES LIPID DROPLETS ACCUMULATION AND PROLIFERATION IN PROSTATE CANCER CELLS

Introduction: To sustain the constant demand of energy associated with a proliferative phenotype, cancer cells undergo metabolic re-programming by increasing their rate of fatty acid (FA) synthesis and storage in lipid droplets (LD). Dysregulation of receptor tyrosine kinase (RTK) signaling can result in aberrant metabolism through disruption of critical metabolic pathways. Here, we show a novel role of EPHB2, an RTK member of the Ephrin family, on LD biogenesis and subsequent accumulation associated with increased prostate cancer (PCa) cell proliferation.

Method: Expression of EPHB2 and LD density was assessed in PCa specimens and PCa cell lines with different degrees of tumorigenicity. EPHB2 silencing was performed in PCa cells. The accumulation and size of LDs were assessed under basal and obesogenic (Oleic acid, OA) environments using a combination of flow cytometry and microscopy. Key molecules involved in lipogenesis and lipolysis were assessed. The biological effects of EPHB2 knock down were tested in vitro.

Results: High grade PCa accumulate significantly more neutral lipid than lower grade tumors. EPHB2 staining of prostate specimens showed a distinct strong membrane expression in benign epithelial glands, compared to diffuse and weak expression in areas with PCa. Expression of EPHB2 was inversely associated with PCa cells tumorigenicity. EPHB2 silencing had a positive effect on PCa cells proliferation. Increased accumulation of LD in the cytoplasmic and nuclear compartments were observed in cells with EPHB2 knock down. LD changes were associated with differential expression of key molecules involved in lipogenesis and lipolysis, notably DGAT1, DGAT2 and ATGL. Inhibition of lipogenesis using a DGAT1-specific inhibitor abolished the effects on LD metabolism induced by EPHB2 loss in PCa cells.

Conclusions: Decreased EPHB2 expression observed in PCa may play a key role in the excessive accumulation of neutral lipids within LDs in cancer cells. PCa cells can use this lipid-rich environment as a source of energy to fuel a more aggressive phenotype. Several DGAT1 inhibitors are currently being evaluated in clinical trials as anti-obesity agents, showing promising results, therefore, the potential anti-tumorigenic utility in high-risk PCa patients with altered ephrin levels requires further study.

Single-cell transcriptomes reveal a MYC-driven reprograming of the androgen receptor cistrome in prostate cancer

Xintao Qiu[1,2], Avery Feit[1,2], Yingtian Xie[1,2], Adrienne M. Luoma[3], Tarek Hallal[4,5], Janie Larocque[4,6], Nadia Boufaied[4], Giorgia Zadra[7,8], Shengqing Gu[1,2,9], Qin Tang[1,2,9], Ji-Heui Seo[2], Connor Bell[2], Edward O'Connor[2], Paloma Cejas[1,2], Leigh Ellis[7,8,10], Massimo Loda[11], Kai W. Wucherpfennig[3], Mark Pomerantz[2], Eva Corey[12], Matthew Freedman[2,10], Shirley X. Liu[1,9,13], Myles Brown[1,2], Henry W. Long[1,2,*], David P. Labbé[4,5,6,14,*]

[1]Center for Functional Cancer Epigenetics, Dana-Farber Cancer Institute, Boston, MA, USA
[2]Department of Medical Oncology, Dana-Farber Cancer Institute, Harvard Medical School, Boston, MA, USA
[3]Department of Cancer Immunology and Virology, Dana-Farber Cancer Institute, Harvard Medical School, Boston, MA, USA
[4]Research Institute of the McGill University Health Centre, Montréal, QC, Canada
[5]Department of Anatomy and Cell Biology, McGill University, Montréal, QC, Canada
[6]Division of Experimental Medicine, Department of Medicine, McGill University, Montréal, QC, Canada
[7]Department of Oncologic Pathology, Dana-Farber Cancer Institute, Boston, MA, USA
[8]Department of Pathology, Brigham and Women's Hospital, Boston, MA, USA.
[9]Department of Biostatistics and Computational Biology, Dana-Farber Cancer Institute, Harvard T.H. Chan School of Public Health, Boston, MA, USA
[10]The Eli and Edythe L. Broad Institute, Cambridge, MA, USA
[11]Department of Pathology and Laboratory Medicine, Weil Cornell Medicine, New York Presbyterian-Weill Cornell Campus, New York, NY, USA
[12]Department of Urology, University of Washington, Seattle, WA, USA
[13]School of Life Science and Technology, Tongji University, Shanghai, China
[14]Division of Urology, Department of Surgery, McGill University, Montréal, QC, Canada
[*]Correspondance to: david.labbe@mcgill.ca (D.P.L.) or henry_long@dfci.harvard.edu (H.W.L.)

Background: Prostate cancer is the most prevalent cancer in men and a leading cause of cancer-related lethality. Prostate cancer development involves corruption of the normal prostate transcriptional network, following deregulated expression or mutation of key transcription factors. MYC is a major driver of prostate cancer tumorigenesis and progression. Although MYC is overexpressed in both early and metastatic disease and associated with poor survival, its impact on prostate transcriptional reprogramming remain elusive.
Methods: We used a genetically engineered mouse model of prostate cancer driven by c-MYC overexpression (Hi-MYC) and patient-derived xenograft models (LuCaP). We performed transcriptomics (bulk and single-cell RNA-seq) and chromatin immunoprecipitation followed by sequencing (ChIP-seq) experiments and analyses.
Results: Using a MYC-driven genetically engineered mouse model of prostate cancer that largely mimics the human disease, we have generated the transcriptome profiling at a single-cell level of both normal and MYC-transformed murine prostate lobes. Here, we demonstrate that MYC overexpression significantly diminish the androgen receptor (AR) transcriptional program in luminal prostate cells without altering its expression. Covariance analysis revealed that upon MYC overexpression, transcripts co-expressed with AR shift from canonical targets to transcripts related to ribosome biogenesis. Importantly, chromatin immunoprecipitation followed by sequencing of

the AR uncovered a profound reprogramming of its cistrome following MYC overexpression. Data integration with single-cell transcriptomics further revealed the establishment of a corrupted AR transcriptional program redirected toward MYC targets. Importantly, analyses of clinical specimens and patient-derived xenograft models also support a diminished canonical AR transcriptional activity associated with high levels of MYC expression as the disease progresses to a castration-resistant state.
Conclusions: Our findings suggest that MYC overexpression contributes to tumour initiation and progression by hijacking the AR transcriptional program.

Acknowledgements
We thank Zach Herbert, Sudeepa Syamala and Noriko Uetani for technical assistance. D.P.L is a Lewis Katz – Young Investigator of the Prostate Cancer Foundation, and is the recipient of a Scholarship for the Next Generation of Scientists from the Cancer Research Society, and is also a Research Scholar – Junior 1 from The Fonds de Recherche du Québec – Santé. The work reported here was funded by a Canadian Institutes of Health Research (CIHR) project grant (PJT-162246) to D.P.L.

Competing financial interests
M.B. receives sponsored research support from Novartis. M.B. is a consultant to Aleta Biotherapeutics and H3 Biomedicine and serves on the SAB of Kronos Bio. The remaining authors declare no competing interests.

Prostate tumor-derived TNFα/TGFβ down regulate AR expression in the prostate cancer stroma through TAK1, NF-κB, and p38 signaling

Shekha Tahsin[1], Cindy K. Miranti[1,2]

1) Cancer Biology Graduate Program, 2) Cellular and Molecular Medicine.
University of Arizona, Tucson, AZ

Background: The ability of stromal AR to secrete differentiation factors that act on the surrounding epithelial cells is a critical determinant of normal prostate gland formation. However, loss of stromal AR is associated with increasing Gleason grade and development of aggressive prostate cancer, resulting in less-differentiated tumors. The mechanisms that lead to stromal AR loss are unknown. In this study, we tested the hypothesis that tumor-secreted factors, such as TGFβ and TNFα, are responsible for AR repression through NF-κB activation.

Methods: Using benign human immortalized prostate stroma cells (BHPrs1) as a model, the mechanistic downregulation of AR was examined. Using cytokine array profiling, we identified TNFα and TGFβ1 as two major factors secreted by two different PCa cell lines, C4-2 and 22RV1. RT-qPCR, immunoblotting, pharmacological inhibitors and shRNA knock-down were utilized to identify the TNFα/TGFβ-mediated signaling pathways contributing AR downregulation.

Results: Treatment of BHPrs1 cells with TNFα or TGFβ leads to loss AR expression within 18-24 hours. This was accompanied by a parallel loss of AR mRNA. TNFα-treated cells showed a time and concentration-dependent activation of NF-κB, TAK1, p38-MAPK, and Jnk, which peaked at 18-24hr. Inhibitors of TAK, p38, and NFκB, but not Jnk, blocked the ability of TNFα to downregulate AR expression. These data indicate that the activation of p38-MAPK and NF-κB via TAK1 are involved in suppressing AR expression in response to TNFα. Future experiments will determine if TGFβ uses the same pathways and whether NF-κB and ATF1 binding sites on the AR promoter are involved.

Conclusion: These results show that there are two pathways downstream of TAK1, p38 and NF-κB, that are responsible for suppressing AR expression in the prostate cancer stroma. Future experiments will explore the significance of these findings in the context of disease.

A neuroanatomical mechanism linking perinatal chemical exposure to prostate smooth muscle hyperactivity and altered voiding function

Background: The historical focus of male lower urinary tract dysfunction (LUTD) has been benign prostatic enlargement and other aging-related processes. Little attention has been directed towards the influence of early life events on urinary physiology in advanced age. Here, we identify the intrauterine environment as a modifier of adult voiding function and risk factor for male LUTD.

Methods: To model environmental chemical exposures, we exposed pregnant mice to the environmental contaminant 2,3,7,8 tetrachlorodibenzo-*p*-dioxin (TCDD, 1 μg/kg), coinciding with initiation of lower urinary tract development in male fetuses. We aged male pups to embryonic day (E) 17.5, postnatal (P) day 9, and 14 weeks of age and collected prostate tissue to stain for noradrenergic axons via immunohistochemistry. RNAseq was performed on E16.75 fetal prostates to identify dysregulated neurotrophic factors. Prostate muscle sensitivity was measured using genetically encoded calcium receptors and tissue bath. Urinary frequency was measured using cystometry.

Results: Fetal TCDD exposure incites abnormal urodynamics in adult male mice, including increased urinary voiding frequency. TCDD also enhances adult prostate sensitivity to electrically evoked muscle contraction, suggesting increased autonomic tone. IUL TCDD exposure stably increases noradrenergic axon density beginning in the fetal period and persisting into adulthood. These changes are accompanied an increase in the abundance of a neurotrophin, Artemin *(Artn*), in the fetal prostate.

Conclusions: This is the first evidence that intrauterine chemical exposures can reprogram prostate neuroanatomical development and drive prostatic smooth muscle hyperactivity in adulthood, which may create a susceptible phenotype for aging-related male lower urinary tract dysfunction.

DNA damage and oxidative stress is higher in high-risk prostate cancer subjects

Background: Prostate cancer is a growing health issue in the Western nations as its incidence increases in the aging population. A major risk factor that contribute to the development of prostate cancer is oxidative stress and oxidant/antioxidant balance. Our objective is to investigate the oxidative DNA damage and changes in antioxidant status in high-risk prostate cancer subjects.

Methods: A total of 40 men in the age range of 52–84 years without any prior drug or treatment involvement were included in the study. Patients were recruited from the Urology clinic of the University Hospitals Cleveland Medical Center between January 2008 and May 2011. Twenty subjects were selected who were diagnosed having precursor high-grade intraepithelial neoplasia lesions confirmed by needle biopsy and serum PSA $\geq$ 4.0 ng/mL and abnormality observed in the prostate during digital rectal exam or transrectal ultrasonography. Twenty age-matched men within the same age group designated as controls were recruited in the study without any history of cancer, benign prostatic hyperplasia or prostatitis. Blood samples were drawn, buffy coat was separated for DNA isolation. The plasma samples and erythrocyte fraction were stored at −80 °C until assayed. We performed the profiling of 8-hydroxydeoxyguanosine (8-OHdG) in leukocytes, plasma antioxidant capacity, guanosine 3',5'-cyclic monophosphate (cyclic GMP), nitrite and nitrate levels, followed by glutathione S-transferase P (GSTP1) and O-6-Methylguanine-DNA Methyltransferase (MGMT**)** using assay kits and the patients' samples were repeated twice in triplicates. All biochemical assays were performed as mentioned in manufacturer's protocol.

Results: Levels of 8-OHdG, cGMP, nitrite and nitrate were significantly increased ($p < 0.0001$) in the buffy coat and plasma samples whereas the levels of GSTP1 and antioxidant capacity were significantly decreased in high risk subjects, compared to control subjects. Simultaneously, an increase in MGMT activity was also noted in the plasma of high-risk subjects, compared to control subjects.

Conclusion: The significant changes observed with an increase in the levels of 8-OHdG, cGMP, MGMT, nitrite and nitrate with a concomitant decrease in the levels of GSTP1 and antioxidant levels in the blood is indicative of increased oxidative stress and changes in antioxidant status susceptible to development of prostate cancer.

Loss of FOXA1 Results in Genome-wide Epigenetic Reprogramming and activation of Interferon-Response Genes including *CD274*/PD-L1

Submission Type: Poster Abstract

Submission Status: Complete / Locked

Submitter: Hironobu Yamashita

Author(s)

Hironobu Yamashita

Research Associate

Penn State College of Medicine

Role: Presenting Author

Disclosure:

Disclosure Status: Complete

Disclosure: Nothing to Disclose

Signed: *Hironobu Yamashita* (9/3/2020, 12:28 PM)

No financial relationships or conflicts of interest.

Wenhuo Hu

Research Associate

Memorial Sloan Kettering Cancer Center

Role: Author

Disclosure:

Disclosure Status: Complete

Disclosure: Nothing to Disclose

Signed: Wenhuo Hu (9/8/2020, 11:23AM)

No financial relationships or conflicts of interest.

Joshua I. Warrick

Assistant Professor

Penn State College of Medicine

Role: Author

Disclosure:

Disclosure Status: Complete

Disclosure: Nothing to Disclose

Signed: Joshua Warrick (9/8/2020, 16:30 PM)

No financial relationships or conflicts of interest.

Vonn Walter

Assistant Professor

Penn State College of Medicine

Role: Author

Disclosure:

Disclosure Status: Complete

Disclosure: Nothing to Disclose

Signed: *Vonn Walter* (9/8/2020, 16:00 PM)

No financial relationships or conflicts of interest.

Jenna Buckwalter

Postdoctoral fellow

Penn State College of Medicine

Role: Author

Disclosure:

Disclosure Status: Complete

Disclosure: Nothing to Disclose

Signed: Jenna Buckwalter (9/8/2020, 14:03PM)

No financial relationships or conflicts of interest.

Hikmat Al-Ahmadie

Associate Attending Pathologist

Memorial Sloan Kettering Cancer Center

Role: Author

Disclosure:

Disclosure Status: Complete

Disclosure: Nothing to Disclose

Signed: Hikmat Al-Ahmadie (9/8/2020, 13:21PM)

No financial relationships or conflicts of interest.

David J. DeGraff

Assistant Professor

Penn State College of Medicine

Role: Author

Disclosure:

Disclosure Status: Complete

Disclosure: Nothing to Disclose

Signed: *David Degraff* (9/8/2020, 17:06 PM)

No financial relationships or conflicts of interest.

Background

Forkhead Box A1 (FOXA1) is a pioneer transcription factor (TF) critical in epigenetic regulation of chromatin state and cell fate determination. Reduced FOXA1 is an independent predictor of poor overall survival in bladder cancer (BC) patients. However, the impact of FOXA1 loss on chromatin epigenetics in BC is unknown. Therefore, we determined the impact of *FOXA1* KO on epigenetic modification of chromatin and associated gene expression. Our integrated analysis identifies FOXA1 as an important regulator of chromatin epigenetic state and expression of immune checkpoint (IC) targets in BC.

Methods

We used CRISPR/Cas9 to delete *FOXA1* in the human luminal BC cells. We performed RNA-seq and Chip-seq for H3K27ac, an epigenetic mark of active enhancers/promoters. Motif and GSEA analysis of RNA/Chip-seq were performed to identify *FOXA1* KO-induced epigenetic differences influencing gene expression. Western blotting (WB)/qPCR confirmed FOXA1-mediated CD274/PD-L1 expression. *In silico* analysis of TCGA data also confirmed relevance to human disease.

Results

We identified 8,230 differentially expressed genes in *FOXA1* KO. Notably, GSEA identified IFNα/γ gene signatures as enriched in *FOXA1* KO. As expected, the majority of differences in H3K27ac across genomic areas in *FOXA1* KO were mapped to intergenic (n=6,250 peaks; 42% of total peaks) and intronic (n= 6,490 ; 43%) regions. In addition, differential H3K27ac levels were also mapped to proximal promoters (n= 1,306 ; 9%) as well as within gene bodies (n=931 ; 6%). Integrated analysis of RNA/ChIP-seq shows changes in gene expression are mirrored by differences in H3K27ac.

Motif analysis of DNA sequence enriched for H3K27ac identified significant increases in TF binding motifs including the interferon (IFN) sensitive response element (ISRE) and IFN response factors such as IRF1. Moreover, we identified increased H3K27ac of regulatory elements as being associated with several upregulated ISGs in *FOXA1* KO. These include *ISG15*, *IFIT2/3*, *IFI44L* and *CD274*/PD-L1. WB/qPCR confirmed upregulation of several ISGs, including *CD274*/PD-L1 following *FOXA1* KO. Analysis of TCGA data confirmed an inverse relationship between *FOXA1* and *CD274* in BC and other cancers.

Conclusions

In summary, we provide evidence of widespread epigenetic reprogramming after *FOXA1* KO in BC cells. Additionally, we provide evidence that epigenetic changes contribute to activation of a global IFN-dominant signature, including *CD274*/PD-L1 in a cancer cell-intrinsic manner in *FOXA1* KO.

Funding and Keywords

Supported in part by RSG 17-233–01-TBE from the American Cancer Society (D.J.D.), The W.W. Smith Charitable Trust (D.J.D.), the Ruth Heisey Cagnoli Endowment in Urology at Penn State College of Medicine and the Bladder Cancer Support Group at Penn State Health.

Keyword 1

Bladder cancer

Keyword 2

Pioneer factor

Keyword 3

Epigenetic reprogramming

MEIS proteins inhibit HOXB13-dependent prostate cancer metastasis and Androgen Receptor signaling

Perike, S., Van Opstall, C., Brown, R., Lamperis, S., Vander Griend, D. J.

Department of Pathology, The University of Illinois at Chicago

Background: Prostate cancer (PCa) is one of the most frequently diagnosed malignancies in men, and its incidence and mortality continue to be a significant clinical problem. Recent evidence from our lab identified MEIS1, an important HOX protein cofactor, as a potential tumor suppressor. Patients bearing MEIS1-positive prostate tumors were less likely to have biochemical recurrence and metastasis compared to men bearing MEIS-negative tumors. Androgen receptor (AR), the major oncogene in PCa, has been shown to interact with HOXB13 to promote prostate cancer progression, but the function of MEIS proteins to antagonize AR/HOXB13 interactions are unknown. We hypothesize that MEIS1 proteins interact with HOXB13 to suppress cancer initiation and progression, and loss of MEIS1 expression in a portion of prostate tumors enables oncogenic AR/HOXB13 interactions.

Methods: We determined the impact of MEIS1 expression and dependency of HOXB13 on AR signaling using cell lines ectopically expressing MEIS1 and/or CRISPR-mediated HOXB13 deletion in both androgen-sensitive LAPC4 and castration-resistant CWR22Rv1 cells. Western blots, qPCR, Proximity Ligation Assay and co-IPs were performed to evaluate the relationship among MEIS1, HOXB13 and AR. Hormonally-intact and castrated male nude mice were used to test the *in vivo* capability of MEIS1-mediated tumor formation and rate of tumor growth in the presence and absence of AR ligand.

Results: We found that AR expression was significantly increased when MEIS1 was ectopically expressed compared to controls and HOXB13 knock-out lines. Re-expression of MEIS1 enhanced the binding between HOXB13-MEIS and AR-MEIS, and reduced the AR-HOXB13 interaction. In castrated mice, re-expression of MEIS1 significantly decreased the tumor formation and tumor growth rate compared to hormonally intact nude mice. Conversely, xenografts of HOXB13-knockout tumors showed an increased rate of tumor growth and tumor formation compared to MEIS1-expressing cells and controls in both hormonally intact and castrated nude mice.

Conclusion: Our collective data supports our hypothesis that increased MEIS1 expression reduces the AR/HOXB13 interaction and increases the *in vivo* sensitivity to host castration; this suggests that MEIS-positive cells have decreased oncogenic AR signaling. Future RNAseq studies will determine the global impact of MEIS expression on AR gene targeting in PCa and provide us a strong rationale to support the potential utility of MEIS proteins as predictive clinical biomarkers of metastatic progression.

Funding: This work was supported by the Urology Care Foundation Research Scholar Award, DOD grant PC130587, and DOD grant PC180414.

Conflict of Interest Disclosure statement: No disclosures and no conflicts of interest

GSTP1 regulates the growth and metastasis of castrate resistant prostate cancer

Merve Aslan[1], En-Chi Hsu[1], Abel Bermudez[1], Fernando Jose Garcia-Marques[1], Michelle Shen[1], Shiqin Liu[1], Meghan A. Rice[1], Rosalie Nolley[2], Christian A. Kunder[3], Sharon J. Pitteri[1], James D. Brooks[2], Eva Corey[4], and Tanya Stoyanova[1]

1. Department of Radiology, Canary Center at Stanford for Cancer Early Detection, Stanford University, Stanford, CA. 2. Department of Urology, Stanford University, Stanford, CA. 3. Department of Pathology, Stanford University, Stanford, CA. 4. Department of Urology, University of Washington, Seattle, WA

Introduction & Objective
Prostate cancer is the second leading cause of cancer related deaths among men in the United States. Although, hormone deprivation therapies are initially effective for prostate cancer patients, the disease commonly recurs and advances into a castration resistant state (CRPC). Neuroendocrine prostate cancer (NEPC) is a highly aggressive variant of prostate cancer that usually emerges post treatment resistance. Since there are no curative treatments for CRPC or NEPC, elucidating new therapeutic strategies for advanced disease is urgently needed. GSTP1 promoter hypermethylation is one of the earliest genetic alterations found in localized prostate cancer. Surprisingly, we identified that GSTP1 protein is significantly elevated in a recently developed NEPC model and further demonstrated that GSTP1 can affect advanced prostate cancer growth and metastasis.

Methods
Protein levels of GSTP1 in benign prostate, CRPC, and NEPC patient-derived xenografts (PDXs) were analyzed by immunohistochemistry. Knockdown of GSTP1 was achieved by short hairpin RNAs in a TROP2-driven NEPC cell line model and in DU145 and PC3 cell lines. The effect of GSTP1 knockdown was assessed by colony formation, cell proliferation, and matrigel drop invasion assays *in vitro*. The role of GSTP1 expression on prostate cancer growth and metastatic colonization was evaluated *in vivo* by subcutaneous xenograft implantation and intracardiac injection.

Results
GSTP1 protein expression was elevated in CRPC and NEPC cell lines and PDXs. Knockdown of GSTP1 expression decreased prostate cancer tumor growth and invasion *in vitro* and metastatic colonization *in vivo*. Furthermore, GSTP1 inhibition by Piperlongumine (PPLGM) suppressed prostate cancer cell growth, migration, and invasion.

Conclusions

GSTP1 is a novel druggable target for CRPC and NEPC. GSTP1 knockdown by shRNA or a small molecule inhibitor, PPLGM, decreases tumor growth and migration in prostate cancer.

GATA3 REGULATES LIPID CONTENT AND COOPERATES WITH AURORA B KINASE IN THE MITOTIC SPINDLE OF HORMONE-REFRACTORY PROSTATE CANCER CELLS

Victoria Gil[1], Philip Fitchev[1], Francesca Nardi[1], Adrian Scheibler[1], Max H Greenberg[1], Kim C. Lim[2], Omar E. Franco[1], Simon W. Hayward[1], Jianfeng Xu[1], James Douglas Engel[2], Susan E. Crawford[1]
[1]Department of Surgery, NorthShore University HealthSystem Research Institute, Affiliate of University of Chicago Pritzker School of Medicine, Evanston, IL 60201
[2]Department of Cell and Developmental Biology, University of Michigan Medical School, Ann Arbor, MI 48109

Background
GATA3 is an important determinant for cell lineage in prostate development and loss of this transcription factor has been implicated in more aggressive prostate tumor growth. The tumor inhibiting mechanisms of GATA3 remain unclear. A critical protein in mitosis, Aurora B kinase, is upregulated in prostate cancer and its targeted inhibitor can suppress tumor growth. We postulated that GATA3 in prostate cancer directly regulates cell growth via cyclin D1 and controls mitotic spindle assembly by cooperating with aurora B kinase.

Methods
To assess the mitotic spindle, immunofluorescence (IF) stains were performed for DAPI, Aurora B kinase and GATA3. Prostate cancer cell line, C4-2b, was transfected with GATA3 siRNA and cell cycle proteins analyzed. GATA3 heterozygote murine embryos were phenotyped and immunostained for Ki67, adipose triglyceride lipase (ATGL), perilipin 2, pigment epithelium-derived factor (PEDF) and angiogenic factors (VEGF and PEDF). To simulate a lipid-enriched tumor microenvironment, C42b cells were treated with oleic acid (OA) and stained for Oil-Red-O and GATA3.

Results
IF studies revealed that in the early phase of mitosis, GATA3 was dispersed in the nucleus. As mitosis progressed GATA3 condensed and aligned with chromatids. GATA3 co-localized with Aurora B kinase at opposing ends of each daughter nucleus until they were cleaved. In the lipid-rich OA-treated experimental group demonstrated malalignment of the mitotic spindle orientation and mitotic progression. Reducing GATA3 in prostate cancer cells showed a 38% increase in cell cycle regulator, cyclin D1, elevated intracytoplasmic lipid and more than a twofold increase in cell number. $GATA3^{+/-}$ embryos demonstrated an increased number of proliferating cells in many organ systems associated with an increased vascular density. The liver had excessive neutral lipid accumulation and increased binucleation of the hepatocytes.

Conclusions
A role for GATA3 in mitotic spindle assembly was discovered with co-localization of an essential cell division regulator, Aurora B kinase. GATA3 knockdown in tumor cells resulted in an increase in proliferating cells and cyclin D1 and this pro-proliferative phenotype was exacerbated by a lipid stimulus. GATA3 deficiency in mice revealed hepatic steatosis supporting a new function for GATA3 in lipid metabolism. Therapeutic targeting of the lipid-GATA3 axis could be effective at arresting tumor growth and progression.

MCT inhibition as a potential therapeutic strategy to target enzalutamide-resistant prostate cancer

Sayani Bhattacharjee, Jonathan Doan, Jerred Pletcher, Rebecca Wynn, Firas Petros, Puneet Sindhwani, Nagalakshmi Nadiminty

Department of Urology, College of Medicine and Life Sciences, University of Toledo Health Science Campus, Toledo, OH

Background: The majority of prostate cancer (PCa) patients treated with androgen deprivation therapy develop resistance to the therapy, thus generating a dire need for establishing newer targets and approaches for the management of therapy resistant PCa. Enzalutamide is a second generation antiandrogen used for the treatment of metastatic castration-resistant PCa. However, resistance to enzalutamide is a significant issue and the mechanisms involved and strategies to overcome the resistance are under intense investigation.

PCa energetic metabolism is unique. Primary PCa are not predominantly glycolytic with increased glycolysis being found only in advanced stages, indicating that PCa are more heterogeneous in their use of energy sources. However, accumulation of the metabolic end product lactate is toxic and cancer cells upregulate the expression of monocarboxylate transporters (MCTs) to facilitate lactate efflux. Different MCT isoforms are differentially expressed in PCa with an increase in the expression of MCT2 and MCT4 during progression from benign prostate to carcinoma and high MCT4 expression in invasive PCa. Based on preliminary data, we hypothesized that MCT inhibition may be an attractive therapeutic strategy against enzalutamide-resistant PCa cells.

Methods: We analyzed the expression levels of MCTs in PCa tissues using public datasets from Oncomine and the relative expression levels of MCTs in enzalutamide-resistant and parental PCa cells using qPCR. We treated enzalutamide-resistant and parental PCa cells with varying concentrations of MCT inhibitors AR-C155858, AZD3965, or syrosingopine either singly or in combination with enzalutamide and assessed cell survival, proliferation, clonogenic ability, and tumorigenicity.

Results: We found that the suppression of MCT activity using the MCT antagonists AR-C155858, AZD3965, or syrosingopine not only diminished the proliferation, survival, clonogenic ability, and tumorigenicity of PCa cells, but also resensitized resistant cells to treatment with enzalutamide. These findings imply that MCTs may have an intrinsic role in resistance to therapy, which can be disrupted using MCT inhibitors.

Conclusions: MCT inhibition may be an effective strategy to overcome enzalutamide resistance in PCa.

Setanaxib attenuates NADPH oxidase 4-driven activation of prostate cancer-associated fibroblasts and alters signaling pathways involved in cellular adhesion and migration

Background

The development and progression of prostate cancer (PCa) is highly influenced by a pro-tumorigenic environment, where cancer-associated fibroblasts (CAFs) influence cancer cell proliferation, metastatic progression and therapy resistance through secretion of soluble factors and remodeling of the extracellular matrix. We previously showed that the H_2O_2-producing enzyme NADPH oxidase 4 (Nox4) is crucial for the transformation of benign fibroblasts to a CAF phenotype and that its increased expression is associated with biochemical relapse and poor survival of PCa patients. The current study aims to evaluate the potential of pharmacological Nox4 inhibition as an adjuvant therapeutic strategy for PCa and to identify Nox4-induced molecular players in the tumor microenvironment that promote tumor development and progression.

Methods

To test the therapeutic application of Nox4 inhibition, primary prostate CAFs and *ex vivo* cultured human PCa tissue were treated with Setanaxib, a dual Nox1/Nox4 inhibitor, and ROS levels, expression of reactive stroma markers and PCa progression markers were determined. In a next step we aim to identify Nox4 effectors and their key regulators via an integrative "omics" approach encompassing the secretome, proteome and transcriptome of primary prostate CAFs and patient-matched normal fibroblasts treated with Setanaxib.

Results

Pharmacological Nox4 inhibition decreased the expression of CAF markers and PCa progression markers in primary CAFs and *ex vivo* tissue cultures, respectively. Notably, treatment with Setanaxib also attenuated the secretion of PSA, a key clinical biomarker of PCa progression. Integrative bioinformatics suggests that Nox4 influences various pathways in the tumor microenvironment, including the secretion of paracrine factors and signaling pathways involved in cellular adhesion and migration. This is supported by functional assays which showed that Nox4 inhibition reduces CAF adhesion and migration, which is directly implicated in facilitating tumor cell migration and metastasis.

Conclusion & Outlook

Current data suggest that Nox4 is a central mediator of stromal-epithelial crosstalk in the PCa microenvironment and thus represents a promising therapeutic target. Candidate Nox4-regulated effectors identified by large scale analyses will be further validated at the functional level to determine their effects on tumor development and progression.

TRIGLYCERIDE RICH ADENOCARCINOMA OF THE PROSTATE (TRAP): A HIGH-GRADE TUMOR VARIANT ASSOCIATED WITH AN IMBALANCE OF LIPID REGULATING PROTEINS DGAT1 & ATGL

Max H. Greenberg, Victoria Gil, Omar E. Franco, Renee E. Vickman, Yana Filipovich, Simon W. Hayward, Susan E. Crawford
Department of Surgery, NorthShore University HealthSystem Research Institute, Affiliate of University of Chicago Pritzker School of Medicine, Evanston, IL 60201

Background:
Lipogenesis and lipolysis are tightly regulated to maintain adequate flux of triglycerides to meet the metabolic needs of a tissue. An adaptive mechanism to promote growth, tumor cells undergo metabolic reprogramming to favor increased neutral lipid accumulation. We postulated that the neutral lipid imbalance could be the result of altered expression of diacylglycerol O-acyltransferase 1 (DGAT1), a key lipogenesis protein, and adipose triglyceride lipase (ATGL), the rate-limiting enzyme in lipolysis.
Methods:
We analyzed protein expression for DGAT1 and ATGL in prostate tumors (n=46) from varying Gleason grades, scored the staining intensity (grade 1-4), and assessed the quantity of vacuoles within the epithelial and stromal compartments. Prostate cancer (PC) cells were co-cultured with human periprostatic fat (PPF) to simulate an obesogenic microenvironment and intracellular lipid evaluated by Oil-Red-O staining and immunofluorescence.
Results:
We found that higher intratumoral DGAT1 protein expression correlated with higher Gleason scores while ATGL often resided on the surface of the vacuoles or lipid droplets (LDs) in both the tumor epithelial and stromal muscle cells. The co-culture of PC cells with PPF exacerbated the intratumoral lipid content. Interestingly, a distinctive histologic phenotype emerged in a subset of tumors (9/46). We termed this tumor subtype as triglyceride-rich adenocarcinoma of the prostate (TRAP). Microscopically, TRAP was characterized by diffuse vacuoles streaming through the stroma, especially the smooth muscle cells and fibroblasts. Grape-like clusters of vacuoles were observed within the cytoplasm of most tumors cells. These vacuoles stained for DGAT1 > ATGL. All TRAP tumors had lipogenesis and lipolysis proteins on the surface of LDs and correlated with higher Gleason scores (8-9).
Conclusion:
These data suggest that lipid re-programming in PC can create nutrient sources to support high-grade tumor growth. Recognition of histologic TRAP tumor subtype could assist in identifying a group of patients who would benefit from DGAT1 inhibition therapy.

Development of Urinary RNA Biomarkers for Renal Cell Carcinoma Prognosis

Justin F. Cotellessa[1, 2], Susan Patalano[2], Todd Riley, Ph.D. [1], Jill A Macoska, Ph.D. [1, 2]
[1]Department of Biology, University of Massachusetts-Boston, [2]Center for Personalized Cancer Therapy, University of Massachusetts-Boston

Background. Renal Cell Carcinoma (RCC) is diagnosed in approximately 65,000 people annually in the United States, accounting for ~3% of all human cancers. The death rate for patients diagnosed with RCC is about 22%. Additionally, recurrence-free survival of patients deemed high-risk using conventional tumor stage and grade criteria is only 44%, and the molecular components that drive high grade, metastatic disease, remain largely unknown. Since tumor histology has limited value in determining patient outcome, there is a clear need for better predictive tools to guide treatment strategies. The ability to predict the risk of tumor recurrence at the time of diagnosis could modulate RCC treatment strategies to include more aggressive approaches for patients deemed high risk. This personalized approach would help to further stratify patients where traditional histological diagnoses fall short. Urine provides an easily obtainable liquid biopsy that is suitable RNA purification and NextGen sequencing, and can be used to identify biomarkers at the transcript level capable of distinguishing between metastatic and non-metastatic patients.
Methods. Urine was collected at the time of diagnosis from 24 patients whose tumors did not recur (>5 years follow-up) and 28 patients who experienced metastatic disease. The samples were centrifuged, cellular debris discarded, and RNA was purified from the resulting supernatant. RNA sequencing was carried out on the Illumina HiSeq 2500 platform. ROC, MDS and random forest approaches were used to investigate the predictive accuracy of the 20 urinary transcript molecular signature. ATCG, Protein Atlas, and GEO datasets were queried to investigate the normal/tumor tissue specificity of the signature.
Results. 20 transcripts were identified that reliably classified non-metastatic and metastatic patients using dimensionality reduction. Additionally, a previously unobserved isoform was discovered for one of the gene transcripts. Furthermore, the biomarker panel has promising classification power in publicly available data.
Conclusions. The results of these studies show that urine is a suitable biospecimen for biomarker discovery. The validation of such a panel of biomarkers could have significant clinical utility in understanding the prognosis of a patent at a critical early junction when treatment plans are established. Additionally this study could provide a roadmap for the development of additional prognostic and diagnostic tests.

Manzamine-A targets androgen receptor signaling and synergizes with cisplatin to kill prostate cancer cells

Manohar Singh[1], Seema Dubey[1], Mark T Hamann[2], and Dev Karan[1]

[1]Department of Pathology and Laboratory Medicine, MCW Cancer Center and Prostate Cancer Center of Excellence, Medical College of Wisconsin, Milwaukee, WI

[2]Department of Drug Discovery and Biomedical Sciences, Medical University of South Carolina, Charleston SC

Background: Androgen receptor (AR) plays a vital role in the development and progression of prostate cancer metastasis, and androgen deprivation therapy (ADT) remains a fundamental clinical treatment for the metastatic stage of this disease. However, the progression of the disease resistant to ADT leads to castration-resistant prostate cancer, along with the development of new AR variants (AR-V7).

Methods: Manzamine-A (MA) is a natural product from the marine sponge and has shown its biological effects in several cancer types. This study demonstrates the antiproliferative and proapoptotic effect of MA in both androgen-responsive (LNCaP and 22Rv1) and androgen-resistant (PC3 and DU145) prostate cancer cell lines.

Results: We demonstrated that the MA significantly inhibited the growth of the tested cell lines in a dose- and time-dependent manner, as evidenced by the cell viability, cell proliferation, and colony formation assays. MA blocked the cell cycle and their regulating proteins CDK4, CDK6, Cyclin D1, and p21. The proapoptotic activity of MA was exerted following PARP cleavage and caspase-3 activation in LNCaP, 22Rv1, and DU145 cells. Interestingly, MA downregulates the AR protein and its downstream target PSA, and AR variant (AR-V7). Examination of molecular signaling revealed that the MA differentially regulates expression levels of total AKT, GSK-3β, pAKT, and pGSK3β proteins in androgen-responsive and -resistant prostate cancer cell lines. Finally, MA sensitizes prostate cancer cells for an effective killing by the chemotherapy drug cisplatin.

Conclusions: The differential activity of MA against androgen-responsive LNCaP and 22Rv1, and androgen-resistant PC3 and DU145 prostate cancer cells suggests a novel mechanism of marine natural product MA targeting cancer cells at different stages of tumor progression. The molecular mechanism and the therapeutic potency of MA as a single agent or in combination with chemotherapy drugs targeting prostate cancer will be determined in future studies.

Macrophage-Derived Tumor Necrosis Factor Contributes to Benign Prostatic Hyperplasia through Increased Fibroblast Proliferation

Background: Benign prostatic hyperplasia (BPH) is characterized by enlargement of the prostate. High-grade inflammation has been demonstrated to limit the success of current BPH therapies. However, the mechanisms by which immune cells promote expansion of the prostate and whether these can be controlled therapeutically are not well elucidated. Previous evaluation of patient medical records indicate that men with an autoimmune disease (AID) diagnoses were significantly more likely to also be diagnosed with BPH, while systemic therapy of AID using tumor necrosis factor (TNF)α-antagonists reduced BPH diagnoses back to a baseline incidence rate. Here, we investigated inflammation in human BPH tissues and assessed whether TNFα regulates proliferation of epithelial or stromal cells from BPH tissues.
Methods: These studies utilized histological evaluation of human BPH tissues from our prostate tissue repository as well as *in vitro* cell proliferation assays using benign prostate epithelial (BHPrE-1 and NHPrE-1) or stromal (BHPrS-1) cell lines, monocyte-like THP-1 cells, and primary fibroblast cultures isolated from BPH tissues following simple prostatectomy. We also isolated transition zone tissue from small (<60 grams) *versus* large (>70 grams) human prostates and sorted viable CD45+EpCAM-CD200- immune cells for single-cell mRNA-sequencing (scRNA-seq) analysis using the 10x Genomics Chromium System. CellRanger and Seurat were used for data analysis and evaluation of cell clusters.
Results: All inflammatory cell types accumulate in large BPH tissues and single-cell mRNA-sequencing (scRNA-seq) analysis of CD45+ immune cells indicates significantly altered pathways related to autoimmune inflammatory (AI) conditions in macrophages from large *versus* small tissues. TNFα is primarily expressed by macrophages within the immune compartment and *in vitro* studies demonstrate that TNFα stimulates proliferation in fibroblasts but not epithelial cells. Furthermore, primary fibroblast proliferation is stimulated by conditioned medium from M1-polarized THP-1 cells. Finally, histological evaluation of prostate specimens from seven patients taking TNFα-antagonists at the time of procedure indicate these tissues have decreased inflammation and reduced proliferation compared to matched controls.
Conclusions: These studies implicate macrophage-derived TNF as a driver of BPH. Studies to determine whether TNF targeting may yield therapeutic benefit for BPH patients are ongoing.

Unraveling and targeting the lipidome of clinical prostate cancer.

Lisa M. Butler[1,2], Chui Yan Mah[1,2], Jelle Machiels[3], Andrew Vincent[1,2], Xander Spotbeen[1,3], Shadrack Mutuku[1,2], Rajdeep Das[2], Rita Derua[4], Etienne Waelkens[4], Paul Trim[1], Marten Snel[1], Margaret M Centenera[1,2], Johannes V. Swinnen[3]

[1]South Australian Health and Medical Research Institute
[2]Adelaide Medical School and Freemasons Foundation Centre for Men's Health, University of Adelaide
[3]Laboratory for Experimental Medicine and Endocrinology, K.U.Leuven, B-3000 Leuven, Belgium
[4]Department of Molecular Cell Biology and the ProMeta Center, K.U.Leuven, B-3000 Leuven, Belgium

Background. Metabolic rewiring is both a hallmark feature of prostate cancer cells and a potential therapeutic vulnerability, but remains a critical gap in the molecular profiling of this disease. Herein, we detail and spatially visualize the lipidomic landscape of clinical prostate cancer.
Experimental Design. Mass spectrometry-based imaging and lipidomics were used to measure and spatially visualize the lipidome of a cohort of prostate tumors and matched benign tissues (n=21), an independent validation cohort (n=47), and primary prostate explants cultured in the absence or presence of a clinical AR antagonist, enzalutamide (n=43).
Results. Significant differences in phospholipid (PL) composition were evident in tumors compared to matched benign samples. Notably, tumors featured higher proportions of monounsaturated lipids across all PL classes and elongated fatty acid chains specifically in phosphatidylinositol and phosphatidylserine-based lipids. Associations between abundance of individual PLs and malignancy were identified for both patient cohorts, and PL composition was characteristically altered in patient tissues that responded to AR inhibition. Moreover, targeting of the observed tumor-related changes in lipid synthesis, saturation and elongation, via inhibition of acetyl-CoA carboxylase or stearoyl-CoA desaturase, significantly reduced cellular proliferation.
Conclusion. This first characterization of the prostate cancer lipidome in a clinical tissue context revealed enhanced fatty acid synthesis, elongation and desaturation as tumor-defining features, with potential for therapeutic targeting to improve patient outcomes.

Increased DNA methylation of genes regulating intracellular calcium levels alter androgen receptor expression and activity in prostate cancer from African American men

Swathi Ramakrishnan[1*], Xuan Peng[1], Eduardo Cortes Gomez[1], Kristopher Attwood[1], Ivan V. Maly[2], Wilma A. Hofmann[2], Wendy Huss[1], Gissou Azabdaftari[1], Li Yan[1], Jianmin Wang[1], and Anna Woloszynska[1]
[1]Roswell Park Comprehensive Cancer Center, [2]Jacobs School of Medicine and Biomedical Sciences

Background: African American (AA) men are 1.7 times more likely to develop and 2.4 times more likely to die of prostate cancer (PrCa) than their European American (EA) counterparts; however, the underlying biology causing this disparity is unknown. The purpose of this study was to determine how DNA methylation mediated transcriptomic changes drive PrCa health disparity in AA men.

Methods: Illumina arrays and RNA-sequencing were used to identify transcriptomic alterations potentially mediated by DNA methylation in PrCa from 32 EA and 30 AA men. MDA PCa 2a (2a)/MDA PCa 2b (2b) cells derived from an AA man and DU145/LaPC-4 cells derived from EA men were stimulated with ionomycin, a calcium ionophore, followed by intracellular calcium measurement using fluorescent-based live imaging. Androgen receptor (AR) protein expression was measured in cells treated with a calcium chelator (BAPTA-AM) and T and in PrCa tissue microarrays from 95 EA and 92 AA men.

Results: Unsupervised hierarchical clustering revealed a DNA methylation cluster (Cluster A) enriched in loci regulating intracellular calcium, including RYR2, TRPC6, and TRPA1, which was associated with reduced disease-free time (DFT) (21.65 vs 46.71 months, $p<0.05$) only in AA men with PrCa. RYR2 (-0.122 vs -0.004, $p=0.69$), TRPC6 (0.006 vs -0.639, $p=0.06$), and TRPA1 (-0.070 vs -0.269, $p<0.05$) transcripts were lower in Cluster A. These data suggest DNA methylation potentially reduces calcium regulatory gene and thus protein expression which can lower their activity. We found rapid increase in intracellular calcium in ionomycin stimulated 2a/2b cells (within 60 seconds) compared to DU145/LAPC-4 cells (120-300 seconds). This suggests that calcium regulatory genes in PrCa cells from an AA man have reduced intracellular calcium buffering capacity. Additionally, we found that depleting calcium in the presence of T increased AR expression only in PrCa cells derived from an AA man. Furthermore, AR protein expression in a subset of tumors and adjacent non-tumor was lower in Cluster A. AR low PrCa with basal-like features respond poorly to androgen deprivation therapy. We found that AR target and PAM50 basal-luminal genes were differentially expressed in AA and EA PrCa and between 2b and DU145 cells.

Conclusion: Our study shows that AA patients with worse DFT have epigenetically dysregulated calcium signaling that can alter AR expression and activity. Our ongoing work seeks to dissect the mechanisms of DNA methylation mediated changes in PrCa models from AA men. We will investigate how these molecular lesions can serve as novel subtypes and guide the design of rationale therapies for AA men with PrCa.

Metabolomic Analysis of Renal Cell Carcinoma with High Resolution Magic Angle Spinning Magnetic Resonance Spectroscopy

Background

Renal cell carcinoma (RCC) is a metabolic disease, with the various subtypes exhibiting aberrations in different metabolic pathways. Metabolomics may offer greater sensitivity for revealing disease biology than evaluation of tissue morphology. In this study, we investigate the metabolomic profile of RCC using high resolution magic angle spinning (HRMAS) magnetic resonance spectroscopy (MRS).

Methods

Tissue samples were obtained from radical or partial nephrectomy specimens that were fresh frozen & stored at -80°C. Tissue HRMAS MRS was performed by a Bruker AVANCE spectrometer. Metabolomic profiles of RCC & adjacent benign renal tissue were compared, and false discovery rates (FDR) were used to account for multiple testing. Regions of interest (ROI) with FDR <0.05 were selected as potential predictors of malignancy. The Wilcoxon rank sum test was used to compare median MRS relative intensities for the candidate predictors. Logistic regression was used to determine odds ratios for risk of malignancy based on abundance of each metabolite.

Results

There were 38 RCC (16 clear cell, 11 papillary, 11 chromophobe) & 13 adjacent normal tissue specimens (matched pairs). Metabolic predictors of malignancy based on FDR include histidine, phenylalanine, phosphocholine, serine, phosphocreatine, creatine, glycerophosphocholine, valine, glycine, myo-inositol, scylla-inositol, taurine, glutamine, spermine, acetoacetate & lactate. Higher levels of spermine, histidine & phenylalanine at 3.15-3.13 ppm were associated with a decreased risk of RCC (OR $4x10^{-5}$, 95% CI $7.42x10^{-8}$, 0.02), while 2.84-2.82 ppm increased the risk of malignant pathology (OR 7158.67, 95% CI 6.3, $8.3x10^{6}$), and the specific metabolites characterizing this region remain to be identified. Tumor stage did not appear to affect the metabolomics of malignant tumors, suggesting that metabolites are more dependent on histologic subtype.

Conclusions

HRMAS-MRS identified many metabolites that may predict RCC. We demonstrated that those in the 3.14-3.13 ppm ROI were present in lower levels in RCC, while higher levels of metabolites in the 2.84-2.82 ppm ROI substantially increased the risk of RCC.

Table 1: Summary of metabolites that were significantly different between malignant and benign adjacent tissue, with odds ratios for risk of malignancy

	RCC (N=38)	Adjacent benign parenchyma (N=13)	P-value			
Age (years)	55.3 ± 11.4	50.8 ± 7.3	0.1818			
Males (n, %)	27 (71.1)	8 (61.5)	0.7302			
Race (n, %)	37 (97.4)	13 (100)	1.00			
Median MRS relative intensities (IQR)				**FDR P-value**	**Odds ratios (OR, 95% CI)**	**P-value for OR**
4.07-4.05 (Myo-Inositol)	0.80 (0.48, 1.32)	1.84 (1.27, 2.24)	0.0026	0.027	0.38 (0.18, 0.82)	0.013
4.02-4.00 (TBD)	1.21 (0.68, 2.07)	0.50 (0.06, 0.88)	0.0073	0.034	3.12 (1.10, 8.84)	0.032
3.99-3.96 (Histidine, Phenylalanine, Phosphocholine, Serine)	1.26 (0.84, 1.93)	2.56 (1.19, 3.50)	0.0092	0.013	0.34 (0.16, 0.71)	0.004
3.95-3.94 (Serine, Phosphocreatine)	0.77 (0.33, 1.24)	0.30 (0, 0.53)	0.0006	0.003	29.2 (2.47. 345.24)	0.007
3.93-3.91 (Creatine, Glycerophosphocholine)	1.28 (0.90, 1.61)	0.69 (0.24, 1.34)	0.0071	0.012	8.17 (1.77, 37.78)	0.007
3.61-3.59 (Myo-Inositol, Glycerophosphocholine, Phosphocholine, Valine)	0.96 (0.63, 1.24)	1.68 (1.39, 1.96)	0.0006	0.005	0.13 (0.03, 0.49)	0.003
3.55-3.52 (Glycine)	1.92 (0.77, 3.17)	4.02 (2.87, 4.42)	0.0019	0.024	0.59 (0.39, 0.90)	0.014
3.36-3.34 (Scylla-Inositol)	0.55 (0.35, 0.78)	1.34 (0.75, 1.54)	0.0019	0.005	0.08 (0.02, 0.42)	0.003
3.24-3.23 (Myo-Inositol, Taurine)	5.86 (3.95, 9.46)	4.32 (2.43, 5.40)	0.0267	0.030	1.35 (1.04, 1.76)	0.027
3.22-3.21 (Phosphocholine, Glycerophosphocholine, Histidine)	0.69 (0.22, 2.16)	4.23 (3.05, 5.53)	<0.001	<0.001	0.41 (0.35, 0.67)	<0.001
3.15-3.13 (Spermine, Histidine, Phenylalanine)	0.21 (0.11, 0.35)	0.83 (0.49, 1.02)	<0.001	<0.001	4 x10^{-5} (7.42x10^{-8}, 0.02)	0.001
2.84-2.82 (TBD)	0.28 (0.18, 0.45)	0.18 (0.10, 0.23)	0.0021	0.009	7158.67 (6.3, 8.3x10^{6})	0.013
2.45-2.42 (Glutamine)	0.51 (0.30, 0.74)	0.32 (0.21, 0.38)	0.0098	0.017	121.5 (2.16, 6820)	0.02
2.15-2.11 (TBD)	1.45 (1.15, 1.97)	1.95 (1.46, 2.50)	0.0370	0.035	3.96 (1.18, 13.28)	0.026
1.93-1.92 (Acetoacetate)	0.31 (0.18, 0.67)	0.77 (0.54, 2.83)	0.0008	0.012	0.38 (0.13, 1.09)	0.072
1.35-1.33 (Lactate)	8.74 (5.26,13.23)	5.2 (3.06, 8.30)	0.0150	0.033	1.22 (1.03, 1.45)	0.023

*TBD denotes that the specific metabolites characterizing this region remain to be identified

Decreases in NKX2-5 expression during prostate carcinogenesis induce malignant prostate features

Dhirodatta Senapati, Salma Ben-Salem, Hong Qiu, Varadha Balaji Venkadakrishnan, Qiang Hu, Giridhar Mudduluru, Eduardo Cortes, Song Liu, Byron Lee and Hannelore V. Heemers

Background: Prostate cancer (CaP) causes more than 33,000 American cancer deaths annually because therapies for metastatic CaP fail. Novel targets are needed for functionally diverse treatments. We explored whether cancer-initiating events rather than drivers of CaP progression can provide such alternatives. We determined the functional consequences of NKX2-5 CpG island promoter hypermethylation, a recurrent epigenetic alteration that marks the transition from benign to malignant prostate and is maintained in metastatic treatment-resistant CaP. NKX2-5 is a cardiac transcription factor whose role in prostate (cancer) is unknown.
Methods: LNCaP and C4-2 CaP cells, the transformed prostate epithelial cell lines RWPE1 and RWPE2, and non-targeting control siRNAs and NKX2-5 targeting siRNAs were used in rhodamine phalloidin staining, immunofluorescence staining, cell proliferation, cell migration and cell-matrix adhesion assays, ATAC-Seq and RNA-Seq followed by GSEA and Homer analyses, and ChIP and CoIP studies.
Results: Silencing of NKX2-5 in both benign and malignant prostate cells increased cell size, number of cellular extensions, and nuclear size but decreased nuclear heterochromatin content -- all morphological features on which pathologists rely for a CaP diagnosis. These changes were accompanied by decreased CaP cell-matrix adhesion, an initiating step in cancer metastasis. Integrated ATAC-Seq and RNA-Seq assays confirmed a preferential association with metastasis and revealed that loss of NKX2-5 increased accessible chromatin regions, which were significantly enriched for binding sites for TEAD1. TEAD1 is a transcription factor that executes Hippo signaling, which is frequently altered in human malignancies, linked to aggressive cancer morphology and progression, but not yet implicated in CaP. ChIP and CoIP studies confirmed TEAD1 regulation of genes whose expression was induced by loss of NKX2-5 and verified formation of functional TEAD1 transcriptional complexes upon NKX2-5 silencing.
Conclusions: NKX2-5 promoter hypermethylation, a biomarker of prostate carcinogenesis, induces aggressive CaP morphology and behavior that is mediated by activation of Hippo signaling, whose pharmacological inhibition may serve as alternative CaP treatment.

Prolyl hydroxylase 3 knockdown accelerates *VHL*-mutant kidney cancer growth *in vivo*

Von Hippel Lindau (VHL) inactivation, which is common in clear cell renal cell carcinoma (ccRCC), leads directly to the disruption of oxygen homoeostasis. VHL works through hypoxia-inducible factors (HIFs). Within this VHL-HIF system, prolyl hydroxylases (PHDs) are the intermediary proteins that initiate degradation of HIFs. PHD isoform 3's (PHD3) role in ccRCC growth *in vivo* is poorly understood. Using viral transduction, we knocked down expression of PHD3 in the human ccRCC cell line UMRC3. Compared with control cells transduced with scrambled vector (UMRC3-SC cells), PHD3-knockdown cells (UMRC3-PHD3KD cells) had increased cell invasion and tumor growth and were responsive to sunitinib (Tumor Growth Figure). PHD3 knockdown reduced HIF2α expression and increased phosphorylated epidermal growth factor (EGFR) expression in untreated tumor models. However, after sunitinib treatment expression of HIF2α and phosphorylated EGFR in tumor tissue did not significantly differ (Densitometry Table). In addition, PHD3 knockdown changed the overall redox state of the cell. Concentrations of free glutathione are significantly higher in UMRC3-PHD3KD tumors compared to UMRC3-SC tumors. UMRC3-PHD3KD cells proliferate faster when grown in the presence of 1.5 mM hydrogen peroxide compared to control cells. Our findings illustrate 1) that PHD3's ability to affect HIF2α expression is variable, 2) reduction of PHD3 expression leads to faster tumor growth in a ccRCC animal model and 3) PHD3 plays an important role in the redox state of the cell and enhances UMRC3 cells ability to grow in a toxic microenvironment. Our results provide an improved understanding of PHD3's potential role in ccRCC progression and the possible role determining PHD3 expression in ccRCC could guide clinical therapeutic decisions.

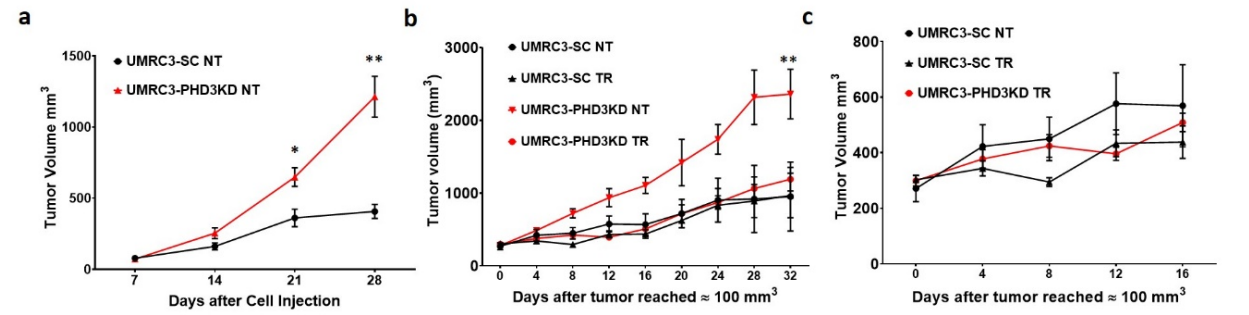

Tumor Growth Figure: no treatment (NT), sunitinib-treated (TR), * P < 0.02, ** P < 0.001

Tumor Type	PHD3/ β-actin	HIF1α/ β-actin	HIF2α/ β-actin	pEGFR/ β-actin	EGFR/ β-actin
UMRC3-PHD3 NT	0.38 ± 0.15	0.40 ± 0.11	* 0.50 ± 0.15	* 0.13 ± 0.02	5.59 ± 0.03
UMRC3-SC NT	0.59 ± 0.03	0.44 ± 0.11	* 0.95 ± 0.27	* 0.05 ± 0.01	5.32 ± 0.43
UMRC3-PHD3 TR	* 0.21 ± 0.09	0.23 ± 0.19	0.92 ± 0.18	0.21 ± 0.07	0.50 ± 0.08
UMRC3-SC TR	* 0.54 ± 0.06	0.25 ± 0.10	0.77 ± 0.42	0.23 ± 0.03	0.52 ±0.07

Densitometry Table, * indicates statistically significant differences P < 0.05

Development of a Metabolomic Profile for Fat-Poor Angiomyolipoma Using Magnetic Resonance Spectroscopy

Background

Fat-poor angiomyolipoma (AML) can be difficult to differentiate from renal cell carcinoma (RCC) radiographically and may lead to biopsy or unnecessary intervention. *In vivo* platforms with the ability to identify tumor histology based on metabolic profiles may avoid unnecessary procedures & their complications. The metabolomics of AML have not been characterized, & research into this area may provide targetable molecules for large AMLs. In this study, we investigate the metabolomic profile of AMLs compared to clear cell RCC (ccRCC) using high resolution magic angle spinning (HRMAS) magnetic resonance spectroscopy (MRS).

Methods

Tissue samples were obtained from radical or partial nephrectomy specimens that were fresh frozen & stored at -80°C. Tissue HRMAS MRS was performed by a Bruker AVANCE spectrometer. Metabolomic profiles of RCC & adjacent benign renal tissue were compared, and false discovery rates (FDR) accounted for multiple testing. Regions of interest (ROI) with FDR <0.05 were considered potential predictors of ccRCC rather than AML. The Wilcoxon rank sum test was used to compare median MRS relative intensities for candidate predictors. Logistic regression was used to determine odds ratios for risk of malignancy based on abundance of each metabolite.

Results

There were 16 ccRCC samples & 7 AML specimens. Candidate predictors of malignancy rather than AML based on FDR p-values include histidine, phenylalanine, phosphocholine, serine, alanine, glutamate, glutathione, glycerophosphocholine, & glutamine. While an abundance of these metabolites is associated with higher risk of malignancy, the odds ratio was particularly high in the 3.5-3.49 ppm spectral region (OR 2.99×10^{6}, 95% CI 3.27, 2.73×10^{12}, p=0.033) in ccRCC samples.

Conclusions

HRMAS MRS identified metabolites that may help differentiate fat-poor AML from ccRCC. In particular, metabolites in the 3.5-3.49 ppm spectral region increased the risk of harboring RCC. Our findings may contribute to future *in vivo* studies to help identify which patients require intervention for malignancy & which may be observed for benign AML without requiring biopsy.

Table 1: Summary of metabolites found to be significantly different between fat-poor AML and clear cell RCC, with odds ratios for risk of malignancy

	ccRCC (N=16)	AML (N=7)	P-value			
Median MRS relative intensities (IQR)				**FDR P-value**	**Odds ratios (OR, 95% CI)**	**P-value for OR**
4.67-4.66 (TBD)	1.22 (0.55, 4.62)	0.042 (0, 0.455)	0.007	0.00046275	4723.55 (1.54, $1.45x10^7$)	0.039
4.02-4 (TBD)	0.80 (0.56, 1.32)	0.46 (0.01, 0.67)	0.0299	0.03685893	17.89 (1.00, 319.6)	0.05
3.99-3.96 (Histidine, Phenylalanine, Phosphocholine, Serine)	1.80 (0.97, 2.61)	0.32 (0.03, 0.49)	0.0009	0.00052614	109.72 (1.25, $9.63x10^3$)	0.04
3.9-3.89 (TBD)	0.84 (0.56, 0.85)	0.10 (0.01, 0.42)	0.0019	0.00105305	674.29 (2.87, $1.58x10^5$)	0.019
3.84-3.81 (TBD)	1.51 (1.22, 1.89)	0.15 (0.03, 0.76)	0.0009	0.00055658	59.25 (2.15, $1.63x10^3$)	0.016
3.8-3.78 (Alanine, Glutamate, Glutamine, Glutathione)	2.34 (1.18, 3.23)	1.11 (0.02, 1.43)	0.0083	0.00293991	9.94 (1.08, 91.66)	0.043
3.77-3.74 Alanine, Glutamate, Glutamine)	2.75 (2.42, 3.31)	0.62 (0.03, 2.38)	0.0029	0.01004921	3.48 (1.26, 9.55)	0.016
3.57-3.56 (TBD)	1.83 (1.44, 2.45)	0.04 (0.02, 0.70)	0.0009	0.00046275	29.61 (2.23, 393.8)	0.01
3.5-3.49 (TBD)	0.53 (0.27, 0.63)	0.008 (0, 0.12)	0.0013	0.00052614	$2.99x10^6$ (3.27, $2.73x10^{12}$)	0.033
3.48-3.46 (TBD)	0.64 (0.36, 1.16)	0.01 (0.006, 0.35)	0.0045	0.0016087	1258.41 (3.2, $4.9x10^5$)	0.019
3.45-3.43(TBD)	1.31 (0.42, 2.13)	0.42 (0.03, 0.87)	0.0083	0.00418794	25.24 (1.21, 527.58)	0.037
3.42-3.39 (TBD)	1.73 (0.98, 2.81)	0.54 (0.02, 0.78)	0.0045	0.00534601	8.37 (1.14, 61.31)	0.037
3.22-3.21(Phosphocholine, Glycerophosphocholine, Histidine)	1.81 (1.03, 2.95)	0.03 (0, 0.19)	0.0003	0.00020209	888.36 (1.31, $6.04x10^5$)	0.041
2.38-2.37 (TBD)	0.22 (0.19, 0.28)	0.04 (0.008, 0.14)	0.0009	0.00052614	$2.44x10^{16}$ (0.73, $8.13x10^{32}$)	0.052
2.36-2.31 (Glutamate)	2.37 (1.67, 3.15)	0.90 (0.04, 1.33)	0.0015	0.00105305	15.05 (1.37, 165)	0.026
2.15-2.11 (TBD)	1.89 (1.43, 2.56)	0.68 (0.002, 1.27)	0.0009	0.00052614	62.62 (1.24, $3.12 x10^3$)	0.038

TBD denotes that the specific metabolites characterizing this region remain to be identified

Background:

Recurrence after BCG therapy for non-muscle invasive bladder cancer (NMIBC) occurs in approximately 40% of the cases at 5 years. Understanding the mechanisms of action of intravesical BCG may help in improving treatment outcomes. Describe changes in the tumor microenvironment upon BCG therapy and biomarkers associated with worse oncological outcomes.

Methods

Formalin-fixed and paraffin-embedded (FFPE) tissue sections before (Pre-BCG) and after (post-BCG) BCG therapy were obtained from our institutional biorepository and used for bulk targeted gene expression analysis. Tumor specimens for single cell RNAseq (scRNAseq) were analyzed fresh.

Results:

An upregulation of genes involved in B cell function was observed after BCG therapy. Pathway analyses revealed a significant enrichment in genes associated with switched memory B cells and a downregulation in genes associated with marginal zone B cells uniquely in post-BCG tumors. Additionally, there was a significant reduction in genes encoding PD-1, PD-L1, and PD-L2. *IGHA1* expression was significantly enriched in tumors that recur ≥ 6 months compared to those that recur ≤ 6 months. Single-cell RNA sequencing analysis revealed the presence of B cell subsets at different maturation stages.

Conclusions:

An upregulation of genes involved in B cell function was observed in the TME after BCG therapy. Pathway analyses revealed a significant enrichment in genes associated with switched memory B cells and a downregulation in genes associated with marginal zone B cells uniquely in post-BCG

tumors. Additionally, there was a significant reduction in genes encoding PD-1, PD-L1, and PD-L2. *IGHA1* expression was significantly enriched in tumors that recur ≥ 6 months compared to those that recur ≤ 6 months. Single-cell RNA sequencing analysis revealed the presence of B cell subsets at different maturation stages.

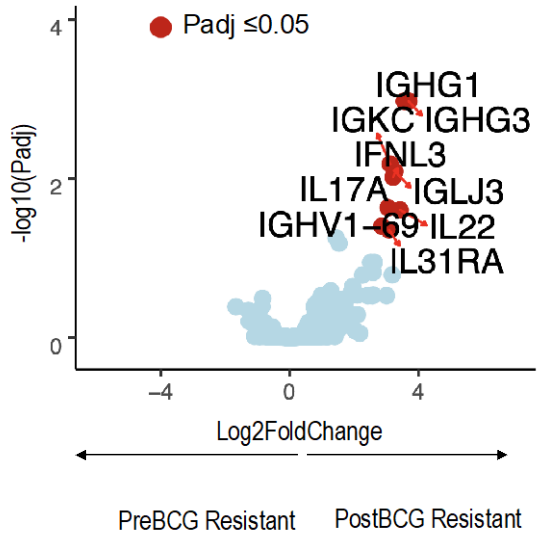

Figure 1. Differentially expressed genes between pre and postBCG bladder tumors from resistant patients. BCG therapy may induce expression of genes that promote synthesis of Immunoglobulins and B cell recruitment

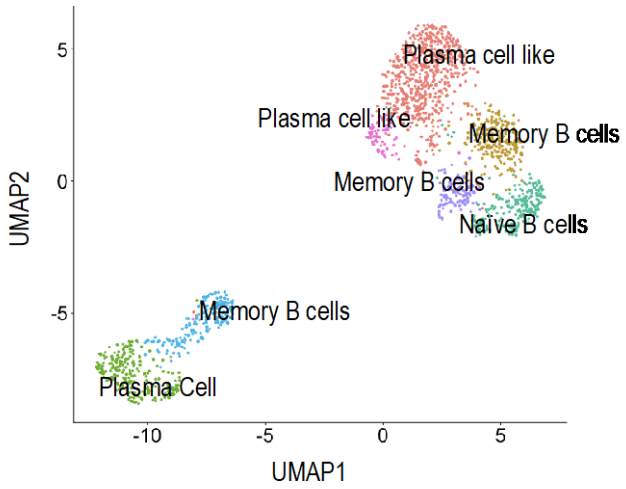

Figure 2. UMAP displaying tumor infiltrating B cell subsets in unmatched pre-BCG and Post-BCG specimen

The AR-CAMKK2-AMPK signaling axis regulates adipose triglyceride lipase in prostate cancer, controlling access to intracellular lipid depots and promoting disease progression

Background: Late-stage prostate cancer patients are treated with androgen deprivation therapy. However, the majority will relapse within 2-3 years. The androgen receptor (AR) and the processes downstream of the receptor remain viable therapeutic targets in prostate cancer. We previously identified the AR-CAMKK2-AMPK signaling axis as a major driver of prostate cancer metabolism. To identify, in an unbiased manner, AMPK downstream targets potentially involved in prostate cancer progression, we leveraged an improved AMPK substrate motif to mine phosphoproteomics data obtained from men with benign disease, localized, hormone-sensitive or metastatic, castration-resistant prostate cancer (mCRPC) samples. Using this approach, we were able to identify high-confidence AMPK targets across subgroups. The screen revealed that phosphorylation of adipose triglyceride lipase (ATGL), the rate-limiting step in the breakdown of triglycerides in lipid droplets, tracks with disease progression.

Methods: A battery of molecular (inducible shRNAs), biochemical (kinase activity), genetic (CRISPR/add-backs) and pharmacological approaches were used to investigate ATGL's regulation and role in prostate cancer cell biology.

Results: Increased AR-CAMKK2-AMPK signaling increased ATGL phosphorylation and subsequent lipolysis. Conversely, knockdown or knockout of ATGL led to an accumulation of neutral lipids in various prostate cancer cell models and inhibited proliferation and migration of CRPC cell models. Using pharmacological or genetic approaches, we were able to show that the inhibition of ATGL impaired intracellular lipid shuttling that could be exploited therapeutically.

Conclusions: Research on lipid metabolism in prostate cancer has centered on lipid uptake and *de novo* lipogenesis, little consideration has been given to how cancer cells accommodate and later access these new lipids. Our study gives important insights into how intracellular fat depots are accessed during prostate cancer progression and suggests that regulation of ATGL is a key mediator of this step. Hence, ATGL represents a potential novel therapeutic target for the treatment of advanced prostate cancer.

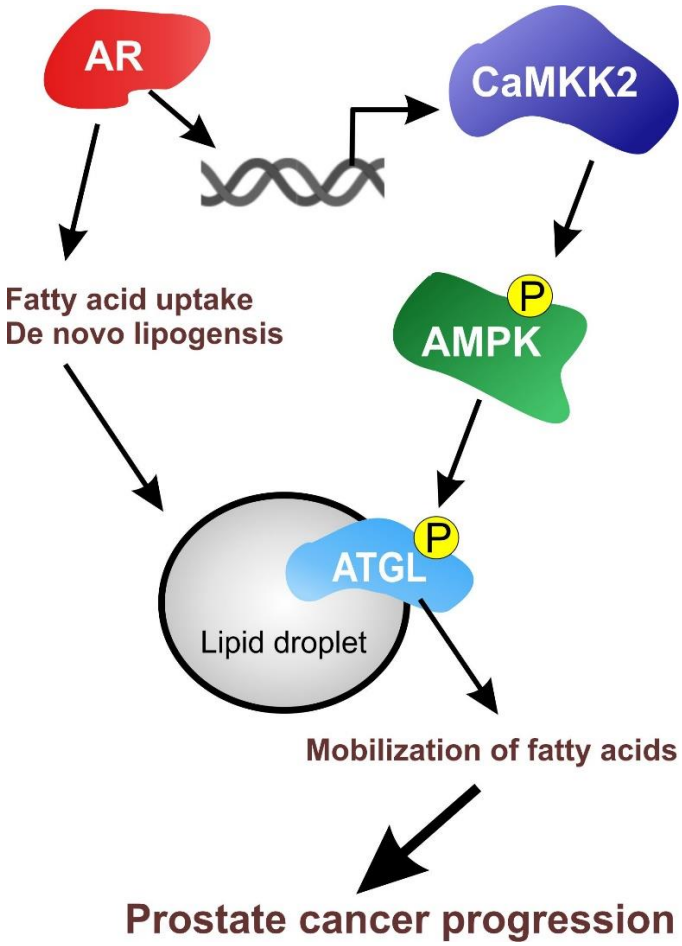
AR
CaMKK2
Fatty acid uptake
De novo lipogensis
P
AMPK
P
ATGL
Lipid droplet
Mobilization of fatty acids
Prostate cancer progression

Single-cell atlas of epithelial and stromal cell heterogeneity by lobe and strain in the mouse prostate

Background:
The mouse prostate is comprised of four lobes: anterior, dorsal, lateral, and ventral. While the lobes are known to differ in tissue morphology and secretions, rigorous single-cell assessments of the transcriptional profile of both epithelial and stromal cell types for each lobe and in multiple mouse strains are lacking.

Methods:
We dissected individual prostate lobes from two commonly used mouse strains, FVB/NJ (N = 2) and C57BL/6J (N = 3), and prepared single-cell RNA-sequencing (scRNA-seq) libraries for each lobe. Mouse prostate scRNA-seq data (27,896 cells) were pre-processed using CellRanger and Seurat, and visualized using Uniform Manifold Approximation and Projection (UMAP) dimensionality reduction and Louvain clustering, as implemented in Seurat (v 3.1.5).

Results:
Data dimensionality reduction and clustering analysis revealed that epithelial cells possessed strain-specific differences, with luminal cells also displaying striking lobe-specific differences. However, two populations of luminal epithelial cells clustered independently of lobe and strain, including a rare population of luminal cells (0.25%) expressing Foxi1 and components of the vacuolar ATPase proton pump (Atp6v1a, Atp6v0d2), and a progenitor-like population (1.8%) expressing stem cell-associated genes (Ly6a/Sca-1, Tacstd2/Trop-2, Psca). In contrast to the epithelial cells, stromal cell clusters (smooth muscle, pericytes, immune cells, and fibroblasts) were largely conserved across strain and lobe. Notably, two fibroblast populations clustered separately when data dimensionality was restricted to stromal cell types, with one cluster having an upregulation in the immune-associated chemokine receptor, Ccr2, as assessed by Ingenuity Pathway Analysis.

Conclusions:
In these foundational single-cell studies of strain and lobe-specific differences in the mouse prostate, we have uncovered previously uncharacterized cell types and nominated unique molecular markers for a more granular in situ examination of prostate tissues. The combination of lobe-specific differences in luminal cells and the stromal composition in the mouse prostate likely contribute to the histological differences observed between lobes. Overall, the findings of this study help establish the fundamental cell types residing in the normal mouse prostate of common mouse strains and serve as a reference to better understand how genetic alterations in transgenic mouse models are impacted by the normal biology of cells in the prostate.

Title: Disrupted Vitamin D Receptor signaling in Prostate Cancer Progression

Authors: Hsu-Chang Wu[1], Moray J. Campbell[1]

[1]The Ohio State University, College of Pharmacy, Columbus OH 43210

Introduction: The miR-106b-93-25 cluster is located in intron 13 of the DNA licensing factor, MCM7. In prostate cancer (PCa), there is strong evidence that altered cluster expression associates with more aggressive disease and therapy resistance. Our previous studies established in non-malignant prostate cells that the nuclear hormone receptor, Vitamin D receptor (VDR), regulates MCM7 as part of a feed-forward loop to control expression of the miRNA cluster and its downstream targets such as CDKN1A (encodes $p21^{(wa1/cip1)}$). The current study was undertaken to test how this signaling axis is altered in PCa, by considering how MYC binding to MCM7 favors miR-106b-25 up-regulation.

Methods: We have exploited miR-106b-93-25 antagomirs and examined regulation of target genes in nonmalignant prostate HPr1AR and malignant LNCaP cells, alongside proliferation assays to test how antagomirs plus $1,25(OH)_2,D_3$ worked co-operatively.

Results:

Cell line data – expression miRNAs was measured in both HPr1AR and LNCaP cell lines; proliferation with antagomirs; gene expression of antagomir and antagomirs plus $1,25(OH)_2,D_3$ - Figure 1 showed that the expression of the mRNAs, the downstream effectors of MCM7 and the cluster, differ between cell lines and if the treatment of $1,25(OH)_2,D_3$ was added.

Finally, we are currently undertaking MYC ChIP-qPCR to reveal how MYC binding patterns on MCM7 relate to time-resolved expression of MCM7 mRNA and protein, and the miR-106b-93-25 cluster.

These results suggest that regulation of MCM7, the miRNAs and downstream effecters differ between HPr1AR and LNCaP cells. The data are supported by analyses in TCGA cohorts, revealing that miR-106b expression in high grade PCa tumors significantly impacted the correlations between VDR and its target genes.

Conclusion:

Our studies demonstrate that VDR regulates MCM7 as part of a feed-forward loop to control expression of the miRNA cluster and its downstream targets, which in turn mediates cancer growth progression. This regulation varies across different prostate cell models and stages.

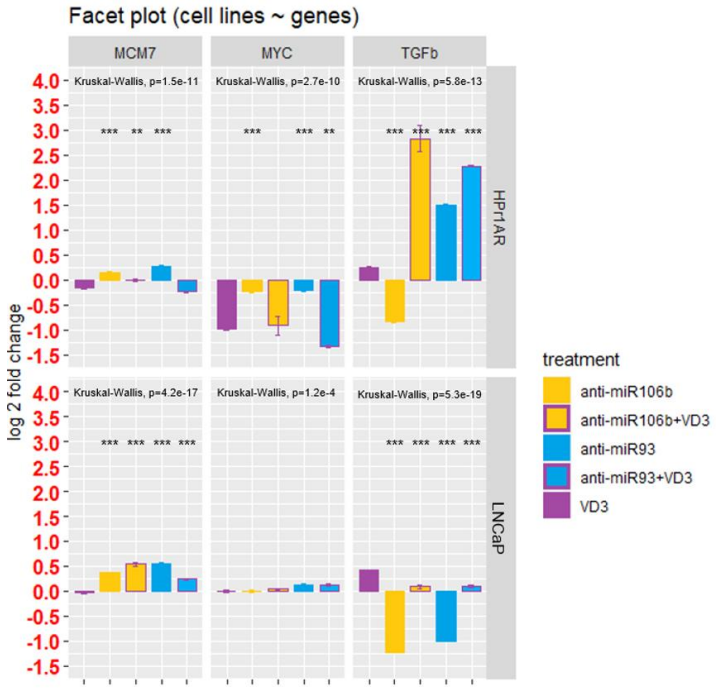

Figure 1: Real time RT-PCR was used to measure changes in expression of the indicated genes following treatment with the VDR ligand 1a,25(OH)$_2$D$_3$ (VD3, 100 nM), miRNA antagomir (35 nM) either alone or in combination.

Background: Outcomes of radiation therapy are highly positive for localized prostate cancer; however, local recurrence remains a potential negative outcome. One mechanism of recurrence is radioresistance. Current practice groups patients between active surveillance, prostatectomy, or radiation therapy based upon patient life expectancy and risk group. Physician-patient shared decision ultimately determines a treatment regimen which includes understanding the side effects, impact on life, and pitfalls of each treatment. Therefore, there is benefit in discovering a radiation therapy outcome specific biomarker to decipher between the two treatment regimens. Recently, SOX2, an established stem maintenance transcription factor, is emerging as a protein of interest in prostate cancer as a key driver of lineage plasticity and therapy resistance. Further, immunohistochemical analyses of prostate tumors demonstrate tumors are either ubiquitously SOX2 positive or negative, thus making it a potential ideal biomarker candidate.

Methods: We eliminated SOX2 expression in SOX2 endogenous prostate cancer cells, CWR-R1s, through CRISPR/Cas9 gene editing. ChIP-Seq and RNA-Seq was conducted to determine SOX2 binding sites and SOX2-associated gene regulation, and bioinformatic pathway prioritization determined potential SOX2-mediated pathways. Functional assays and protein analyses we conducted to mechanistically define roles for SOX2 in prostate therapy resistance.

Results: We found the loss of SOX2 led to decreased cell growth. Further, analyses prioritized SOX2-assoicted changes in DNA damage signaling and responses. DNA damage signaling genes via Qiagen pathway array showed differential expression between SOX2 expressing and non-expressing cells. This led us to examine the DNA damage sensing protein γH2AX, which demonstrated constitutive activation of γH2AX and accumulations of foci upon loss of SOX2.

Applied Deep Learning to Prostate Cancer Tissue Images with Genomic Profiling to Classify Tumor Progression

Purpose

Deep learning techniques can aid the automation of prostate cancer grading from histologic samples, thereby improving diagnostic accuracy and treatment selection.

Introduction

Among the most valuable tools in the evaluation of prostate cancer is the Gleason Score (GS) that is assigned by a pathologist to prostatic biopsies. This score represents the aggressiveness of the tumor and ranges from 3 to 5 (least to most aggressive) in a primary and secondary pattern. Here we describe how deep learning techniques can automate the classification of prostate samples by GS. By automating this process, we are able to reduce the human subjectivity and potential error of Gleason grading and are able to create a pipeline by which we can integrate gene expression to quickly determine cancer progression in individual patients.

Methods

733 prostate tissue slide images were downloaded along with clinical information on 500 individuals from the PRAD study contained in The Cancer Genome Atlas (TCGA). We used the Xception network architecture within the Keras software package and TensorFlow backend in Python. We used 80 images that were scored by a board-certified pathologist as training images (with data augmentation) to create a refined deep convolutional neural network to automate Gleason grading to identify cancer regions of interest on test training slides. We then used this model to score new unannotated slides blindly. Additionally, we have looked at gene expression by combining patients within a specific GS, and compared profiles within each group with gene expression software. From this we were able to select a set of unique markers to identify new patients by GS as well as identify the amount of genetic variance within a given dataset.

Results

We compared the model results of the Gleason grading from 10 images with the score that was reported in the TCGA and found that the system was able to correctly identify 7 of the 10 GS. We were able to identify 6,411 differentially expressed genes (DEG) between normal adjacent tissue and GS6, 186 DEGs between GS6 and GS7, 1,855 DEGs between GS7 and GS8, and 603 DEGs between GS8 and GS9.

Conclusions

Deep learning can be applied to determine the histologic severity of tissue images. Given future modifications to improve the accuracy of our current model, we can be hopeful of producing an automated software workflow that will aid in identifying tumor areas, determining their severity, and influencing treatment decisions.

COVID-19 Associated Cystitis (CAC): Infection with SARS-CoV-2 and Subsequent Urinary Symptoms

Ryan Timar[1], Nevedita Dhar[2,3], Melissa Wills[1], Laura E. Lamb[4,5], Michael B. Chancellor[4,5]

[1] Wayne State University School of Medicine, Detroit, MI, USA

[2] Detroit Medical Center, Detroit, MI, USA

[3] John D. Dingell VA Medical Center, Detroit, MI, USA

[4] Oakland University William Beaumont School of Medicine, Rochester Hills, MI, USA

[5] Department of Urology, Beaumont Health System, Royal Oak, MI, USA

Corresponding author: Laura E. Lamb

Address: 3811 W. 13 Mile Road, Suite 504, Royal Oak, MI 48073

Phone: 248-551-0579

Fax: 248-551-0486

Purpose

Coronavirus disease 2019 (COVID-19) causes many symptoms in various organ systems, and other viral infections are known to result in lower urinary tract symptoms (LUTS). However, there is scarce literature regarding genitourinary symptoms in COVID-19 disease. We sought to determine if patients with COVID-19 experienced any new or different urologic symptoms.

Materials and Methods

With IRB approval, hospital discharged COVID-19 patients completed an AUA Urology Care Foundation Overactive Bladder (OAB) Assessment Tool to determine their current urinary symptoms, and if applicable, how their symptoms changed after recovering from COVID-19. Patients responded to five symptom and five quality-of-life questions (QOL). All questions range from 0 to 5 based on severity for a maximum score of 25. People with normal urinary habits should expect to score near 0 using this assessment tool.

Results

We identified 44 patients with new or worsening OAB symptoms, most notably frequency, urgency, and nocturia. The median total OAB symptom score in both men and women with COVID-19 was 18. The median total QOL score for both men and women with COVID-19 was 19. Median age was 64.5 (range 47-82). Median length-of-stay (LOS) was 10 days (range 5-30).

Conclusion

COVID-19 patients reported severe de novo genitourinary symptoms, most notably an increase in urgency, frequency, and nocturia. We called these associated urinary symptoms COVID-19 associate cystitis (CAC). It is unclear if these urological symptoms are caused directly by the virus, indirectly through increased inflammation, or through another mechanism. Research is needed to elucidate the specific pathophysiology of OAB symptoms in the context of COVID-19 so urologists can timely and appropriately treat their patients.

Classification (n)		Symptom score (median)	Range	QoL score (median)	Range
New (39)		*18*	*12-21*	*19*	*16-24*
Worsening (5)					
	Before	*8*	*4-10*	*9*	*8-10*
	After	*19*	*17-21*	*20*	*19-20*
Female (12)		*18*	*15-21*	*19*	*16-21*
Male (32)		*18*	*12-20*	*19*	*16-20*

Table. Primary outcomes for symptom & quality of life (QoL) scores
**only "after" symptom scores are included in male/female analysis*

Role of Prx4 in Prostate Cancer Development and Radiation Resistance

Na Ding[1], Hong Jiang[1], Pratik Thapa[1], Yanning Hao[1], Aziza Alshahrani[1], Shengming Yang[3], Vivek M Rangnekar[2], Xiaoqi Liu[1,2], Qiou Wei[1,2]*

[1]Department of Toxicology and Cancer Biology, [2]Markey Cancer Center, College of Medicine; [3]College of Agriculture, University of Kentucky, Lexington, KY 40536

*Corresponding to qiou.wei@uky.edu

Introduction & Objective

The peroxiredoxin (Prx) family of proteins functions as major cellular antioxidants that mediate oxidative signaling under physiological conditions as well as scavenge extra hydrogen peroxide in the context of oxidative stress. Among them, Prx4 is encoded by *PRDX4* gene on X chromosome and has been found to contribute to the development of male reproduction system. Previous studies indicate that Prxs are frequently upregulated in various types of human cancer. However, the role of Prx4 in prostate cancer has not been well defined. The purpose of this study is to examine the expression of Prx4 in prostate cancer and to explore its functional significance in cancer radiation resistance and recurrence.

Methods

Bioinformatic tools were used to evaluate genetic alterations of *PRDX4* gene as well as the levels of its transcripts in prostate normal and cancer populations. Kaplan-Meier survival analysis was used to explore the association of Prx4 levels with the prognosis of prostate cancer patients. Western blot and immunohistochemistry were used to evaluate the expression of Prx4 protein in cell lines and patient specimens. Loss of Prx4 in cells was achieved by knock down using lentiviral shRNA or knockout using CRISPR-Cas9 techniques. Cell proliferation, survival, and protein profiler kinase arrays were used to examine the differences between control and Prx4-depleted cells with or without ionizing radiation.

Results

We demonstrated that *PRDX4* gene is frequently amplified in prostate cancer and the level of its transcript is highly elevated. Patients with Prx4 at higher quartile have significantly reduced probability of survival compared with those in lower quartile. Prostate cancer cells express much higher levels of Prx4 than normal epithelial cells. Moreover, Prx4 is upregulated by the activation of AR-dependent signaling, and depletion of Prx4 sensitizes prostate cancer cells to radiation-induced cell death. Mechanistically, Prx4 contributes to prostate cancer radiation resistance through the activation of PI3K/AKT signaling pathway (Figure).

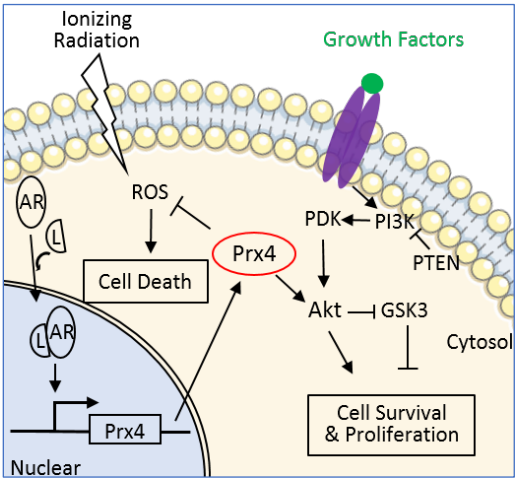

Conclusions

A combination of bioinformatic, histochemical, cellular, and molecular methods reveals that Prx4 plays a critical role in prostate cancer cell proliferation, radioresistance and reoccurrence.

Background: In prostate cancer (PCa), the surrounding stromal cells are activated to a disease phenotype termed cancer-associated fibroblasts (CAFs). While stromal cells are not mutated in PCa, their secretome changes to enhance prostate cancer survival and progression. Extracellular vesicles (EVs) released from the cells of the tumor microenvironment have been implicated in various aspects of prostate cancer progression and metastasis. Proteins, mRNAs, and small noncoding RNAs within these EVs communicate with surrounding cells. Our goal is to study EV microRNAs (miRs) secreted from patient-derived prostate epithelial and stromal cells and determine their effects on prostate biology and cancer.

Methods: Patient radical prostatectomy tissue was dissociated to single cells followed by selection for epithelial and stromal cells using cell type-specific media. Patient-derived prostate cells were fully characterized using prostate epithelial and stromal markers by qPCR. Prostate epithelial and stromal cell EVs were isolated from culture media via differential ultracentrifugation. Small RNAs from patient prostate cells and cell EVs were sequenced by next generation sequencing (NGS) and were validated by microRNA in situ hybridization (ISH) of prostate tissue (miRScope) and qPCR. NGS data was analyzed with edgeR.

Results: There were 190 differentially expressed miRs between epithelial and stromal cells and 278 differentially expressed miRs between EVs released from epithelial and stromal cells ($Q<0.05$). Of these miRs, 79 were differentially expressed in both comparisons. Of interest, miR-199a-5p and miR-199a-3p were specific to the stromal cells and stromal cell EVs. The localization of miR-199a in the stromal compartment was confirmed by miR ISH staining of patient radical prostatectomy tissue. Both miR-199a-5p and miR-199a-3p were robustly expressed in patient serum EVs as quantified by NGS.

Conclusions: We demonstrate that miR-199a is specific to the prostate stroma and circulates in serum EVs. We are currently working to determine the role of miR-199a in the prostate stroma and the effects it may have on prostate cancer via EV communication in the tumor microenvironment. Future experiments include overexpressing and knocking down miR-199a in prostate stroma cells and quantifying levels of target genes in both prostate cell types. A prostate cancer patient tissue microarray will be used to quantify miR-199a levels in patient-matched cancer and benign tissues. We hope to determine the role of miR-199a in promoting the CAF phenotype and CAF-mediated effects via extracellular vesicle signaling.

Temporal evolution of cellular heterogeneity during the progression to advanced, AR-negative prostate cancer

Background:
The progression from castration-resistant prostate cancer (CRPC) to neuroendocrine (NE) prostate cancer (NEPC) is driven by a number of molecular events, such as the amplification and overexpression of *MYCN* (encoding the transcription factor N-Myc). In a cohort of advanced prostate cancer patients, we found an enrichment for the co-occurrence of N-Myc overexpression and the loss of the tumor suppressor *RB1*. Moreover, patients harboring both genetic events have significantly reduced overall survival. We have previously showed that N-Myc overexpression in a genetically engineered mouse model (GEMM) of prostate cancer can induce a transcriptional profile similar to what is observed in the context of RB1 loss-of-function. However, the molecular programs underlying these changes are not understood.

Methods:
We recently developed a novel GEMM with N-Myc overexpression in a Pten- and Rb1-null background that develops NE-like disease. We have extensively characterized tumor histology and metastatic spread over time. Moreover, we have used single-cell based approaches, such as scRNA-seq and scATAC-seq, in conjunction with genome-wide N-Myc ChIP-seq and DNA methylation studies, to fully characterize the development of NEPC. We have also compared the results from our GEMM to a cohort of clinical prostate cancer patients, including two scRNA-seq profiles from NEPC patient samples.

Results:
Tumors formed in the new GEMM significantly faster than animals with wild-type *Rb1*, beginning as early as 8 weeks of age. The tumors contained foci of AR-negative, poorly differentiated disease. Distant metastases were found in the lymph nodes, lungs and liver and consisted entirely of AR-negative tumor cells that were positive for NE markers. Additionally, surgical castration followed by longitudinal MRI revealed that these tumors were resistant to castration compared to control groups. Bulk RNA-seq, N-Myc ChIP-seq, and RRBS performed on regions of conventional adenocarcinoma compared to poorly differentiated tumor regions revealed an enrichment for a number of neural- and stem cell-related genes and clinically relevant changes to the methylome. To understand the heterogeneity in the developing tumors, we performed scRNA-seq and scATAC-seq on mouse prostates collected at 6 and 8 weeks of age. While a large number of cells at these early time points were N-Myc^{+} and AR^{-}, a distinct subpopulation of cells was present that were N-Myc^{+} and AR^{+} but showed low expression of AR target genes, suggesting a transition away from an AR-dependent state. Combined analysis of scRNA-seq and scATAC-seq data revealed the existence of a population of cells expressing a novel transcription factor which may be implicated in the transition to an NE-like state.

Conclusions:
We have identified that N-Myc overexpression in conjunction with Rb1 loss-of-function is enriched in NEPC patients and confers reduced overall survival. Using a novel GEMM, we have shown that N-Myc overexpression and Rb1 loss-of-function can synergize to dramatically accelerate tumorigenesis, promote castration resistance, and drive the acquisition of an NE-like state. Future studies will assess the temporal regulation of transcriptional programs following castration and reveal the mechanistic underpinnings of the development of NEPC.

Arginine vasopressin receptors as therapeutic targets for castration-resistant prostate cancer

L. Heidman and K. Burnstein

Department of Molecular and Cellular Pharmacology, University of Miami Miller School of Medicine; Sylvester Comprehensive Cancer Center

BACKGROUND

Improved drugs to combat castration-resistant prostate cancer (CRPC) are needed. We identified the G protein-coupled receptor, arginine vasopressin receptor type 1A (AVPR1A) as a potential therapeutic target in CRPC. AVP is the ligand for AVPR1A and all AVPR subtypes. AVPR1A signals via Gq11 subunits to stimulate intracellular calcium release. AVPR1A mRNA levels are elevated in CRPC patients compared to primary PC and depletion of AVPR1A decreases CRPC cell proliferation. Safe and effective AVPR1A antagonists have been evaluated in clinical trials for non-cancer conditions. The AVPR1A selective antagonist, relcovaptan, inhibits CRPC tumor growth in vivo in three distinct preclinical settings: newly emergent, established and late stage growth in the bone metastatic niche. Because osteoblasts and osteoclasts express AVPR1A, we investigated possible autocrine and paracrine signaling by the ligand AVP. Since AVP stimulates all AVPRs including AVPR2, which is also expressed in CRPC, we investigated the effects of AVPR2 antagonism on PC cell proliferation.

METHODS

We examined AVP stimulated pathways using pharmacologic inhibitors, analyzed human PC datasets, and investigated AVP production by CRPC cell lines. We evaluated AVPR2 mRNA expression in PC cells and the combined effects of selective antagonists of AVPR1A and AVPR2 on CRPC cell proliferation.

RESULTS

Pre-provasopressin (the precursor to mature AVP) mRNA is present at higher levels in advanced PC patient datasets. We discovered that AVP was synthesized by several CRPC cell lines. AVP stimulates ERK phosphorylation leading to activation of CREB in CRPC and this pathway was blocked by a Gq11 inhibitor but was independent of calcium signaling. AVPR2 was co-expressed with AVPR1A in patient samples as well as in select CRPC cell lines. The combination of AVPR1A and AVPR2 antagonists inhibited CRPC cell proliferation and promoted apoptosis to a significantly greater extent than treatment with the individual antagonists.

CONCLUSION

These data reveal the potential for AVP autocrine and paracrine signaling in CRPC and suggest that AVP-mediated activation of both AVPR1A and AVPR2 may occur. These findings support the repurposing of drugs that target AVPRs in CRPC.

STAG2 role in gene regulation in muscle invasive bladder cancer (MIBC)

Zara Kazmierczak, Lanni Aquila, Nithya Krishnan, Swathi Ramakrishnan, Jianmin Wang, Eduardo Cortes Gomez, Anna Woloszynska-Read

Background:
Stromal Antigen 2 (STAG2) is one of the major subunits comprising the cohesin complex and is the most frequently mutated cohesin component in muscle invasive bladder cancer (MIBC). Independent of its role in chromatid segregation, STAG2 is thought to have a role in gene regulation. Based on evidence that STAG2 binding sites correspond to tissue-specific enhancers, we hypothesize that STAG2 acts as a transcription factor. Our objective is to investigate how STAG2 impacts BC biology through gene regulation and how this knowledge can be utilized in therapies.

Methods:
Whole and targeted exome sequencing revealed the presence of STAG2 functional mutations in over 10% of patients, with tumor immunochemistry confirming loss of STAG2 protein expression in mutated tumors. To study the impact of STAG2 loss on gene regulation in MIBC, we stably knocked down STAG2 in T24 cells via shRNA. Integrated analysis of ChIP (WT STAG2) and RNA sequencing (upon STAG2 knockdown) using Cistrome algorithm allowed us to identify STAG2 target genes. To map genome-wide chromatin accessibility upon loss of STAG2, we utilized ATAC sequencing. We used integrated analysis of increased accessibility (ATACseq) and gene expression (RNAseq) in T24 STAG2 wild type and knockdown cells to identify specific genomic regions of STAG2 transcriptional activity.

Results:
We observed that patients (n=330) with no STAG2 expression had prolonged median overall (34 vs. 24.5 months, p=.049) and progression free survival (23 vs. 13.5 months, p=.016) compared to STAG2 positive tumors. Integration of ChIP-seq and RNA-seq data identified epithelial-mesenchymal transition genes, such as MMP2, MMP9, SLUG, and SNAIL, targeted by STAG2. Cistrome with GeneHancer overlaps of STAG2 targets indicated 2811 potential enhancers regulated by STAG2. Integrated analysis of RNAseq and ATACseq data showed a decrease in chromatin accessibility upon knockdown of STAG2. shRNA-induced loss of STAG2 in T24 led to reduced chromatin accessibility. This correlated with increased expression of genes involving sister chromosomes resolution, cell cycles, rRNA modification and reduced expression of genes involving interferon signaling pathway and cellular matrix organization.

Conclusions:
Our results support the hypothesis that STAG2 promotes MIBC progression through transcriptional regulation and changes in chromatin accessibility. Our ongoing work will focus on functional validation of newly identified STAG2-regulated pathways and how STAG2-driven biology in bladder cancer can be exploited for new interventions.

Title: Androgen play critical roles in epithelium proliferation in BPH not normal adjacent

Authors: Wei Chen, Laura E. Pascal, Rajiv Dhir, Uma Chandran, Alex Chang and Zhou Wang

Background: The androgen receptor (AR) is expressed by both stromal and epithelial cells in the prostate, and plays a critical role in normal development and homeostasis as well as prostate pathogenesis. Our preliminary data showed that stromal AR signaling was essential for the proliferation of epithelial cells in BPH, but not in normal adjacent prostate (NAP). However, the underlying mechanisms of this phenomenon are still unknown.

Method: Human prostate specimens obtained from BPH patients undergoing simple prostatectomy for symptomatic BPH. Patient derived explants (PDE) and stromal cell cultures from BPH and NAP tissues were established and utilized to evaluate the impact of androgens. Proliferation, cytokines and androgen-responsive genes were quantified in clinical BPH specimens and paired normal prostatic specimens via immunohistochemistry, RNA-Seq and qPCR.

Results: PDEs derived from BPH and paired NAP tissues were able to maintain their original architecture and AR signaling in culture for at least 4 days. Androgen could induce epithelial proliferation in BPH, but not NAP explants. Stromal cells derived from BPH tissues secreted higher levels of CCL family proteins (CCL8, CCL7, CCL11, CCL13 and CCL28), CXCL proteins (CXCL6, CXCL12), interleukins (IL6, IL7 and IL32), and growth factors than those derived from the paired NAP tissues. RNA sequencing identified several cytokines and growth factors which were up-regulated after androgen stimulation in BPH, but not NAP. These results were confirmed by qPCR.

Conclusions: Androgens could increase epithelial proliferation in BPH but not NAP in the PDE model. Androgens were shown to influence the expression of several genes including CXC and interleukins in BPH stromal cells, but not NAP stromal cells. Our results suggest that androgen signaling in BPH stromal cells is dysregulated and could contribute to prostatic epithelial growth and provide a strong foundation to elucidate the mechanisms of androgen-dependent stromal regulation of epithelial cell growth in BPH.

Title: Claudin 1 is down-regulated in the aging prostate and associated with increased inflammation in BPH

Authors: Laura E. Pascal, Rajiv Dhir, Goundappa K. Balasubramani, Wei Chen, Chandler Hudson, Pooja Srivistava, Anthony Green, Donald B. DeFranco, Naoki Yoshimura and Zhou Wang

Background: Benign prostatic hyperplasia (BPH) is an age-related disease that is frequently associated with chronic prostatic inflammation. In our previous studies, we detected the presence of PSA protein in the stroma of BPH nodules and down-regulation of junction proteins E-cadherin and claudin 1. Transmission electron microscopy (TEM) imaging showed a decrease in tight junctions suggesting the luminal epithelial barrier in BPH tissues may be altered. Recent in vitro studies showed that stimulation of benign prostate epithelial cell lines with TGFβ1 induced a decrease in claudin 1 expression suggesting that inflammation might be associated with alterations in the prostate epithelial barrier. This study explored the potential associations between aging and loss of junction proteins and the presence of inflammatory cells in prostate tissue specimens from young healthy donors and aged BPH patients.

Method: Immunostaining of serial prostate sections from BPH patients and healthy young donors was performed for claudin 1, CD4, CD8, CD20 and CD68. H-Scores and the number of inflammatory cells were calculated for the same area in donor, normal adjacent prostate to BPH (NAP) and BPH specimens. Quantification and statistical correlation analyses were performed.

Results: Down-regulation of junction protein claudin 1 was associated with increasing age and inflammation in NAP and BPH compared to young healthy donor prostate.

Conclusions: These findings suggest that aging is associated with down-regulation of claudin 1 and claudin 1 is further decreased in BPH. Claudin 1 down-regulation was associated with increased infiltration of inflammatory cells in both NAP and BPH tissues. Claudin down-regulation in the aging prostate could contribute to increased prostatic inflammation, subsequently contributing to BPH pathogenesis.

Immune cell RNA sequencing and interaction analyses suggest a role for mast cells in benign prostatic hyperplasia

Introduction and objective

Single cell mRNA sequencing (scRNA-Seq) is a valuable tool in identification and comparison of gene expression and interactions among various cell types. scRNA-Seq data was used to identify immune cell populations in BPH and normal prostates and compare ligand-receptor interactions between immune cells. Initial analyses predicted numerous interactions involving mast cells (MC), suggesting a potential role for MC interactions in BPH. Here we use scRNA-Seq data to further explore MC and their role in BPH.

Methods

scRNA-Seq was performed on immune cells isolated from 10 small (<60g) and 3 large (>70g) BPH prostates. Distinct immune cell subtypes were clustered based on differential gene expression (DGE). These data were combined with previously published scRNA-Seq data from three normal prostates. Ligand-receptor interactions were predicted and scored based on ligand and receptor gene expression and cell number while referencing databases of known ligand-receptor pairs. MC gene expression and ligand-receptor interactions scores were compared between sample types.

Results

Unsupervised clustering of combined scRNA-Seq data segregated immune cells into 11 main clusters, including a prominent MC cluster, which was further divided into 6 subclusters. Significant gene expression alterations between BPH and normal samples MC included multiple pro-inflammatory cytokines such as CSF1, TNF, and CCL2. Initial interaction scoring across all immune cell subtypes predicted and scored a total of 5515 ligand-receptor pairs, 2018 scores were significantly different between BPH and normal samples. 1,001 of predicted interactions involved MC, 492 with significantly different scores between small BPH and normal and/or large BPH and normal. These included both MC-MC interactions and MC interactions with other immune cell types. Highly scored interactions include ligand-receptor pairs that have been associated with cell adhesion and migration such as VIM/CD44, TIMP1/CD63, and HBEGF/CD9. Also, CD63 and CD9 have been implicated in mast cell activation and chemotaxis.

Conclusion

While the role of MC in BPH is not well understood, these results indicate that MC and their interactions are altered in BPH compared to normal prostates, suggesting a potential role in the disease. And while further studies are needed to define the biological significance of these alterations, the scRNA-Seq and bioinformatic analysis techniques described here aid in identification of potential targets for future studies.

Stromal estrogen receptor-alpha is involved in the development of lower urinary tract dysfunction.

AUTHORS
Debra R. Garvey[1], Kristen S. Uchtmann[1], Richard E. Peterson[2], and Chad M. Vezina [1,3,4] and William A. Ricke[1,3]

[1]George M. O'Brien Center of Research Excellence, Department of Urology, University of Wisconsin-Madison, Madison, WI,
[2]School of Pharmacy, University of Wisconsin-Madison, Madison, WI, USA;
[3]Molecular and Environmental Toxicology Center, University of Wisconsin-Madison, Madison, WI, USA;
[4]School of Veterinary Medicine, University of Wisconsin-Madison, Madison, WI, USA

ABSTRACT
Introduction: Aging men exhibit a shift in hormone levels which contribute to the development of lower urinary tract dysfunction (LUTD). We recently determined that *in utero* and lactational exposure to the persistent environmental toxicant, 2,3,7,8-tetrachlorodibenzo-*p*-dioxin (TCDD), exacerbates voiding dysfunction in the testosterone (T) and 17b-estradiol (E2) model of LUTD. It was also demonstrated that estrogen receptor-alpha (ER-α) was necessary for the development of LUTD in C57Bl/6 male mice. The objective of this study was to determine if stromal ER-α was necessary for the development of LUTD.
Methods: To determine the specific role of estrogen receptor-alpha (ER-α) in prostatic stroma we used stromal specific smooth muscle-cre (B6.Cg-Tg(TgIn-cre)1Her/J) mice crossed to ER-α floxed mice, which deleted prostatic stroma ER-α. These mice were exposed *in utero* to TCDD at embryonic day 13.5 (or corn oil), then in adulthood at six weeks were treated with T and E2 or sham using slow release subcutaneous implants. To assess voiding behavior, we utilized void spot assays (VSA) each week for four weeks following hormone treatment. Mice were necropsied after the 4th VSA to assess the bladder and prostate.
Results: We observed decreased bladder mass and void dribbling in the stromal ER-α knockout in comparison to wild type for the TCDD and hormone treated groups.
Conclusion: These findings suggest that stromal ER-α plays a key role in the development of lower urinary tract dysfunction (LUTD) in this 2-hit model of LUTD. To further investigate the role of ER-α in other cell types future work will use epithelial-specific cre: B6.Cg-Shh $^{tm1(EGFP/cre)Cit}$/J mice.

Title: Deciphering Human Prostate Carcinoma-Associated Fibroblast Heterogeneity using scRNA-seq

Background: Carcinoma-associated fibroblasts (CAF) are a heterogenous component of the prostate tumor microenvironment and have been demonstrated to regulate prostate cancer growth and progression in a variety of ways. The extent of CAF heterogeneity in prostate cancer tissues has not been well described.

Methods: These studies expand upon our recent description of the heterogeneity of cultured CAF by isolating fibroblasts directly from human prostate cancer and matched normal tissues for single-cell mRNA-sequencing (scRNA-seq) analysis. These studies evaluated several digestion conditions for isolation of prostatic fibroblasts. Sorting of primary fibroblasts was conducted by excluding CD45 (immune), CD200 (endothelial), and EpCAM (epithelial) cells. Prostate cancer-containing peripheral zone (PZ) and matched cancer-free transition zone (TZ) tissues were digested and sorted for viable CD45-CD200-EpCAM- cells for downstream scRNA-seq analysis using the 10X Chromium System. Normal fibroblasts from young, healthy donors were used as a comparison. CellRanger and Seurat were used for cell clustering and differential gene expression analysis.

Results: Successful isolation of fibroblasts requires longer tissue digestion protocols than for immune or epithelial cells. Clustering of fibroblasts from cancer-containing PZ or cancer-free TZ identifies a more heterogeneous population of fibroblasts from the PZ compared to the TZ of the same patient. Although nearly all of these cells express vimentin, there is heterogeneous expression of other fibroblast markers. When all fibroblasts from the same patient are clustered together, a subset of PZ fibroblasts form isolated cell clusters. Finally, prostate fibroblasts freshly isolated from a cancer patient cluster separately from cultured CAF and also from normal prostate fibroblasts isolated from a young, healthy donor.

Conclusions: These studies suggest prostate CAF are more transcriptionally heterogeneous than normal fibroblasts within the same patient. These results will initiate further investigation of the unique CAF subpopulations present in prostate cancer tissue which aid in prostate cancer progression or limit therapeutic potential.

Background

Prior analysis of mammalian mucosal chemosensory brush cells have largely focused on those present in the gastrointestinal tract, respiratory tract, pancreas, gall bladder, and thymus. More recently brush cells in the lower urinary tract of mice have been identified that exhibit tufted morphology, express choline acetyltransferase, and possess chemosensory activity. Serotonin-expressing cells in the lower urinary tract have similar chemosensory potential given their association with nerve terminals in adult animals and have been termed paraneurones. When these cells initially appear in development and their spatial distribution throughout the lower urinary tract during organogenesis has been not been determined. We assessed the timing and distribution of these cells, referred to hereafter as "neuromodulatory cells" (NM) based on their expression of neurotransmitters. Using a combination of immunohistochemistry (IHC) and transgene expression we mapped the spatial distribution of these cells over the interval from 14 days post coitus (dpc) in the mouse through to early postnatal stages.

Methods

To determine the initial appearance of NM during organogenesis, we relied on IHC for serotonin (5-HT) and transgenes driven from Villin1 (Vil1) and Choline acetyl transferase (ChAT). We related the distribution of these cells to nerve terminals by staining for sensory nerve processes expressing Calcitonin Gene Related Peptide (CGRP) and the pan-neuronal marker TuJ1. Fetal tissues were collected in daily increments, fixed, cryo-sectioned and imaged by confocal microscopy. Whole mount imaging was accomplished through clearing in a modified CUBIC solution accompanied by confocal ribbon microscopy

Results

We observed that Vil1-Cre NMs largely colocalize with 5HT+ cells in both male and female mice. In contrast ChAT-EGFP+ cells label a distinct population that does not express 5-HT. Vil1-cre+ cells first appear in the mid region of the pelvic urethra and become more widely distributed along the urethra at later stages. Vil1-cre lineage traced NM cells only begin to exhibit 5-HT+ granules at 16.5dpc. Initially Vil1-cre cells are not associated with nerve terminals and become innervated by CGRP+ nerve processes several days after their initial appearance. In contrast ChAT-EGFP expressing NM cells were only observed at later fetal stages despite the presence of ChAT-EGFP+ nerve terminals throughout the bladder wall at earlier stages.

Conclusion

NM cells in the lower urinary tract are both heterogeneous in the genes they express (Vil1 versus ChAT) and in their temporal appearance during development. The timeline of regionality of NM cells we have established lays the groundwork for future analysis of the function and physiology of these populations.

Emergence of novel basal-luminal hybrid cells and loss of SARS-CoV-2 factors, TMPRSS2 and ACE2, in prostate cancer organoids under androgen deprivation treatment

Jamieson, Christina, Mendoza, Theresa*, Lee, Sanghee*, Burner, Danielle*, Muldong, Michelle, Wu, Christina, Arreola, Catalina, Zuniga, Abril, Miakicheva-Greenburg, Zhu, William, Cacalano, Nicholas, Jamieson, Catriona, Kane, Christopher, Kulidjian, Anna, Gaasterland, Terry.

BACKGROUND: Over 80% of advanced prostate cancer (PCa) patients develop bone metastases which inevitably become resistant to androgen deprivation therapy (ADT). To address the need for more predictive pre-clinical research models we established previously new patient-derived xenograft (PDX) models for bone metastatic prostate cancer. We used these PDX models to establish new three-dimensional (3D) organoids and tested their response to ADT.

METHODS Intra-femoral xenograft tumors of the PDX, PCSD1, were harvested and cells embedded in growth factor-reduced Matrigel domes in prostate organoid culture medium with 10% FBS. Organoids were grown with either: no DHT, 1nM DHT, 1nM DHT plus vehicle control (0.1% DMSO), or 1nM DHT plus 10uM Enzalutamide. The number and size of cysts and spheroids were quantified using a Keyence microscope. Alamar Blue viability assay was performed. Quantitative RT-PCR was performed for Prostate-Specific Antigen (PSA), Androgen Receptor (AR) and Prostate-Specific Membrane Antigen (PSMA). Immunohistochemistry (IHC) and immunofluorescence (IFC) analyses of prostate markers PSA, AR, cytokeratin-5 (CK-5) and cytokeratin-8 (CK-8), Ki67 were performed. Next generation RNA sequencing was performed utilizing an Illumina NovaSeq 6000 and samples were demultiplexed using bcl2fastq v2.20 Conversion Software (Illumina, San Diego, CA).

RESULTS: In the presence of DHT, the organoids grew as a heterogeneous population of epithelial cysts and spheroids. These recapitulated cyst- and small gland-like structures in the PDX and Gleason grade 10 (5+5) histomorphology of the donor patient's primary prostate tumor and bone metastatic prostate cancer. Androgen deprivation (no DHT) or enzalutamide treatment resulted in loss of cysts and smaller, yet still viable, spheroids. Transcriptomic and protein analyses in IHC and IFC revealed that the ADT resistant cells were CK5+CK8+ hybrid epithelial cells which had re-acquired stem-cell transcription factors, up-regulated steroidogenic and neurogenic pathways while down-regulating cell cycle, cell division and circadian pacemaker machinery, as well as TMPRSS2 and, surprisingly, ACE2.

CONCLUSIONS: Androgen deprivation or enzalutamide treatment of PCa PDX organoids led to the emergence of castrate resistant, quiescent, basal-luminal hybrid cells. Furthermore, ADT decreased expression of both SARS-CoV-2 host cell viral entry factors, TMPRSS2 and ACE2. Therefore, 3D PDX prostate cancer organoids can be used to screen for therapies that target mechanisms of ADT resistance and also for therapies that reduce TMPRSS2 and ACE2, thus inhibiting SARS-CoV2 infection.

Funding: The Leo and Anne Albert Charitable Trust Foundation, The JM Foundation

Single Cell RNAseq Analysis of Benign Prostate Hyperplasia Reveals Distinct Wound Repair Macrophage Phenotype

Authors

Gregory M. Cresswell[1], Meaghan M. Broman[1], Nadia A. Lanman[2], Renee E. Vickman[3], Douglas Strand[4], Gervaise Henry[4], Simon Hayward[3], Timothy L. Ratliff[1,2]

Affiliations:

[1]Purdue University, Department of Comparative Pathobiology, West Lafayette, IN

[2]Purdue University, Purdue Center for Cancer Research, West Lafayette, IN

3NorthShore University HealthSystem, Department of Surgery, Evanston, IL

[4]University of Texas Southwestern, Department of Urology, Dallas, TX

Background

Benign prostatic hyperplasia (BPH) is a common disease in older men, causing difficulty in urination followed by possible urinary tract or kidney problems. It is unclear what causes BPH with several risk factors, such as, age, diabetes, and obesity. Studies have linked inflammation to the initiation and progression of the disease, particularly in driving hyperplasia of the prostate. However, the role and the extent to which inflammation drives development or progression of BPH is poorly understood. The goal of this project is to use single cell RNAseq to characterize the immune populations present in the transitional zone of BPH patients through the course of the disease to better understand the interplay between the immune system and BPH.

Methods

BPH sampling was done by collecting tissue from large prostates (>70 grams) and small prostates (<60 grams) for comparison. From those samples, CD45+ populations were isolated and processed using the 10x genomics platform for scRNAseq. Data were analyzed for distinct immune populations based on existing human cell databases, as well as, potential interactions between immune populations using predictive ligand/receptor scoring. Additionally, populations of interest were further sub clustered to identify immune population diversity and function. BPH data sets were also compared against a publicly available normal prostate single cell database generated by the Strand Lab at UT Southwestern.

Results

Unsupervised clustering revealed 12 immune populations in BPH patients with macrophages representing the second largest cluster by cell number. Further sub-clustering of macrophages, as defined by the Human Cell Atlas, identified 10 unique macrophage populations. Based on gene

expression from the total macrophage cluster with *IER5, SERPINH1, KLF2, ISG15, HSPA1B,* and *MT1G* representing a group of highly upregulated genes that are involved in wound repair and M2 macrophage polarization suggesting possible tissue growth stimulated by BPH macrophages. Additionally, a subset of macrophages appear to express *AREG* which has the potential to drive prostate epithelial hyperplasia.

Conclusions

These data demonstrate an interesting and poorly understood immune profile that is present in BPH patients. The macrophage gene profile present in BPH suggests a strong wound repair phenotype with genes tissue recover strongly expressed. These data are suggestive of a macrophage driven environment of hyperplastic stimulation. These data set the stage for further study and exploration of macrophage targeted therapy for BPH patients to control the immune stimulation that could be driving hyperplasia.

Tumor-derived catabolic TGFß-family myokine blockade induces prostate cancer regression

Background:
A prominent side effect of androgen deprivation therapy (ADT), the mainstay treatment for advanced prostate cancer (PrCa) is an obese frailty syndrome that includes fat gain and sarcopenia, a progressive loss of skeletal muscle mass and strength. Previously, we showed that ADT induces catabolic TGFβ family myokines in muscle. Blocking these catabolic myokines using the ligand trap ActRIIB-Fc prevents ADT-induced sarcopenia. Recently we discovered that these myokines are also expressed in tumor, and that tumor derived myokines in the circulation signal from tumor to muscle to accelerate both muscle and strength loss in the PTEN null PrCa mouse model.

Methods:
Following ActRIIB-Fc treatment, we measured tumor volume in Pb-Cre4 x $Pten^{fl/fl}$ mice using high-resolution high-frequency ultrasound (HFUS) imaging and quantitated the reconstructed 3D tumor image using AMIRA. Growth of CaP8 cells and organoids from PTEN null prostate tumors treated with myokines and ActRIIB-Fc was quantitated. VEGF protein levels were assayed in cell lysates and conditioned media using ELISA, and microvessels in tumors quantitated using CD31 IHC. RNAseq of myokine-treated cells was analyzed using CAMERA to agnostically identify affected Hallmark pathways. TCGA expression analysis combined partial correlation graphs, model-based clustering and case level classification.

Results:
Myokines are secreted by tumor constitutively in Pten PrCa mice and are induced by ADT. Tumor-sourced catabolic myokines exacerbate the sarcopenic effects of the muscle-derived ADT-induced catabolic myokines. Unexpectedly, tumor volume decreased markedly in both sham and castrated mice treated with ActRIIB-Fc. Analysis of clinical PrCa gene expression demonstrate that there is a subset of PrCa patient tumors with myokine affected signaling. Mechanistically, myokines induced angiogenic factors including VEGF from PrCa epithelial cells, and blockade damaged tumor endothelium, suggesting tumor growth control is mediated via the microenvironment. Growth of tumor in Pten null mice treated with anti-VEGFR2 mAb was arrested.

Conclusions:
Catabolic TGFß-family myokines regulate tumor growth by increasing two distinct pro-growth activities. One is an angiogenic factor secreted into the tumor microenvironment that signals via VEGFR2. However, VEGF blockade only arrests tumor growth. Blockade of a second myokine induced activity results in frank tumor regression.

Ex vivo culture of prostate needle biopsies to assess macrophage immune phenotype changes following exposure to therapeutic drugs

C. Boibessot[1,2], F-H Joncas[1,2], A. Park[1,2], J.F Pelletier[1,2], A. Bergeron[1,2,3] and P. Toren[1,2,3].

[1]Laboratoire d'Uro-Oncologie Expérimentale, CHU de Québec-Université Laval Research Center, Oncology Division; [2]Centre de recherche sur le cancer de l'Université Laval; [3]Department of Surgery, Faculty of Medicine, Université Laval. Quebec City, Quebec, Canada

ABSTRACT

BACKGROUND

Within the prostate tumor microenvironment (TME) there are complex multi-faceted and dynamic communication occurring between cancer cells and immune cells. Macrophages are key cells which infiltrate and surround tumor cells and are recognized to significantly contribute to progression and resistance to therapies. Our understanding of their function in the TME and response to therapies is commonly based on *in vitro* and *in vivo* models, with limited research to confirm these model observations in human prostates.

METHODS

Macrophages within the TME of human prostates were evaluated after 72h culture of fresh biopsies samples in the presence of enzalutamide or control. In addition to immunohistochemistry, an optimized protocol for multi-parametric evaluation of macrophage-related cell surface markers was developed using flow cytometry. Marker expression data were compared to clinicopathological features.

RESULTS

Immunohistochemistry staining for 19 patients with paired samples suggested enzalutamide increased the proportion of $CD163^+$ cells relative to $CD68^+$ cells. However, this was not validated in a second cohort of 29 patients with Gleason grade group ≥2 where analysis was performed by multiparametric flow cytometry on dissociated cells. Our exploratory analyses of multi-parametric flow cytometry data for multiple macrophage markers suggest novel associations between circulating biomarkers such as neutrophil- to lymphocyte ratio (NLR) and the phenotype of immune cells within the prostate TME. Further, we observed an association between $B7\text{-}H3^+$ macrophages and the presence of intraductal carcinoma.

CONCLUSIONS

The use of flow cytometry to evaluate *ex vivo* cultured prostate biopsies fills an important gap in our ability to understand the immune cell composition of the prostate TME.

Michelle Muldong; mmuldong@health.ucsd.edu
Christopher Oh; cso003@health.ucsd.edu
Juliana Velez; jvelezlujan@health.ucsd.edu
Christina Wu; c5wu@health.ucsd.edu
Sanghee Lee; salee@health.ucsd.edu
Charles Prussak; cprussak@health.ucsd.edu
Christina Jamieson; camjamieson@ucsd.edu

Advancing anti-ROR1 CAR-T cells employing a cirmtuzumab based T-cell CAR to eradicate lethal castration resistant ROR1^{pos} prostate cancer.

Background:
One in six men will be diagnosed with prostate cancer (PCa), making it one of the leading health problems affecting men. The main treatment for advanced prostate cancer (PCa) affecting up to one quarter of PCa patients is androgen deprivation therapy (ADT) which targets androgen receptor (AR) signaling. These patients, however, inevitably become resistant to ADT and develop lethal castration resistant prostate cancer. A particularly malignant form of CRPC called neuroendocrine prostate cancer (NEPC), is emerging with increasing frequency in patients treated with ADT.

Methods:
Cirmtuzumab-based T-cell CAR was generated to target treatment resistant ROR1^{pos} cancers. To test and demonstrate the activity of this CAR product, a series of 2nd generation T-cell CAR constructs were produced that when transduced into human T-cells demonstrated highly potent and specific anti-tumoral activity and specificity in *in vitro* and *in vivo* test systems of hematological and human solid tumor cancers. LDH cytotoxicity and Incucyte assays were performed using various effector to target ratios (E:T) of ROR1 CAR-T cells against ROR1 positive NEPC prostate cancer cell lines.

Results: Anti-ROR1 T-cell CAR is highly potent in targeting and killing ROR1 expressing NEPC cell lines even at low effector to target (E:T) ratios when compared to mock transduced control T cells in Incucyte assay and LDH release assay.

Conclusion: The highly potent, prolonged and specific activities we observe with the cirmtuzumab-based anti-ROR1 T-cell CARS encourage the advancement of this product into human clinical studies.

Three-dimensional (3D) co-culture system for organoids plus tissue infiltrating lymphocytes (TILs) derived from patient benign normal and hyperplastic proliferative ureter specimens

Lee, Sanghee, Muldong, Michelle, Kang, Sung Gu, Hsu, Jonathan, Kane, Christopher, Salmasi, Amirali, Jamieson, Christina

BACKGROUND: Three-dimensional (3D) co-culture systems recapitulates *in vivo*-like autocrine and paracrine signaling in culture systems which retain the cellular heterogeneity of the original tissue. However, such systems have not been established for benign inflammatory changes in ureter. We established a 3D organoids and tissue infiltrating lymphocytes (TILs) co-culture system to model host-immune interplay in normal ureter and ureter with benign proliferative changes in human.

METHODS: 10 mg of normal tissue and 10 mg of tissue with benign proliferative changes (abnormal) were harvested from upper ureter from a 78-year-old female patient. 3D organoid and TILs cultures were prepared and maintained for three weeks separately. Host-immune interplay of benign ureter was modeled in co-culture of 3D ureter organoids and 480,000 TILs. The TILs from abnormal tissues were not proliferating as much as the TILs from benign normal, therefore, TILs were added as a 1:1 mixture of TILs from benign normal and abnormal tissues to have total of 480,000 TILs, a pre-determined number for successful co-culture. Four areas within each co-culture plate were imaged by EVOS microscope at 0, 4, 28, 56, 84 and 91 hr. 3D organoids alone, co-cultured organoids plus TILs were processed for H&E staining and Immunohistochemistry using antibodies specific to Keratin 5 (CK5), P63 and Uroplakin III (UpkIII).

RESULTS: The abnormal tissues were later determined by the pathologist to be benign hyperplasia. 3D organoid cultures of benign normal vs benign hyperplastic proliferation of ureter contained a mix of cell masses. Strikingly, microscopic imaging of co-cultures revealed that TILs migrated into the matrigel dome and finally infiltrated ureter organoids. TILs retained their original ability to infiltrate host benign normal ureter organoids even after their surrounding environment had changed. Ureter organoids were CK5 and P63 positive but Upk III negative. A functional consequence of TILs infiltration of the organoids was a morphological change in organoids structure, an irregular boarder of organoids and an extrusion of luminal components. Both types of TILs infiltration were observed in both benign normal vs benign hyperplastic proliferation ureter.

CONCLUSIONS: Our study provides the first patient-derived model of benign ureter organoids plus TILs which maintained functional and cellular phenotype of urothelial cells and TILs.

Funding: The Leo and Anne Albert Charitable Trust Foundation, The JM Foundation

Macrophage re-education in prostate cancer: subversion of inflammatory macrophages to a mixed immunosuppressive tumor associated-macrophage phenotype

C. Boibessot[1,2], O. Molina[1,2], G. Lachance[1,2], C. Tav[1,2], A. Champagne[1,2], B. Neveu[1,2], J-F. Pelletier[1,2], F. Pouliot[1,2,3], V. Fradet[1,2,3], S. Bilodeau[1,2,4], Y. Fradet[1,2,3], A. Bergeron[1,2,3] and P. Toren*[1,2,3]
[1] Centre de recherche du CHU de Québec-Université Laval, Axe Oncologie, Québec; [2] Centre de recherche sur le cancer de l'Université Laval, Québec; [3] Département de chirurgie, Université Laval; [4] Centre de Recherche en Données Massives de l'Université Laval, Québec

Background
Tumor-associated macrophages (TAMs) are known to influence the tumor microenvironment (TME) supporting tumor progression. TAM are versatile cells implicated in different immune functions influenced by local factors, whether immune-stimulatory or immunosuppressive. Many questions remain as to the origin, development and function of TAMs within the TME. To understand the origin of this population, we analyzed phenotypical and functional aspects of human macrophages using

Methods
Immunohistochemistry (IHC) for the immunosuppressive TAM marker CD163 was performed in a cohort of 98 patients with locally advanced PCa and long clinical follow-up. Biopsies of surgically removed prostates, including tumoral and non-tumoral zones, were cultured for 72 ex vivo, followed by cellular dissociation and rlow cytometry analyses for a panel of immunosuppressive myeloid markers. Human peripheral blood mononuclear cells were used to derive inflammatory M1 or immunosuppressive M2 macrophages in vitro according to validated protocols.

Results
IHC studies identified CD163 in tumor-adjacent normal epithelium, but not tumoral regions, as a significant predictor of the development of metastases or PCa death. Flow cytometry analyses of radical prostatectomy specimens identified prostate TAMs as frequently expressing both pro-inflammatory M1 (CCR7+) and immunosuppressive M2 (CD163+) markers. We show that prostate cancer cells subvert M1 macrophages into M2 macrophage by loss of function and up-regulation of CD163 marker. Further, we observed that the milieu-induced transition between immunosuppressive M2 to pro-inflammatory M1 macrophage is abrogated by the presence of PCa cells. Using RNA sequencing, we show that human macrophages subverted by PCa cells show alterations in the chemokine network which may recapitulate TAMs characteristics.

Conclusion
Together, our results suggest that prostate TAMs originate from infiltrating inflammatory M1 macrophages which are subsequently reprogrammed by PCa cells and the cytokine milieu. We also showed that PCa cells influence TAM function more importantly than pro-inflammatory milieu by changes in chemokine network.

INTRODUCTION

Tumor-associated macrophages (TAMs) are a major component of the tumor microenvironment (TME) and play an important role in the progression of many cancers [1, 2]. The origin of TAMs may include resident tissue macrophages, but the majority is thought to be related to infiltration of circulating monocytes derived from bone marrow hematopoietic progenitors [3-5]. Macrophages are known to quickly detect and adapt to changes in their microenvironment [6]. They participate in the elimination of invading bodies or cell debris and drive inflammation to promote the recruitment of other immune cells and present antigens to T lymphocytes, therefore contributing to the shaping of the microenvironment [7]. In contrast to normal macrophages, TAMs favor local immunosuppression, have lower cytotoxic function, decreased antigen presenting capability and promote matrix remodelling and angiogenesis [6, 8-10].

Historically, macrophages were divided into classically activated M1 macrophages and alternatively activated M2 macrophages characterized by anti-tumor and pro-tumor properties, respectively [11]. However, this oversimplified binary classification is now referred to as a polarization spectrum to reflect the complexity and plasticity of macrophages within different contexts, including the TME [12]. A recent study using single cell RNA sequencing in breast cancer samples reported expression of both M1 and M2 gene signatures in tumors [13]. These findings were also reported in gliomas, suggesting a model wherein TAMs reside along a spectrum and not in mutually exclusive M1 or M2 polarization states [14].

In PCa, the TME is preferentially enriched with myeloid cells compared to lymphocytes in both human and murine models [9, 15, 16]. TAMs, which can represent up to 30% of total tumor infiltrating immune cells, are characterized by immunosuppressive phenotype and function [17]. In general, a higher density of macrophages is associated with a poorer prognosis [18], but the impact of macrophage profiles on specific clinical events is not well understood. Prior research suggested that, in localized tumors, the expression of CD163 and CD206, both markers of M2 macrophages, was associated with an increased risk of metastasis [15, 20, 21]. It was also shown that the proportion of $CD206^{+}$ macrophages was increased in metastatic castration resistant prostate cancer (CRPC) compared to localized PCa [19]. Moreover, a meta-analysis suggested that a higher density of prostate TAMs was associated with poorer overall survival. More recent studies suggested that treatment resistance following PCa progression may be driven by an increase in TAMs [17, 22].

A recent analysis of PCa metastates suggested there exist two subtypes of CRPC: a first one characterized by higher androgen receptor (AR) and metabolic activities and a second characterized by higher immune cell infiltration [15]. For the past decade, immunotherapy based on T cell reactivation using immune checkpoint inhibitors is emerging as an effective strategy to treat cancers. However, T cell-based strategies do not appear effective in all tumor types. PCa is notably known to not be or poorly responsive to these immunotherapeutic approaches. A better understanding of how macrophages contribute to therapeutic resistance and how they could be reprogrammed to avoid resistance would be important for the elaboration of better therapeutic approaches.

In this study we characterized TAM infiltrating human PCa specimens and investigated the crosstalk between PCa cells and macrophages. Using classical markers of M1 and M2 macrophages, our analyses help to understand the complex phenotype, origin and identity of prostate TAMs. We further demonstrate that this particular phenotype can be modelized using polarized human macrophages, media re-education and particularly direct contact with PCa cells. We also observed how PCa-subverted macrophages may be more supportive to PCa cell growth. Together, our results help to better understand PCa TAMs and highlight the importance of these cells on PCa progression and resistance.

MATERIAL AND METHODS

Patient samples

Three patient cohorts were used in this study. A first retrospective cohort of 98 men with localized PCa treated by radical prostatectomy at Centre Hospitalier Universitaire de Québec, L'Hôtel-Dieu de Québec Hospital (QC, Canada) between March 1996 and November 1998 was used to study macrophage infiltration in tumors. These men provided written consent for the use of their tissue and medical data for research through their participation to our uro-oncology biobank (URO-1). The clinical database includes patient demographics, tumor clinico-pathological characteristics, as well as data on biochemical recurrence, metastases and death. Formalin-fixed paraffin-embedded (FFPE) tumors from these patients were obtained and whole tumor sections were used for immunohistochemical analysis. The research ethics committee of the Centre Hospitalier Universitaire de Québec-Université Laval approved the use of these specimens and clinical data for this study (#2012-1059).

A second cohort consists of 21 men with Gleason Grade Group (GGG) ≥ 3 PCa on pre-operative biopsy that underwent radical prostatectomy bbetween 2019 and 2020 at Centre Hospitalier Universitaire de Québec, L'Hôtel-Dieu de Québec Hospital (QC, Canada) and who accepted to participate in the URO-1 biobank and provide fresh prostate biopsy and blood samples at time of surgery. Ethics approval for this study was obtained from the Centre Hospitalier Universitaire de Québec-Université Laval (#2019-4181).

Finally, a third cohort consisting of healthy male donors aged between 45 to 70 years was enrolled at the Héma-Québec blood center or at the Centre de recherche du CHU de Québec-Université Laval to provide blood samples for the production and analyses of monocyte-derived macrophages. Volunteers with known infectious disease and preexistent cancer or autoimmune disease were excluded. These men accepted to participate to the local uro-oncology biobank with ethics approval obtained from the Centre Hospitalier Universitaire de Québec-Université Laval (#2012-1002).

Immunohistochemistry

Formalin-fixed and paraffin-embedded (FFPE) prostate tumors were cut into 5 µm-thick sections and dried overnight at 37°C. Sections were deparaffinized, and heat-induced antigen retrieval was performed using a PT Link, Pre-Treatment Module for Tissue Specimens (Dako, Burlington, ON, Canada) with Tris/EDTA, pH 9 (Dako Code K8004: EnVision™ FLEX, High pH (Link). Endogenous peroxidase activity was blocked by incubation in 3% peroxide solution for 10 min. The immunodetection was performed using the IDetect super stain HRP polymer kit (ID labs, London, Ontario, Canada) as follows. First, slides were incubated for 10 min at room temperature with Super block solution to block nonspecific background staining. Then, incubation with anti-CD163 monoclonal antibody (mAb)(clone 2G12, dilution 1:2000, Abcam, Toronto, ON) was carried out for 1 hour at room temperature. After washes, slides were incubated for 30 min with HRP-Polymer Conjugate according to manufacturer's recommendations. After a 5 min DAB staining, slides were rinsed, counterstained with hematoxylin, dehydrated and mounted with coverslip using MM 24 low viscosity mounting medium (Leica Microsystems, Durham, USA). Slides were digitalized using a Nanozoomer (Hamamatsu Photonics, Bidgewater NJ, USA) and visualized using the NDP.view2 software (Hamamatsu Photonics).

Immunohistochemistry scoring

The density of $CD163^+$ cell infiltration was analyzed in tumor and normal-appearing adjacent tissue. In each area, ten randomly selected visual fields at 20x magnification (surface area of 0.460 μm^2) were chosen and the number of positive cells in these fields was determined by semi-automatic digitized image analysis using the Calopix software (RTIBVN Healthcare, Châtillon, France). For quality control of the scoring, 10% of the slides were randomly selected and the scoring was confirmed by a genitourinary pathologist.

Cell culture

LNCaP cells were cultured in RPMI 1640 supplemented with 10% heat-inactivated fetal bovine serum (FBS) (Wisent Bioproducts, St-Bruno, QC, Canada). Enzalutamide-resistant MR49C and MR49F cells (kindly provided by Dr. Amina Zoubeidi from the Vancouver Prostate Cancer Centre, Vancouver, BC, Canada) were cultured in RPMI 1640 supplemented with 10% heat-inactivated FBS and with 5 μM enzalutamide (MedChemExpress LLC, Monmouth Junction, NJ, USA, #HY-70002). PC3 and LAPC4 cells were cultured in Dubelcco's modified Eagle's minimal essential medium (DMEM medium, 1g glucose/L) supplemented with 10% heat-inactivated FBS. RWPE-1 and PZ-HPV7 cells were cultured in keratinocyte serum-free medium supplemented with prequalified human recombinant epidermal growth factor 1-53, bovine pituitary extract and 10 nM dihydrotestosterone . Authentication of LNCaP, PC3 and RWPE-1 cells was performed using the GlobalFiler IQC PCR Amplification Kit (ThermoFisher Scientific Inc., Ottawa, ON, Canada).

Monocyte-derived macrophages preparation and polarization

Monocyte-derived macrophages (MDM) were prepared from peripheral blood mononuclear cells (PBMCs) of healthy male volunteers aged between 45 and 70 years. Briefly, whole blood was collected in EDTA tubes and PBMCs were isolated by Ficoll-PAQUE Plus density gradient centrifugation (GE Healthcare Life Sciences, endotoxin tested, #17- 1440-02). Monocytes were purified from PBMCs by magnetic-activated cell sorting (MACS) positive selection using a CD14 microbeads isolation kit (Miltenyi Biotec, Gaithersburg, MD, USA, #130-050-20) and LS Columns (Miltenyi Biotec, #130-042-401). The purified $CD14^+$ monocytes were seeded in 12-well plates ($1x10^6$ cells/well) or in 24-well plates ($4x10^5$ cells/well) in RPMI supplemented with 10% heat-inactivated FBS, 2,38 g/L of D-glucose (AnalR, #10117), 2,50 g/L of HEPES (Sigma-Aldrich, Oakville, ON, Canada) and 10 ng/ml recombinant human monocyte-colony stimulating factor (M-CSF, Peprotech, Cranbury, NJ, USA, #300-25) for 5 days to differentiate the monocytes into M0 macrophages. On day 5, 50% of volume of fresh medium supplemented with M-CSF (10 ng/ml) was added. On day 6, M0 macrophages were polarized into M1 or M2 macrophages. To obtain M1 macrophages, 20 ng/ml of IFN-γ (Cedarlane, Burlington, ON, Canada, #CL-101-06) and 10 ng/ml of LPS (Sigma-Aldrich) were added to the medium, while to obtain M2 macrophages, 20 ng/ml of interleukin-4 (IL-4; Cedarlane, #CL-101-04) and 20 ng/ml of IL-13 (Cedarlane, #CL-101-13) were added to the medium and the culture was continued for 4 additional days.

For the re-education of macrophages, cytokines were added to M0 macrophages to polarize them into M1 or M2 macrophages as described above. Then three approaches for re-education were used. MDMs were re-educated by co-culturing them with PCa cells, by the addition of conditioned media of polarized macrophages and by both co-culturing them with PCa cells and conditioned media.

Briefly, for *MDMs re-educated by cancer cells*, 5×10^5 MDMs were polarized into M1 or M2 macrophages in 6-well plates as described above. After 24h of polarization, 5×10^5 PCa cells were added to the wells for 96 h of co-culture.

For MDMs re-educated by conditioned media, 5×10^5 MDM were polarized as above for 48 h into 6-well plates. After 48 h of polarization, supernatant was collected, cells were washed two times with PBS and conditioned supernatant from M1 macrophages was added to M2 macrophages and supernatant from M2 macrophages was added to M1 macrophages for an additional 2 - 6 days of culture.

For MDM re-educated by cancer cells and conditioned media, 5×10^5 MDMs were polarized for 48h into 6-well plates as described above. After 48h of polarization, supernatant was collected, cells were washed two times with PBS and conditioned supernatant from M1 macrophages was added to M2 macrophages along with the addition of 5×10^5 PCa cells and supernatant from M2 macrophages was added to M1 macrophages along with the addition of 5×10^5 PCa cells for an additional 2 - 6 days of culture.

Macrophage analysis from fresh prostate tissue specimens

Biopsy procurement. Fresh prostate biopsies were obtained from men undergoing radical prostatectomy (second cohort). Less than one hour after prostate was resected, the prostate was brought to the pathology

department where a total of six 18-gauge needle biopsies (2 from the tumor area and 4 from the adjacent non-tumor area) were taken by a pathologist. The localization of the tumor area was indicated by palpation, MRI and/or prior biopsy pathology results.

***Short-term culture*.** For each participant, biopsies were washed in HBSS without Ca^{2+} Mg^{2+} then cultured for 72 h in freshly prepared complete autologous media. Complete medium consists of Advanced DMEM-F12 media supplemented with 50 mg/L of antimicrobial agent Primocin (InvivoGen, San Diego, CA), 5 ml/L of Glutamax (ThermoFisher Scientific, #35050061), 1489 mg/L of HEPES added with 10% autologous participant's serum.

***Tissue dissociation*.** Biopsies were washed two times with HBSS with Ca^{2+} Mg^{2+}, then incubated overnight at 37°C with 5% CO2 in complete medium without autologous serum. Media was supplemented with Type II collagenase (ThermoFisher Scientific, #17101015, final concentration of 300 U/ml) and 2 U/ml of DNase (Sigma #10104159001). The day after, dissociated biopsies were washed with HBSS with Ca^{2+} Mg^{2+} then incubated with 1 ml Accutase (Corning, #25-058-ci) for 20 min at 37°C. Dissociated cells were then collected, washed, stained and filtered for flow cytometry analyses.

Cytokine analyses

The levels of cytokines in the supernatant of cultured macrophages were determined using the Bio-Plex Pro Human Cytokine Th1/Th2 immunoassay (Bio-Rad, Mississauga, ON, Canada, #M5000005L3) which measures GM-CSF, IFN-γ, IL-2, IL-4, IL-5, IL-10, IL-12(p70), IL-13 and TNF-α using the Luminex technology. Medium alone was used as blank and non-treated samples were compared with treated samples. Assays were run on a Bio-Plex® 200 System and data analyzed using Bio-Plex Manager™ Software 6.1 (Bio-Rad).

Proliferation assay

Cells were centrifuged, washed 2 times with PBS and then incubated with 10 μM CFSE/1x10^6 cells/ml for 20 min in the dark at room temperature. Cells were washed two times with complete medium then added to macrophage cultures for 96 h. After the incubation period, cells were harvested, marked with V500-labelled anti-CD45 monoclonal antibodies (mAb) (see supplementary Table S1) according to manufacturer's recommendation and then analyzed by flow cytometry.

Cell staining and flow cytometry analyses

Multiparameter flow cytometry analyses were performed on fresh samples. Compensation controls were done using compensation beads (BD CompBeads, BD Biosciences, San Jose, Ca, USA, #552843) and Fluorescence Minus One (FMO) control strategy on fresh samples to identify gating boundaries.

For *in vitro* grown PCa cells and MDM, cells were mechanically detached from the plate and washed twice with PBS. For these cells as well as for those obtained after biopsy dissociation, cells were incubated with Seroblock (Bio-Rad, #BUF070B) for 5 min, and then then with a cocktail of mAbs against CD11b, HLA-DR, CCR7, CD163, CD206, PD-L1, PD-1 and B7-H3 (see supplementary Table S1). Cells were analyzed using a BD LSRFortessa cytometer (BD Biosciences) and data analysis was performed using FlowJo software (v10.5.2) (Treestar, Inc., Ashland, OR). Cell viability was analyzed using the BD Horizon fixable viability stain (FVS-780, BD Biosciences) and doublets were excluded based on forward scatter-A against forward scatter-H gating.

Fluorescent activating cell sorting

Re-educated macrophages were harvested and labelled with viability stain FVS-780, V500-labelled anti-CD45, PE-labelled anti-CCR7 and AF-647-labelled anti-CD163 mAbs and sorted on ARIA II (BD Biosciences). Then, sorted cells were maintained in complete medium supplemented with Primocin to avoid contamination before being snap frozen for further RNA sequencing analyses or seeded in 24-well plate for 6 h before a new 72 h of co-culture with MR49C cancer cells.

High-dimensional t-SNE visualization of flow cytometry data

Flow cytometry datasets were cleaned by the exclusion of dead cells and doublets. New files were generated for total immune cells ($CD45^+$), total macrophages ($CD45^+$, $HLA\text{-}DR^+$, $CD11b^+$) and total $CCR7^{Hi}$ macrophages ($CD45^+$, $HLA\text{-}DR^+$, $CD11b^+$, $CCR7^{Hi}$) and analyzed separately to generate t-SNE map using FlowJo software (v10.5.2). The global geometry was evaluated with 3 different values of perplexity (30, 50, 100) and steps (1000, 3000, 5000). Values of 100 for perplexity and 5000 for geometry were chosen based on the maximum resolution of cluster on total immune cells. Major clusters were identified by manually gating in different population by the fluorescence intensity of selected markers, then overlay the gates on top of the t-SNE map.

RNA-sequencing

Cells were homogenized in Qiazol buffer (Qiagen, Germantown, MD, USA) and total RNA was extracted using the miRNeasy micro kit on-column DNase (Qiagen, Hilden, DE) treatment following the manufacturer's instructions. Quantity of total RNA was measured using a NanoDrop ND-1000 Spectrophotometer (NanoDrop Technologies, Wilmington, DE, USA) and total RNA quality was assayed on an Agilent BioAnalyzer 2100 (Agilent Technologies, Santa Clara, CA, USA).

NEBNext Ultra II directional RNA library prep kit for Illumina (New Englands Biolabs Inc., Ipswich, MA, USA) was used to prepare 21 mRNA sequencing libraries, according to manufacturer's instructions. Briefly, 350 ng of total RNA were purified using the NEBNext poly(A) (New Englands Biolabs Inc.) and used as a template for cDNA synthesis by reverse transcriptase with random primers. The specificity of the strand was obtained by replacing the dTTP with dUTP. This cDNA was subsequently converted to double-stranded DNA that was end-repaired. Ligation of adaptors was followed by a purification step with AxyPrep Mag PCR Clean-up kit (Axygen, Big Flats, NY, USA), by an excision of the strands containing the dUTPs and finally, by a PCR enrichment step of 11 cycles to incorporate specific indexed adapters for the multiplexing. The quality of final amplified libraries was examined with a DNA screentape D1000 on a TapeStation 2200 and the quantification was done on the QuBit 3.0 fluorometer (ThermoFisher Scientific, Canada). Subsequently, mRNA-seq librairies with unique index were pooled together in equimolar ratio and sequenced for paired-end 100 pb sequencing on an NovaSeq 6000 flowcell S2 at the Next-Generation Sequencing Platform, Genomics Center, CHU de Québec-Université Laval Research Center, Québec City, Canada. The average insert size for the librairies was 280 bp. The mean coverage/sample was ~22M paired-end reads. Analysis of raw sequencing reads was performed using the MUGQIC RNA-Seq pipeline (version 3.1.5). Briefly, reads were trimmed for adaptor sequences using Trimmomatic (version 0.36). High-quality reads were aligned to the human reference genome (GRCh38.p7, Ensembl 87) with STAR aligner (version 2.5.3a). PCR duplicates were removed with picard MarkDuplicates (version 2.9.0). Number of mapped reads to each gene was calculated using the count function of HTSeq (version 0.6.0) (Anders, 2015).

Count matrix underwent the variance stabilizing transformation to stabilize the variance across the mean, using the vst function of DESeq2 R package. The 500 genes with the higher variance across samples were then analyzed using Principal Component Analysis (PCA) from the prcomp function in R (https://www.r-project.org). PCA was visualized using plotly R package (https://plot.ly).

Differentially expressed genes were identified with DESeq2 (Love, 2014) (genes with zero coverage in all samples were excluded) and called with a significance at Benjamini-Hochberg corrected p-value < 0.05. Upregulated genes were selected at a minimum log2 fold change of 1.5 and down-regulated genes at a minimum log2 fold change of -1.5.

Pathway enrichment scores were calculated by Gene Set Enrichment Analysis Pathway (GSEA) (Subramanian, 2005). The preRanked mode of GSEA was applied using 2000 random permutations and selecting only the gene-sets associated with a FDR < 0.05. The database of pathway gene sets used for pathway

enrichment analysis has been retrieved from http://download.baderlab.org/EM_Genesets (Release August 2020). This database has been built from eight data sources: GO, Reactome, Panther, NetPath, NCI, MSigDB curated gene sets (C2 collection, excluding Reactome and KEGG), MSigDB Hallmark (H collection) and HumanCyc.

Gene expression profiling dataset

Clinicopathological profiles and expression data from TCGA-PRAD [16] and GSE21032 [17] were downloaded respectively on GDC (Genomic Data Common; https://portal.gdc.cancer.gov/) and GEO (Gene Expression Omnibus; https://www.ncbi.nlm.nih.gov/geo/) data portal (n = 333 and n = 218, respectively). The expression of *CCR7*, *CD163*, *CD276*, *CD274* and *MRC1* in these mRNA datasets was analyzed using GraphPad Prism 8.0 in PCa patients linked with their clinical parameters.

Statistical analyses

Immunohistochemistry data: Infiltration of $CD163^+$ cells was categorized into quartiles. Survival analyses were performed using the Kaplan-Meier method and log-rank test. For test association analysis, CD163 expression was expressed as median and interquartile range.

Univariate and multivariable proportional hazard Cox models assessed the effect of CD163 immune cell infiltration on clinical outcome (metastasis and PCa-specific death), with propensity score adjustment estimated using age, PSA, T stage, N Stage, Gleason and invasive margin. All survival analyses were done with time-to-event variables calculated from the date of radical prostatectomy to the first biochemical recurrence date for the biochemical recurrence-free survival analyses, to the date of first metastasis discovery for the metastasis-free survival analyses, and to death date for PCa-specific death-free survival analyses. Statistical analyses were performed using SAS Statistical Software v.9.4 (SAS Institute, Cary, NC, USA) with a two-sided significance level set at $p < 0.05$.

In vitro assays: Specimen biopsy normality was evaluated by both D'Agostino & Pearson normality test and Shapiro-Wilk normality test using GraphPad Prism 8.0. For nonparametric distribution, unpaired Mann-Whitney test or paired Wilcoxon matched-pairs signed rank test were used. For parametric distribution, Student's T-test was used.

RESULTS

$CD163^+$ macrophages in tumor-adjacent normal areas predict clinical outcomes

To understand the impact of immunosuppressive TAMs in the TME of PCa, we evaluated CD163 staining in a cohort of 98 locally advanced PCa radical prostatectomy specimens selected for adverse pathology (pT2 with positive margins or ≥pT3) (Table S2). We first divided TME in tumor and tumor-adjacent normal areas to evaluate the impact of localisation on clinical outcomes (Figure S1a and b). CD163+ cells were scattered in the tissue and a wide difference in staining levels was observed. However, the staining pattern was similar from one tumor to another. Positive cells were more abundant in the tumor areas (mean of 23 cells/visual field) than in the adjacent normal areas (mean of 14 cells/visual field) (Figure 1a, Figure S1a). Survival analysis demonstrated that a higher $CD163^+$ cell infiltration (4^{th} quartile) in the tumor-adjacent normal epithelium, but not in the tumor, was significantly associated with shorter survival without metastases (p=0.0001) and PCa-specific mortality (p=0.012) (Figure 1b) as well as with CRPC-free survival (p=0.016) (Figure S1b). In multivariable analyses, a high $CD163^+$ cell infiltration in tumor-adjacent normal tissue significantly increased the risk of developing metastases (adjusted HR=9.43, 95%CI 1.52-58.82, p=0.02) and PCa-specific death (adjusted HR=3.03, 95% CI 1.28-7.14, p=0.01) (Figure 1c) as well as CRPC (adjusted 4.88 95% CI 0.97-24.39, p=0.05), (Table S3). In contrast, neither $CD163^+$ cell infiltration in tumor area was associated with these outcomes (Figure 1c, Table S3). These findings support the prognostic importance of immunosuppressive macrophages in locally advanced prostate tumors,

with intriguing findings that the level of infiltration of $CD163^+$ macrophages in tumor-adjacent normal epithelium is the strongest independent predictor of adverse clinical outcomes.

Dual $CD163^+$ $CCR7^+$ macrophages are present in tumor-adjacent normal tissue

To better understand macrophages within the prostate TME, we analyzed their phenotype in *ex vivo* cultured prostate biopsies using multi-parametric flow cytometry. Only patients with (Gleason Grade Group $\geqslant$ 3) were included to avoid indolent tumors; from each patient a pool of 6 prostate needle biopsies were evaluated using our optimized dissociation protocol. Because $CD163^+$ macrophages with the strongest prognostic index of metastases and PCa-specific mortality were identified in the peri-tumoral zone, 2 of these 6 biopsies were taken from the tumoral zones and 4 from the adjacent sextants with no tumor on pre-operative biopsy.

In all dissociated biopsies, approximately 25 to 30% of the viable cells represented immune lineage cells ($CD45^+$, Figure 2a), with macrophages constituting about 40% of these cells ($CD45^+$/$CD11b^+$/HLD-DR^+, Figure 2b). In addition to conventional sequential biaxial plot-based analysis, we utilized t-SNE visualization to evaluate macrophages within the total immune cell ($CD45^+$) population of each patient. On the global t-SNE map, 8 main clusters were identified by smooth density plots (Figure 2d) and the proportion of macrophages (CD11b, HLA-DR), M1-associated marker (CCR7), M2-associated marker (CD163, CD206) and immune checkpoints (PD-L1, B7-H3) was evaluated in each cluster (Figure 2d, Figure S2a). Of these clusters, cluster #1 (red) and #8 (light green) were myeloid populations expressing both high level of CD11b and HLA-DR markers (Figure 2d, S2a). Interestingly, cluster #8 represents a macrophage population that expresses both M1 (CCR7) and M2 (CD163, CD206, B7-H3 and PD-L1) markers (Figure 2d). To investigate this M1 and M2 marker co-expression further, we manually divided the global macrophage population according to high and low marker expression for each patient (Figure S2b) and observed that the CCR7 M1-associated marker was highly expressed in our macrophage population ($CD45^+$/$CD11b^+$/HLA-DR^+) (Figure 2c). By combining these data, we observed that $CD163^{Hi}$ macrophages also expressed high levels of CCR7. The same observations were made with CCR7 and all the other M2-associated markers, supporting high co-expression of both M1 and M2 markers in human PCa associated macrophages (Figure 2e). Moreover, starting from global immune population to macrophage population and then $CCR7^{Hi}$ macrophage population on the global t-SNE analysis, we also detected an enrichment of $CD163^{Hi}$, $CD206^{Hi}$, PD-$L1^{Hi}$, B7-$H3^{Hi}$ populations (Figure S2c).

To corroborate our findings, we analyzed M1 and M2-marker expression in the publicly available TCGA (n=333) and GSE21032 (n=131) gene expression profiling datasets of primary PCa samples. In both datasets, gene expression of M1 (CCR7) and M2 markers (CD163, CD206 and PD-L1) were positively correlated (Figure 2f). Taking together, these data strongly suggest a dual expression of both M1 and M2 markers on macrophages infiltrated into the prostate tumors.

PCa cells subvert M1 macrophages into macrophages expressing both M1 and M2 characteristics

Dual expression of M1 and M2 markers on macrophages infiltrating prostate tissues suggests that the TME re-educates infiltrating inflammatory macrophages toward a mixed phenotype. We therefore sought to explore this hypothesis using human PCa cells and monocyte-derived macrophages (MDM). First, M1 and M2 macrophages were produced from $CD14^+$ monocytes isolated from whole blood of healthy male donors according to validated protocols. As expected, we observed high expression of CCR7 and low expression CD163, CD206 and B7-H3 in M1 polarized macrophages (Figure 3a, Figure S3a). Further, we observed that M1 macrophages secrete IL-12 and TNF-α (Figure S3b) and inhibit the proliferation of PCa cells by 70% (Figure 3e). To assess direct effects of PCa cells on human macrophages, we used a co-culture model. Different PCa cells were tested and enzalutamide-resistant MR49C PCa cells were chosen because of their aggressivity and capacity to induce CD163 expression (Figure S3c). Following macrophage M1 polarization, MR49C cells were co-cultured in a 1:1 ratio for 48h to 6 days or with MR49C conditioned media (Figure 3b). Following contact with these PCa

cells, M1 macrophages showed an increased proportion of cells expressing M2 markers as up to 60-70% of the cells expressed CD163 and B7-H3 after 96h of co-culture (Figure 3b and c) with a concurrent significant increase of intensity (Figure S3e). CCR7 intensity at cell surface decreased by two-fold but 100% of cells were still positive for this marker (Figure 3d, S3e). The proportion of PD-L1^{+} macrophages was significantly reduced after 48 or 96 h of co-culture with MR49C cells (Figure S3d) while that of CD206^{+} cells was not increased by these PCa cells (Figure S3f). Notably, these changes were not observed when macrophages were put in direct co-culture with PZ-HPV7 benign prostate epithelial cells (Figure S4f) or with MR49C conditioned media (Figure 3b), while we saw the same induction of CD163 when M1 macrophages were cultured with different PCa cell lines (*e.g.* LAPC4, MR49F or LNCaP) (Figure S3c).

Next, we sought to evaluate the anti-cancer properties of dual CCR7 and CD163-positive macrophages (M1$^{CCR7+/CD163+}$) in our model. Cell sorting by flow cytometry was used to isolate M1$^{CCR7+/CD163+}$ macrophages which were subsequently put in direct co-culture with PCa cells as previously. These experiments confirmed that these subverted macrophages significantly lost their cytotoxicity towards MR49C cells compared to M1 macrophages but did not completely resemble M2 macrophages, used as a negative control (Figure 3e).

M1 and M2 macrophages can switch their phenotype

To further characterize the plasticity of macrophages, we next assessed the capacity of polarized macrophages to be re-educated into their opposite phenotypes through exposure to conditioned culture media of polarized macrophages. Freshly isolated CD14^{+} monocytes from healthy donors were polarized into M1 or M2 macrophages as above, followed by an exchange of culture media (*e.g.* culture medium of M1 macrophages replaced that of M2 macrophages (1→2) and vice-versa) (Figure 4a). We observed that both M1 and M2 phenotypes can be re-polarized into the opposing phenotype in a time-dependant fashion. After 96h to 6 days of re-polarization, an increasing proportion of 1→2 macrophages expressed CD163, CD206 and B7-H3 markers on their surface and after 6 days the proportions were close to that observed in M2 macrophages (Figure 4b, c, d and e). The number of molecules on their cell surface also gradually increased over time (Figure S4a). Conversely, M2 macrophages re-educated with M1 media showed a decreasing proportion of cells positive for CD163, CD206 and B7-H3 markers (Figure 4f, 4g and 4e). After 6 days, less than 20% of M2 macrophages re-educated to M1 (2→1) still expressed CD163, CD206 and B7-H3. We also observed a concordant important decrease in the number of these cell surface molecules over the time (Figure S4d). Interestingly, CCR7 expression was maintained independently of the direction of re-education (Figure S4b, S4e). We also observed that PD-L1, expression found in nearly 100% of M1 macrophages (Figure 4f, S3a, S3d), was downregulated by the transition from M1 to M2 as very few cells expressed it after transition while the proportion of cells expressing it was significantly increased when M2 macrophages were switch into M1 (Figure S4c and S4f).

Direct interaction of M1 and M2 macrophages with PCa cells prevent their re-education

To understand how re-education of macrophages in the context of the prostate TME could occur, we performed co-culture experiments of polarized macrophages in the presence of MR49C PCa cells (Figure 5a). These experiments demonstrated that the presence of PCa cells promotes the retention of M2-associated markers and thus prevents the switching of 2→1 macrophages (Figure 5). Around 65% to 85% of M2 macrophages re-educated into M1 macrophages retained high levels of CD163, CD206 and B7-H3 expression (Figure 5b, c, d and e; Figure S5a). CCR7 expression was not affected by co-culture with MR49C cells (Figure 5f; Figure S5a). Inversely, the presence of PCa cells prevented the increase in the proportion of PD-L1^{+} macrophages (Figure S5f). On the other hand, the presence of MR49C cells helped to the switching of M1 to M2 (1→2) macrophages since we observed a greater proportion of macrophages expressing CD163, CD206 and B7-H3 and with a higher amount of molecules at the cell surface when cultured in presence of PCa cells (Figure S5b, c, d).

As above, we used cell sorting by flow cytometry to isolate dual positive CCR7^{+} CD163^{+} macrophages obtained from these re-education experiments in presence of MR49C cells (1→2$^{CCR7+/CD163+}$ or the inverse

2→1$^{CCR7+/CD163+}$) in order to assess their cytolytic function. We observed that subverted macrophages (1→2$^{CCR7+/CD163+}$ and 2→1$^{CCR7+/CD163+}$) exert the same pro-tumoral function favoring PCa cells viability compared to PCa cells co-cultured with M1 (Figure 5g). However, M1 macrophages re-educated into M2 macrophages in the presence of PCa cells had a higher immunosuppressive activity compared to 1→2 re-education without PCa cells (1→2$^{CCR7+/CD163+}$ vs 1→2) (Figure 5g). The presence of PCa cells during 2→1 re-education (2→1$^{CCR7+/CD163+}$ vs 2→1) resulted in a loss of M1 macrophage killer activity (Figure 5g). Both re-education of M1 or M2 macrophages by PCa cells is accompanied by a significant decrease in PD-L1 expression (Figure S5e and f).

Macrophage re-education in presence of PCa cells leads to concomitant specific changes in chemokine signature for M1$^{CCR7+/CD163+}$ and 2→1$^{CCR7+\ CD163+}$

We next performed RNA-seq to evaluate the transcriptional similarities and differences of macrophages from two donors (A and B) re-educated by the cytokine milieu compared to the changes induced by contact with MR49C cells (Figure 6). This included total macrophages (M1, M2, 1→2 or 2→1) and flow-sorted macrophages from mixed co-cultures (M1$^{CCR7+/CD163+}$, 1→2$^{CCR7+/CD163+}$ or 2→1$^{CCR7+\ CD163+}$). Principal component analysis (PCA) demonstrated overall highly comparable results for biological replicates and overall differences in transcriptomic profiles (Figure 6a). Macrophages polarized by media conditions (M1, M2, 1→2, 2→1) clustered separately from tumor-educated macrophages (M1$^{CCR7+/CD163+}$, 1→2$^{CCR7+/CD163+}$ or 2→1$^{CCR7+\ CD163+}$). As expected, differential expression analysis (DEA) revealed more differentially expressed genes (DEGs) between M1 vs M2 macrophages (1006 upregulated and 784 downregulated; false discovery rate [FDR] <5%) compared to re-educated macrophages 1→2 and M2 (350 upregulated and 169 downregulated; FDR <5%) or 2→1 and M1 (12 upregulated and 8 downregulated; FDR <5%) (Figure 6b, Table S3). Macrophages co-cultured with MR49C (M1$^{CCR7+/CD163+}$, 1→2$^{CCR7+/CD163+}$ or 2→1$^{CCR7+\ CD163+}$) had relatively more up-regulated genes compared to down-regulated genes (Table S3).

Upset analysis revealed the number of shared genes between DEG cut-off list for the subverted macrophages compared to M1 reference for both up- and down-regulated gene sets (Figure 6b). We identified relatively more up- and down-regulated genes using M2 reference (Figure S6) compared to M1 reference (Figure 6b). We then evaluated chemokine network of subverted macrophage using M1 reference to decipher how M1 original function could be overpassed and found that both M1$^{CCR7+/CD163+}$ and 2→1$^{CCR7+\ CD163+}$ shared similar modulations since the numbers of transcripts for CXCL2, CXCL8, CCL2 and CCL8 were increased whereas the number of CXCL10 transcripts were decrease (Figure 6c, 6d). This modulation was not observed in 1→2$^{CCR7+/CD163+}$ and neither in M1, M2, 1→2 or 2→1 macrophages (Figure 6c).

DISCUSSION

PCa is a poorly immunogenic cancer that to date has only shown rare responses to immune checkpoints inhibitors [18]. TAMs, as abundant components of the prostate TME, may contribute to this poor immunogenicity. Our findings highlight the importance of the transition of macrophage from a pro-inflammatory state to became TAM. With the classic M1/M2 paradigm very limited delineate macrophage sub-populations, we focused our analyses directly on human samples and sought to elucidate the relative contributions of the cytokine milieu and PCa cell contact which subvert an infiltrating inflammatory macrophage to become a TAM. Our results showing the persistence of inflammatory markers suggest that prostate TAMs origins are principally infiltrating myeloid cell, which are then subverted by prostate tumor cells. Notably, our multi-marker analyses suggest the importance of B7-H3 as a factor associated with poor M1 anti-cancer function of macrophage and loss of PD-L1 expression.

The finding that CD163^{+} cells in tumor adjacent normal epithelia was more prognostic than CD163^{+} cells within the tumor core was unexpected and striking in magnitude. Our cytometric analysis of the prostate TME presents a global analysis of the immune infiltration but does not capture different subcompartments.

Nonetheless, this detailed multi-parametric information on the prostate immune cell infiltration was biased to include greater sampling of non-tumoral areas than tumoral areas. This therefore complements our initial findings and perhaps increased our capacity to understand the role of immunosuppressive macrophages within the prostate TME. CD163 and CD206 were previously described as immunosuppressive macrophage markers associated with clinicopathological outcomes and poor prognoses in patients with aggressive PCa [19, 20]. We then identified one specific sub-population of macrophages which express M1 (CCR7) and M2 (CD206, CD163) phenotypic characteristics. Further, this same mixed phenotype was recapitulated using an *in vitro* monolayer co-culture model of human blood-derived macrophages and PCa cells ($1\rightarrow2^{CCR7+/CD163+}$ and $2\rightarrow1^{CCR7+/CD163+}$). Isolation of these macrophages by fluorescence-activated cell sorting further demonstrated that these cells exert low cytotoxic functions compare to original M1 inflammatory macrophages. Based on this data, we propose that M1 macrophages recruited into the TME of PCa are subverted by PCa cells and surrounding immunosuppressive context to become TAMs with pro-tumoral functions, low expression of PD-L1, high B7-H3 expression. Moreover, our model suggests that in the presence of PCa cells, these macrophages lose their capacity to revert to their orginal phenotype. We also noticed that only $2\rightarrow1^{CCR7+/CD163+}$ macrophages resemble closely to TAM observed in patient samples with matching phenotype and modulations of known chemokine network transcripts [21, 22].

Immune checkpoint inhibition remains effective for a very small proportion of advanced PCa patients [23]. As in other cancers, the results of the phase Ib KEYNOTE-028 trial in PCa [24] suggest the PD-1 inhibitor pembrolizumab is more effective in patients with PD-L1 positive immune and non-immune cells, though it represents a small subgroup of patients [25, 26]. As we observed that PCa-subverted macrophages had lower expression of PD-L1 but higher expression of B7-H3, we can hypothesize that, in a time-dependent manner, this is one of the multiple ways how PCa may escape immune surveillance. Further, results in our model correspond to patient studies which highlight the correlation between B7-H3 and poor clinical outcomes in PCa [8, 27] as well as other solid tumors [27-29].

We are aware of some limitations in our study. Only 21 patients underwent the identical full panel of immunosuppressive marker for our flow cytometry studies, though almost all these patients had GGG ≥3 disease with at least two prostate zones negative for PCa. This selection for more aggressive, focal disease may incur unknown bias into our results. Another limitation was noted in our co-culture system where the M2 macrophages seemed to exert a little anti-tumoral function by decreasing PCa cell viability which could be attributed to the non-autologous co-culture system between healthy donor samples and PCa cell lines or the simplify polarization environment [30]. The phagocytic activity of macrophages limited our capacity to accurately evaluate the proliferation of PCa cells using CSFE (data not shown) [30] in our co-culture system. Further, this phagocytic activity also appeared to influence the results for the RNA sequencing. Indeed, mRNAs from several PCa-associated genes (*e.g. KLK3, STEAP, NKX3.1*) where found in the list of upregulated genes in all macrophage co-cultures suggesting phagocytosis of PCa cells (not shown). These exogenous mRNAs limit the interpretation of affected signaling pathways in macrophages between different experimental conditions. While our model demonstrates the differential effects of the cytokine milieu and PCa cell contact, further work needs to be done to evaluate strategies to re-educate TAMs using our co-culture model. This includes impact of B7-H3 targeting or other macrophage-specific targets (add refs). Nonetheless, our studies highlight that our model mirrors both the phenotype and function respectively observed and anticipated in human prostate tumors. Further studies evaluating other cancer cell lines, particularly those associated with different TAM phenotypes (*e.g.* in colon, gastric cancers) may provide further insights into interactions induced by these infiltrating myeloid cells.

In summary, this study provides new insights into the origin of PCa immune-driven resistance mechanisms and contributes to a better understanding of the origin of TAMs within the prostate TME.

REFERENCES

1. Takeya, M. and Y. Komohara, *Role of tumor-associated macrophages in human malignancies: friend or foe?* Pathol Int, 2016. **66**(9): p. 491-505.
2. Weigert, A., et al., *Killing Is Not Enough: How Apoptosis Hijacks Tumor-Associated Macrophages to Promote Cancer Progression.* Adv Exp Med Biol, 2016. **930**: p. 205-39.
3. Franklin, R.A., et al., *The cellular and molecular origin of tumor-associated macrophages.* Science, 2014. **344**(6186): p. 921-5.
4. Franklin, R.A. and M.O. Li, *The ontogeny of tumor-associated macrophages: a new understanding of cancer-elicited inflammation.* Oncoimmunology, 2014. **3**(9): p. e955346.
5. Varol, C., A. Mildner, and S. Jung, *Macrophages: development and tissue specialization.* Annu Rev Immunol, 2015. **33**: p. 643-75.
6. Wynn, T.A., A. Chawla, and J.W. Pollard, *Macrophage biology in development, homeostasis and disease.* Nature, 2013. **496**(7446): p. 445-55.
7. Noy, R. and J.W. Pollard, *Tumor-associated macrophages: from mechanisms to therapy.* Immunity, 2014. **41**(1): p. 49-61.
8. Benzon, B., et al., *Correlation of B7-H3 with androgen receptor, immune pathways and poor outcome in prostate cancer: an expression-based analysis.* Prostate Cancer Prostatic Dis, 2017. **20**(1): p. 28-35.
9. Muliaditan, T., et al., *Macrophages are exploited from an innate wound healing response to facilitate cancer metastasis.* Nat Commun, 2018. **9**(1): p. 2951.
10. Aras, S. and M.R. Zaidi, *TAMeless traitors: macrophages in cancer progression and metastasis.* Br J Cancer, 2017. **117**(11): p. 1583-1591.
11. Mantovani, A., et al., *Cancer-promoting tumor-associated macrophages: new vistas and open questions.* Eur J Immunol, 2011. **41**(9): p. 2522-5.
12. Keeley, T., D.L. Costanzo-Garvey, and L.M. Cook, *Unmasking the Many Faces of Tumor-Associated Neutrophils and Macrophages: Considerations for Targeting Innate Immune Cells in Cancer.* Trends Cancer, 2019. **5**(12): p. 789-798.
13. Azizi, E., et al., *Single-Cell Map of Diverse Immune Phenotypes in the Breast Tumor Microenvironment.* Cell, 2018. **174**(5): p. 1293-1308 e36.
14. Muller, S., et al., *Single-cell profiling of human gliomas reveals macrophage ontogeny as a basis for regional differences in macrophage activation in the tumor microenvironment.* Genome Biol, 2017. **18**(1): p. 234.
15. Ylitalo, E.B., et al., *Subgroups of Castration-resistant Prostate Cancer Bone Metastases Defined Through an Inverse Relationship Between Androgen Receptor Activity and Immune Response.* Eur Urol, 2017. **71**(5): p. 776-787.
16. Aran, D., Z. Hu, and A.J. Butte, *xCell: digitally portraying the tissue cellular heterogeneity landscape.* Genome Biol, 2017. **18**(1): p. 220.
17. Taylor, B.S., et al., *Integrative genomic profiling of human prostate cancer.* Cancer Cell, 2010. **18**(1): p. 11-22.
18. Kim, T.J. and K.C. Koo, *Current Status and Future Perspectives of Checkpoint Inhibitor Immunotherapy for Prostate Cancer: A Comprehensive Review.* Int J Mol Sci, 2020. **21**(15).
19. Cao, J., et al., *Prognostic role of tumour-associated macrophages and macrophage scavenger receptor 1 in prostate cancer: a systematic review and meta-analysis.* Oncotarget, 2017. **8**(47): p. 83261-83269.
20. Zarif, J.C., et al., *Mannose Receptor-positive Macrophage Infiltration Correlates with Prostate Cancer Onset and Metastatic Castration-resistant Disease.* Eur Urol Oncol, 2019. **2**(4): p. 429-436.

21. Argyle, D. and T. Kitamura, *Targeting Macrophage-Recruiting Chemokines as a Novel Therapeutic Strategy to Prevent the Progression of Solid Tumors.* Front Immunol, 2018. **9**: p. 2629.
22. Farmaki, E., et al., *CCL8 Promotes Postpartum Breast Cancer by Recruiting M2 Macrophages.* iScience, 2020. **23**(6): p. 101217.
23. Topalian, S.L., et al., *Safety, activity, and immune correlates of anti-PD-1 antibody in cancer.* N Engl J Med, 2012. **366**(26): p. 2443-54.
24. Chung, H.C., et al., *Pembrolizumab After Two or More Lines of Previous Therapy in Patients With Recurrent or Metastatic SCLC: Results From the KEYNOTE-028 and KEYNOTE-158 Studies.* J Thorac Oncol, 2020. **15**(4): p. 618-627.
25. Haffner, M.C., et al., *Comprehensive Evaluation of Programmed Death-Ligand 1 Expression in Primary and Metastatic Prostate Cancer.* Am J Pathol, 2018. **188**(6): p. 1478-1485.
26. Mehnert, J.M., et al., *Safety and antitumor activity of the anti-PD-1 antibody pembrolizumab in patients with advanced, PD-L1-positive papillary or follicular thyroid cancer.* BMC Cancer, 2019. **19**(1): p. 196.
27. Castellanos, J.R., et al., *B7-H3 role in the immune landscape of cancer.* Am J Clin Exp Immunol, 2017. **6**(4): p. 66-75.
28. Baral, A., et al., *B7-H3 and B7-H1 expression in cerebral spinal fluid and tumor tissue correlates with the malignancy grade of glioma patients.* Oncol Lett, 2014. **8**(3): p. 1195-1201.
29. Chen, L., et al., *B7-H3 expression associates with tumor invasion and patient's poor survival in human esophageal cancer.* Am J Transl Res, 2015. **7**(12): p. 2646-60.
30. Chung, S., et al., *Quantitative analysis of cell proliferation by a dye dilution assay: Application to cell lines and cocultures.* Cytometry A, 2017. **91**(7): p. 704-712.

Macrophage regulates androgen receptor activation in prostate cancer

Asmaa El-Kenawi[1*], Min Liu[2], William Dominguez Viqueira[3], Xiaoqing Yu[4], John Koomen[2], Robert Gatenby[5] and Brian Ruffell[1*]
[1]Department of Immunology; [2] Proteomics and Metabolomics Core (PMC); [3] Small Animal Imaging Lab (SAIL); [4] Department of Biostatistics ; [5] Department of Radiology, H. Lee Moffitt Cancer Center, Tampa, Florida 33612, USA

Background
Castration-resistant prostate cancer (CRPC) is a lethal stage of disease. A wealth of clinical and experimental data supports the persistence of androgen receptor (AR) signaling in many cases of CRPC, despite androgen-deprivation therapy (ADT).
Methods
Here we sought to determine the role of macrophages in CRPC using an animal model that reflects the mutational landscape of prostate cancer.
Results
Our findings showed that depleting macrophage using a neutralizing antibody against the colony-stimulating factor (CSF)-1 in combination with ADT (Lupron) significantly extended survival of mice-bearing orthotoptic prostate tumors, compared with each agent alone. To determine the mechanism by which macrophages enhance response to ADT, we performed an unbiased transcriptomic analysis of prostate tumors following macrophage depletion, and, found that macrophage infiltration was associated with molecular signatures of AR activation. This was confirmed by immunohistochemistry, with both macrophage depletion and Lupron treatment leading to reduced AR nuclear localization in prostate tumors. These findings were recapitulated in vitro, with the co-culture of macrophages and prostate cancer cells enhancing AR nuclear localization, increasing cancer cell proliferation in androgen-deprived conditions, and reducing sensitivity to the AR antagonist, enzalutamide.
Conclusion
Tumor macrophages directly promote AR activation and resistance to ADT in prostate cancer.

CHD1-loss Promotes Tumor Heterogeneity, Lineage Plasticity and Therapy Resistance

Background: Targeted therapies for driver oncogenes have transformed the management of many cancers but the magnitude and duration of response remains variable. One potential explanation is the presence of additional genomic alterations which modify the degree of dependence on the targeted driver mutation. Metastatic castration resistant prostate cancer (mCRPC) serves as an example, where the target is the androgen receptor (AR). Compared to primary disease, mCRPC is characterized by extensive heterogeneity at both genomic and transcriptional levels, including genomic copy number alterations (CNAs), which are presumed to contribute to the resistance to AR targeted therapies.

Method: To gain functional insight into the genes impacted by the CNAs in mCRPC, we screened 730 genes often deleted in mCRPC for CNAs that confer *in vivo* resistance and identified the chromodomain helicase DNA-binding protein 1 (*CHD1*) as a top candidate modifying resistance, a finding supported by patient data showing that *CHD1* expression is inversely correlated with clinical benefit from therapy.

Results: Depletion of *CHD1* confers significant resistance to enzalutamide both *in vitro* and *in vivo*. Furthermore, we observed global changes in open and closed chromatin after the depletion of *CHD1*, indicative of an altered chromatin state, with associated changes in gene expression. Integrative analysis of ATAC-seq and RNA-seq, combining with CRISPR-based screen, identified four heterogenous resistance drivers (*GR, BRN2, NR2F1, TBX2*), which are elevated in different independently derived, resistant, *CHD1*-deleted subclones. Significantly increased transcriptional heterogeneity, as well as lineage plasticity was observed in these resistant tumors and in the tumor samples from a large mCRPC patients' cohort. Finally, GR inhibition with both genetic and pharmacological approaches restored the enzalutamide sensitiivty in resistant tumors with elevated GR signaling.

Conclusion: These results suggest *CHD1*-loss establishes a state of chromatin plasticity that accelerates the development of AR targeted therapy resistance through activation of heterogeneous downstream effectors, which mediated the transition away from luminal lineage identity and AR dependency. This model not only provides an innovative explanation for the increased transcriptional heterogeneity in mCRPC, but also suggests that proper clinical interventions targeting these heterogenous resistance drivers may be a novel avenue to overcome resistance towards AR targeted therapies.

Title: Identification of Novel Therapies for RB-deficient Castration-Resistant Prostate Cancer

Authors: Deborah L. Burkhart (1), Justin H. Hwang (1,2), John G. Doench (2), Kent Mouw (1,3), Atish D. Choudhury (1,2), and Leigh Ellis (1,2,3)

Institutions
(1) Dana-Farber Cancer Institute, Boston, MA
(2) Broad Institute of Harvard and MIT, Cambridge, MA
(3) Brigham & Women's Hospital, Boston, MA

Background: Metastatic castration-resistant prostate cancer (mCRPC) is currently incurable. The majority of mCRPC remains reliant on androgen receptor (AR) signaling. With next generation AR targeted therapies including enzalutamide, the frequency of patients who develop ADT-resistant tumors that no longer rely on AR signaling (CRPC-AI) is increasing. Patients' progression to CRPC-AI involves combinatorial loss of function of tumor suppressor genes like PTEN, RB1, and TP53. Furthermore, these highly lethal tumors adapt to ADT via lineage plasticity, driven largely by Ezh2, and adopt a phenotype no longer dependent on AR expression and signaling.

Recent data from patients with mCRPC identified genetic aberrations in the RB tumor suppressor as the strongest predictor of poor outcome. These data implicate RB dysfunction as a dominant molecular mechanism driving lethal prostate cancer. Currently there are no therapies to provide durable response in patients with RB loss-of-function (LOF). Therefore, there is a critical need to delineate downstream effectors of RB LOF so that therapeutic targets can be identified and validated in clinical trials. RB is a known regulator of the cell cycle, differentiation status, and genomic stability. Absence of RB impairs the DNA damage response (DDR) through multiple mechanisms, therefore increasing the potential sensitivity of RB-deficient cells to inhibitors of the kinases required for DNA repair.

Methods: Using an RB-deficient mouse cell line derived from our novel genetically engineered mouse model, we have performed a genome-wide CRISPR knockout screen. Negatively selected genes identified in this screen have been cross compared to a similar screen performed in RB-deficient small cell lung cancer cells. Selected targets identified by the screen have been validated using small molecule inhibitors.

Results: We have identified 1723 genes whose knockout is detrimental to the growth of RB-deficient mouse prostate cancer cells. Gene set enrichment analysis of these genes found enrichment of genes involved in the G2/M checkpoint and DNA damage response. Specifically, 6 kinases with roles in these checkpoints were amongst the significant genes negatively selected in DKO cells. These included Atm, Atr, Plk1, Chek1, AurkA, and AurkB, which have also been identified as vulnerabilities in RB-deficient small cell lung cancer.

We are currently validating these genes in mouse and human models of CRPC-AI with an ultimate goal to provide novel mechanistic insight and therapeutic trials within patients who

progress to CRPC-AI involving RB loss of function. Furthermore, we are investigating the correlation between absence of RB and response to the ATR inhibitor M6620 in combination with carboplatin in an ongoing clinical trial (NCT03517969). Future studies will extend these findings to use preclinical models to explore the efficacy of combination therapies using ATR inhibition, EZH2 inhibition, and immune checkpoint blockade in RB-deficient CRPC.

ADT/ANTI-AR THERAPY RESULTS IN GAPDH UPREGULATION IN PROSTATE CANCER

Wang Liu, **Ting Li**, Haixia Xu, Changlin Li, Jeffrey Holzbeierlein and Benyi Li

Departments of Urology, The University of Kansas Medical Center, Kansas City, KS 66160

Introduction

As the widespread use of potent anti-AR drugs in castration-resistant prostate cancer patients, neuroendocrine progression (t-NEPC or CRPC-NE) has emerged as a major clinical obstacle, accounting for more than 25-30% mortality of prostate cancers. Recent studies with patient-derived xenografts (PDX) revealed that t-NEPC model LTL-331R exerted a highly upregulated glycolytic activity, indicating a metabolic reprogramming in t-NEPC progression. Currently, targeting the altered glycolysis pathway in cancer cells has emerged as a potent cancer therapy. Especially, inhibition of glyceraldehyde-3-phosphate dehydrogenase (GAPDH), a critical glycolytic enzyme, achieved a profound anti-cancer outcome specifically in highly glycolytic cancers. Therefore, we investigated the role of GAPDH alteration in t-NEPC/CRPC-NE models and identified a novel GAPDH inhibitor Alternol as a potential therapy for NEPC patients.

Methods

GAPDH gene expression profiles in prostate cancers were analyzed using the published NCBI GDS datasets. GAPDH promoter-driven luciferase reporter assay and glucose consumption assay was conducted in LNCaP cells after Enzalutamide treatment. GAPDH protein expression was evaluated in tissue microarray sections, NEPC PDX tissue and xenograft tissues by immunohistochemistry. The novel small compound Alternol isolated from fungi fermentation was used in multiple prostate cancer cell lines for GAPDH activity assay. Cellular thermal shift assay (CETSA) was used to verify the interaction of Alternol with GAPDH protein in cells.

Results

Data mining for GAPDH expression showed that it is slightly higher in primary (1.7-2.18 folds) and significantly higher in metastatic prostate cancers (>5-folds) compared to normal or benign adjacent tissues (Fig 1). In addition, castration in mice caused a significant increase of GAPDH expression in prostate gland or subcutaneous xenograft tissues of prostate cancer (Fig 2). Consistently, GAPDH-LUC reporter activity was increased about 2-fold after androgen depravation, which was further enhanced (> 9-fold) by Enzalutamide in LNCaP cells. Interestingly, Enzalutamide also enhanced glucose consumption rate under androgen depravation condition (Fig 3). Molecular docking study confirmed our previous report that Alternol interacts with GAPDH at the catalytic active/NAD+ binding sites with a binding affinity at -10.1 kcal/mol (Fig 4A). This interaction was validated in CETSA assay in C4-2 and 22RV1 cells (Fig 4B & 4C). The functional consequence of Alternol-GAPDH interaction was evaluated using in vitro and in vivo GAPDH assays (Fig 5).

Conclusion

Androgen depravation plus anti-AR therapy resulted in GAPDH up-regulation in prostate cancer cells and tissues, suggesting a strong clinical relevance of GAPDH up-regulation in anti-AR treatment-induced NE progression of CRPC patients. Alternol interacts with GAPDH and potently suppressed GAPDH glycolytic activity *in vitro* (IC_{50} = 5.794 nM), which is 37.5-fold more potent than an existing GAPDH inhibitor Korningic Acid (IC_{50} = 217.6 nM). Alternol also lowered down the excessive GAPDH glycolytic activity in prostate cancer cells to the level close to benign cells without a total blockage, indicating a safe therapeutic feature.

Funding

DoD PCRP190026

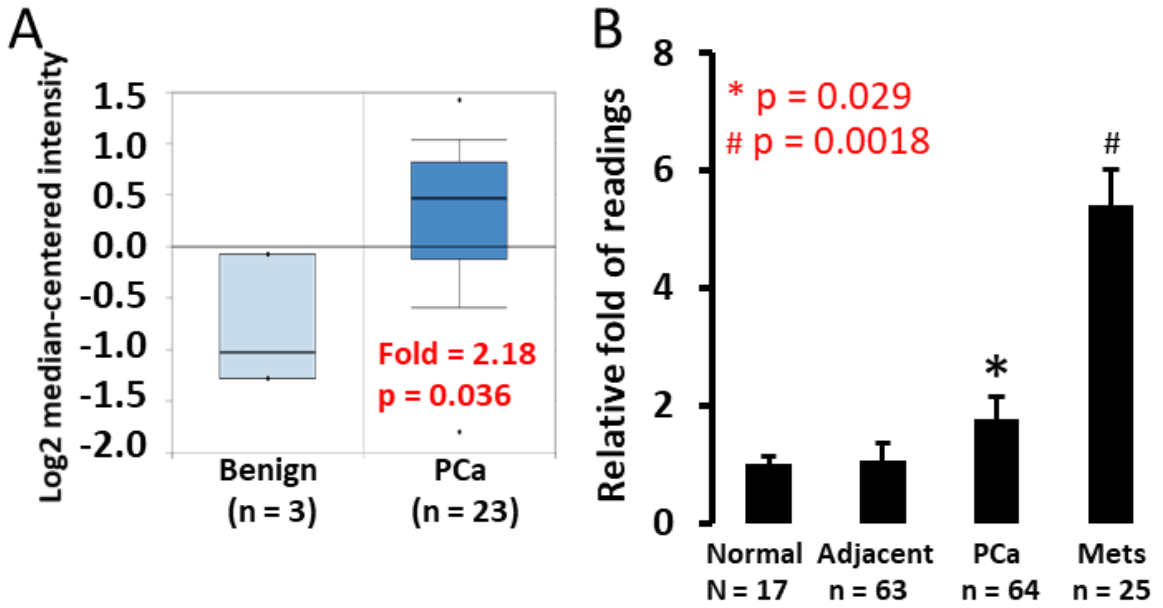

Fig 1. GAPDH expression in prostate cancers. Data mining for GAPDH expression was conducted using datasets from human prostate specimens (A, GSE6888236 and (B, GDS254537).

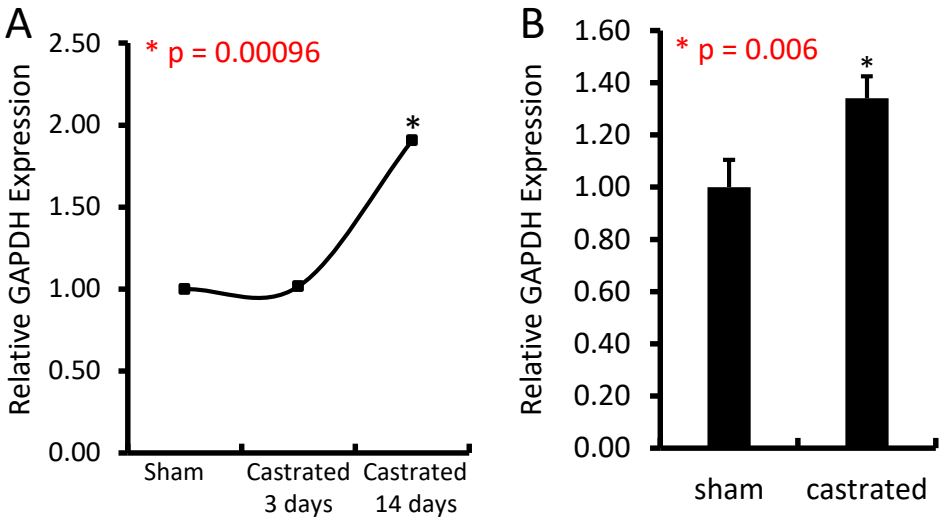

Fig 2. GAPDH expression after castration. Data mining for GAPDH expression was conducted using datasets from (A) mouse prostate tissue after 3-14 days of castration (GDS2562) and (B) LuCaP35 s.c. xenografts in SCID mice after 4-weeks castration (GDS4120). Epithelium-specific gene KRT18 was used for data normalization.

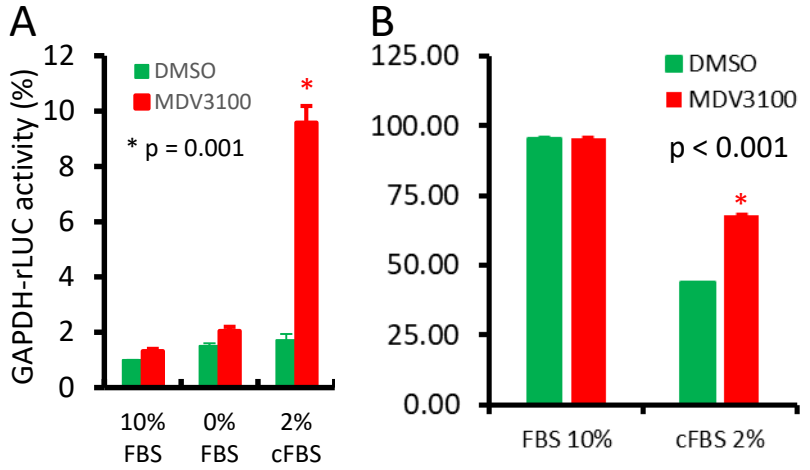

Fig 3. Enzalutamide enhances GAPDH expression and activity. **A** LNCaP cells transfected with GAPDH-rLUC constructs (Addgene#82479) were treated with DMSO or MDV3100 (Enzalutamide, 10 μM) for 24 h. Reporter activities were normalized with protein concentrations in corresponding samples. **B** Glucose levels in cell culture media were measured with a pre-assembled kit from Signa (catalog #GAGO20) in LNCaP cells after 24-h treatment as indicated.

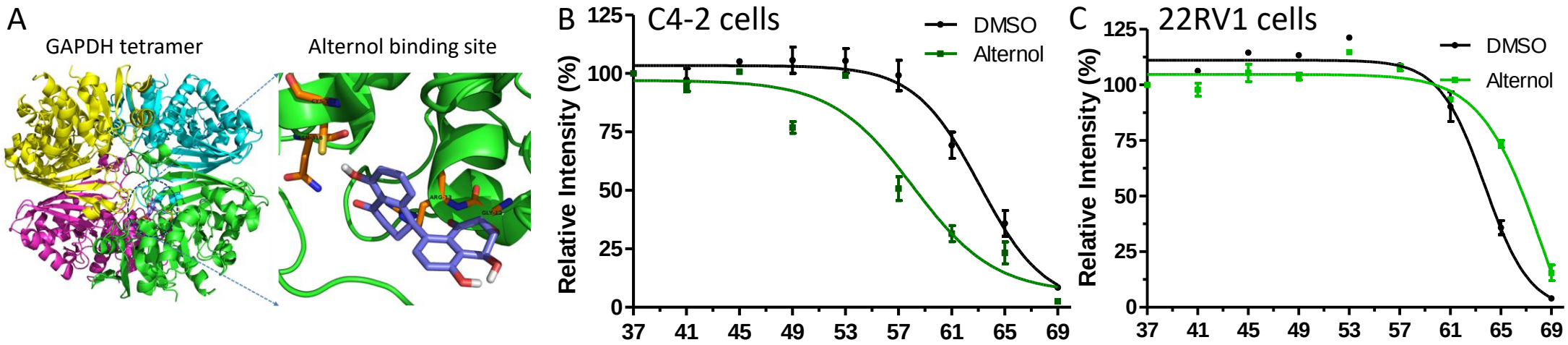

Fig 4. Alternol interacts with GAPDH. **A** in silicon docking analysis was conducted using crystal structure for human liver GAPDH protein derived from Research Collaboratory for Structural Bioinformatics Protein Data Bank (1ZNQ). **B&C** C4-2 and 22RV1 cells were treated with Alternol (10 μM) for 4 h, followed by CETSA assays.

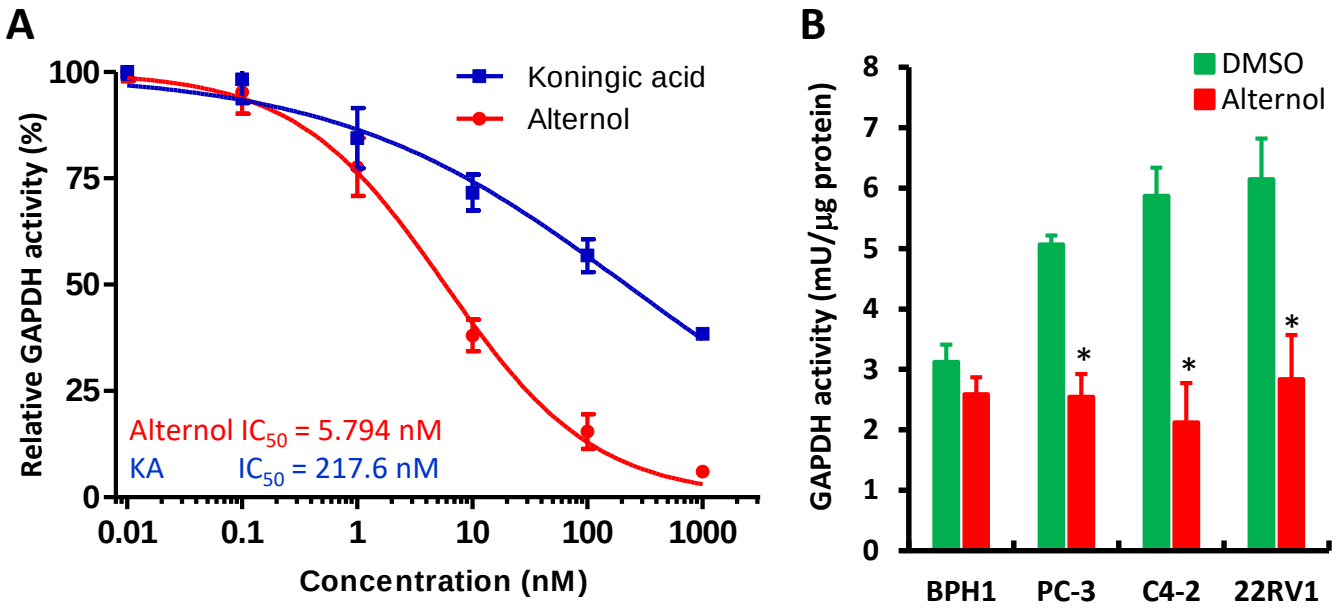

Fig 5. Alternol suppresses GAPDH activity. **A** GAPDH in vitro activity assay. **B** Cells were treated with DMSO or Alternol (10 μM) for 4 h and cellular proteins were extracted for GAPDH activity assay using the BioVision kit. The asterisk indicates a significant difference compared to DMSO ($p < 0.05$, Student t-test).